SCIENTIFIC REPORT

2001-2002

**Photo : Intensity maps measured using
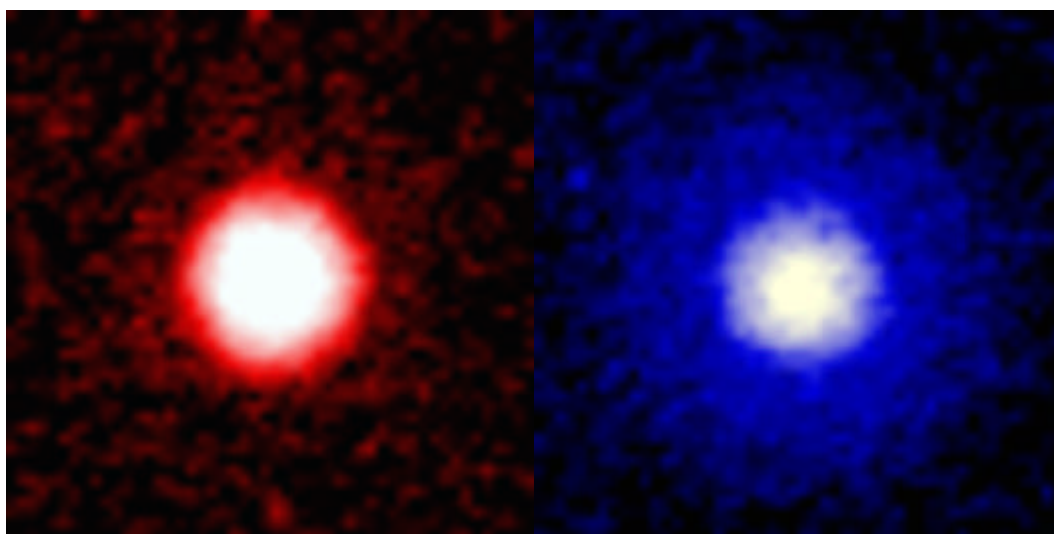Fresnel Zone Plates as neutron focussing lenses**

LABORATOIRE LEON BRILLOUIN

SCIENTIFIC REPORT 2001-2002

Centre d'Etudes de Saclay
Bâtiment 563
91191 Gif-sur-Yvette cedex, France
Internet : http://www.llb.cea.fr

CENTRE NATIONAL
DE LA RECHERCHE
SCIENTIFIQUE

CONTENTS

1 - STRUCTURES AND PHASE TRANSITIONS

2 - MAGNETISM AND SUPERCONDUCTIVITY

3 - MATERIALS SCIENCE

4 - LIQUIDS AND DISORDERED SYSTEMS

5 - SOFT MATTER AND BIOMATERIALS

6 - LIFE SCIENCES

7 - MODELLING

8 - TECHNICAL AND INSTRUMENTAL DEVELOPMENTS

Director's Report

This report presents an overview of the scientific activities of the Laboratoire Léon Brillouin LLB during the 2001-2002 period.

The LLB is a CNRS-CEA mixed research unit ("Unité mixte de recherche" UMR12) funded by the "Centre National de la Recherche Scientifique" (CNRS) and the "Commissariat à l'Energie Atomique" (CEA).

The LLB is a neutron laboratory dedicated to a triple mission:

- Large national facility to perform neutron scattering experiments proposed by external users, including industrial firms, in the best conditions
- Training centre for young researchers, in particular thesis students preparing PhD diploma essentially based on neutron scattering techniques and instrumentation
- Research laboratory with its own scientific activity centred on the use of the LLB facilities and performed by permanent or associated teams.

This triple character of the LLB mission, neutron facility, training centre and research laboratory, leads to an integrated scientific environment for neutron scattering of excellence and the research performed at the LLB is acknowledged worldwide in many scientific fields. The LLB, as the French national neutron facility, benefits from the quality of the Orphée reactor, one of the best neutron steady sources in the world, almost exclusively dedicated to research. Orphée is perfectly run and maintained by the Direction of the Nuclear Energy (DEN) of the CEA.

Neutron beam time: Around 3600 beam time days are delivered per year on 25 spectrometers: 65% for the French community, 22% for CEE countries, 4% for Russia and 5% for ex-PECO countries which will join the CEE in 2004. Six (6) spectrometers benefit from a Collaborative Research Group agreement with Germany (3), Russia, Italy and Austria.

Orphée-LLB and the European Community: The LLB has been selected by Brussels since 1993 in the access programs for large installations. In the framework of the fifth program (FP5) running until February 2004, the LLB delivers 170 days of neutron beam time to the research teams of the CEE and associated countries. Orphée-LLB participates actively in the "Neutron Integrated Initiative" of the sixth EU framework programme for Research and Technological Development (FP6). Aside the access program, several research projects have been defined, two of which being coordinated by LLB researchers.

Research done at LLB is following the main strategic schemes and topmost priorities of the French research agencies, in particular the CNRS and the CEA.

Nanosciences: The LLB uses neutron techniques to bring valuable contributions in the field. Adhesion phenomena, solubilization, chemical reactivity and grafting on nanocomposites, protein interactions are important processes operating at interfaces that can be studied by standard neutron reflectivity whereas polarised neutron techniques probe the magnetic structures of layered devices for the future spin electronics.

Life sciences: The research activities in this field are in constant increase at the LLB. The focus is on protein unfolding and the structure-function relationship in biological systems. Neutron diffusion allows to characterize both the folded and the unfolded states of proteins modified by temperature, pH, chemicals and hydrostatic pressure and can bring important clues for a complete understanding of the factors stabilizing their folded conformation. As for the dynamics at physiological temperatures, the diffusion in protein solutions is very complex due to the rich variety of possible correlations under the influence of concentration or hydration. Neutron spectroscopy is a powerful tool to resolve the protein motions in the time range from picoseconds to tens of nanoseconds (time of flight, backscattering, spin echo techniques), with the help of the large cross section of hydrogen/deuterium atoms. For example, work on myoglobin and haemoglobin, done in biological conditions i.e. at 37°C in very concentrated solutions, is very promising to understand fundamental aspects of oxygen transport.

New projects are developed at the LLB concerning environmental problems, earth sciences, innovative materials for cleaner energies like membranes for fuel cells, Lithium batteries, special steels for new reactors (e.g. the aging behaviour under irradiation).

Industrial developments and technological transfers: The activity of LLB in Engineering Sciences has significantly increased in the last years. Numerous industrial problems were studied, in general within the framework of contracts (Man technologies AC, EADS, PSA and SNCF), or by the means of European programs (in particular TRAINSS). As an example, the residual thermal stresses of Ti-SiC composites have been analysed by neutron diffraction to model their long-term behaviour during in-service operation, as they are considered by SNECMA to be used in a near future for compressor parts in their motors. In 2002, a CEA researcher from the LLB, Alain Menelle was the co-laureate, together with the CILAS company, of the ROCARD prize of the "Societe Francaise de Physique" for his work on technological transfers for supermirror neutron guides.

Instrumental developments at Orphee-LLB: These projects are gathered under the theme CAP2010. The neutron spectrometers must be continuously refurbished and upgraded to be kept attractive at an international level. First, it is proposed to stop the less efficient spectrometers, in particular the G4.4 machine for diffuse scattering, the G4.3 cold triple-axis "VALSE" and the MESS spin echo. The first priority of the LLB is now modernize the high-resolution powder diffractometer 3T2, highly demanded by the solid-state chemistry laboratories. In parallel, the time-of flight reflectometer EROS will be upgraded to face the growing studies on liquid surfaces and interfaces in soft matter and complex systems. We plan to shorten the collimator system in a first step and then move the whole spectrometer to an end position to increase the flux and flexibility. The last project concerns the time of flight spectrometer Mibemol that still performs very well in terms of energy resolution but could benefit of a higher flux. A new time of flight spectrometer is under study, to be placed also on an end guide position. Aside these three major instrumental projects, there is a rising request of large two-dimensional detectors to be financed and built.

It has been decided to discontinue the LLB users' meeting "Tables Rondes"organized every year before the fall scientific committee. It will be replaced by regular workshops focusing on scientific or technical subjects of interest for the neutron and synchrotron community. The aim is to make of the "Saclay Plateau" a meeting point for complementary techniques as successful on a French stand as in other countries or in Grenoble on a European level with the ILL and the ESRF.

The following pages illustrate the LLB activities in the 2001-2002 period. For each research domain, Structures, Magnetism, Material Science, Liquids and disordered systems, Soft matter and Life sciences, a outline of the LLB scientific activity is presented, focussing mainly on in-house research and close collaborations. Each summary is followed by a few selected recent highlights illustrating the work performed on the LLB instruments by our researchers and the external users. This report contains a new chapter dealing with the theory and modelling of scientific problems related to neutron scattering and data reduction. It is followed by a chapter on instrumentation, a presentation of the LLB activity with statistics summarizing the user activities and a list of publications for 2001-2002.

We are in a stimulating phase when the main European countries, like Great Britain and Germany, develop their national neutron sources while reinforcing their association with the ILL, the European high-flux reactor. The Munich reactor FRMII will soon start and complement the neutron work done at Julich and Berlin. ISIS will invest 100M£ to build a second target station and the related instrumentation. The researchers of the LLB have collaborated closely with all these centres to promote the case of the European spallation source ESS in the last years. Now the spotlight has moved on the SNS, the new spallation source built in the United States, showing that Neutron is an essential technique in many research domains like material science, superconductivity, nanosciences, chemical physics and life science. We heartily hope that ORPHEE-LLB will continue to play a fundamental role in all these domains.

M. ALBA,   P. MONCEAU
May 6, 2003

SCIENTIFIC HIGHLIGHTS

STRUCTURES AND PHASE TRANSITIONS
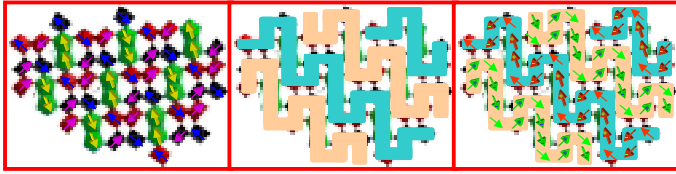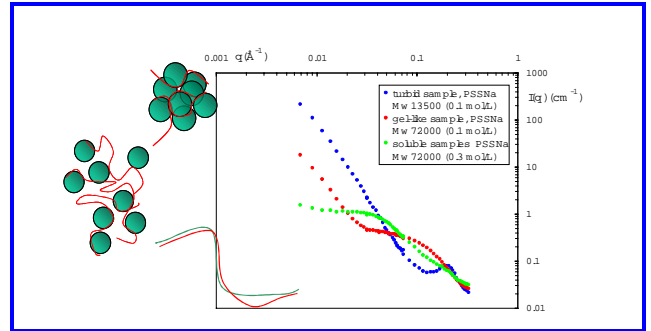
MAGNETISM AND SUPERCONDUCTIVITY

MATERIAL SCIENCE

LIQUIDS AND DISORDERED SYSTEMS

SOFT MATTER AND BIOMATERIALS
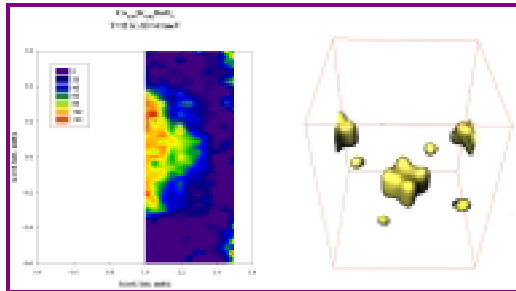
LIFE SCIENCES
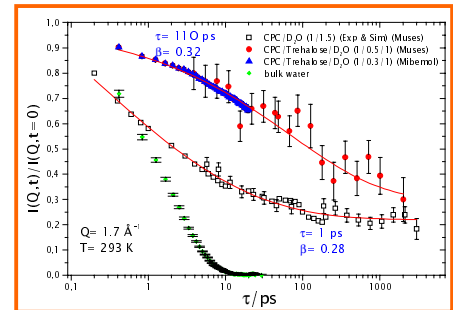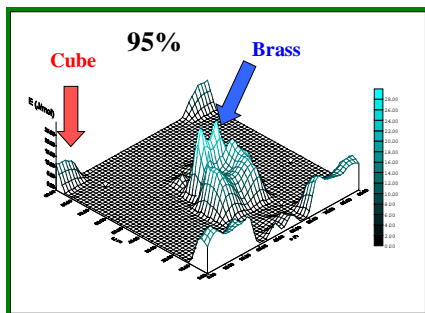
MODELLING
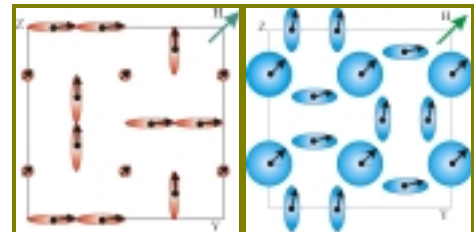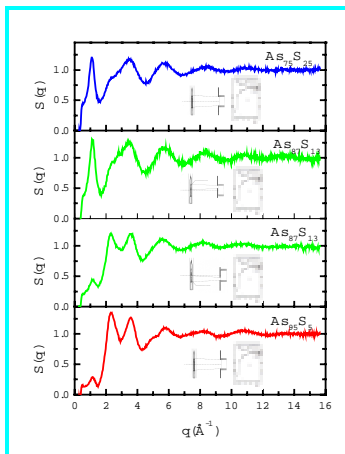
TECHNICAL AND INSTRUMENTAL DEVELOPMENTS
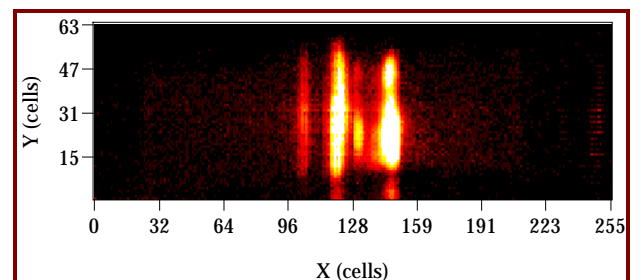
1 - STRUCTURES AND PHASE TRANSITIONS

The study of both crystallographic and magnetic structural phase transitions is an important part in the activity of Léon Brillouin Laboratory. Besides macroscopic techniques, such as electrical resistivity, specific heat and magnetic measurements, such studies need microscopic techniques, and among them neutron diffraction and inelastic scattering play an essential role, in order to look simultaneously at light and heavy elements in the crystal structure, at crystal and magnetic structures and/or excitations.

Neutron studies, either diffraction or inelastic scattering, are performed as a function of external parameters, namely temperature and pressure. Many different physical problems, both fundamental and applied, are in connection with phase transitions and the present summary intends to show the main results of the research in the field in 2001 and 2002, from perovskites to molecular crystals, from hydride systems to quantum tunnelling, from commensurate to incommensurate materials…

HYDRIDES: STRUCTURAL STUDIES

Most of the intermetallic alloys of general formula AB_n (A = Mg, Ti, Zr, Y or R = rare earth; B = Mn, Fe, Co, Ni…; n = 1, 2, 3, 5…) are able to store large amounts of hydrogen to create metallic hydrides. The absorption/desorption reaction is reversible in a large domain of temperature and pressure. Therefore these compounds have been developed for energy storage applications. Among the hydride forming compounds, $LaNi_5$ is able to store more than 6H/formula unit at room temperature.

Neutron diffraction is crucial for the determination of the structural properties of these phases: symmetry, nature of occupied insertion sites and occupation factor. Moreover, due to the neutron penetration depth, structural studies can be performed in closed cell under hydrogen pressure up to 100 bar allowing accurate control of the hydrogen composition. The accurate description of crystal structures of AB_5 host matrices and their hydrides remains our most important contribution in the hydride field, including superstoechiometric AB_{5+x} intermetallic alloys.

$LaY_2Ni_9H_{12}$

New materials are also investigated, such as RY_2Ni_9 (R = La, Ce) compounds, structurally described as an ordered intergrowth of $(R,Y)Ni_5$ and $(R,Y)Ni_2$ structure-types. In a more fundamental point of view, the magnetic structures of Laves phases have been studied in connection with their absorption properties, thus allowing a careful description of their phase diagrams and the relationships existing between inserted hydrogen (deuterium) structural order and magnetic order. [Collaboration: Laboratoire de Chimie Métallurgique des Terres Rares-CNRS, Thiais]
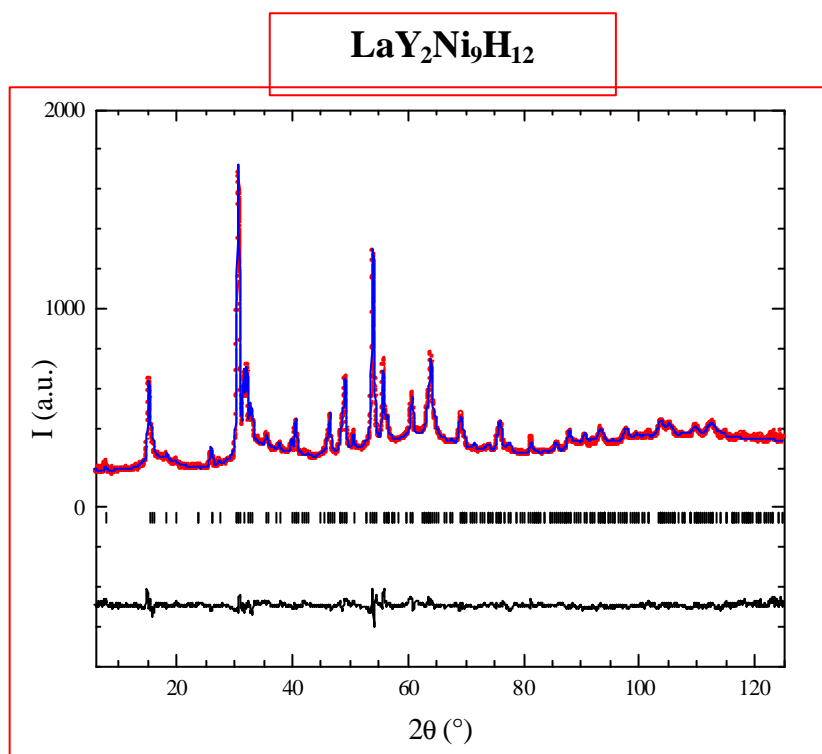
MOLECULAR CRYSTALS: QUANTUM EFFECTS AND BIOMOLECULAR SYSTEMS
Quantum entanglement in hydrogenated molecule vs "classic" deuterated analogue

Differences between quantum mechanics and classical physics are specially underlined in $KHCO_3$. Quantum entanglement observed in the $KHCO_3$ crystal then further demonstrates the validity of quantum mechanics at the macroscopic level (see subsequent "$KHCO_3$" **Highlight**).

Lithium acetate ($LiCH_3COO,2H_2O$) is another prototype system to investigate the interplay of crystal structure and rotational dynamics of nearly free quantum methyl rotors. For the methyl-deuterated salt we [Collaboration: LADIR, Thiais, F. Fillaux; LLB: B. Nicolaï (PostDoc), A Cousson] have observed a phase transition at (17.5±0.5) K that does not occur for the hydrogenated derivative. The disordered CD_3 groups in the high temperature phase become ordered at low temperature, whereas all other atomic positions remain virtually unchanged. The transition is due to quantum effects arising from the increased mass of the methyl groups upon deuteration. It can be said that CD_3 rotors are "more" classical than CH_3 groups. The probability density maps in the rotational plane of the methyl groups combined with the tunnelling spectra of various partially deuterated samples shed a new light onto the quantum rotational dynamics.

Thus we demonstrate that complementary neutron diffraction and inelastic neutron scattering techniques may reveal the otherwise hidden interplay of crystal structures and quantum rotational dynamics, at levels of accuracy and physical understanding far beyond what can be obtained with the most advanced computational methods of quantum chemistry [B. Nicolaï, A. Cousson and F. Fillaux Chem. Phys. **290** (2003) 101-120].

Localisation of water molecules

Determination of the crystal structure of molecular crystals is most easily accessed via single crystal neutron diffraction. The localisation of water molecules and hence the characteristics of hydrogen bonds, respectively in $Sr[Fe(CN)_5NO].4H_2O$ and 1-hydroxy-1-phosphono-pentyl-phosphonic acid dimethylammonium salt was studied in connection with biology [Collaboration: Laboratoire de Chimie et Spectroscopie Biomoléculaire, Université Paris XIII, A. Navaza; LLB, G. Chevrier]. $Sr[Fe(CN)_5NO].4H_2O$ has also been investigated in the 77K-300K temperature range via X-ray powder diffraction (XRD), differential thermal analysis (DTA) and infrared spectroscopy (IRS). The crystal structure of 1-hydroxy-1-phosphono-pentyl-phosphonic acid dimethylammonium salt at room temperature (triclinic, space group P-1) has evidenced a hydrogen bond network formed by the dimethylammonium cation linking hydroxybisphosphonate groups in columns parallel to the [0 1 0] direction. Results have shown that acids of the hydroxybisphosphonic family can protonate volatile alkaline species like dimethylamine to get particularly stable crystals.

Radioprotective systems

As for the study of medical preparates, 2-thione and 2-cyanoiminepyrimidine compounds were synthesized for applications in the medical treatment of radiation damages on human organisms [Petersburg Nuclear Physics Institute, Moscow State University and Moscow State Academy of Fine Chemical Technology, Russia]. By combining NMR-, IR-spectroscopy, single crystal X-ray diffraction and neutron powder diffraction, more than ten (10) crystal structures were solved, in order to correlate the molecular structures of these compounds and their radioprotective properties.

PHASE TRANSITIONS: LATTICE DYNAMICS UNDER PRESSURE

The study of phonons is one of the main domains accessible to Inelastic Neutron Scattering. A common program [Collaboration: Physique des Milieux Condensés, Université P&M Curie, S. Klotz & al.] on the study of **phonon dispersion curves at very high pressures** continues to be pretty efficient and very successful. As an example, a highly anomalous pressure dependence of acoustic phonons in the chalcopyrite $AgGaSe_2$ up to 4.5 GPa across a subtle structural phase transition has been discovered (**see Highlight**). Very recently, record pressures of 20 GPa (200 kbars) have been reached using this technique in measurements of the pressure-induced mode softening in $SrTiO_3$.

The LLB is the only neutron facility in the world that is able to carry out such studies, and at the same time offers such techniques fully to the user community. Using more standard high pressure methods, soft modes have also been studied in ice Ih (normal ice) up to 0.5 GPa, which revealed for the first time the origin if its negative thermal expansion coefficient.

APERIODIC MATERIALS

An important domain of research at LLB concerns aperiodic materials both in their structural and dynamical aspects. In addition to quasi-crystals systems, aperiodicity is observed into two different classes of materials, incommensurate systems and composite systems with two chemical species or with non-stoechiometric

chemical composition. In contrast to the former case, one cannot define a mean structure in the latter case. Instead, two different sublattices coexist with incommensurate periodicities. The main question in the field concerns the nature and magnitude of interactions between the two sub-systems in order to understand the peculiar electronic or magnetic properties of these composites.

Incommensurate Composite systems

Incommensurate composites are constructed from at least two interpenetrating subsystems with different periodicities in at least one crystallographic direction. The structural properties using the superspace formalism begin now to be well understood, but the lattice dynamics via the phonon modes needs to be elucidated. Following the different coupling mechanisms (nuclear and/or electronic ones), one expects to interpret the acoustic branches and the sliding mode response, which reflects a relative displacement of the subsystems along the incommensurate direction.

The most studied incommensurate crystals are the Bi-based high-Tc superconductors $\mathbf{Bi_2Sr_2Ca_{n-1}Cu_{2n}O_{2n+4+d}}$ (n = 1, 2). In a composite description, these compounds are assumed to be formed by a rigid perovskite block ($Sr_2Ca_{n-1}Cu_{2n}O_{2n+2}$) strongly coupled to the $Bi_2O_{2+\delta}$ slabs. Recent single crystal neutron diffraction data about Bi-2212 (n = 2) have been used to obtain Fourier maps within the superspace formalism, which show discontinuous modulation functions for the oxygen atoms in the BiO layers. The competition between the couplings to the perovskite neighbouring slabs is directly related to the oxygen content δ. The low frequency dynamics (n = 1, 2), investigated by inelastic neutron scattering, has given different behaviours for the acoustic and sliding mode branches emerging from main Bragg reflections of each subsystem. Comparison with other oxide materials (spin-chain ladder systems, $Sr_{14-x}Ca_xCu_{24}O_{41+\delta}$) is made in order to progress in the understanding of the charge ordering effects in the physical properties.

[Collaboration: J. Etrillard (Université de Rennes), P. Bourges (LLB), B. Keimer (MPI, Stuttgart), J.M. Perez-Mato (Universidad del Pais Vasco, Bilbao), M. Braden (University, Köln), A. Revcolevschi (Université Paris-Sud)].

Another approach to the study of incommensurate composite systems is obtained by applying an external pressure on the crystal and measuring the strain induced on each sublattice via neutron diffraction. This was done in the **Alcane-Urea** system and the original results are described in a subsequent **Highlight** [L. Bourgeois, B. Toudic, C. Ecolivet, GPMC, Université de Rennes].

An incommensurate system, BCCD

Solids with an incommensurate structural thermal instability can exhibit complex phase sequence as a function of temperature with several intermediate commensurate phases where the structural modulation locks into different multiple periodicities of the underlying basic lattice.

Betaine Calcium Chloride Dihydrate (**BCCD**) is the most conspicuous experimental case with more than fifteen intermediate phases. Three axis elastic neutron scattering results demonstrate that the five-fold modulated phase exhibits under electric field a phase transition without change of the superlattice periodicity. The transition is caused by the flip of the average polarization of one of the interface layers. This type of polarization-flip phase transition had been detected and characterized in one-dimensional theoretical models as generalized Frenkel-Kontorova models or spins chains with elastic couplings. We have demonstrated, using a general phenomenological displacive model, the occurrence of this peculiar transition in systems like BCCD. Spin-flip phase transitions yield very peculiar phase diagrams with a checkerboard topological structure and self-similar features. In particular, they may present special critical points as so-called upsilon points. BCCD may be then the first experimental system where they could be observed.

[Collaboration: M. Quilichini (LLB), O. Hernandez (Université de Rennes), J.M. Perez-Mato (Universidad del Pais Vasco, Bilbao), G. Schaak (Würzburg University) and L. Vieira (Minho University, Braga)].

Modulated structure of photo refractive compounds

To make a smooth transition to the next paragraph dealing with ferroelectric systems used in industry, let us also mention the **highlight** on the modulated structure of $(Sr, Ba)Nb_2O_6$ from a Swiss neutron team. [PhD, D Schaniel, ETH 2003]

FERROELECTRICS MATERIALS
Giant piezo-electricity in lead-based ferroelectrics relaxors.

Correlation between device-based properties of relaxor compound and their microstructures is a problem extensively studied at LLB by the Laboratoire "Structures, Propriétés et Modélisation des Solides" of Ecole

Centrale de Paris [UMR-CNRS 8580; J.M. Kiat, C. Malibert, B. Dkhil, ECP]. In these compounds, such as $PbMg_{1/3}Nb_{2/3}O_3/PbTiO_3$ (PMN/PT), giant piezoelectric and electrostrictive properties, high dielectric permittivity etc… are evidenced in a large region of temperatures but in a narrow range of concentrations, called **morphotropic compositions**. These materials are largely used for industrial applications such as high capacity condensators, transducers and actuators, DRAM memories…. Up to now, coexistence of several ferroelectrics phases was assumed to explain the outstanding properties of these mixed compounds. Combination of neutron and X ray diffraction has allowed to evidence new monoclinic phases [PRB 65 (2001) 024104; PRB 65 (2002) 064106] which bridge the ferroelectric phases of the end members of PZN/PT, PMN/PT, PSN/PT systems, allowing a quasi-continuous rotation of the polarization between the well-known antagonist tetragonal and rhombohedral phases. The existence of these low symmetry phases allows understanding why these systems are very «soft» from the standpoint of polar properties and manifesting high technological properties.

Order and disorder in lead-free ferroelectric BST ($Sr_{1-x}Ba_xTiO_3$)

Thin films of ferroelectric materials are more and more studied for their integration in silicium-based devices. BST is of peculiar interest because it is the lead-free system with the highest performances when downsizing from bulk systems toward thin films. Studies at LLB and UMR 8580 have allowed understanding the competition between short and long-range polar orders that results in high dielectric performances. [*Thèse C. Menoret [ECP], 18 Décembre 2002, ECP*] [PRB 65 (2002) 224104].

MAGNETIC STRUCTURES IN INTERMETALLIC COMPOUNDS

Rare-earth (R) based intermetallics are generally associated to localized R^{3+} magnetism, as R belongs to the second series of the rare-earth elements. At LLB, we were more interested in Cerium and Uranium compounds where Magnetism is partly "delocalised" (see also next section).

Cerium intermetallics

A systematic study of magnetic properties was investigated in the ternary Ce-Ni-Ge system, for which more than 20 stoechiometric compounds were known to exist, in order to connect chemical composition and magnetic properties [Collaboration: ICMCB, Bordeaux; LLB / PhD, L. Durivault, November 2002, Université de Bordeaux]. Both macroscopic (magnetic susceptibility, electrical resistivity, specific heat measurements) and microscopic techniques (X-ray and neutron diffraction, XANES) were used in order to characterise the magnetic state of the systems. See the results in a subsequent **Highlight**.
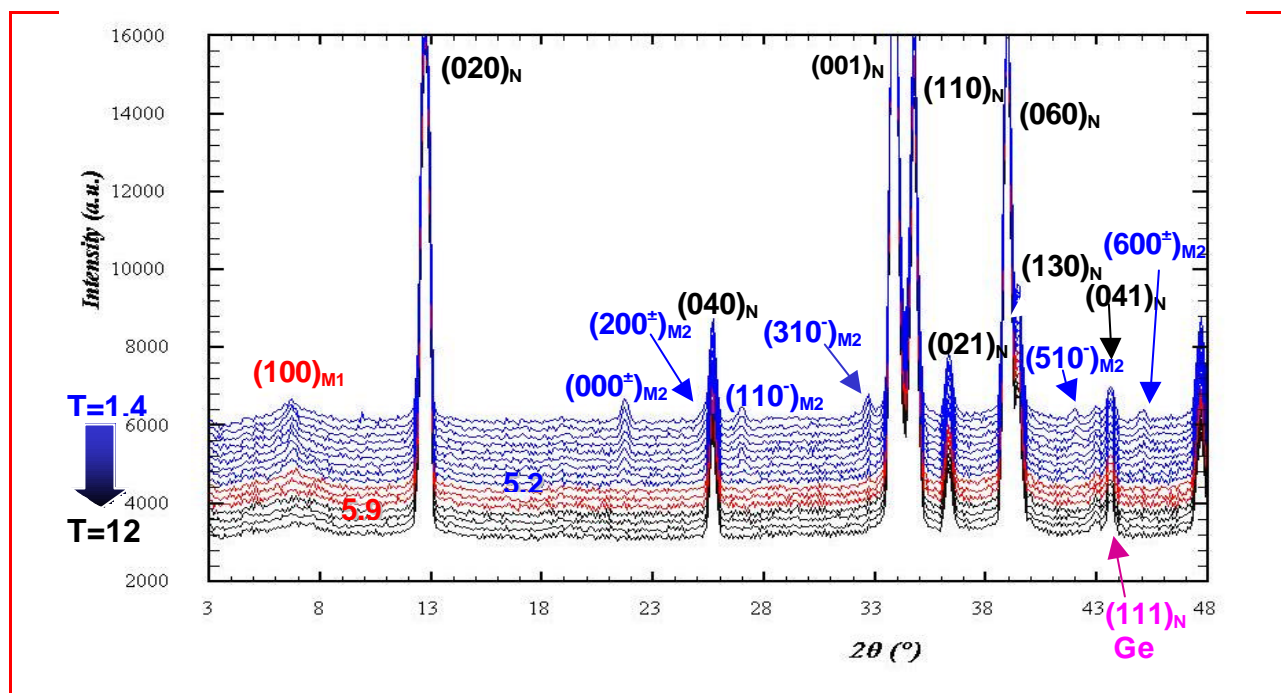
Neutron thermodiffractogram of CeNiGe$_3$ between 1.4 K and 12 K showing the **k$_1$** (100) commensurate magnetic order in red and the **k$_2$** (0 0.4 0.5) incommensurate magnetic order in blue obtained on G4.1.

Uranium intermetallics

Crystal structures in binary U-Sn intermetallic system have only been recently obtained [1995]: USn_3, U_3Sn_7, USn_2, USn and U_5Sn_4 are known to exist. Depending of the stoechiometry, different types of magnetic behaviours are observed, from ferromagnetic U_5Sn_4 and USn to antiferromagnetic USn_2 and U_3Sn_7 and non-magnetically long range ordered USn_3. In order to establish a relationship between the crystal and magnetic structures in the series, USn_2 and U_3Sn_7 have been investigated via neutron powder diffraction [Collaboration: LCSIM, Rennes; LLB]. Below T_N=75K, the USn_2 magnetic structure is associated to **k** = (0 0 ½) propagation vector (Cmmm space-group) and alternating "+-+-"ferromagnetic (0 0 1) planes with magnetic moments along **c** (T=1.4K , M=1.55μ_B). As for U_3Sn_7 magnetic structure (T_N=50K, from magnetic measurements), the main result we got from neutron powder diffraction is an upper limit for the uranium magnetic moment, namely 0.3 μ_B [JAC 329 (2001) 47-49].

MAGNETIC STRUCTURES IN IONIC COMPOUNDS

Among ionic compounds, transition metal oxides attract a lot of interest from the solid-state chemist community, due to "remarkable" properties of some of these materials, such as manganese perovskites and ferroelectrics. Magnetic properties of some of these oxides are also very interesting, showing either reduced dimensionality effects ($CuGeO_3$, Y_2BaNiO_5), or frustration (pyrochlore-type oxides with antiferromagnetic interactions…). Magnetic structure determination in insulating compounds was recently renewed by ab-initio methods able to predict the fundamental states from the super-exchange (M-O-M') and/or super-super-exchange M-O-O-M' interactions. Computing programs for analysing the topology of exchange interactions [SIMBO] and the classical magnetic energy [ENERMAG] have then been developed (see corresponding **Highlight**, in the "Modelling" section of this report). Two "real" systems are described below, which are controlled by super-exchange (M-O-M') and super-super-exchange (M-O-O-M') magnetic interactions.

Terbium ionic compounds

Fluoroterbates magnetic structures, obtained via neutron powder diffraction, are analysed (see subsequent **Highlight**) in order to correlate crystal structures and magnetic properties [Collaboration: **L**aboratoire des **M**atériaux **I**norganiques (LMI), Université Blaise Pascal, Aubière, France ; LLB ; High Magnetic Field Laboratory (HMFL), Grenoble]. Let us note that the magnetic transition temperature in all of the already studied compounds is less than 4.2K, resulting both from super-exchange (R-F⁻-R') and/or super-super-exchange R-F⁻-F⁻-R' magnetic interactions (R and R' stand for either Tb^{3+} or Tb^{4+} ions) and dipolar interactions.
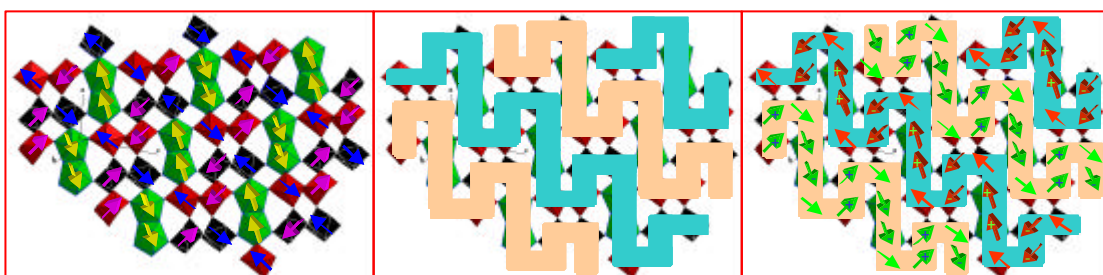
$KTbF_5$ magnetic structure (left and right parts of the figure); edge-sharing $[TbF_8]^{4-}$ polyhedral chains (middle and right parts of the figure).

Magnetic phosphates

Magnetic structures of $MFePO_5$ (with M a divalent transition element, M = Fe, Co, Ni, Cu) and $CuFe_2(P_2O_7)_2$ phosphates have been obtained and "theoretically" analysed [Collaboration: LLB ; Département de Physique, Faculté des Sciences, Rabat,Maroc; Laboratoire de Chimie du Solide Appliquée, Faculté des Sciences, Rabat, Maroc] / N. El Khayati, PhD, Décembre 2001, Université de Rabat, Maroc]. $MFePO_5$ oxyphosphates are all isomorphic, with orthorhombic Pnma space-group, M^{2+} and Fe^{3+} metallic ions being located on distinct crystallographic sites. The $M^{2+}O_6$ and $Fe^{3+}O_6$ topological arrangement leads to the existence of a complex map for super-exchange interactions (J_1, J_2, J_3 et J_4), which allowed to explain the observed antiferromagnetic structures, which are collinear, with magnetic moment along **b**-axis, except for M = Co

[European Journal of Physics B : Condensed Matter Physics 22 (2001) 429-442]. Let us note that Goodenough-Kanamori-Anderson rules give positive J_1 and J_2 exchange parameters.

The crystal structure of $CuFe_2(P_2O_7)_2$ pyrophosphate [monoclinic, $P2_1/n$ space-group] has centrosymetric Fe^{3+}-Cu^{2+}-Fe^{3+} trimers, with square-planed coordinated Cu^{2+} [CuO_4], and 6- coordinated Fe^{3+} [FeO_6 octahedra]. Within this topological arrangement, both Cu-O-Fe super-exchange (inside the same Fe^{3+}-Cu^{2+}-Fe^{3+} trimer), and Cu-O-O-Fe and Fe-O-O-Fe super-super-exchange interactions (between metallic ions in neighbouring trimers) are present. Magnetic structure below T_N=15.5K is described with a (½ 0 ½) propagation vector, the magnetic moments of the metallic ions within a trimer being parallel to each other (ferromagnetic trimer) and to **b**-axis. The observed magnetic structure was then analysed via SIMBO and ENERMAG, with seven (J_{1-7}) exchange constants [Solid State Science 4 (2002) 1273-1283].

CMR MANGANITES AND PEROVSKITES

As for manganese perovskites with Colossal MagnetoResistance (CMR) behaviour, an essential problem is the existence, or non-existence, of Mn^{3+} and Mn^{4+} charge ordering at low temperature, according to the nature of the cations and the stoechiometry of the structure. This problem has been "revisited" by a careful analysis of the crystal structure of a half-doped manganite (single crystal X-ray and neutron diffraction) [M. Daoud-Aladine, PhD, 2001, Université Paris VI; J. Rodriguez-Carvajal, LLB; in collaboration with L. Pinsard-Gaudart, A. Revcolevschi, Laboratoire de Physico-Chimie des Solides, Université Paris-Sud; M.T. Fernandez-Diaz, ILL] and new insights obtained in a polaronic approach of the Mn-Mn couplings. These results are described in one of the following **Highlights**.

Seeking for new oxides materials (cuprates, manganites…) with defined properties, either superconductive and/or magnetoresistive, is an essential task for the « New Materials » scientific team in CRISMAT, Caen. A collaboration does exist between CRISMAT and LLB, in order to get via neutron diffraction a precise description of the crystal and magnetic structures of the synthesized compounds. Half-doped manganites $Pr_{0.5}Sr_{0.5-x}Ba_xMnO_3$ have been considered and their crystal and magnetic phase diagrams carefully established as a function of temperature and $<r_A>$ and σ_A , the mean values characteristic of the cation atomic radius [C. Autret, PhD, 2002, Université de Caen].
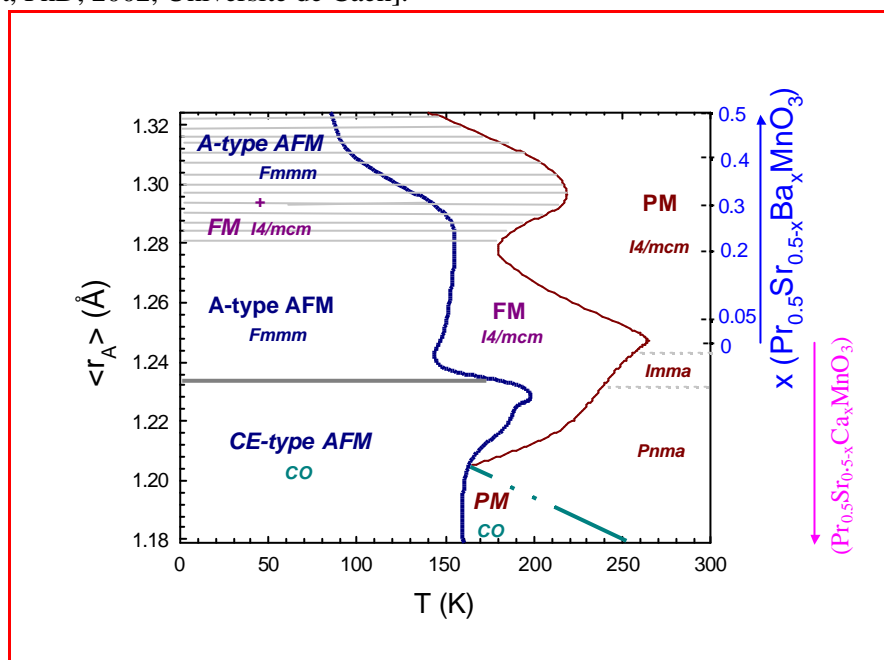
Structural and magnetic phase diagram ($<r_A>$ vs T) for half-doped manganites: $Pr_{0.5}Sr_{0.5-x}Ba_xMnO_3$ and $Pr_{0.5}Sr_{0.5-x}Ca_xMnO_3$ (from neutron powder diffraction results). AFM, FM and PM stand for AntiFerromagnetism (A-type and CE-type), Ferromagnetism and ParaMagnetism, CO for Charge Order. The crystallographic structures are described by the Fmmm, I4/mcm, Imma and Pmma space groups.

In the same work, and in order to connect crystal and magnetic properties, the n=1 Ruddlesden-Popper "bidimensional" components $Pr_{2-x}Ca_xMnO_4$ were characterized ($1.5 \leq x \leq 1.75$). Let us note that the crystal structure of these compounds (K_2NiF_4-type) is derived from the perovskite crystal structure, alternating perovskite and NaCl type-layers and that electron microscopy and neutron diffraction revealed the existence of Mn^{3+}/Mn^{4+} charge ordering (x=1.5).

Another goal of this CRISMAT team is to study the effect of substitution on the Mn site of the perovskite. In fact, an efficient way to destabilize the charge ordering is to substitute Mn with other elements, in accordance with the formula $Pr_{0.5}Ca_{0.5}Mn_{1-x}M_xO_3$ and M = Cr, Ru, Al… Depending on the x values and the substituting cations, different behaviours are observed, leading, more often, to interesting properties due to the existence of a phase-separated system at low temperature. Within this framework, two compounds were first studied by neutron diffraction: $Pr_{0.5}Ca_{0.5}Mn_{0.95}Cr_{0.05}O_3$ and $Pr_{0.5}Ca_{0.5}Mn_{0.95}Al_{0.05}O_3$ and it was thus shown that 5% Cr induces long-range ferromagnetism (FM) while 5% Al only weakens the charge ordering (CO) and the associated CE-type antiferromagnetism (AFM). Nevertheless, due to the FM-AFM competition, CMR is evidenced in both cases. For the phase separation scenario, the second type of compounds exhibits, of course, more interest. It is why the study of other Mn-site doped $Pr_{0.5}Ca_{0.5}MnO_3$ samples is always a subject of research and recently, a puzzling effect was reported in the low level substituted $Pr_{0.5}Ca_{0.5}Mn_{1-x}M_xO_3$ compounds (x < 0.10). Actually, their field dependent magnetization curves, collected at low temperature, exhibit abrupt steps, that are attributed to transformations of AFM regions into FM ones. The occurrence of steps in the magnetization is a general feature of these doped manganites, but particularly large jumps are obtained for the Ga substituted compounds, and a careful structural study is now in progress on the 3%Ga compound, by combining neutron diffraction (3T2, G41 and PAXY) and electron microscopy (CRISMAT) in connection with transport and magnetic measurements (resistivity, susceptibility, magnetization and specific heat). See also the 1c paragraph and the **highlight** manganites in the next section "Magnetism and superconductivity".

In 2001-2002, our Russian collaborators on G4.2 performed neutron diffraction experiments on "magnetoresistive" manganites. Crystal and magnetic structures of $^{154}Sm_{1-x}Sr_xMnO_3$ were obtained, also derived from resistivity, magnetic susceptibility and second harmonic magnetic measurements [Petersburg Nuclear Physics Institute, Moscow State University, Russia]. The influence of Fe doping was characterized in a second series $La_{0.7}Ca_{0.3}Mn_{1-x}Fe_xO_3$: transformation from a weakly frustrated FM (ferromagnetic) phase in the 0-0.05 x-range to a strongly frustrated, mixed FM and glassy phase in the 0.07-0.09 x-range [Petersburg Nuclear Physics Institute, Russia and Wihuri Laboratory, University of Turku, Finland]. The magnetic properties of lightly doped $Nd_{1-x}Ca_xMnO_3$ manganites, with both Nd and Mn magnetic sublattices, have also been considered [Petersburg Nuclear Physics Institute, Russia and Low Temperature Physics and Engineering Institute, Kharkov, Ukraine].

GEOMETRICALLY FRUSTRATED MAGNETIC SYSTEMS

Study of geometrical frustration and magnetic instability is a long-term activity in LLB. In geometrically frustrated systems, the lattice geometry of chemically ordered compounds does not allow all magnetic interactions to be minimised at the same time. In this respect, they differ from classical spin glasses, which combine frustration and chemical disorder. A well-known case of geometrical frustration is obtained by antiferromagnetic first neighbour interactions in a triangle. The 2D Kagomé and 3D pyrochlore lattices are other extensively studied systems. Especially when combined with magnetic instability (transition from localized to itinerant magnetism), geometrically frustration leads to numerous and spectacular effects in the field of phase transitions. Some recent results are given below**,** on

- (i) Laves phases RMn_2 and their hydrides RMn_2H_x [I. Goncharenko, I. Mirebeau, P. Cadavez-Peres, O. Makarova, F. Bourée, R. Kahn, I. Golosovsky (PNPI, Gatchina, Russia), A. Irodova (Kurchatov Institute, Moscow), A. Markosyan (Moscow University)] and
- (ii) $Tb_2Ti_2O_7$ [I. Mirebeau, I. Goncharenko, P. Cadavez-Peres, G. Dhalenne and A. Revcolevschi (Université Paris-Sud), S. Bramwell (UK), M. Gingras and J. Gardner (Canada)].

Let us mention also the neutron single crystal diffraction study of the magnetic structure of paramélaconite Cu_4O_3, a system with a spin $S = 1/2$ pyrochlore lattice [J. Rodríguez-Carvajal, A. Gukasov (LLB) — L. Pinsard-Gaudart (LPCES, Univ. Paris-Sud) — Ph. Monod (LPS, ESPCI Paris)].

Laves phases RMn₂ and their hydrides

In the RMn_2 compounds, the Mn atoms are also situated in a pyrochlore lattice, and they exhibit magnetic instability, depending on the Mn-Mn first neighbour distance. The study of $GdMn_2$ and $Ho(Mn_{0.9}Al_{0.1})_2$ under high pressure revealed several phases transitions: starting from complex short range ordered phases at ambient pressure, new ferromagnetic phases are induced under high pressure, (6-8GPa), with a stabilization of ferrimagnetic phases (either canted or collinear) at intermediate pressures. The experiment allowed separating the different contributions to the magnetic energy (from dominant AF Mn-Mn interactions at P=0,

to dominant R-R ferromagnetic interactions at high pressure). The influence of Al substitution which combines two opposite effects, a negative chemical pressure and a magnetic dilution of the frustrated Mn lattice, was also studied in a wide range of concentration in RMn_2 compounds with R=Ho, Dy, Er.

In the Laves hydrides RMn_2H_x, the H lattice strongly interacts with the frustrated Mn lattice. The cubic Laves hydrides R = Y, Gd, Tb, Dy, Ho (PhD, P. Cadavez-Peres, Décembre 2002) show number of magnetic transitions controlled by existence of R magnetism, the substitution in the Mn lattice and the chemical ordering of the H sublattice. Hydrogen disorder may induce new short range ordered magnetic phases with unusually high freezing temperatures. The magnetic structure and spin excitations in these phases have been studied by powder neutron diffraction and inelastic neutron scattering. Experiments under applied pressure helped to discover other unusual phase transitions in these compounds: chemical segregation in the hydrogen sublattice and transitions from short-range to long range ordered magnetic structures.

Oscillating chemical and magnetic order of hexagonal hydrides

Study of the hexagonal hydrides R=Er, Tm, Lu (PhD, O. Makarova, 2002) revealed a very surprising feature: an oscillating dependence between the chemical and magnetic orders. Whereas the H sublattice progressively orders with increasing H content denoted x, inducing ordered superstructures at high concentrations, the correlation length in the magnetic sublattice oscillates between long range (LRO) and short range (SRO) ordered structures: SRO for x=2→ LRO for x=3, propagation vector $\mathbf{k}$=1/2 0 0 → SRO for x=4.2 →LRO for x =4.6, $\mathbf{k}$=1/3 1/3 0. For the first time, a long-range magnetic order was induced by short-range order in the chemical lattice (transition x=4.2→x=3). This surprising effect is still unexplained.

Crystallisation of a spin liquid under pressure

$Tb_2Ti_2O_7$ is an ideal spin liquid where magnetic moments still fluctuate down to very low temperatures (10 mK), well below the Curie-Weiss temperature (-19K) which characterizes the strength of the magnetic interactions. Under high pressure (up to 8 GPa), we observed by powder neutron diffraction the onset of long-range antiferromagnetic order, coexisting with the spin liquid state below 2.1K (see the **highlight**).

New pressure experiments on oriented single crystals, with different types of pressure (hydrostatic, quasi-hydrostatic, and uniaxial) are now in process to investigate the origin of this effect, and follow it down to very low temperatures (0.1K). The future prospects concern the characterization of the new observed phases and the understanding of their stability. The pyrochlore lattice with S=1/2 is an excellent candidate to test the validity of recent theories about quantum fluctuations in these frustrated systems and their predictions: existence of a quantum spin liquid state, analogous to the Resonant Valence Bond (RVB) one, nature of the spin excitations. In rare earth pyrochlores, where the spin values are high, the mechanisms that govern the onset of magnetic phases are still rather poorly understood. High-pressure neutron diffraction (a unique feature available in LLB) is a very powerful tool to study the stability of such phases. Pressure could also induce new magnetic phase transitions like those quoted above, or the transition from metallic ferromagnet to insulating spin glass in $R_2Mo_2O_7$ pyrochlores, whose study is foreseen.

CONCLUSION

If we had to have a short summary of the above results, the first characteristics to be pointed out would be the wide diversity of the subjects needing neutron scattering, in both fundamental and applied research. Another character is the high number of collaborations existing between physicists or chemists in LLB and out LLB, either in France or Europe. As for experimental conditions, non "ambient" temperatures and samples under controlled atmospheres are easily available with neutron scattering. A "new" parameter is also more and more used in neutron experiments: "high pressure". And, in the recent years, neutron diffraction experiments under very high hydrostatic or quasi-hydrostatic pressures became available at the LLB. At the present moment, the LLB disposes of higher pressures (up to 500 kbars) than any other neutron source in the world. The development is based on a combination of high-intensity neutron diffraction and compact pressure cells with sapphire (pressures up to 100 kbars) or diamond (pressures up to 500 kbars) anvils. New high-pressure version of the G6.1 diffractometer ("MICRO"), equipped by a special focusing system, allows studying samples as small as 0.1-0.001 mm^3 in the wide range of pressures and temperatures.

1 - STRUCTURES AND PHASE TRANSITIONS

OBSERVATION OF THE DYNAMICAL STRUCTURE ARISING FROM SPATIALLY EXTENDED QUANTUM ENTANGLEMENT AND LONG-LIVED QUANTUM COHERENCE IN THE KHCO₃ CRYSTAL

François Fillaux[1], Alain Cousson[2], David Keen[3]

[1]LADIR-CNRS, UMR 7075 Université P. et M. Curie, 2 rue Henry Dunant, 94320 Thiais, France
[2]Laboratoire Léon Brillouin (CEA-CNRS), CEA-Saclay, 91191 Gif-sur-Yvette, cedex, France
[3]ISIS Facility, Rutherford Appleton Laboratory, Chilton, Didcot, OX11 0QX, UK
Physics Department, Oxford University, Clarendon Laboratory, Parks Road, Oxford OX1 3PU, UK

The nonlocal nature of quantum entanglement has remained a subject of great interest since the earliest days of quantum mechanics as it causes many of the paradoxes and lies at the heart of the profound difference between quantum mechanics and classical physics. Quantum entanglement is observed primarily for simple quantum objects (photons or/and atoms) in environments specially designed to minimize quantum decoherence and dissipation.

In the condensed matter, an initially entangled subsystem loses its ability to exhibit quantum interference by getting entangled *via* interaction with the ambient degrees of freedom. However, the exotic behavior of superconductivity and superfluidity, along with that of laser light, are manifestations of macroscopic quantum effects.
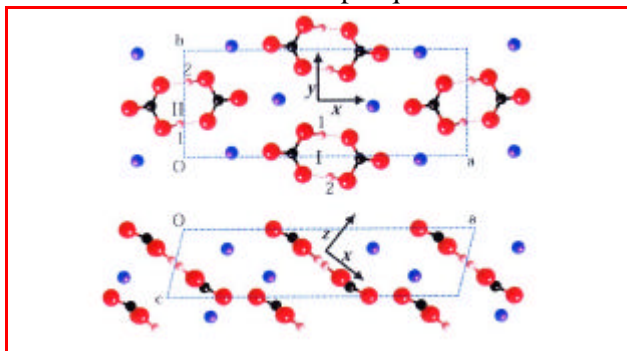
Figure 1. Schematic view of the crystalline structure of KHCO₃ at 14 K, measured on 5C2 at LLB [2]. The dotted lines represent the unit cell. The crystal is monoclinic, space group $P2_1/a$ (C_{2h}^5), with four KHCO₃ entities per unit cell. The dimers at Ci sites are parallel to planes at ≫ 42° with respect to the (a; b) planes. There is no visible proton disorder. The same conclusion applies to the deuterated derivative.

An ideal situation to observing long-lived quantum entanglement is realized for protons in the potassium hydrogen carbonate crystal (KHCO₃, Fig. 1) [1]. In this system all protons are equivalent and indistinguishable. The crystal is composed of centrosymmetric dimmers $(HCO_3^-)_2$ linked by hydrogen bonds. The local dynamics of protons is represented with symmetric pairs of coupled oscillators. In the degenerate ground state, the Pauli principle imposes antisymmetrization of the vibrational wave function with respect to permutation of the indistinguishable fermions and, consequently, strict separation of the proton dynamics from other atoms [1]. The main decoherence mechanism is forbidden and probing the long-lasting quantum coherence with neutrons gives rise to interference that resemble those commonly observed during double-slit experiments in optic (Fig. 2) [3].
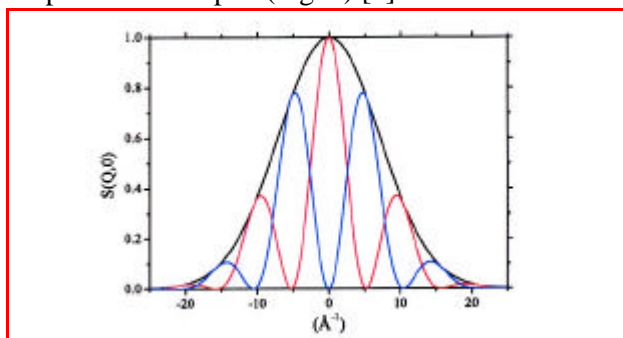
Figure 2. Calculated quantum interference observed with the neutron scattering technique for a pair of protons in KHCO₃ at 14 K [1,3]. Black: uncorrelated protons. Red: singlet state for the symmetric mode. Blue: Triplet state for the antisymmetric mode. Similar profiles were observed along the three directions labelled x, y and z in Figure 1

In order to demonstrate the macroscopic character of the quantum entanglement, we have performed neutron diffraction experiments. The diffraction pattern anticipated for the dynamical structure of the sublattice of entangled protons is quite different from the Bragg-peaks of the crystal lattice. The overall shape of the pattern depends on the dimensionality of the quantum correlation. Moreover, the pattern is not determined solely by the spatial distribution of entangled protons. It is also related to the proton dynamics and the symmetry of the phonon states imposes specific constraints to the phase of the scattered neutrons. The intensity is proportional to the total cross section for protons (¼ 80 barns).

With the SXD diffractometer (ISIS, Rutherford Appleton Laboratory, UK) we have measured a rather 2 large volume of the reciprocal space parallel to the (a¤, c¤)plane of KHCO₃ and KDCO3 at 15 K (Fig. 3 and 4, respectively) [2]. Compared to the four-circle diffractometer, the advantage of SXD is twofold. Firstly, with the time-of-flight technique, the whole accessible range of reciprocal space is measured all at once for each neutron pulse. This is convenient for seeking signals in addition to the Bragg intensities. Secondly, with the high flux of epithermal neutrons delivered by the spallation source, one can probe a much larger domain of reciprocal space than at a reactor source.
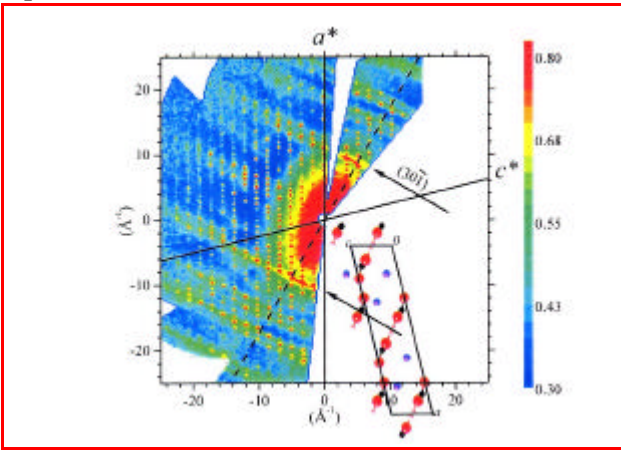
Figure 3. Diffraction pattern in the (a*; *¤) plane of KHCO₃ at 15 K [2]. The dash line and the ridges of intensity along the $(30\bar{1})$ correspond to diffraction parallel and perpendicular to the dimer planes, respectively.

On the other hand, only a limited number of detectors was available on SXD at the time of these measurements. In addition, with the time-of-flight technique the data analysis is more complex In the present work, we have gained advantage from both techniques. The structure was determined at the best accuracy with the four-circles technique and quantum interference were quickly detected in the overview of the reciprocal space obtained with the time-of-flight technique.

For KHCO₃, the ridges of intensity along the $(30\bar{1})$ direction observed at $\pm(10.25 \pm 0.25)$ Å^{-1}
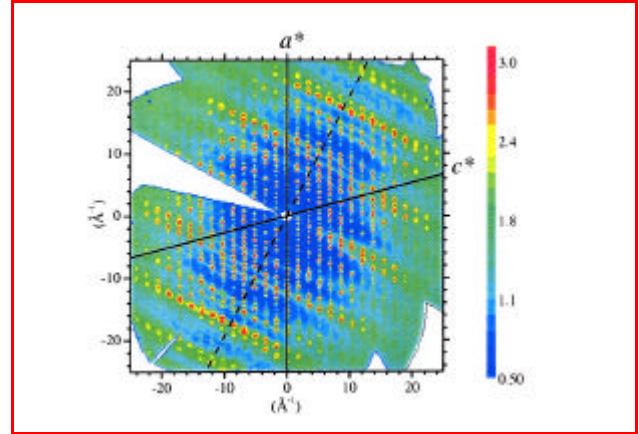
Figure 4. Diffraction pattern in the (a*; c*) plane of KDCO₃ at 15 K [2]. The dash line corresponds to diffraction parallelto the dimer planes.

from the center have all the characteristics anticipated for coherent scattering by entangled protons in planes containing the dimer entities: (i) the ridges are not due to coherent scattering by the whole lattice; (ii) they are not observed for the deuterated analogue; (iii) they have rod-like shapes; (iv) orientations and positions are in accord with the structure of the proton sublattice. Additional ripples of diffuse scattering observed at » ±17 and ±22 Å^{-1} for KHCO₃ are rather weak and broad. As they survive in the deuterated analogue they are not related to quantum statistics.

In conclusion, KHCO₃ can be termed a "quantalcrystal" (or Q'stal). The superposition of fully entangled macroscopic vibrational states with long life-time is a dramatic burst of the quantum paradoxes into the macroscopic world. Compared to superconductivity and superfluidity, the KHCO₃ Q'stal shows some remarkable similarities, such as entangled pairs of fermions and largescale long-lived quantum coherence in the ground state. Indeed, these similarities are natural consequences of the basic principles of quantum physics. At the same time, the Q'stal is quite different from other macroscopic quantum systems. The entangled pairs are not mobile, they are totally decoupled from the host lattice and the quantum coherence could survive at rather high temperature.

This new state of the matter deserves further investigations.

References

[1] F. Fillaux, Physica D **113** (1998) 172.
[2] F. Fillaux, A. Cousson, and D. Keen, Phys. Rev. B **67** (2003) 054301.
[3] S. Ikeda and F. Fillaux, Phys. Rev. B **59** (1999) 4134.

ANOMALOUS PRESSURE DEPENDENCE OF ACOUSTIC PHONONS OF AgGaSe$_2$ INVESTIGATED BY INELASTIC NEUTRON SCATTERING TO 4.3 GPa

S. Klotz[1], P. Derollez[2], R. Fouret[2], R. Debord[1], M. Braden[3], B. Hennion[4], J. Gonzalez[5]

[1]Physique des Milieux Condensés, UMR 7602, Université P&M Curie B77, 4 Place Jussieu, 75252 Paris
[2]Laboratoire de Dynamique et Structure des Matériaux Moléculaires, ESA 8024, Université de Lille I, 59655 Villeneuve d'Ascq Cedex
[3]II. Physikalisches Institut, Universität zu Köln, Zülpicher Str. 77, 50937 Köln, Germany
[4]Laboratoire Léon Brillouin (CEA-CNRS), CEA-Saclay, 91191 Gif-sur-Yvette
[5]Centro de Estudios de Semiconductores, Facultad de Ciencias, Universidad de Los Andes, Mérida 5101, Venezuela.

Silver gallium diselenide AgGaSe$_2$ belongs to the semiconductor family A^I-B^{III}-X$_2$^{VI} (where A = Cu, Ag, B = Al, Ga, In, and X = S, Se, Te) that adopts the tetragonal chalcopyrite structure. X-ray diffraction studies [1] have shown that the chalcopyrite structure undergoes a quasi second-order phase transition at ~2.6 GPa to an α-phase which is stable up to ~ 6 GPa, where a first-order transition to a orthorhombic phase occurs. The structures of the α phase is not yet clearly identified, but single crystal x-ray work [2,3] on AgGaS$_2$ indicates that the α-phase is a monoclinic distortion of the chalcopyrite structure with space group symmetry Cc, and the same appears to be the case for AgGaSe$_2$ [4]. We have investigated the frequency variations of the TA phonon and low-energy optical phonon modes across this phase transition by inelastic neutron scattering to 4.3 GPa using the Paris-Edinburgh cell, at the 1T triple-axis spectrometer of the LLB [4,5]. The results reveal an exceptionally large pressure-induced phonon softening which suggest that the structural phase transition at 2.6 GPa is an instability due to a soft acoustic phonon associated with the elastic coefficient C$_{44}$.

Figure 1 shows typical scans at constant reduced wave vectors (00ξ) with ξ=0.3 and ξ=0.7 across the TA[001] branch for different pressures: P = 0, 2.2 (in the chalcopyrite phase) and P=3.0 GPa (in the α phase). A strong shift to lower frequencies is observed for the TA frequencies in the chalcopyrite phase. Above ~ 2.6 GPa, however, the phonon frequencies show in general a normal behaviour with a positive pressure coefficient. Figure 2 shows the corresponding frequency variations. The softening is strong at the Γ-point and for small wave-vectors (ξ=0.3), with Grüneisen parameters as low as -10. The shifts are less pronounced for intermediate wave-vectors (ξ=0.4 to 0.7) and become again important at the boundary of the Brillouin zone.
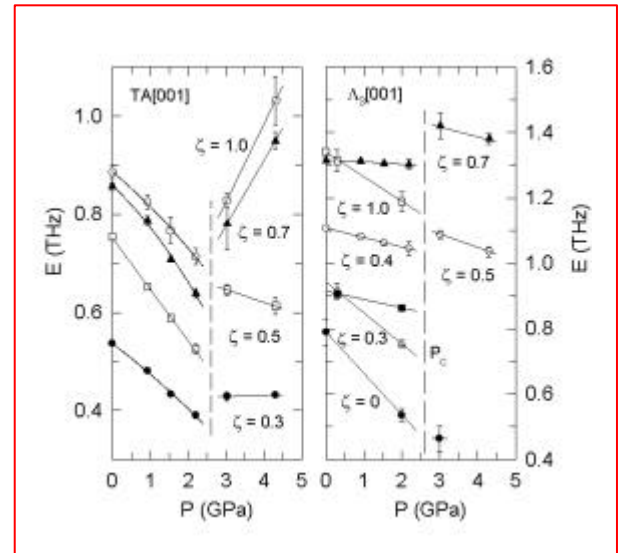
Figure 2. Frequency variations of the TA phonon (left) and the optical phonon Λ_3 (right) for different q-values along the [001] direction as a function of pressure

In Figure 3 we show the variation of the elastic coefficient C$_{44}$ which is associated to the slope of the investigated TA[001] and TA[100] branches at Γ. The value of C$_{44}$ decreases by ~ 50% from 24.6

Figure 1. Constant-Q scans of the transverse acoustic phonons along the [001] direction in AgGaSe$_2$ at different pressures.

GPa at atmospheric pressure to 12.8 GPa at 2.2 GPa. These results have been confirmed recently by ultrasonic measurements to 0.8 GPa, which are also shown in Fig. 3. Extrapolation of these data shows indeed that C_{44} attains very low values in the vicinity of 3 GPa.

The behaviour of TA phonons under pressure discovered here is exceptional in several aspects: the Grüneisen parameters are larger than in *any other* tetrahedral semiconductor investigated so far, the mode softening seems to be directly related to the symmetry of the high pressure phase, and finally, $AgGaSe_2$ is the first and only example of a semiconductor where the phonon dispersion could be studied in a high-pressure phase.
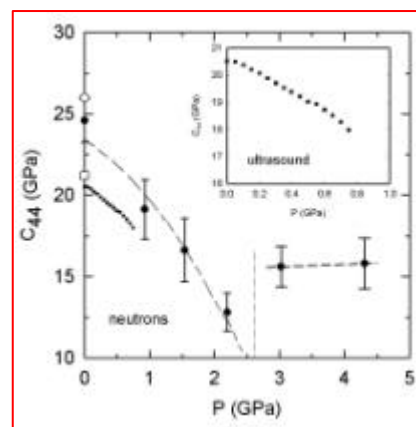
Figure 3. Pressure dependence of elastic coefficient C_{44} determined from the neutron data (large dots) and by ultrasonic measurements to 0.8 GPa. The square and the diamond correspond to ambient pressure results from measurements and ab initio calculations, respectively.

References

[1] T. Tinoco, A. Polian, J.P. Itié, E. Moya and J. González, J. Phys. Chem. Solids **56** (1995) 481.

[2] H. Kitahara, F. Marumo, Y. Noda, Phys. Rev. B **55** (1997) 2690.

[3] H. Kitahara, N. Ishizawa, F. Marumo, Y. Noda, Phys. Rev. B **61** (2000) 3310.

[4] S. Klotz, P. Derollez, R. Fouret, M. Braden, B.Hennion, Ch. Hubert, F. Meducin, J. Lazewski, J. Gonzales, phys. stat. sol. (b) **235** (2003) 331.

[5] P. Derollez, S. Klotz, J. Lazewski, M. Braden, B. Hennion, R. Fouret, and J. Gonzáles, High Pressure Research **22** (2002) 283.

ONE-DIMENSIONAL STRESS-STRAIN EXPERIMENT INSIDE AN APERIODIC INCLUSION SINGLE CRYSTAL

L. Bourgeois[1], B. Toudic[1], C. Ecolivet[1], P. Bourges[2], T. Breczewski[3]

[1] Groupe Matière Condensée et Matériaux -UMR CNRS 6626,Université de Rennes1, 35042 Rennes ,France
[2] Laboratoire Léon Brillouin (CEA-CNRS), CEA-Saclay, 91191 Gif -sur-Yvette, France
[3] Faculdad de Ciencias, Universidad del Pais Vasco, Apdo 644, Bilbao, Spain

Certain small molecules, such as urea, thiourea, perhydrotriphenylene can co-crystallise with long-chain hydrocarbon molecules to form aperiodic inclusion compounds[1]. The guest chains are confined to narrow, approximately cylindrical channels created by the host small-molecule lattice. The stoichiometry and the conformations of the chains included inside the channels are function of internal interactions such as intrachain interaction, but also of overall co-operative properties of the resulting three dimensionally ordered single crystal. The feasibility of a selective stress-strain experiment inside such a composite relies on the aperiodicity of the structure, which theoretically enables an homogeneous displacement of one sublattice with respect to the other one without any restoring force. This property results from an infinitely degenerate ground state for an infinite aperiodic structure. The stiffness of the matrix is a further necessary condition since this matrix plays the role of a compression cylinder.

This is the case with urea host molecules which are known for their ability to form, via hydrogen bonds, solid 1d channels, almost cylindrical with an available diameter of 5.5 Å, which can accommodate linear guest molecules like n-alkanes. Inside these honeycomb-like channels, these latter are confined in an ordered 1d dense packing with some 3d ordering despite some rotational and translational disorder.
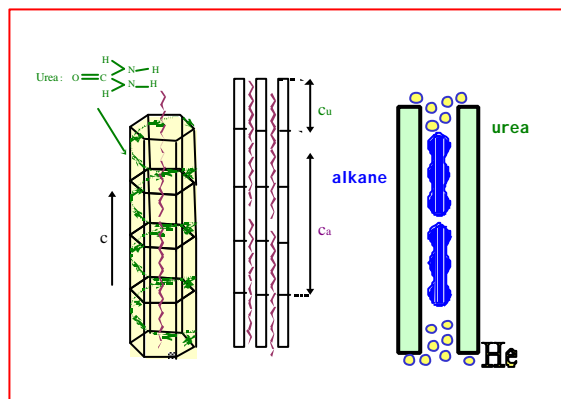
The compound we have studied is the nonadecane $(C_{19}D_{40})$ / urea $(CO(ND_2)_2)$ which is a paradigm of such intergrowth crystals. The mean high symmetry structure of the urea host subsystem is described by the hexagonal $P6_122$ space group, with cell parameters $a = b = 8.22$ Å and $c_u = 11.02$ Å at room temperature and atmospheric pressure. The a and b parameters are shared by both subsystems. The aperiodicity of the composite results from the two independent periods of the sublattices: the alkane lattice parameter (C_a=26.36 Å at 300K and 1bar) and the pitch of the urea helices constituting the host structure independently of the guest length. Their ratio is called the misfit parameter. In composites, a major consequence of aperiodicity is the existence of four kinds of Bragg reflections located at different positions in the reciprocal space. We distinguish common reflections (h k 0 0) generated by both sublattices in the commensurate plane, and along the incommensurate direction, either main sublattice reflections labeled (h k l 0) for the host and (h k 0 m) for the guest, together with pure intermodulation satellites at combinatory positions (h k l m)[2,3].

A convenient way to directly measure the lattice and sublattice strains is to apply hydrostatic pressure and to perform neutron diffraction. This experiment was performed on the triple axis spectrometer **4F1** with an incident wave vector $k_i = 1.55$ Å^{-1}. Hydrostatic pressure up to 5.3 kbars was obtained in a helium gas pressure cell at room temperature. The retained scattering plane was (**a***,**c***) with a fully deuterated single crystal.

Figure 1. schematic drawing of one of the three urea helices building a channel occupied by alkane molecules. Middle: Schematic representation of the urea and alkane periodicities. Right: principle of the "molecular press" with helium pressure gaz.
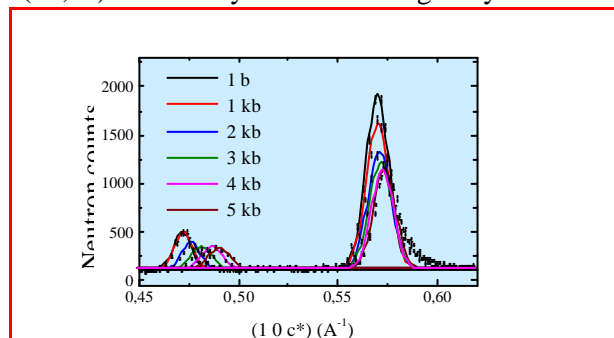
Figure 2. Evolution of two Bragg peaks related respectively to the alkane (1 0 0 2) (left) and to the urea (1 0 1 0) (right) sublattices.

The figure 2 shows the evolution versus pressure of two Bragg peaks observed on the reciprocal line (1, 0, l, m) which are (1 0 1 0) and (1 0 0 2). Obviously, these peaks, related respectively to the urea and the alkane sublattices, shift with a different pressure sensitivity.
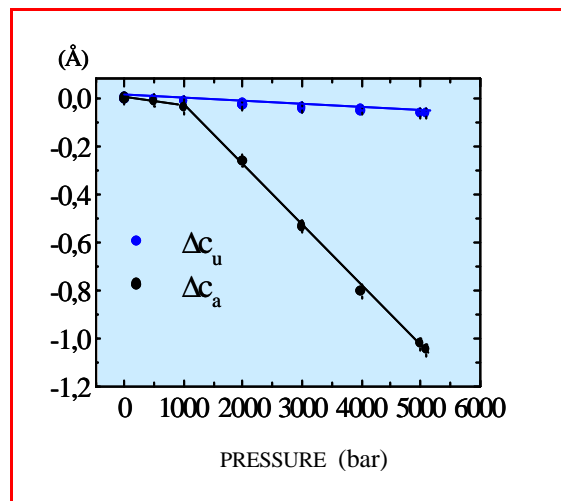
Figure 3. Evolution versus pressure of the sublattice parameter variations along the incommensurate direction c for the alkane (?) and the urea (•) one (lines are guides for the eye)

Original features appear along this incommensurate direction [4]:

- Below 1 kbar the measured strains are comparable within the experimental accuracy to the computed values of the elastic constants measured in standard conditions where the composite behaves as a regular crystal.

- Above 1 kbar, one observes different strains for the two sublattices direction, which appear as the individual responses of each sublattice. The variations observed which are an order of magnitude larger for the alkane sublattice than for the urea one are reversible and so indicate that the composite is neither destroyed nor altered under pressure. One can interpret the alkane behavior as due to the application of pressure at both ends of the urea channels by the He atoms on the alkane molecules. Then, on increasing pressure, He atoms with a Van der Waals diameter of ca 2.8 Å can play the role of a piston inside each cylinder made of urea molecules by pushing the alkanes towards the inside of the crystal.

From the lattice parameter variation shown in figure 3, it is possible to determine experimentally the elastic properties of the alkane sublattice. One can estimate the pushing force by multiplying the pressure by the free area of the hexagonal channel 19 ± 1 Å^2. A pressure of 5kbars corresponds then to a force of 95 ± 5 pN acting on the far ends of the alkane sublattice. This force is acting mainly on the inter-molecular degrees of freedom and lead to a compression end-to-end of the molecules

The slope of the alkane deformation versus pressure shows that for 5 kbars, the elongation of the alkane sublattice should be 1.3 Å. However it has to be corrected from the influence of the conformational defects of the chain ends which also alter the chain length [5]. This correction leads to an actual elastic displacement of 1.0 ± 0.1 Å. Consequently, the alkane intermolecular force constant k is found equal to 1.0 ± 0.15 N/m.

In conclusion, we have observed selective compressions in a crystal due to its aperiodic nature. This experiment shows furthermore that the relative motion of a sub lattices are pinned at low pressures and that a depinning occurs under the effect of pressure like CDW under the effect of an electric field above some threshold. The knowledge of the inter alkane force constant will help the definition of better experimental conditions for the sliding mode observation in this family of aperiodic organic composite.

References

[1] M. D. Hollingsworth and K. D. M.Harris, in *Comprehensive Supramolecular Chemistry* Pergamon Press **6** (1996) 177.

[2] R. Lefort, J. Etrillard, B. Toudic, F. Guillaume, T. Breczewski and P. Bourges, *Phys. Rev. Lett.* **77** (1996) 4027.

[3] T. Weber, H. Boysen, M. Honal, F. Frey, R.B. Neder, *Zeit. Für Kristallog.* **211** (1996) 238.

[4] Lydie Bourgeois, Claude Ecolivet, Bertrand Toudic, Philippe Bourges, Tomasz Breczewski, *Phys. Rev. Lett.* **91**, (2003) 025504

[5] L. Bourgeois, PhD thesis Rennes (2002)

NEUTRON DIFFRACTION EXPERIMENTS
ON THE MODULATED STRUCTURE OF $Sr_xBa_{1-x}Nb_2O_6$

D. Schaniel [1,2], A. Cousson [3], J. Schefer [1], T. Woike [2] and M. Imlau [4]

[1] Laboratory for Neutron Scattering, ETHZ & PSI, CH-5232 Villigen PSI
[2] Institut für Mineralogie und Geochemie, Universität zu Köln, DE-50674 Köln, Germany
[3] Laboratoire Léon Brillouin (CEA-CNRS), CEA-Saclay, F-91191-Gif-sur-Yvette, France
[4] Fachbereich Physik, Universität Osnabrück, DE-49069 Osnabrück, Germany

$Sr_xBa_{1-x}Nb_2O_6$ (0.25<x<0.75) is a very attractive material for technological applications and basic research because of its high electro-optic, piezoelectric and pyroelectric coefficients and its favorable photorefractive properties, for example holographic data storage (Fig. 1).
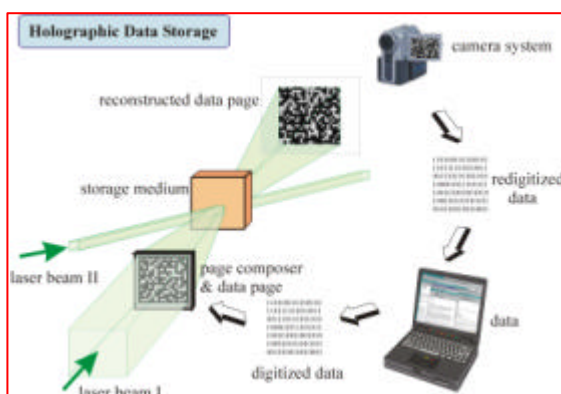
Figure 1. Schematic layout for holographic data storage. The holograms are written from different direction into the crystal, therefore taking advantage of 3-dimenstional data storage

It belongs to the class of oxygen octahedral ferroelectrics possessing tetragonal potassium tungsten bronze structure [1]. The average structure of congruently melting $Sr_{0.61}Ba_{0.39}Nb_2O_6$, space group P4bm, has been determined by X-ray diffraction [2], showing that the structure is a three-dimensional network of NbO_6 octahedra linked by their corners forming alternating five- and four-membered rings (see Fig. 2). The five Sr/Ba atoms are statistically distributed over 6 possible lattice places.

Two full data sets on a poled (300V/mm) single crystal of $Sr_{0.61}Ba_{0.39}Nb_2O_6$ (size: a=b=4mm, c=5mm) were measured on the two four-circle diffractometers TriCS at the Swiss Neutron Spallation Source SINQ at PSI, Villigen/Switzerland and 5C2 at the Laboratoire Léon Brillouin (LLB) in Saclay/France. We were interested in the origin of the modulated structure, especially if it is due to occupational or distortional

modulation, and if this modulation is harmonic or not (appearance of higher order satellites).
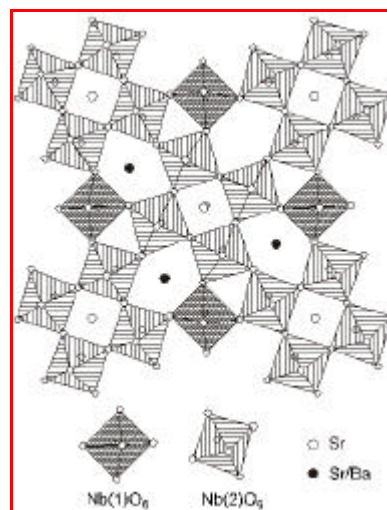
Figure 2. Average structure of $Sr_{0.61}Ba_{0.39}Nb_2O_6$, projected onto the ab-plane.

Modulated crystal structures are characterized by appearance of reflections at non-Bragg positions. The positions of these reflections in reciprocal space can be described using

$$\mathbf{Q}(h,k,l,m_i) = h\mathbf{b}_1 + k\mathbf{b}_2 + l\mathbf{b}_3 + \sum_{i=1}^{n} m_i\mathbf{Q}_i$$

where

$$\mathbf{Q}_i = Q_{i,a}\mathbf{b}_1 + Q_{i,b}\mathbf{b}_2 + Q_{i,c}\mathbf{b}_3$$

are called modulation vectors. The modulation is called commensurate if all $Q_{i,j}$ (j=a,b,c) are rational and incommensurate if at least one of the $Q_{i,j}$ is irrational. Reflections with $m_i=0$ are called main reflections (Bragg positions), whereas diffraction spots with $m_i \neq 0$ are called satellites (non-Bragg positions). The Fourier transform of the main reflections is the average structure in real space. Taking into account the satellite reflections, the Fourier transform yields a structure in real space, which does not exhibit translation symmetry anymore. To overcome this problem de Wolff and Janner [3] developed the so-called superspace

approach. Thereby the reciprocal lattice is embedded in a higher dimensional space R_{d+n} (d= dimension of average structure, n=number of modulation vectors). The measured reflections are considered as the projection of this higher dimensional lattice onto R_d. The Fourier transform of this projection is a section of a higher dimensional structure, which possesses again the full translational symmetry in real space.

The measurements were performed at room temperature well below the ferroelectric phase transition at 80º Celsius. The refinement was carried out with the program JANA2000 [4]. The average structure determined from the main reflections is shown in Fig. 2 and is in agreement with previous X-ray measurements [2].

From the positions of the satellites the modulation vectors $Q_{1,2}$=(0.3075,±0.3075,0.5) found in X-ray experiments [5] could be verified. For the refinement of the modulated structure two modulation vectors $Q_{1,2}$=(0.3075,±0.3075,0) in 5-dimensional superspace (space group X4bm with centering vectors (0,0,0,0,0) and (0,0,0.5,0.5,0.5))

were used. The third component of the modulation vectors was taken into account by doubling the cell along the c-axis (a=12.52 Å, c=7.87 Å). Because two modulation vectors are present, the modulation of position, occupation and temperature factors are described with two harmonic waves. The refinement of the positional parameters of the oxygen atoms resulted in a stronger modulation of O(4) than found with X-rays (Fig.3). The two oxygen atoms O(4) and O(5) show the largest modulation amplitude of all the atoms in this compound. The O(4,5) atoms are modulated mainly in the tetragonal plane while the O(1,2,3) atoms exhibit a strong modulation along z. This is due to the fact that O(4) and O(5) are lying in the same plane as the Sr and Ba atoms. They are therefore most affected by the statistical distribution of these atoms. The O(1,2,3)-atoms react on the deformation of the octahedra produced by the O(4,5) atoms and this results in a modulation along the z-direction [6]. Since the Nb atoms are positionally modulated only weakly, the whole modulation can be seen as a rotational modulation of almost rigid NbO_6 octahedra [7,8].
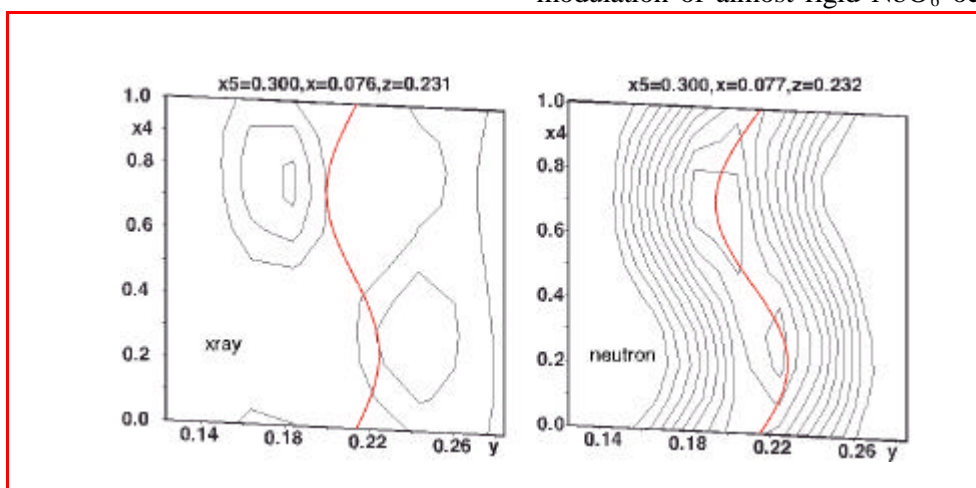
Figure 3. Modulation of O(4) obtained by X-rays (left) [5] and after refining the positional parameters of O(4) using the neutron data (right). Axes are given in fractional coordinates. x4=$(r+n)Q_1$, x5=$(r+n)Q_2$.

As we did not see higher order satellites, even in the Saclay measurement, we cannot refine any anharmonic distortions. Such a specialized refinement needs to be fixed not only quantitatively on the intensity of first order satellites, but also qualitatively on the appearance of second order reflections in order to allow such an advanced interpretation.

References
[1] P.B. Jamieson *et al*., J. Chem. Phys. **48** (1968) 5048.
[2] T.S. Chernaya *et al*., Cryst. Reports **42** (1997) 375.
[3] P.M. De Wolff, Acta Cryst A30, 399 (1974)
[4] V. Petricek and M. Dusek, The crystallographic computing system JANA2000, Institute of Physics, Praha.
[5] Th. Woike *et al*., Acta Cryst. **B59** (2003) 28.
[6] D. Schaniel *et al*., Appl. Phys. A, **A74** (2002) s963-s965
[7] D. Schaniel *et al*., prepared for publication.
[8] D. Schaniel, Ph.D. thesis, ETH Zurich (No. 14902, 2002)
   http://datastorage.web.psi.ch/pdf/dissertation-ethz-14902.pdf

RELATIONSHIP BETWEEN CHEMICAL COMPOSITION AND MAGNETIC ORDER IN THE Ce-Ni-Ge SYSTEM

L. Durivault[1,2], F. Bourée[2], B. Chevalier[1], G. André[2] and J. Etourneau[1]

[1]Institut de Chimie de la Matière Condensée de Bordeaux (ICMCB), CNRS [UPR 9048], Université Bordeaux I, Avenue du Docteur A. Schweitzer, 33608 Pessac Cedex, France.
[2]Laboratoire Léon Brillouin, (CEA-CNRS), CEA-Saclay, 91191 Gif-sur-Yvette, France.

Unusual properties are often observed at low temperatures for intermetallic Ce compounds, leading to Kondo systems, either magnetic or not, Intermediate Valence and/or Heavy Fermion properties… These ground state properties are governed by the J_{cf} interaction between spins of localized 4f(Ce) electrons and conduction electrons, via a competition between Kondo and RKKY (Ruderman-Kittel-Kasuya-Yosida) interactions, resulting either in the quenching of the 4f (Ce) ion magnetic moment (Kondo interaction) or in the occurrence of long-range magnetic order for 4f (Ce) ion magnetic moments (RKKY interaction). A systematic study of magnetic properties was then investigated in the ternary Ce-Ni-Ge system, for which more than 20 stoechiometric compounds were known to exist, in order to connect chemical composition and magnetic properties. Both macroscopic (magnetic susceptibility, electrical resistivity, specific heat measurements) and microscopic techniques (X-ray and neutron diffraction, XANES) were used in order to characterise the magnetic state of the systems.

Structural similarities can be found in the series. A set of such similarities is illustrated in Figure 1 for Ce_2NiGe_6, $CeNiGe_3$, $CeNiGe_2$ and $Ce_3Ni_2Ge_7$ compounds: the orthorhombic crystal structures of $CeNiGe_3$ and $Ce_3Ni_2Ge_7$ for instance have identical stackings of a $[Ce_4Ge_4]$ antiprism, a $[Ce_6]$ trigonal prism and another $[Ce_4Ge_4]$ antiprism, along the longest crystallographic axis. These sequences are separated either by a $[Ge_8]$ cube in $CeNiGe_3$ or by a $[Ge_{12}]$ cubooctahedron in $Ce_3Ni_2Ge_7$. Going from $CeNiGe_3$ to $Ce_3Ni_2Ge_7$ is then due to the insertion into the $[Ge_8]$ cube of the $CeNiGe_3$ crystal structure of an atomic plane, containing Ce and Ge atoms. Let us notice then that if only one crystallographic site is available for Ce in $CeNiGe_3$, two are now available in $Ce_3Ni_2Ge_7$, adding a "new" Ce position (hereafter referred as Ce1) within the $[Ge_{12}]$ cubooctahedron to the Ce "initial" position (Ce2), common to $[Ce_6]$ and $[Ce_4Ge_4]$ polyhedra,
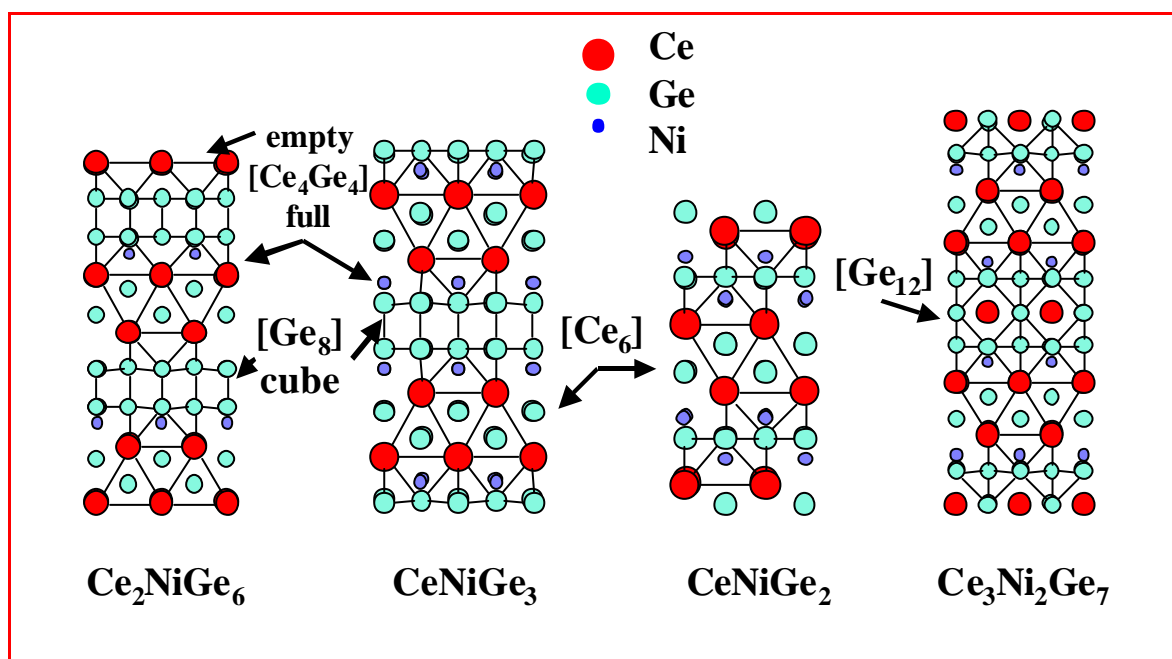
Figure 1. Crystal structures of Ce_2NiGe_6, $CeNiGe_3$, $CeNiGe_2$ and $Ce_3Ni_2Ge_7$. The elementary polyhedra are shown: $[Ce_4Ge_4]$ antiprisms, $[Ce_6]$ trigonal prisms, $[Ge_8]$ cubes and $[Ge_{12}]$ cubooctahedrons.

From magnetic measurements we know that the Ce-Ni-Ge ternary germanides, with more 50 Ge-atomic %, are antiferromagnetic, with Néel temperatures T_N decreasing with Ge-content: Ce_2NiGe_6 (T_N=10.4(2) K), $Ce_3Ni_2Ge_7$ (T_N=7.2(2) K), $CeNiGe_3$ (T_N=5.5(2) K), $Ce_2Ni_3Ge_5$ (T_N=4.8(2) K or 5.1(2) K) and $CeNiGe_2$ (T_N=3.9 K). In this composition range however, Ce_2NiGe_3 exhibits spin glass properties, in connection with its hexagonal crystal structure (AlB_2-type), clearly different from the above described crystal structures.

All the corresponding magnetic structures have been obtained via neutron powder diffraction.

Ce_2NiGe_6, $Ce_3Ni_2Ge_7$ and $Ce_2Ni_3Ge_5$ show collinear antiferromagnetic structures, while $CeNiGe_3$ possesses more complex magnetic properties, with both commensurate and incommensurate magnetic structures coexisting at 1.4 K. The commensurate magnetic structure of $CeNiGe_3$ must be compared to that of $Ce_3Ni_2Ge_7$ (Fig. 2). In the latter compound, the Ce1 atoms do not carry any ordered magnetic moment. As a consequence, these two magnetic structures are identical and can be described by antiferromagnetic stacking of ferromagnetic layers of trigonal $[Ce_6]$ prisms [2].
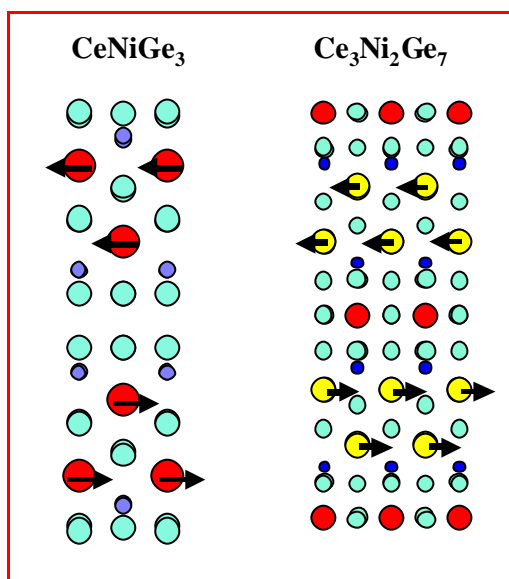
Figure 2. Commensurate $Ce_3Ni_2Ge_7$ and $CeNiGe_3$ magnetic structures.

As the Néel temperatures T_N are decreasing with Ge-content, so the value of the Ce-magnetic moments at 1.4K, with M_{Ce} = 1.98(7)μ_B in $Ce_3Ni_2Ge_7$, M_{Ce} = 0.8(2) μ_B in $CeNiGe_3$ and M_{Ce} = 0.4(1)μ_B in $Ce_2Ni_3Ge_5$. This decrease of Ce-magnetic moment reflects the increasing
strength of Kondo interaction, when going from $Ce_3Ni_2Ge_7$ to $Ce_2Ni_3Ge_5$, a result confirmed by specific heat measurements on $Ce_2Ni_3Ge_5$ showing that the Kondo temperature T_K for this stoechiometry is of the same order of magnitude as k_BT_N.

On the contrary, the Ni-rich compounds ($\geq$ 50 Ni-at. %) don't show any long range magnetic order. $CeNi_{4.25}Ge_{0.75}$ is an intermediate valence compound. $CeNi_9Ge_4$ shows heavy fermion properties with γ=1.2 J/mol^{-1}K^{-2}.

The Ce-Ni-Ge germanides at the borderline between the two families, which have been described above, namely $CeNi_2Ge_2$, $Ce_3Ni_4Ge_4$ and $CeNiGe$, show an intermediate valence behaviour, which is more and more pronounced as we follow the sequence $CeNi_2Ge_2 \rightarrow Ce_3Ni_4Ge_4 \rightarrow CeNiGe$ [2].

The magnetic properties of intermetallic Ce-Ni-Ge compounds have then been investigated, in connection with the stoechiometry and the crystalline geometrical environment of Ce ions. The above work is associated to Laurence Durivault's PhD, defended at Bordeaux University, on November 2002, 4th.

References
[1] L. Durivault et al., J. Phys.: Condens. Matter, 15 (2003) 77-90.
[2] L. Durivault et al., Acta Physica Polonica B, 34 (2003) 1393-1397.

FLUOROTERBATES: CRYSTAL STRUCTURES AND MAGNETIC PROPERTIES

M. Josse[1], M El-Ghozzi[1], D. Avignant[1], F. Bourée[2], G. André [2], M. Guillot[3]

[1]Laboratoire des Matériaux Inorganiques (UMR-6002 CNRS), Université Blaise Pascal, 63177 Aubière, France.
[2]Laboratoire Léon Brillouin (CEA-CNRS), CEA-Saclay, 91191 Gif-sur-Yvette, France.
[3]High magnetic Field Laboratory, MPI/CNRS, BP 166, 38042 Grenoble, Cedex 9, France.

One of the topics under present investigation in LMI [Laboratoire des Matériaux Inorganiques], in collaboration with LLB and HMFL [High Magnetic Field Laboratory] deals with existing relationships between crystal structures and magnetic properties in fluoroterbates. This topic with an essentially basic character has been initiated to understand the singular behaviour of the Li_2TbF_6 representative of the Li_2MF_6 series (M. Guillot et al., J.S.S.C. 97, 2 (1992) 400) and instigated a growing interest both due to the originality and the diversity of the encountered structural types. Our approach consists in comparing the crystal chemistry of the Tb^{4+} ion with that of Zr^{4+} and U^{4+} ions, the ionic radii of which lie on each side of the Tb^{4+} ionic radius value for a given coordination number.

The singular crystal chemical behavior of the Tb^{4+} appears thus much more related to its half-filled $4f^7$ electronic configuration than to its ionic radius despite the ionic character of the fluorides. One of the most significant advance in the comprehensive crystal chemistry of the Tb^{4+} ion comes from its fitness for the 8-coordination as evidenced by numerous crystal structures determination. Indeed, with a set-back bearing over some thirty fluorides, the structures of which have been determined accurately from single-crystal X-ray diffraction and/or neutron powder diffraction, we may ascertain that the Tb^{4+} ions were always found in a F^- ions-8-fold surrounding, with either square antiprisms, dodecahedra or bicapped trigonal prisms as coordination polyhedra. The only exception to these observations comes out from M_3TbF_7 fluorides (M = K, Rb, Cs) where a $[TbF_7]^{3-}$ complex ion with a pentagonal bipyramid-like configuration and a dynamical fluorine disorder is expected by analogy with the isotypic $[ZrF_7]^{3-}$ ion.

The present knowledge about the crystal chemistry of the Tb^{4+} ion in fluorides leads us to lay down the following empirical rule, except for M_3TbF_7 (M=K, Rb, Cs) compounds: Fluoroterbates are isotypic to fluorozirconates with the same stoichiometry only if the Zr^{4+} ions are in 8-fold coordination exclusively. That is, if for a given stoichiometry the Zr^{4+} ions exhibit different coordination numbers (in the 6-8 range), then the homologous tetravalent terbium fluoride does not exist; or, if it does, it crystallises in another crystal structure, being then built from 8-coordination polyhedra exclusively". This empirical rule does not apply to oxides despite the similar sizes of O^{2-} and F^-, thus strengthening the idea that the 4f orbitals play a determinant role in the crystal chemistry of the Tb^{4+} ion in fluorides.

Let us note that this part of our crystal structure investigations could not have been successfully carried out without using neutron diffraction, as small distortions of the anionic sublattice F (F is a "light" element, as compared to Tb) occurring either at room or low temperature have only been "seen" via neutron diffraction, in particular via High Resolution Powder patterns recorded on the 3T2 instrument.

To go further in the comprehensive role played by the 4f orbitals a study of the magnetic properties of the evidenced tetravalent terbium combinations was undertaken. Through the large panel of available compounds some general outstanding features relative to the magnetic behaviour of the Tb^{4+} ($4f^7$ electronic configuration and $^8S_{7/2}$ ground term) have been evidenced. Figure 1 gives a summary of the preliminary results obtained by neutron diffraction (on G4.1 instrument). In particular long range magnetic orderings have been observed in fluorides with edge-sharing $(TbF_8)^{4-}$ polyhedra. For instance, in both β-$BaTbF_6$ and KTb_3F_{12} compounds, which are characterized by infinite $[TbF_6]^{2-}$ chains of edge-sharing $[TbF_8]^{4-}$ dodecahedra, ferromagnetic couplings are observed within the chains and the antiferromagnetic structures result from antiferromagnetic couplings between the nearest chains. In the case of β-$BaTbF_6$, let us mention that an applied magnetic field of a few hundred of oersteds (~ 200 oersteds) is sufficient to induce a ferromagnetic state. This emphasizes the weakness of the inter-chain couplings.

For some representatives of the M_2TbF_6 series (M=Li, K, Rb), incommensurate magnetic structures have been observed; for instance a square modulated magnetic structure with $\mathbf{k}$=(0 0.0162(1) 0) propagation vector is obtained

for Li_2TbF_6 from the position and intensity analysis of first, third and fifth order magnetic Bragg peaks down to 1.4K.

For compounds with a crystal structure built from edge- and corner-sharing coordination polyhedra ($KTbF_5$, $RbTbF_5$, $K_2Tb_4F_{17}$), the magnetic transition temperature is a function of the PCM (Polyhedra Connection Mode), the higher is the % of corner- sharing, the lower is the magnetic transition temperature temperature (Figure 1).

In the near future this research will be developed

and extended to statistically disordered mixed-valence compounds obtained by taking advantage of the partial thermal decomposition of the tetravalent terbium tetrafluoride in terbium trifluoride and elemental fluorine which occurs in compositions rich in terbium tetrafluoride.

This work is associated to M. Josse PhD [2003]. And has already given rise to Communications either in National [1] and International [2] Conferences and to Publications in specialized reviews [3,4].

Compound	Structural characteristics		Long range magnetic order
	Polyhedral linking (CN* [8] for Tb^{4+})	PCM*	
Li_2TbF_6 (K_2TbF_6) (Rb_2TbF_6)		100% edges	$T_N = 2.00$ K $T_N = 1.60$ K (K) $T_N = 2.10$ K (Rb)
β-$BaTbF_6$ ($CaTbF_6$) ($SrTbF_6$) ($CdTbF_6$)		100% edges	$T_N = 2.10$ K ($T_N \cong 2.15$ K) ($T_N = 2.65$ K) ($T_N \cong 2.75$ K)
α-$BaTbF_6$		66.6% corners and 33.3% edges	None down to 1.4K
$KTbF_5$ ($RbTbF_5$)		50% edges and 50% corners	$T_N = 1.60$ K ($T_N \cong 1.4$ K)
$CsTbF_5$		80% corners and 20% edges	None down to 1.4K
$Na_7Tb_6F_{31}$		80% corners 20% edges	None down to 1.4K
$Tb^{III}Tb^{IV}_3F_{15}$		100% corners	None down to 1.4K
$K_2Tb^{III}Tb^{IV}_3F_{17}$		edges Corner	$T_N = 1.65$K
$KTb^{III}Tb^{IV}_2F_{12}$		100% edges (Tb^{4+}-Tb^{4+}) 100% corners (Tb^{3+}-Tb^{4+})	$T_N = 3.65$K

References

[1] M. Josse, M. Dubois, M. El-Ghozzi, D. Avignant, G. André, F. Bourée, M. Guillot
    JDN10, Trégastel, Côtes d'Armor, Mai 2001; JDN11, Presqu'île de Giens, Var, Mai 2002;
    MATÉRIAUX 2002, Tours, Octobre 2002.
[2] M. Guillot, M. El-Ghozzi, D. Avignant, G. André, F. Bourée, A Cousson
    46th Annual Conference on Magnetism and Magnetic Materials, Seattle, U.S.A., November 2001.
[3] M. Guillot, M. El-Ghozzi, D. Avignant, G. André, F. Bourée, A Cousson
    J. Applied Physics, 91, 10 (2002) 8519
[4] E. Largeau, M. El-Ghozzi, D. Avignant, M. Guillot, F. Bourée, G. André, A Cousson,
    J. Magn. Magn. Mater., 261 (2003) 93.

A NEW INTERPRETATION OF THE CO STATE IN HALF-DOPED MANGANITES: THE ORDERING OF ZENER POLARONS.

A. Daoud-Aladine [1], J. Rodríguez-Carvajal[1], L. Pinsard-Gaudart[1,2], M.T. Fernández-Díaz[3], A. Revcolevschi[2].

[1]Laboratoire Léon Brillouin (CEA-CNRS), CEA-Saclay, 91191 Gif sur Yvette, France.
[2]Laboratoire de Physico-Chimie des Solides, 91405 Orsay, France
[3]Institute Laue-Langevin, 38042 Grenoble, France

The calcium-doped manganites $R_{1-x}Ca_xMnO_3$ (x~0.5) (R: rare-earth) are known to display a structural phase transition at T_{CO}. This transition is usually attributed to charge and orbital ordering (CO/OO) because it is associated with a jump of the resistivity and to the onset of superstructure reflections in the low temperature (LT) phase. Moreover their complex spin ordering, at a temperature $T_N < T_{CO}$, has been traditionally interpreted by using the semi-empirical Goodenough-Kanamori-Anderson rules for the superexchange interactions. These rules have been applied to a model of Mn^{3+} d_{z^2} orbital ordering in the (**a**, **b**) plane, proposed in the late fifties by Goodenough [1]. The fact that this model suggests

a charge ordered pattern of Mn^{3+} and Mn^{4+} ions, has promoted the idea that the magneto-transport properties of these compounds are strongly influenced by dynamic CO/OO driven by the combined effect of Coulomb repulsion and Jahn-Teller distortion around the Mn^{3+} sites. It is expected that CO will result in the setting up of MnO_6 octahedra of different average Mn-O distances ($\langle d_{Mn-O} \rangle$). The experimental determination of these displacements has been attempted on $La_{1/2}Ca_{1/2}MnO_3$ by neutron and synchrotron powder diffraction [2] making use of *a priori* constraints, and symmetry, according to the pattern shown in Figure 1(left).
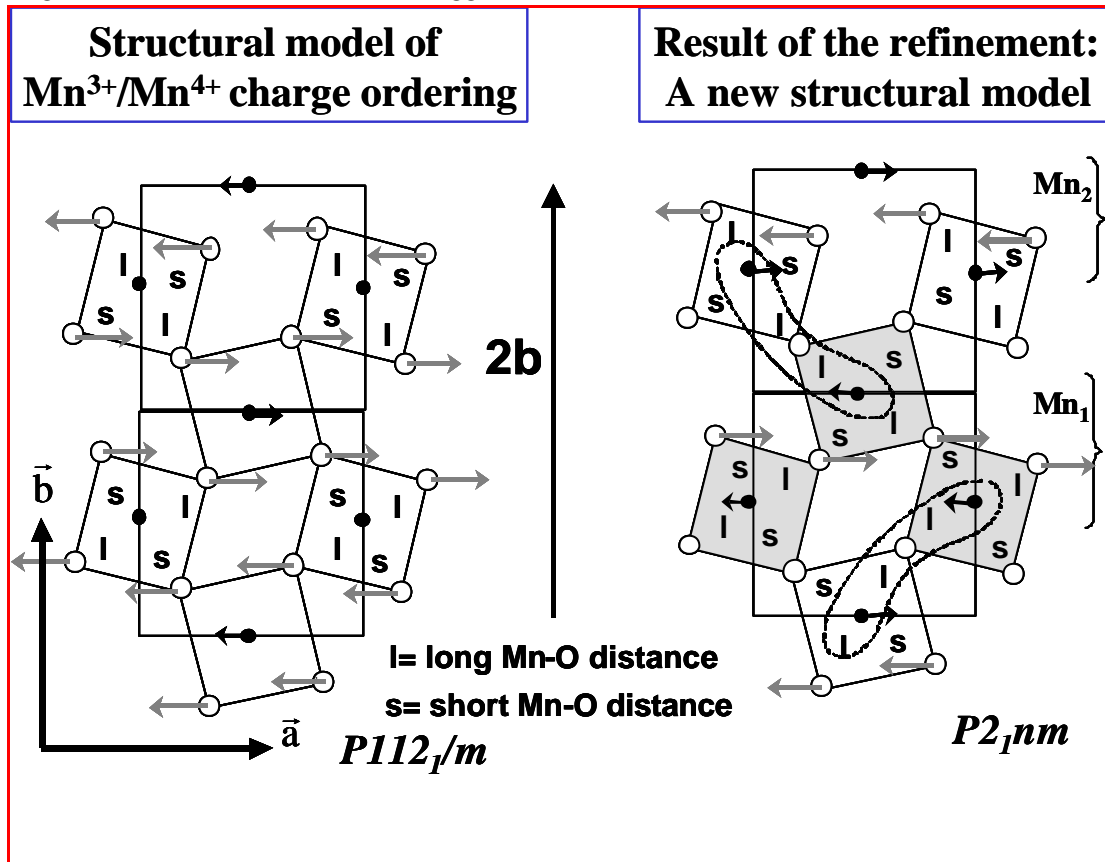
Figure 1. (left) Schematic atomic displacements of the conventional Mn^{3+}/Mn^{4+} model for the CO in half doped manganites with respect to the high temperature phase, (right) experimentally determined pattern of atomic displacement. The amplitude of displacements, represented by arrows, is exaggerated for clarity.

We have performed a neutron diffraction experiment on a single crystal of $Pr_{0.6}Ca_{0.4}MnO_3$ [3] that has provided a quite different picture of the displacement pattern (see Figure 1(right)). Instead of the distortion pattern expected for the CO/OO picture the two non-equivalent MnO_6 octahedra have similar $\langle d_{Mn-O} \rangle$. There is also an off centering of the Mn ions resulting from the loss of the inversion center at the Mn sites. These structural details are inconsistent with the picture of Mn^{3+}/Mn^{4+} charge ordering. The persistence of mixed valence state of Mn atoms in the LT phase is confirmed by the nearly equal $\langle d_{Mn-O} \rangle$ on the two sites. This result is totally in agreement with previous XANES studies that have already mentioned a unique intermediate valence state displayed by half-doped manganites across the CO/OO transition.

The analysis of the atom displacements indicates that the Mn_1-O_3-Mn_2 angle is the most opened angle in the LT structure. The elongation of the octahedra further suggests that one electron is shared by the $Mn_1(e_g)$-$O_3(2p)$-$Mn_2(e_g)$ units, keeping the intermediate valence of both Mn atoms. This is consistent with Mn_1-Mn_2 pairs coupled via a local double exchange (DE) process mediated by the O_3 oxygen, corresponding to the image of a Zener polaron. The electronic localization below T_{CO}, in these compounds, can be then explained by a partial localization of the electrons beyond the atomic limit. This interpretation of the structural distortions suggests the appearance, below T_{CO}, of ordered Mn_1-O_3-

Mn_2 molecular objects (Zener polarons) with ferromagnetically coupled Mn moments (see Fig. 2). This hypothesis gives also a clue to interpret the anomaly in the magnetic susceptibility observed at the, supposedly purely structural, transition for compounds that remain in a paramagnetic state below T_{CO} [3]. The formation of Zener polarons leads to new elemental paramagnetic units with a higher effective moment. The extension of this image to other compounds of the manganites family is being investigated. In particular the CO in $La_{1/3}Ca_{2/3}MnO_3$ may be interpreted in terms of Zener polarons involving three Mn atoms.
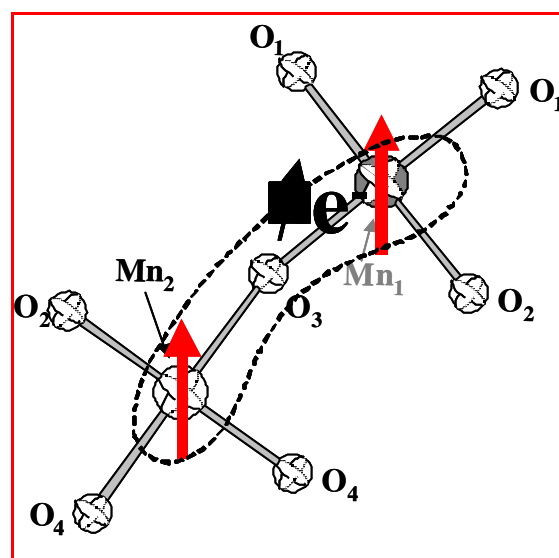
Figure 2. Schematic image of a Zener polaron

References

[1] J. B. Goodenough, Phys. Rev. **100** (1955) 564.

[2] P. Radaelli, D.E. Cox, M. Marezio and S-W. Cheong, Phys. Rev. **B55** (1997) 3015.

[3] A. Daoud-Aladine, J. Rodríguez-Carvajal, L. Pinsard-Gaudart, M.T. Fernández-Díaz and A. Revcolevschi., Phys. Rev. Lett.**89** (2002) 097205

PRESSURE INDUCED CRYSTALLIZATION OF A SPIN LIQUID

I.Mirebeau[1], I.N. Goncharenko[1], P. Cadavez-Peres[1],
S.T. Bramwell[2], M.J.P. Gingras [3,4], J.S. Gardner[5]

[1]Laboratoire Léon Brillouin (CEA-CNRS), CEA-Saclay, 91191 Gif-sur-Yvette, France.
[2]University College London, London, United Kingdom.
[3]University of Waterloo, Waterloo, Ontario, Canada.
[4]Canadian Institute for Advanced Research, Toronto, Ontario, Canada
[5]National Research Council of Canada, Chalk River, Ontario, Canada

$Tb_2Ti_2O_7$ is an insulating pyrochlore oxide in which localized Tb^{3+} spins occupy a lattice of corner-linked tetrahedra. Antiferromagnetic Heisenberg interactions on this lattice are highly frustrated, giving rise to macroscopic degeneracy in the ground state. In general this degeneracy is lifted by perturbations arising from chemical disorder or additional magnetic interactions, yielding either spin glass-like or long range ordering transitions. $Tb_2Ti_2O_7$ is the only compound which remains in a fluctuating paramagnetic state down to 70 mK [1]. Short range antiferromagnetic correlations between the Tb spins develop below 100 K, corresponding to a "spin liquid" state. The single ion ground state in $Tb_2Ti_2O_7$ is a crystal field doublet, which interacts with its neighbors via superexchange and dipolar coupling. Given these simple interactions, the absence of magnetic order is surprising. Applied pressure allows one to study this stability, by perturbing the balance of the various interactions, which have different dependencies on interatomic distance.

We used LLb-Kurchatov pressure cells and the specialized high pressure diffractometer G6-1, the only apparatus that allows neutron scattering at both very low temperatures (1.4 K) and very high pressures, (10-50 GPa) (2). Figure 1 shows neutron diffraction spectra at 1.4 K for three pressures, focusing on the diffuse intensity in the region of the 111 nuclear peak. At P = 0, the diffuse intensity arising from liquid-like magnetic correlations shows no indication of magnetic long range order. At 1.5 GPa, small magnetic Bragg peaks start to emerge from the diffuse background. At 8.6 GPa, the average intensity becomes much lower, but the magnetic peaks are now very clearly seen. Concomitantly, the diffuse intensity shows a stronger modulation. The onset of narrow Bragg peaks shows the development of magnetic long range order, or crystallization of the spin liquid state, induced by pressure.
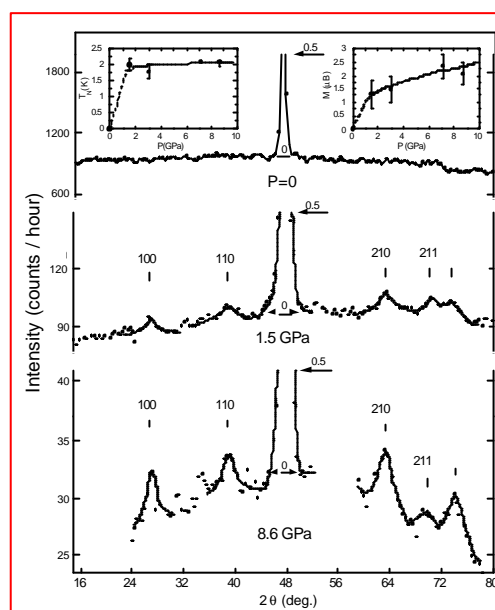
Figure 1. $Tb_2Ti_2O_7$: raw neutron diffraction spectra (neutron counts/hour) for three pressures at 1.4 K. The incident neutron wavelength is 4.741 Å. Intensity scales are chosen to show the magnetic peaks as compared with the 111 structural peak. Half intensity of the 111 peak is shown at the center of the spectra. Insets: the Néel temperature (left) and ordered magnetic moment at 1.4 K (right) vs. pressure.

The ordered magnetic structure has a simple cubic unit cell, derived from the chemical one of Fd-3m symmetry by a propagation vector $\mathbf{k}$ = 100 or 110. There is no magnetic contribution to the structural peaks. The antiferromagnetic structure is not predicted by theoretical models and differs from the few ordered structures reported in pyrochlore compounds. The Néel temperature T_N = 2.1 K is pressure independent. Below T_N, the ordered and spin liquid phases coexist. The ordered moment increases with pressure, but remains always below the calculated value of $5 \mu_{B'}$ as expected due to the coexistence of liquid and ordered states.

The modulation amplitude of the diffuse scattering A(P,T) shows clear evidence of this coexistence. A(P,T) defined experimentally as I_{max}-I_{min}, where I_{max} and I_{min} are the extrema of the diffuse intensity, is proportional to the thermal average of the first neighbor spin correlations. It increases with decreasing temperature, and this effect becomes more pronounced as pressure increases (Fig. 2). The onset of long range order at T_N coincides with a sharp kink of A. Below T_N, the decrease of A mirrors the increase of the Bragg intensity, showing that spin liquid and ordered phases coexist. The magnetic state below T_N reminds one of a mixed solid-liquid phase, with both static and dynamical character, and a gradual transfer of intensity from liquid to ordered state as temperature decreases.

The coexistence of spin liquid and ordered states and the fact that T_N is pressure independent suggest that the transition may be of first order. The pressure induced order provides further compelling evidence that the spin liquid state in $Tb_2Ti_2O_7$ is most unusual. In liquid helium, pressure induces crystallization by simply strenghtening the interatomic interactions, which reduces the quantum fluctuations. Here the role of pressure is more intricate. One possibility is that the frustration is relieved by a pressure induced structural distortion, but this has not been observed. A more intriguing possibility is that in the spin liquid state, exchange dipolar and crystal field interactions are naturally balanced in such a way as to make quantum fluctuations significant. This delicate balance is then destroyed by pressure, resulting in magnetic order.
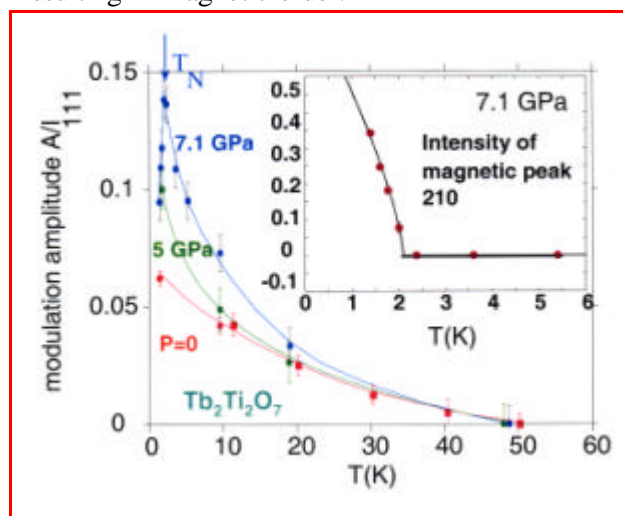
Figure 2. Temperature dependence of the modulation amplitude A(P,T) for the pressures P = 0, 5 and 7.1 GPa, where A(P,T) = I_{max}-I_{min}, the difference in extrema of intensity in our experimental range. To compare data at different pressures, A(P,T) is scaled to the integrated intensity of the 111 Bragg peak. At 5 and 7.1 GPa, solid lines above T_N are fits with the law -ln(T/T_{up}), T_{up} = 46 K. At 5 GPa, only the paramagnetic regime was investigated. Inset: integrated intensity of the 210 magnetic peak (scaled to the 111 peak intensity) vs. temperature at 7.1 GPa. The solid line is a guide to the eye.

References
[1] J. S. Gardner. *et al. Phys. Rev. Lett.* **82** (1999) 1012.
[2] I. Goncharenko and I. Mirebeau, *Rev. High Pressure Sci. and Technol.* **7** (1998) 475.

Results published in Nature **420**, 55, (2002).
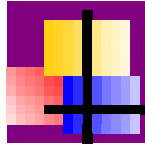
2 - MAGNETISM AND SUPERCONDUCTIVITY

Of all physical probes used for studying magnetism in solids, neutrons offer by far the most extended spectrum of experimental techniques. Whereas classical diffraction and inelastic scattering methods remain unsurpassed for disentangling complex magnetic structures or deriving exchange parameters from magnon dispersion branches, neutron scattering has also proved remarkably versatile in targeting new problems at the cutting edge of modern magnetism.

New types of magnetic objects can be studied, such as large-spin clusters in molecular magnets, or transition-metal monoxides in confined geometries. Specific phenomena occurring at magnetic interfaces can be studied in thin-film specimens using neutron reflectometry. Our current understanding of "strongly correlated electron systems", including a variety of transition-metal oxides (ruthenates, high-T_c cuprates, manganites) and unstable f-electron compounds (Kondo insulators, heavy-fermion superconductors, quadrupole-order compounds), is based to a large extent on the knowledge of their ground-states and low-energy excitations gained from unpolarized and polarized neutron scattering experiments.

To keep pace with other techniques, neutron instrumentation continuously extends the range of experimental parameters accessible to measurements. To observe new photo-induced phenomena in "switchable" molecular materials, *in situ* illumination by a laser beam has been implemented in a polarized-neutron diffractometer. Various types of materials are studied at the LLB under multi-extreme conditions (high pressure + high field + very low temperature) making it possible to stabilize and investigate novel magnetic states.

1. COMPLEX ELECTRONIC SYSTEMS
1.a. Ruthenates
M. Braden and coworkers (Köln University) - Y. Sidis, Ph. Bourges, O. Friedt (thesis), P. Pfeuty, A. Gukasov, R. Papoular (LLB) - J. Kulda (ILL) - Y. Maeno (Kyoto University).

Sr_2RuO_4 is the only superconducting layered perovskite isostructural with cuprates. It is now well established that its superconductivity is unconventional (spin-triplet, p-wave symmetry with line nodes). The supposed pairing via ferromagnetic fluctuations has not been confirmed by inelastic neutron scattering measurements, which show a spin excitation spectrum dominated by incommensurate spin fluctuations. The fluctuations are related to a dynamical nesting effect between quasi-1D sheets of the Fermi surface (α and β bands). While the role of these fluctuations is still a subject of debate, it has been shown recently that the strong incommensurate spin fluctuations were induced by a spin-density wave instability nearby. That instability
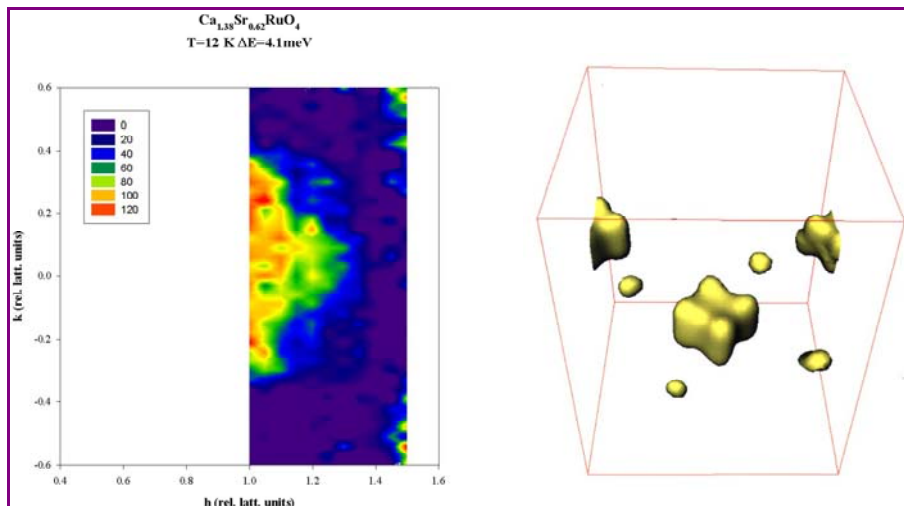
Left) Incommensurate spin fluctuations located at wavevectors $Q_{inc} = (\pm0.2,0,0)$ and $(0,\pm0.2,0)$ in $Ca_{1.38}Sr_{0.62}RuO_4$. Right) the spin density spreads mainly on $4d_{xy}$ orbital and is partially distributed on O^{2-} ligands in $Ca_{1.5}Sr_{0.5}RuO_4$.

controls non-Fermi liquid properties observed in the normal state of Sr_2RuO_4 (T-linear resistivity, ω/T scaling of the incommensurate spin fluctuation). Furthermore, substituting Ti^{4+} for Ru^{4+} destroys superconductivity and stabilizes the spin-density-wave state. Quantum critical phenomena are under investigation in $Sr_2Ru_{1-x}Ti_xO_4$ ($x = 0.04$).

Substitution of Ca^{2+} for Sr^{2+} gives rise to a tilt and a rotation of oxygen octahedra, leading to deep modifications in both the electronic structure and the magnetic properties. In $Ca_{1.38}Sr_{0.62}RuO_4$, the spin excitation spectrum is dominated by incommensurate spin fluctuations around the ferromagnetic point. These fluctuations are likely associated with a change in the Fermi surface topology, which reinforces the role of the γ band. In $Ca_{1.5}Sr_{0.5}RuO_4$, the spin density, mapped out by polarized neutron diffraction and analysed by the maximum entropy method confirms the dominant influence of $4d_{xy}$ orbitals (γ band) on the magnetic properties.

1.b. High-T_c cuprates

LLB Inelastic group (Ph. Bourges, Y. Sidis, P. Pailhès) - B. Keimer and coworkers (MPI Stuttgart) - L.-P. Regnault (CEA/Grenoble), - A. Ivanov (ILL) - LLB Theory group (F. Onufrieva, P. Pfeuty).

The resonance mode (see [highlight](#))

An unusual spin excitation mode, the so-called magnetic resonance mode, has stimulated numerous theoretical studies on the interplay between charged quasiparticles and collective spin excitations in copper oxide superconductors. The mode had, so far, only been observed in materials with crystal structures consisting of copper oxide bilayers, and was absent in single-layer $La_{2-x}Sr_xCuO_4$. Neutron scattering data have shown that the magnetic resonance mode is present in $Tl_2Ba_2CuO_{6+\delta}$, a single-layer compound with a superconducting transition temperature of ~ 90 K, demonstrating that it is a generic feature of copper oxide superconductors, independent of the layer sequence.

In slightly underdoped $YBa_2Cu_3O_{6.85}$ ($T_c = 89$ K), previous inelastic neutron studies had shown that the magnetic resonance mode displays a downward dispersion. This rather peculiar dispersion was predicted in the "spin-exciton" model by the LLB Theory group. Alternatively, it has been argued that the dispersive magnetic resonance mode could be similar to magnons in incommensurate antiferromagnets. To test this suggestion, the spin excitation spectrum in a stripe-ordered nickelate, $La_{2-x}Sr_xNiO_4$ ($x = 0.31$), was determined using inelastic neutron scattering. The spin excitation spectrum is found to be surprisingly similar to that of a standard incommensurate antiferromagnet. While interesting in their own right, the results do not provide an adequate model for the magnetic resonance observed in several cuprates. (Collaboration: LLB Inelastic Group, M. Braden (Köln Univ.) - J. M. Tranquada (Brookhaven National Lab.)).

Coexistence of antiferromagnetism and superconductivity

J. Hodges (SPEC), LLB (Ph. Bourges, Y. Sidis, M. Hennion, I. Mirebeau), X. Chaud (CRETA).

Weak commensurate antiferromagnetism has been reported in superconducting compounds $YBa_2Cu_3O_{6.5}$ ($T_c = 55$ K) by the LLB group and in $YBa_2Cu_3O_{6.6}$ ($T_c = 63$ K) by other groups. The anomalously fast decrease in the magnetic form factor gave rise to a controversy about the origin of the antiferromagnetic order:
(i)   A spin-density wave (LLB Theory Group), or
(ii)   A d-wave charge-density wave.

In $YBa_2(Cu_{1-y}Co_y)O_7$ ($y = 0.013$, $T_c = 94$ K), recent neutron scattering measurements have revealed the existence of a commensurate antiferromagnetic order ($T_N = 330$ K, $\mu = 0.14 \mu_B$). Cobalt substitution leads to a state in which superconductivity and antiferromagnetism coexist, without strong interference, on the microscopic scale. The anomalous magnetic form factor was also observed in a Co-substituted sample at optimal doping. This result brings into question the existence of a d-wave charge-density wave, expected in the underdoped regime only. The exact reason for the observed structure factor remains unclear at present.

Density wave phases and their precursor fluctuations in high T_c cuprates

LLB Theory group (F. Onufrieva, P. Pfeuty).

The LLB theory group have analysed different density wave ordered phases (SDW, CDW, Orbital magnetism and Spin current) in 2D strongly correlated metals, their stability in different parts of the T-x diagram (where x is the electron concentration), their compatibility with d-wave superconductivity and the

precursor dynamic fluctuations associated with these orders. The LLB theoretical work allows one to understand the origin of different phenomena observed in the high T_c hole doped cuprates: namely the magnetic ordered phases observed by neutrons at low hole doping δ as well as their strong sensibility to different external factors, and their disappearance with increasing doping, the spin current phase observed recently by ARPES near optimal doping, the dynamical fluctuations observed by neutrons by NMR and by Raman scattering at intermediate doping and their influence on ARPES spectra as well as recent observation of the coexistence of DW+SC orders.

1.c. CMR Maganites

Hole-doped manganites $A_{1-x}B_x$MnO$_3$ (A = {La, Pr,...}, B = {Sr, Ca}), display a very rich phase diagram where nuclear and magnetic structures, as well as transport properties, evolve with doping. The purpose of the neutron scattering studies is to shed light on the origin of the "colossal" magneto-resistance observed in the ferromagnetic and metallic state. This paragraph focus on dynamical and large-scale studies complementing the structural work of the previous chapter "Structure and Phase Transitions" of this scientific report.

Spin-charge-lattice interactions in manganites

P. Kober (thesis), F.W. Wang (postdoc), M. Hennion, F. Moussa, J. Rodrigez-Carvajal (LLB) – L. Pinsard, P. Reutler, A. Revcolevschi (LPCES, Univ. Paris-Sud)

Experiments performed on triple-axis spectrometers in the canted antiferromagnetic state of La$_{1-x}B_x$MnO$_3$ (B = Ca, Sr) have brought to light the existence of ferromagnetic platelets of nanometric size. In addition, they have revealed a complex spin excitation spectrum made of two magnon dispersion branches: one reminiscent of the pure antiferromagnetic compound, and the other one showing strong ferromagnetic character. Recent measurements under magnetic field do not indicate any splitting of the antiferromagnetic-like branches, pointing out that the two modes in zero field are actually due to the intrinsic splitting of the antiferromagnetic magnon branch by the inhomogeneous magnetic-field distribution induced by ferromagnetic clusters. The absence of crossing between the two branches might also be related the inhomogeneous character of the system. At the ferromagnetic cluster percolation, the compounds become ferromagnetic and metallic at T_c. However, a new and unexpected metal-insulator transition takes place upon cooling. In two similar compounds, La$_{0.8}$Ca$_{0.2}$MnO$_3$ and La$_{0.875}$Sr$_{0.125}$MnO$_3$, the inelastic neutron scattering studies of the spin excitation spectrum reveal the opening of gaps in the magnons dispersion curve. The gap energies coincide with phonon energies, pointing out a spin-lattice-charge coupling on the microscopic scale that could stabilize a charge order at low temperature. A spin-phonon coupling has been already reported in the metallic state (Ca, Sr: x = 0.3) and ascribed to the coupling between magnons and orbital fluctuations. The comparison between spin excitation spectra in both insulating and metallic ferromagnetic states is in progress.

Magnon dispersion in (La,Ca)MnO$_3$ along [001] at 17 K, showing two gaps, at q_0 and q = 3/8. Full (empty) symbols indicate the main (weak) magnons. Phonon dispersions are displayed as red lines). The gap at q_0 is interpreted as a folding of the dispersion curve with an anti-crossing effect due to magnon-phonon coupling.

Spin and charge inhomogeneities in manganites (see highlight)

Ch. Simon and coworkers (CRISMAT), D. Saurel (thesis), G. André, A. Brûlet (LLB)

As a result of the competition between ferromagnetic double exchange, induced by hole hopping, and the antiferromagnetic superexchange coupling, it was originally proposed that a uniform canted antiferromagnetic state should develop as a result of hole doping in manganites. More recent theoretical and experimental studies [M. Hennion *et al., Phys. Rev. Lett. 98*] rather suggest the occurrence of an inhomogeneous electronic phase separation, leading to the appearance of anisotropic ferromagnetic clusters. With increasing doping, the percolation of such clusters could explain the colossal magnetoresistance effect observed in these materials. The dimensions and shape of the ferromagnetic domains of nanometric size, which are embedded in an otherwise antiferromagnetic medium, have been determined by small angle neutron scattering in $Pr_{0.67}Ca_{0.33}MnO_3$.

1.d. Mixed-valence and Kondo systems.
Kondo insulators, mixed-valence semiconductors (see <u>highlight</u>)
J.-M. Mignot (LLB) – P. A. Alekseev, K. S. Nemkovski (RRC Kurchatov Inst., Moscow) – L.-P. Regnault (DRFMC/SPSMS, CEA/Grenoble) – F. Iga (ADSM, Hiroshima Univ.)

One challenging problem in correlated *f*-electron systems is to understand the emergence of an insulating ground state upon cooling in compounds that initially behave as metals near room temperature. The opening of a narrow gap ($E_g \sim 10$ meV) in the electron density of states near the Fermi level is actually predicted by the "periodic Anderson" or the "Kondo lattice" models for the special case of exactly one conduction electron per magnetic 4*f* site, but their applicability to real materials remains controversial. Inelastic neutron scattering can probe subtle changes in the low-energy magnetic response associated with the formation of the gap state. Detailed measurements on the Kondo insulator YbB_{12}, recently made possible by the availability of large single crystals from Japan, confirmed the existence of a spin gap below 10–15 meV at $T = 10$ K, and provided strong evidence that the excitations just near the gap edge have pronounced antiferromagnetic character.

In $Sm_{1-x}Y_xS$ alloys, a mixed-valence (MV) state is achieved by substituting Y into the originally divalent semiconductor SmS. In the latter compound, Sm^{2+}–Sm^{2+} exchange interactions are known to produce a dispersion in the $J = 0 \rightarrow J = 1$ spin-orbit transition. In the MV regime ("black phase"), a remarkable splitting of the dispersion curve into two branches occurs over the entire Brillouin zone. It has been suggested previously that the upper and lower branches might correspond to the localized and extended part of the MV Sm wave function, respectively, as predicted theoretically by Kikoin and Mishchenko. This view is supported by measurements for larger Y concentrations ($x = 0.17, 0.25, 0.33$) showing that, as the Sm valence increasingly deviates from +2, the lower branch gains spectral weight while splitting further apart from the upper one.

Orbital degrees of freedom, quadrupole order
K. Iwasa, M. Kohgi (Tokyo Metropolitan Univ.), J.-M. Mignot, C.P. Yang, A. Gukasov (LLB), M. Braden (LLB and FZ Karlruhe)

Neutron diffraction studies of the unique antiferroquadrupolar (AFQ) phase discovered previously in TmTe (rocksalt structure, divalent magnetic semiconductor) have been extended to include the very-low-temperature ($T \geq 100$ mK), high-field ($H \leq 7$ T) region, where one expects an interplay between quadrupole and magnetic dipole order. The results indicate that the pre-existing order of the O_2^2 quadrupolar components competes with Tm-Tm exchange interactions to produce a canting of the antiferromagnetic magnetic structure formed below $T_N = 0.45$ K. Huge irreversibilities observed at 0.1 K as a function of field denote a peculiar behaviour of the AFQ/AFM domains.

Ce monopnictides Ce*X* (*X*: P, As, Sb), order at low temperature in complex magnetic structures, consisting of long-period stacking sequences of ferromagnetic planes. In each plane, the Ce ions can have either large or small ordered magnetic moments, corresponding to two different crystal-field ground states, respectively Γ_8-like or Γ_7-like. In this state, the Ce-4*f* orbital order therefore coexists with the magnetic dipole moment order. Inelastic scattering experiments have revealed an extra, nearly dispersionless, lattice excitation at 7 meV. This mode, which appears only in the orbital order phase, is thought to result from a local vibration within the large-moment planes, coupled to a change in the symmetry of the Ce 4*f* orbital due to its mixing with *p* orbitals of Sb neighbours.

The family of "filled skutterudites" RT_4X_{12} (R = lanthanide, T = {Fe, Ru, Os}, X = {P, As, Sb}) combines an exceptional variety of electronic properties with a potential for thermoelectric applications. Among them, $PrOs_4Sb_{12}$ is thought to be the first example of a Pr-based heavy-fermion superconductor. Diffraction experiments performed both at JAERI (Japan) and at LLB in Saclay have established the existence of a small AF moment in the new ordered phase stabilized below 1 K by a magnetic field $H \geq 4.5$ T. This field-induced AF component is ascribed to an AFQ order of the O_{yz} type.

High-pressure studies of magnetic and valence instabilities
In magnetically unstable $4f$ and $5f$ compounds, the decrease of interatomic distances produced by high hydrostatic pressures can induce substantial changes in the electronic structure. Magnetic powder diffraction experiments have been performed on several systems using the dedicated diffractometer G6.1 ("MICRO"). In Ce_2Fe_{17}, pressure modifies the magnetic structure and the magnetic ordering temperature T_N drops from 215 K at ambient pressure to 125 K at $P = 7$ GPa. (Z. Arnold, O. Prokhnenko, I. Goncharenko). A nonmagnetic state is expected to be achieved in this compound at about 20 GPa. In $YbMn_2Ge_2$, the Yb ions undergo a valence transition at $P \sim 1.5$ GPa. This transition results in a reorientation of the magnetic moments on the Mn sublattice [M. Hofmann P. Link, (IPC Universität Göttingen), I. Goncharenko (LLB).

Dipolar anisotropy of Gd ferromagnetic and antiferromagnetic compounds (see highlight)
In magnetically stable $4f$ compounds, the orbital part of the magnetic moment may be completely cancelled as in Gadolinium compounds and the magnetic anisotropy comes only from very weak dipolar forces or complex exchange mechanisms. Thanks to the high-energy neutrons of the hot source reducing the absorption, the good resolution of the 7C2 spectrometer and the high value of the magnetic moment, a series of Gadolinium magnetic compounds were studied to elucidate their structure and anisotropy. The predominance of the dipolar forces in both ferromagnetic and antiferromagnetic systems is very striking.

1.e. Quantum critical points.
Magnetic filed induced quantum critical point in Pr_2CuO_4
D. Petitgrand, P. Pfeuty (LLB) – A. Ivanov (ILL) – S.V. Maleev (Gatchina)

Pr_2CuO_4 is an insulating parent compound of high-T_c superconducting cuprates. In this system, a pseudo-dipolar interaction gives rise a non-collinear antiferromagnetic state. In a uniform magnetic field applied parallel to the CuO_2 planes, magnetic moments in neighbouring CuO_2 planes rotate and a spin-flop transition occurs. The transition can be either first or second order depending on the direction of the applied field. Studies have first focused on the second-order transition that takes place when a magnetic field $H_{c0} = 3$ T is applied along the [110] direction. H_{c0} is the end point of the critical magnetic field $H_c(T)$ at $T = 0$ and therefore corresponds to a quantum critical point, around which strong quantum fluctuations are expected. Neutron scattering experiments are carried out in order to observe these non-classical dynamical effects.
The order parameter, which vanishes at H_{c0}, exhibits a critical exponent $\beta \sim 0.2$, smaller than the expected classical values. Meanwhile, correlation lengths are strongly anisotropic. On the one hand, the out-of-plane spin correlation length decreases slowly from 80 Å down to 9 Å when varying the field from 3 to 5 T, implying the persistence of strong inter-plane spin fluctuations away from H_{c0}. On the other hand, in-plane spin fluctuations remain long range (> 500 Å). The characteristic frequency scale of the critical fluctuations is beyond the 10 GHz experimental detection threshold. Based on neutron scattering measurements, the system can be pictured as a set of long-range, slowly fluctuating, planar antiferromagnetic islands, weakly coupled perpendicular to the CuO_2 planes. In connection with the experiments, a theoretical model is developed by S. A. Maleev in Gatchina and quantum critical phenomena are studied by P. Pfeuty at LLB.

Quantum criticality in MnSi under pressures (see highlight)
C. Pfleiderer, D. Reznik, L. Pintschovius, H. v. Löhneysen (Karlsruhe Univ., FZ Karlsruhe, LLB)).
The transition metal compound MnSi is one of the most extensively studied itinerant-electron magnets. Below 30 K, it orders magnetically in a helical structure. Using hydrostatic pressure one can induce highly reproducible variations of its bulk magnetic properties, in particular its ordering temperature T_C is suppressed above $p_c = 14.6$ kbars. New single-crystal elastic scattering experiments have been carried out just below p_c

(p = 14.3 kbars, $T_C \approx 3.3$ K) on the cold-neutron triple-axis spectrometer 4F1 using a miniature pressure cell. The results indicate the appearance of a partial order, akin to that found in liquid crystals, with magnetic intensity spread out over a sphere of radius 0.0422 Å^{-1}. More generally, this observation is an important step in the search for novel electronic states in intermetallic compounds.

Heavy-fermion superconductors

The study of critical phenomena occurring close to the quantum critical point (QCP) in heavy-fermion superconductors continues to be investigated in connection with possible dimensionality effects.

A careful study of the Q dependence of magnetic fluctuations in CePd$_2$Si$_2$ by B. Fåk (DRFMC, CEA/Grenoble, and ISIS) and N.H. van Dijk (Delft University of Technology) did not reveal significant anisotropy, contrary to expectations from the electrical resistivity. Experiments on CeRu$_2$Si$_2$ have been undertaken by S. Raymond and W. Knafo (DRFMC, CEA/Grenoble) to search for scaling laws in the (T, ω) dependence of the dynamical susceptibility. This study of the pure compound will complement measurements performed at the ILL on the solid solution containing 7% La located right at the QCP.

The new family of heavy-fermion superconductors CeMIn$_5$ (M = Rh, Co, Ir) presents a layer structure but it is still unclear whether 2D effects are important for their comparatively "high" critical temperatures. The pressure dependence of magnetic order in CeRhIn$_5$ close to the QCP has been determined by neutron diffraction. [J.-M. Mignot, I.N. Goncharenko (LLB), E. Moshopoulou (National Center for Scientific Research «Demokritos», Athens), A. Llobet-Megias (Los Alamos Nal. Lab.)], and inelastic measurements have been carried out on a (Rh, Ir) solid solution to probe the dynamical response close to the QCP.

2. MOLECULAR MAGNETISM

The design of molecules that could be used for information processing or storage is one of the main topics in molecular magnetism. This branch of material science deals with the magnetic properties of molecules, or assemblies of molecules, containing magnetic centres: spin-crossover systems, magnetic clusters or organic magnetic materials for example. The determination of spin density maps provides crucial information on the mechanisms of magnetic interactions, such as spin polarization and spin delocalisation. Polarized neutron diffraction on single crystals is a unique experimental technique that makes it possible to visualize the spin distribution over a whole complex molecule in its ground or metastable state.

2.a. Photo-induced molecular magnetism (see *highlight*)

A. Goujon, B. Gillon, A. Gukassov (LLB) – J. Jeftic, Q. Nau, (Ecole Nationale Supérieure de Chimie de Rennes) – E. Codjovi, F. Varret (Laboratoire de Magnétisme et d'Optique de Versailles)

In a pioneering experiment, carried out on the 5C1 diffractometer at LLB, the photo-induced magnetization density of the photo-switchable spin-crossover compound [Fe(ptz)$_6$](BF$_4$)$_2$ (ptz = 1-propyltetrazole) could be obtained [J. Jeftic *et al., to be published in Polyhedron*]. The photo-switching process was observed using a new experimental set-up in which the sample is illuminated in situ during the polarized neutron diffraction (PND) measurement. The photo-excitation kinetics was followed and a complete photo-process was evidenced. These results emphasize the potential of PND for studies of a variety of systems known to exhibit photo-induced magnetic effects. In particular, when the photo-excitation process is due to a charge transfer (metal-metal, metal ligand), PND technique should give an insight into the photo-excitation process and the metastable state. Therefore, new collaborations are starting off in this field: *i*) photo-magnetism has been evidenced in a high-spin molecule (Mo^{IV}Cu$^{II}_6$) in which the photo-excitation process is assumed to involve an electron transfer from a Mo^{IV} site to one of the six Cu^{II} sites. PND experiments should explain the photo-process mechanism and the magnetic nature of the photo-induced state [collaboration: Laboratoire de Chimie des Métaux de Transition, Univ. Paris VI]; *ii*) the technique will also be applied to the study of the photo-excited magnetic state in materials synthesized with the molecular precursor K$_4$[Mo^{IV}(CN)$_8$]•5(H$_2$O) [collaboration: Laboratoire des Sciences Moléculaires, ICMCB].

2.b. Molecular clusters

The study of molecular clusters with large spins is another important topic in molecular magnetism. Using PND, one can unambiguously determine the magnetic ground state, which is not always possible from bulk magnetic measurements.

The magnetic structure of cyano-bridged (A^{II}, B^V) molecular-based compounds (A = {Mn, Co, Ni} and B = {Mo, W}) has been studied [J. Larianova, M. Pilkington, H. Andres, H. Stoeckli-Evans, H.U. Güdel,

S. Decurtins]. The measurement of the magnetization density in $Ni^{II}_9W^V_6$ has confirmed an $S = 12$ ground state with a collinear spin alignment. In contrast, PND results do not support the proposal of an $S = 51/2$ state for $Mn^{II}_9Mo^V_6$ based on magnetization measurements. [Collaboration: Laboratoire de Chimie Moléculaire ET Organisation du Solide, Montpellier].
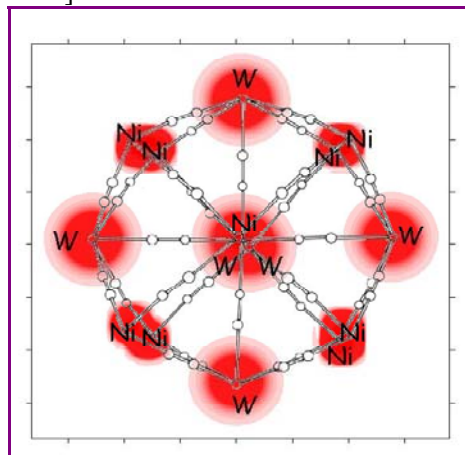
Figure 3. $Ni^{II}_9W^V_6$: projected spin density along the Ni1W3 direction (T=1.5 K, H=5 T)

2.c. Mixed compounds

In a system containing a rare earth (Gd) together with semiquinonate radicals, the combined determination of charge and spin densities sheds light on the mechanism of intramolecular magnetic interactions. In the case of the antiferromagnetic interaction between Gd^{3+} and a semiquinonate radical, it could be shown that there exists a spin delocalisation from the organic radical to the rare earth site in an isostructural compound where Y^{3+} substitutes for Gd^{3+}. This result supports an antiferromagnetic coupling involving the overlap of $4f$ orbitals and the π orbital of the radical [collaboration: University of Florence, Laboratoire de Cristallographie et Modélisation des Matériaux Minéraux et Biologiques, Nancy].

3. NANOMAGNETISM

Investigations of the magnetic interactions in nanostructured systems will help creating new functionality in artificial magnetic materials. The new physics of magnetic superlattices or confined particles will enable major improvement in ultra-strong permanent magnets and magnetic-based electronics.

3.a. Magnetic ordering and phase transitions in confined media

I. V. Golosovsky (Gatchina), I. Mirebeau, G. André (LLB), and Ioffe Physical Institute of St Petersburg.

The study of magnetic ordering and phase transitions in confined media has been developed in two directions. At first, it has focussed on antiferromagnetic transition metal oxides (MnO, FeO, CoO) embedded in the same porous media (Vycor glass). Then, it has been extended to the antiferromagnet MnO embedded in porous matrices with a different topology such as:

i)   porous glass Vycor (irregular matrix with a random interconnected network of pores),
ii)   mesoporous materials of [MCM-41]- and [SBA-15]-type (regular hexagonal array of parallel channels with tuneable diameters of 20-90 Å),
iii)   natural minerals such as Chrysotile asbestos.

For samples embedded in Vycor glass, the recent measurements in CoO confirm previous results on MnO: persistence of magnetic ordering in confined geometry, type of ordering and structural distortions similar to those in the bulk compound, noticeable reduction of the ordered moment ascribed to finite size effects. For samples embedded in natural (asbestos) or artificial (MCM, SBA) channels, neutron diffraction suggests that MnO is adsorbed at the surface of pores walls. The ordered moment is reduced with respect to the bulk moment, but surprisingly this effect is smaller in the smallest pores. Further measurements by complementary techniques (X-ray diffraction, EPR, magnetization) are in progress to confirm this result.

3.b. Dynamic nuclear polarisation (see *highlight*)

E. Leymarie and H. Glatlli (LLB), Collaboration with CEA, DRECAM/SPEC.

A new tool combining NMR techniques and Small Angle Neutron Scattering (SANS) has been developed to image the dynamic nuclear polarisation of paramagnetic centres. The contrast variation induced by this method can be viewed a new alternative to the standard H-D isotopic substitution, commonly used in soft matter and life sciences to study for example the transient dynamics of these complex systems.

3.c. Magnetic thin films (see *highlight*)

The LLB operates a polarized neutron reflectometer with polarization analysis (PRISM) dedicated to the study of magnetic thin films: multilayers of 3d ferromagnets (Fe, Co, Ni), rare earths (Gd, Ce), ferromagnetic oxides (manganites and magnetite), hard magnets (NdFeB) or magnetic semiconductors (GaMnAs). The polarized neutron reflectivity (PNR) technique allows one to determine fine details at magnetic interfaces (magnetization orientation, magnitude, roughness…) but also to determine the magnetic ordering and coupling in magnetic superlattices such as $[Fe/Si]_n$, $[Fe/Ge]_n$, $[GaMnAs/GaMn]_n$. In such superlattices, the magnetic coupling amplitude and sign depend on the thickness of the non-magnetic spacer and the coupling therefore oscillates between antiferromagnetic and ferromagnetic. A quadratic coupling (90°) is even observed for very specific structures. The trend in these last two years has been to study structures involving semiconducting materials that could be coupled to existing industrial microelectronic devices. Such structures are foreseen as possible candidates for spin-memory cells (MRAMs) and spin-transistors based on spin injection properties (see also ***highlight*** on GMR sensor optimisation)

3.d. Spin dynamics in thin films (see *highlight*)

The spin dynamics in confined structures, at the nanometric scale, is still a topic under investigation. Recently, the measurement of the spin-wave dispersion in semiconducting heterostructures (MnTe/ZnTe) has demonstrated the possibility of studying dynamical properties of magnetic thin films. This study has been performed thanks to the very high performance of the upgraded triple axis spectrometers of the LLB and the high-quality of MBE-grown single crystalline films of metastable Zinc Blende structure.

In parallel, a technique based on grazing incidence geometry has been evaluated on the PRISM reflectometer. The technique couples a surface sensitive technique (reflectivity) together with a selective excitation of the sample by a hyper frequency field. It should allow the characterization of very low energy magnetic excitations in thin films. In the first tests performed on Permalloy thin films, the accessible energy range has been found to be limited to 20GHz corresponding to surface magneto-static spin-waves in thin films.

3.e. Magnetic surface diffraction and Grazing Incidence Small Angle Neutron Scattering (GISANS)

"Grazing Incidence SANS", another technique derived from reflectivity, is presently evaluated on the spectrometer PAPOL. The technique will allow us to study the magnetic correlations in planar structures at a nanometric scale. The spectrometer PAPOL is currently being upgraded in order to implement and offer performing GISANS in the coming year. At the moment, the technique has been demonstrated for magnetic structures in the range 50-100 nm and will be extended to smaller sizes. One of the advantages of this technique is that neutrons can probe in-depth structures and give a quantitative magnetic information inaccessible to surface techniques such as Magnetic Force Microscopy for example. Application fields of GISANS concerns magnetic domains in thin films, self organized metallic clusters or nanometric objects fabricated by modern lithographic techniques to study the confinement and reduced dimensionality effects.

Confinement effects due to the finite film thickness or external strains due to epitaxial growth on a substrate strongly affect the magnetic behaviour of thin films. The precise knowledge of the magnetic ordering in thin films at the atomic level is therefore still a question. A new option of grazing incidence surface diffraction with polarized neutrons has been developed on the reflectometer EROS in order to study the magnetic order in epitaxial thin films (see ***highlight*** for a detailed presentation of this set-up).

2 - MAGNETISM AND SUPERCONDUCTIVITY

MAGNETIC RESONANT MODE IN THE SINGLE-LAYER HIGH TEMPERATURE SUPERCONDUCTOR $Tl_2Ba_2CuO_{6+\delta}$

H. He[1], P. Bourges[2], Y. Sidis[2] C. Ulrich[1], L.P. Regnault[3], S. Pailhès[2], N.S. Berzigiarova[4], N.N. Kolesnikov[4], B. Keimer[1]

[1] Max-Planck-Institut für Festkörperforschung, 70569 Stuttgart, Germany
[2] Laboratoire Léon Brillouin, CEA-CNRS, CE Saclay, 91191 Gif-sur-Yvette, France
[3] CEA Grenoble, Département de Recherche Fondamentale sur la matière Condensée, 38054 Grenoble cedex~9, France
[4] Institute of Solid State Physics, Russian Academy of Science, Chernogolovka, 142432 Russia

Electronic conduction in the copper oxide high temperature superconductors takes place predominantly in structural units of chemical composition CuO_2, in which copper and oxygen atoms form an approximately square planar arrangement. Most theoretical models of high temperature superconductivity are therefore based on a two-dimensional square lattice. In real materials, however, deviations from this simple situation are nearly always present. For instance, buckling distortions of the CuO_2 layers that are found in many copper oxides are thought to have a significant influence on the electronic structure and on the superconducting transition temperature T_c. Interlayer interactions in materials with closely spaced CuO_2 layers (forming bi- or trilayer units) or additional copper oxide chains in the crystal structure present further complications whose influence on the superconducting properties remains a subject of debate. Experiments on $Tl_2Ba_2CuO_{6+\delta}$, a material with unbuckled, widely spaced CuO_2 layers and a maximum T_c around 90 K, have therefore played a pivotal role in resolving some issues central to our understanding of these materials.

Inelastic neutron scattering experiments in high-T_C cuprates have revealed a magnetic resonant mode characteristic of only the superconducting state at the antiferromagnetic (AF) wavevector $\mathbf{Q}_{AF}$. Since its discovery [1], this collective mode has been extensively investigated in the bilayer copper oxide $Yba_2Cu_3O_{6+\delta}$, as well as in $Bi_2Sr_2CaCu_2O_{8+\delta}$ (BSCO) another bilayer compound [2]. At all doping levels, strong line shape anomalies of this collective spin excitation below T_c bear witness to a substantial interaction with charged quasiparticles. Conversely, anomalies in the quasiparticle spectra observed by photoemission, optical conductivity, tunneling, and Raman scattering techniques have been interpreted as evidence of coupling to the neutron mode. In the copper oxides the intriguing correspondence between anomalous features in the spectra of spin and charge excitations has stimulated spin fluctuation based pairing scenarios. All of these considerations are, however, only viable if the resonant spin excitation turns out to be a general feature of the various

crystallographically distinct families of superconducting copper oxides. The failure to detect such an excitation in the single-layer compound $La_{2-x}Sr_xCuO_{4+\delta}$, despite much experimental effort, has therefore hampered a unified phenomenology of the copper oxides, and the prospect that the mode could be a spectral feature specific to bilayer materials has cast a cloud over models in which spin excitations play a central role.
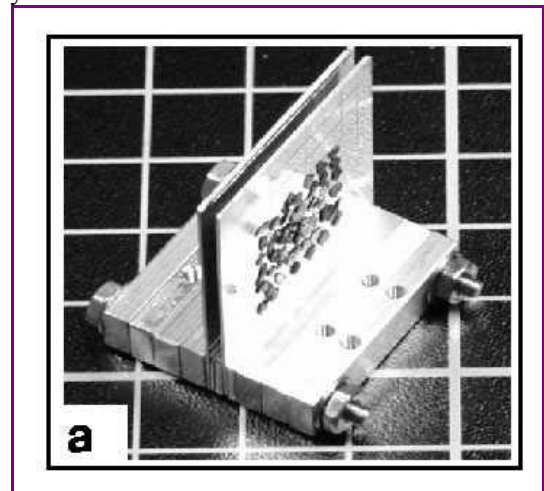
Figure 1. Photograph of a part of the array of co-oriented $Tl_2Ba_2CuO_{6+\delta}$ single crystals, glued onto Al plates. The equivalent single crystal has a mosaicity of $1.5°$ (from [3]).

We therefore recently focused our effort on the magnetic excitations on the one layer system, $Tl_2Ba_2CuO_{6+\delta}$, with $T_C \cong 90$ K. The crystal growth of the Tl-based copper oxide superconductors suffers from technical difficulties arising from the toxicity of Tl, and only single crystals with moderate volumes of about $\sim 0.5\text{-}3$ mm^3 can be obtained through a CuO-rich flux technique at the Institute of Solid State Physics in Chernogolovka (Russia). To obtain the required single crystals volume of ~ 0.1 cm^3 in order to perform inelastic neutron scattering, an array of more than 300 co-aligned single crystals had been assembled at the Max-Planck-Institut in Stuttgart (see photo Fig.1) [3]. Before alignment, the magnetic susceptibilities of all crystals were measured as a

function of temperature. The crystallographic axes of the individual crystals in the array were aligned with an accuracy of about 1.5°. The array of figure 1 is equivalent to a standard single crystal on which we could measured low energy transverse acoustic phonons accurately.
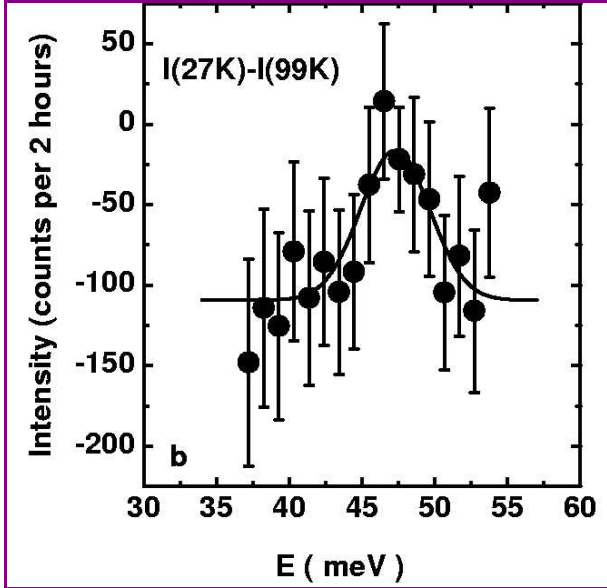
Figure 2. Difference between constant-**Q** scans measured at T=99 K (> T_c) and T=27 K (< T_c) at the antiferromagnetic wave-vector (from [3]).

Using high-flux triple axis spectrometer 2T at LLB, we were able to observe a resonance peak for this array [3]. Constant-energy scans above T_c show a featureless background that gradually decreases in an energy- and **Q**-independent fashion as the temperature is lowered. In the superconducting state, a sharp peak centered at Q_{AF} appears on top of this background. As expected for magnetic scattering that is uncorrelated from layer to layer, the peak intensities measured at two inequivalent *L*-positions are identical within the errors. The identification of this peak with the magnetic resonant mode is further supported by comparing constant-**Q** scans at $Q = Q_{AF}$ above and below T_c. Figure 2 shows that difference: it typically exhibits the characteristic signature of the resonant mode, albeit at an energy of 47 meV that is somewhat larger than the mode energy in the bilayer compounds.

In many aspects, the resonant mode in $Tl_2Ba_2CuO_{6+\delta}$ shows strong similarities with that observed in $YBCO_7$. In both cases, the mode is limited by the resolution in energy and exhibits the same extension

in q-space. Further, the resonance peak spectral weight per CuO_2 layer, defined as $\int d\omega d^3Q \, Im\chi^{res}(Q,\omega)$, equals $(0.02\mu_B^2/eV)$ for both of these systems. In BSCO, where the resonance q-width along the diagonal (110) direction is about twice as large, the spectral weight is larger, but the energy integrated intensity at the AF wavevector, normalized to one CuO_2 layer, is almost identical for the three different cuprates.

The result of our experiment on single-layer $Tl_2Ba_2CuO_{6+\delta}$ (whose $T_c \sim 90$ K is closely similar to that of optimally doped $Yba_2Cu_3O_{6+\delta}$ and $Bi_2Sr_2CaCu_2O_{8+\delta}$ implies that strong magnetic interactions between closely spaced CuO_2 layers are not required for the formation of the resonant mode. The different form of the spin excitation spectrum of $La_{2-x}Sr_xCuO_{4+\delta}$ may be due to the proximity of a competing instability that could also be responsible for the anomalously low $T_c \leq 40K$. The magnetic resonance is therefore a generic feature of high-T_c cuprates, at least for systems with a maximum T_C^{max} of around 90 K. The resonant mode occurs at an energy E_r always lower than twice the superconducting gap $E_r < 2\Delta_{max} \sim 70$ meV $\sim$ 9 k_BT_c, which has been deduced either by photoemission measurements in BSCO or by the position of the B_{1g} mode in Raman scattering; the latter has been measured for all cuprates. This agrees with models which interpret the resonant mode as a magnetic collective mode of the $d_{x^2-y^2}$-wave superconducting state below the electron-hole continuum.

The most important implication of the findings reported here regards the unified phenomenological picture recently developed for spin and charge spectroscopies of the copper oxides. The spectral anomalies that have been interpreted as evidence of coupling to the collective spin excitation are present in single-layer $Tl_2Ba_2CuO_{6+\delta}$, and equally pronounced as in analogous data on bilayer materials. If the mode had turned out to be absent (or its spectral weight substantially diminished) in $Tl_2Ba_2CuO_{6+\delta}$, this model would have become untenable. As it has survived this crucial test, it is now time to quantitatively refine this approach and to fully evaluate its implications for the mechanism of high temperature superconductivity

References
[1] J. Rossat-Mignod et al., Physica C **185-189** (1991) 86-92
[2] H.F. Fong et al.}, Nature **398** (1999) 588-591.
[3] H. He, Ph. Bourges, Y. Sidis, C. Ulrich, L.P. Regnault, S. Pailhès, .S. Berzigiarova, N.N. Kolesnikov, and B. Keimer, Science, **295** (2002) 1045 (cond-mat/0201252).

COMPLEX 2D MAGNETIC CORRELATIONS IN MANGANITES STUDIED BY SANS

Ch. Simon[1], S. Mercone[1], C. Martin[1], D. Saurel[2*], G. André[2], A. Brûlet[2]

[1] CRISMAT, 6 Bd du Maréchal Juin, 14050 Caen
[2] Laboratoire Léon Brillouin (CEA-CNRS), CEA- Saclay, 91191 Gif sur Yvette Cedex
[*] Thèse cofinancée CEA-Région Basse Normandie débutée en octobre 2002.

The colossal magnetoresistance (CMR) effect – the spectacular change of the resistivity in an applied magnetic field from insulating to metallic state- is an interesting unresolved problem in condensed matter physics [1]. Such CMR properties are widely studied in doped perovskite manganites, $A_{1-x}B_xMnO_3$, where A is a trivalent ion (La^{3+}, Pr^{3+}, etc) and B a divalent ion (Ca^{2+}, or Sr^{2+}). A physical problem raised in the manganese oxides is the competition between the double-exchange interaction, which favors the ferromagnetism (F) and super-exchange, which favors the antiferromagnetism (AF). From the competition between these two interactions, it was first proposed (in 1955) that a canting appeared in the magnetic structure. Recently, calculations suggested that the ground state of the CMR compounds could be an inhomogeneous electronic phase separation [2]. An elegant manner to interpret the CMR properties is a percolation of a metallic ferromagnetic phase in an insulating antiferromagnetic matrix, percolation that might be induced by a small change of the fraction or of the arrangement of the ferrodomains. This percolation scenario responsible of the CMR effect is a fascinating problem, which has attracted a lot of physicists.

Among the manganites, the $Pr_{1-x}Ca_xMnO_3$ series is one of prime interest, because Pr and Ca are about the same size and hence minimize the cationic size mismatch effect. Neutron diffraction technique is very well suited to determine their magnetic phase diagram. Figure 1 shows the different states depending on the x value. For the higher Mn^{3+} contents (typically x=0.2), the compounds are insulating ferromagnetic (FMI) at low temperature, and for larger x values (typically x=0.4) they are orbital ordered, antiferromagnetic CE like type. In between, the compositions x~0.3 show a mixing of F and AF phases as shown by neutron diffraction [3]. They also display CMR properties in close relation to the existence of the phase separation, which is now well proved by magnetoresistance, magnetization and specific heat studies [4].
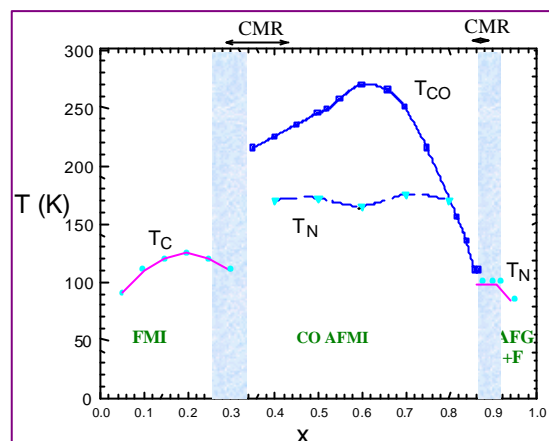
Figure 1. Magnetic phase diagram of $Pr_{1-x}Ca_xMnO_3$ compounds. The compositions close to x~0.3, which display colossal magnetoresistance, have an inhomogeneous low-temperature insulating state, where ferromagnetism (FMI) antiferromagnetism, and charge ordering (CO AFMI) coexist. Compositions close to 0.9 also have CMR properties.

As example, for the composition x=0.33, changes up to 10 orders of magnitude in the resistivity are observed at low temperature under an applied magnetic field of 7T. In revenge, the experimental situation which determines the size of the objects is not clear. Some authors have observed small nanometric ferromagnetic clusters by small angle neutron scattering (SANS), while others found much larger phase separated domains by electron microscopy or neutron diffraction. In principle, SANS is a very good technique to study the size and the shape of the domains of nanometric size and the magnetic contrast between a ferromagnet and an antiferromagnet is very large (the AF does not scatter at small angle).

Recent SANS experiments have been performed on the PAXY spectrometer at LLB to study sintered powder and single crystal samples of different compositions, x=0.20, 0.33 and 0.37. Classical magnetization and transport measurements were done to check their qualities and magnetic behaviours. x=0.2 is isolating and ferromagnetic, x=0.33 presents both ferromagnetic

and antiferromagnetic transitions and x=0.37 is mainly antiferromagnetic (see figure 1). The comparison of their SANS intensities is very interesting. Indeed, at low temperature, for the samples of composition x=0.33, the scattering signal show a q^{-2} dependence in the high q regime. This q dependence is typical of that due to infinite planar ferromagnetic sheets in an antiferromagnetic matrix [5]. The structure envisaged for the composition x=0.33, which displays CMR properties, is that of an isotropic "cabbage" as pictured in figure 2.

Figure 2. Cross section of a red cabbage to describe the 2D sheet structure of the F/AF phase separation in $Pr_{0.67}Ca_{0.33}MnO_3$ sample. At 30K, the phase separation between 1/3 F and 2/3 AF phase fractions occurs between thin ferromagnetic sheets of thickness of about 2.5nm.

The 2D thin sheets in this structure model could be the stripes proposed in the recent theories.

By combining magnetization and neutron diffraction data, we can determine the F and AF phase fractions in the samples. Knowing these magnetic fractions, the quantitative analysis of the SANS signal allows us to determine the ferromagnetic layers thickness of this peculiar 2D sheet structure, of about 2.5nm at 30K.

Further SANS experiments have been achieved to test the role of the magnetic field on such a nanoscopic structure. We have thus determined the magnetic field dependence of the thickness of the different magnetic domains in the phase separated x=0.33 system. The observed changes correspond to a gradual irreversible switch from AF sheets to F ones, transforming the system to complete ferromagnetic state at 6T [6]. At about 3T, the system reaches the percolation of the metallic ferromagnetic phase. The resistance decreases very rapidly, indicating the colossal magnetoresistance appearance.

Finally, SANS and classical magnetic techniques are powerful tools to study the electronic microphase separation occurring the manganese oxides.

References

[1] "Colossal magnetoresistance, charge ordering and related properties of manganese oxides", C.N.R. Rao and B. Raveau Eds., World Scientific, Singapore, 1998. "Colossal magnetoresistive oxides" Y. Tokura Ed., Gordon and Breach Science, New-York.
[2] A. Moreo, S. Yunoki, E. Dagotto, Science 283 (1999) 2034. D. Komskii, Physica B 280 (2000) 325.
[3] Z. Jirak et al. J. Magn. Magn. Mater. 53 (1985) 153.
[4] V. Hardy, A. Wahl, C. Martin, Phys. Rev. B64 (2001) 64402.
[5] Ch. Simon, S. Mercone, N. Guiblin, C. Martin, A. Brûlet, G. André, Phys. Rev. Lett. 89 (2002) 207202 .
[6] Ch. Simon et al., manuscript in preparation.

MAGNETIC SPECTRAL RESPONSE IN THE KONDO INSULATOR YbB$_{12}$

J.-M. Mignot,[1] P.A. Alekseev,[2] K. Nemkovski,[2] L.-P. Regnault,[3] F. Iga[4]

[1] Laboratoire Léon Brillouin (CEA-CNRS), CEA-Saclay, 91191 Gif sur Yvette, France
[2] RRC "Kurchatov Institute", 123182 Moscow, Russian Federation
[3] DRFMC/SPSMS, CEA/Grenoble, 38054 Grenoble Cedex 9, France
[4].ADSM, Hiroshima Univ., Hiroshima 739-8526, Japan

Aside from the well-documented "heavy fermion superconductors", metallic Fermi liquids, or magnetically ordered materials, other strongly correlated (mixed-valence) rare-earth compounds such as SmB$_6$ or TmSe have been known for 30 years or so to develop an intriguing *semiconducting* ground state at low temperature. More recently, the discovery of so-called "Kondo insulators" (Ce$_3$Bi$_4$Pt$_3$, YbB$_{12}$) among Ce- and Yb-based compounds was a significant advance because these elements, having only one electron (or hole) on their 4f shell, are more directly amenable to existing correlated electron theories. Experimentally, the hallmark of Kondo insulators is the gradual opening of a very narrow gap (of the order of 10 meV) in the electronic density of states at the Fermi energy when temperature decreases below ~ 100 K. This gap is thought to be a genuine effect of strong f-electron correlations.

YbB$_{12}$ is an outstanding example of this type of physics: the electronic gap is observed in a number of properties (optical conductivity, photoemission spectra, point-contact spectroscopy, etc.), and the role of coherent Kondo-type magnetic fluctuations is evidenced by the recovery of a conventional single-ion Kondo regime on heating up to near room temperature or, alternatively, diluting Yb by nonmagnetic Lu. The low-temperature magnetic specific heat changes from a linear gT term in the dilute limit to an exponential behavior in pure YbB$_{12}$, indicating that the spectrum of low-lying magnetic excitations is strongly altered.

Previous time-of-flight [1] and triple-axis [2] neutron scattering experiments on YbB$_{12}$ had revealed that the magnetic excitation spectrum at 10 K has a gap structure with no magnetic signal below approximately 10 meV. Furthermore, a group of 3 peaks was found just near the gap edge, at 15, 20, and 38 meV. The distinct dependences of these excitations as a function of temperature and Lu substitution suggested that their origins might be different.

Experiments and results

We have carried out a detailed investigation of the magnetic spectral response in YbB$_{12}$. The experiments were performed on the triple-axis spectrometer 2T using an assembly of two large, high-quality, single crystals (total volume of approximately

0.4 cm^3) grown in an image furnace at Hiroshima University.

In the energy range of the measurement (0-32 meV), two branches of magnetic excitations have been observed, around 14.5 and 19 meV respectively (fig. 1), which correspond to two spectral components identified in the powder experiments. The lower mode (M1) is strongly peaked near the zone-boundary L point, Q = (3/2,3/2,3/2), denoting a main role of antiferromagnetic (AF) Yb–Yb correlations with the wave vector k = (1/2,1/2,1/2). This point also corresponds to a minimum in the energy dispersion (fig. 2). From spectra similar to those shown in fig. 1, we have constructed a map, in the $[1\bar{1}0]$ scattering plane, of the intensity associated with the M1 spectral component (fig. 3). It appears that this intensity is strongly reduced for $q \parallel$ [110], and practically vanishes for $q \parallel$ [001]. Comparing experimental spectra measured at equivalent points Q = (q,q,q), for q = 1.5, 2.5, and 3.5, it was possible to estimate and subtract out the phonon component, then to trace the Q dependence of the magnetic signal M1: within experimental accuracy, its intensity does not deviate from the Yb^{3+} magnetic form factor.
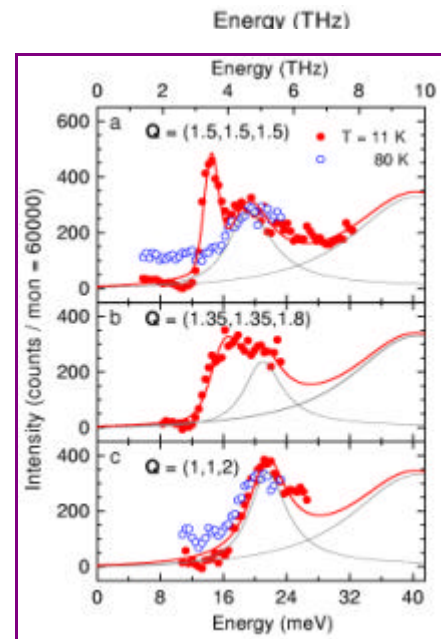
Figure 1. Magnetic neutron spectra of YbB$_{12}$ measured for 3 different Q values on the zone boundary.

The second mode (M2) is much more extended in
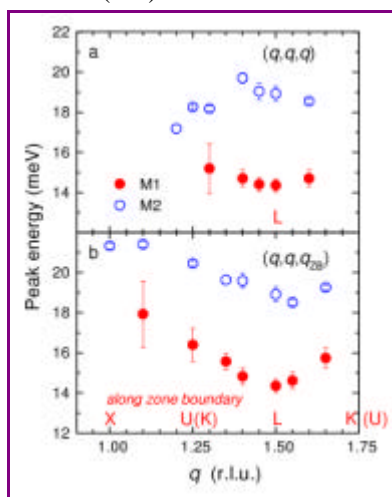
Figure 2. Energy dispersions of the two modes M1 and M2 along [111] (upper frame) and following the zone boundary (lower frame).

Q-space (compare figs. 1a and 1c). Quantitative analysis of this excitation is complicated by the fact that it is superimposed on one weakly dispersive optic phonon mode. However, phonon correction can be performed at least approximately, and the remaining signal, which decreases on going from Q = (1,1,2) to (1,1,4), is clearly magnetic in origin. Spectra measured along the [1,1,q] direction, where the M2 mode dominates, seem to indicate that its intensity varies across the Brillouin zone mainly because of the q dependence of the peak *width*. This result is surprising and may be due to an interplay between phonon and magnetic scattering. It is noteworthy that the energy of M2 exhibits significant dispersion: along the [111] direction, it decreases from zone boundary to zone center (fig. 2a), whereas following the zone boundary it goes through a minimum at the L point (fig. 2b).

Increasing temperature rapidly suppresses the M1 peak, and the corresponding signal becomes undetectable above 60 K. Simultaneously, a broad and q-independent quasielastic component is seen to grow in the spin-gap region, in agreement with the previous powder results [3] On the other hand, temperature below 80 K has no substantial effect on either the intensity or the energy dispersion of M2. The latter signal is only slightly reduced.

It can be noted that the observed Q dependence of the low-energy excitations explains the strong reduction of the bulk susceptibility occurring below 70 K: the

reason is the transfer of magnetic spectral weight in the gap-edge region from zone center toward zone boundary.
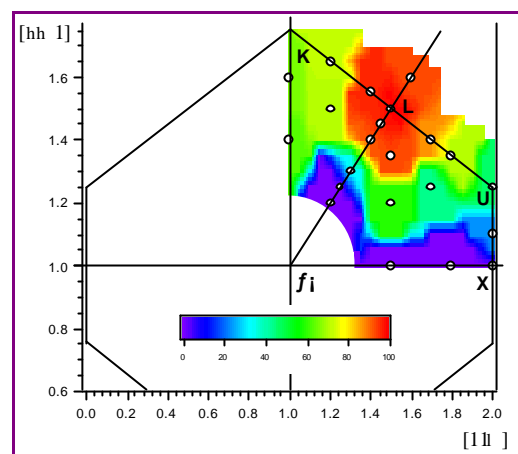
Figure 3. Interpolated intensity map of the M1 mode; circles denote Q-space points at which energy spectra have been measured.

Concerning the physical origin of M1, the fact that this excitation disappears completely above 60 K implies that it is intimately connected with the gap in the electronic structure, which disappears at about the same temperature, as evidenced by the optical conductivity data. The above results suggest that it originates from magnetic fluctuations at the AF L point. Whether the physics of these excitations should rather be treated as localized or itinerant remains an open question. Based on similarities with mixed-valence SmB_6 it is likely that the magnetic wave functions involved in the formation of AF fluctuations may be the same kind of "local bound excitonic states" (extended part of the MV wave functions) proposed to exist in the latter compound. In the present case, these states should probably involve hybridization with orbitals at neighboring Yb sites in order to explain the staggered character of the magnetic response.

As to the M2 mode, comparison with the powder results suggests that it behaves to some extent as a single-ion (e.g. crystal-field) excitation. If so, the observation of appreciable dispersion in the single-crystal spectra should be ascribed to the effect of exchange interactions, as observed many years ago by Shapiro et al. in SmS. However, a possible role of phonons needs to be clarified by polarized neutron experiments.

References

[1] A. Bouvet et al., J. Phys.: Condens. Matter 10 (1998) 5667; E.V. Nefeodova et al., Phys. Rev. B 60 (1999) 13507.

[2] Measurements on IN8 made on one of the crystals used for the present study have been reported in: F. Iga et al., J. Phys. Chem. Solids 60 (1999) 1193.

[3] It was found in the powder measurements that the upper broad peak at 38 meV also collapses above ~ 100 K.

PARTIAL ORDER IN AN ITINERANT-ELECTRON MAGNET

C. Pfleiderer[1], D. Reznik[2,3], L. Pintschovius [3], H. v. Löhneysen[1,3]

[1]Physikalisches Institut, Universität Karlsruhe, D-76137 Karlsruhe, Germany
[2]Laboratoire Léon Brillouin (CEA-CNRS), CEA-Saclay, 91191 Gif-sur-Yvette
[3]Forschungszentrum Karlsruhe, Institut für Festkörperphysik, D-76021 Karlsruhe, Germany.

The transition metal compound MnSi is perhaps the most extensively studied of the itinerant-electron magnets apart from the elemental metals iron, cobalt, nickel and chromium. It is a stable, congruently melting compound that can be produced at high purity and high crystalline perfection in the cubic B20 structure. A large body of information on MnSi is available that includes thermodynamic and transport data as a function of temperature, magnetic field and pressure, and microscopic data based on neutron scattering, nuclear magnetic resonance and quantum oscillations. Though relatively simple, the B20 structure is somewhat unusual in that it lacks inversion symmetry, so that the weak spin-orbit interactions have the Dzyaloshinsky-Moriya (DM) form. In turn, for the $P2_13$ space group of MnSi this causes a helical twist of wavelength $\lambda ? \tilde{} \ 170$ Å of the small ordered magnetic moments m = 0.4 μ_B/f.u. (formula unit) that is locked to Q = <111>, where $m \perp Q$.

Hydrostatic pressure as a clean tuning technique that does not interfere with the crystalline perfection is well established to induce highly reproducible variations of the bulk magnetic properties of MnSi, notably the suppression of the bulk magnetic transition temperature above p_c = 14.6 kbar. [1,2]. This has motivated us to investigate the magnetic state of MnSi microscopically at high pressure using neutron diffraction. Experiments were carried out on the cold thermal neutron triple axis spectrometer 4F1 at the Laboratoire Léon Brillouin where we achieved a high resolution in energy better than 50 μeV. Use of a triple axis spectrometer allowed a significant reduction of the diffuse scattering by the miniature pressure cell.

For our study the helical modulation at ambient pressure proves to be instrumental, because the corresponding Bragg scattering at $Q \tilde{} 0.037$ Å^{-1} is confined to a small volume of reciprocal space, making it easy to track the magnetic order at high pressure. Data were collected near the [110] lattice Bragg point, where the exceptional structural perfection of our sample, evident from a resolution limited mosaic spread $h ? << 0.2°$, allowed for unambiguous results. Shown in Fig. 1 is an illustration of our key results. In the temperature versus pressure plane the Curie temperature of MnSi, $T_c \tilde{} 29.5$ K, determined in resistivity and susceptibility measurements, falls monotonically with pressure, p [1]. The transition is second order up to $p^* \tilde{} 12$ kbar and weakly first order between p^* and p_c, where T_C vanishes. At ambient pressure (top left corner of Fig. 1) resolution limited magnetic Bragg reflections of a coherence length $x ? > 1200$ Å at Q = 0.037 Å^{-1} (111) are observed, that are characteristic of conventional three-dimensional long-range order. This is in excellent agreement with previous studies [3,4]. At p = 14.3 kbar, where $T_C \tilde{} 3.3$ K, the lattice constant is reduced by only 0.4 % in general agreement with the compressibility. For this pressure we observe neutron scattering intensity that is only resolution limited in the radial direction of a sphere with Q = 0.0422 Å^{-1}. The intensity is elastic at the limit of our energy resolution of 50 μeV.

To explore the distribution of intensity on the sphere of radius Q further we have performed various longitudinal, transverse and vertical scans with respect to <111> and <110>. For longitudinal scans we observe resolution limited intensity corresponding to $x ? > 1200$ Å as expected of conventional long range magnetic order. In striking contrast typical transverse scans show intensity over the full arc between <111> that is strongly enhanced at <110>. Scans vertical to the arc between <111> and the longitudinal direction at (110) indicate a gradual decrease along this direction as well. At 1.7 K and <111> we find that approximately 4% of the intensity of ambient pressure is left. A detailed account of the T dependence may be found elsewhere [5].

The total integrated scattering intensity over the sphere at 1.7 K is conserved to within 10 % of that at ambient pressure. This is consistent with measurements of the bulk magnetic moment as function of pressure in a polarising magnetic field of 0.6 T [2] and suggests that we detect within a small margin of error all of the ordered moment present at ambient pressure.

Our data imply a very shallow minimum of the free energy for <110> that is characteristic of a competition of interactions. To shed light on the nature of this competition we note that the conservation of scattering intensity implies that the

partial order, i.e. departure from $3d$ order, must be the result of topological defects weakening the spin rigidity. The reduction of T_C is in particular not the result of soft dynamical modes. In the simplest case these defects are the walls of the magnetic domains. Because the weight of intensity near <110> is incompatible with the DM interaction for the space group of MnSi a modification of these topological defects (domain walls) appears likely. For instance, it has been shown theoretically [6], that the competition of the DM interaction with the ferromagnetic stiffness for the case of MnSi may stabilize the formation of magnetic vortices.

In conclusion, when changing the lattice constant of MnSi by just 0.4 % using hydrostatic pressure, the elastic magnetic neutron diffraction intensities display sharp Bragg reflections in the longitudinal direction only, akin of partial order in liquid crystals. The observation of mesoscopic partial order in high quality single crystals of one of the most extensively studied itinerant-electron magnets has deep implications in the search for novel electronic states of intermetallic compounds in general [7]. For MnSi the temperature dependence of the electrical resistivity of the normal state ($T > T_C$) for $p > p^{*} \sim 12$ kbar suggests a diffusive motion of the electrons resulting from the interactions among the itinerant electrons themselves [2]. It is tempting to associate such a diffusive motion with the only partial order for which we have presented direct microscopic evidence. Further, quasi-elastic neutron spectra of intermetallic materials near quantum critical transitions may this way be recognized as forms of partial itinerant electron magnetism that are driven by unstable topological defects of the magnetic rigidity. This could potentially resolve the controversy of local quantum criticality [8] versus low dimensional dynamics [9] as well as uniting itinerant with local moment magnetism.
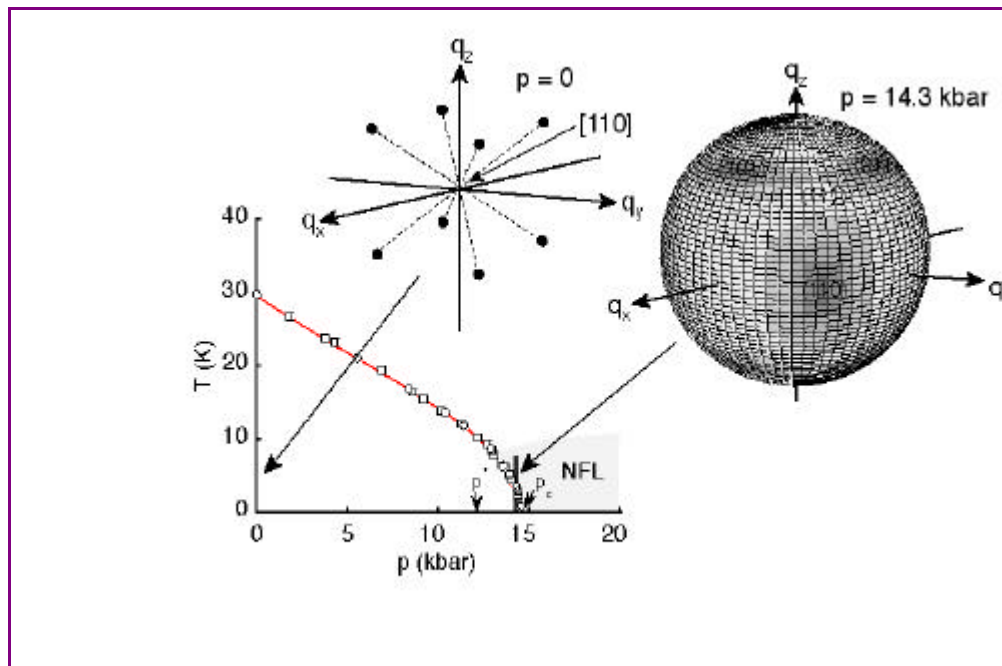
Figure 1. Schematic temperature T versus pressure p phase diagram of MnSi and qualitative illustration of the scattering intensity characteristic of the magnetic state. Data points of $T_C(p)$ are taken from reference [1]. Data were collected near the [110] lattice Bragg peak. At ambient pressure resolution limited magnetic satellites are observed at a distance $Q=0.0375$ Å^{-1}, characteristic of long range magnetic order. At high pressure intensity on a sphere of radius $Q=0.0422$ Å^{-1} is found with the highest intensity at <110> indicated by dark shading.

References

[1]   C. Pfleiderer et al., *Phys. Rev. B* **55** (1997) 8330.

[2]   C. Pfleiderer et al., *Nature* **414** (2001) 427.

[3]   Y. Ishikawa and M. Arai, *J. Phys. Soc. Jpn.*, **53** (1984) 2726.

[4]   B. Lebech in Recent Advances in Magnetism of Transition Metal Compounds, World Scientific, 167 (1993).

[5]   C. Pfleiderer, D. Reznik, L. Pintschovius and H. v. Löhneysen, submitted for publication.

[6]   A. N. Bogdanov and A. Hubert, *J. of Mag. Mag. Mat.* **138** (1994) 255.

[7]   C. Pfleiderer, Novel electronic states of magnetic metals, to appear in Modern Tracts of Physics, Springer, Heidelberg.

[8]   A. Schröder et al., *Nature* **407** (2001) 351.

[9]   A. Rosch et al., *Phys. Rev. Lett.* **79** (1997) 159

USING HOT NEUTRONS TO SPOT SMALL SOURCES OF MAGNETIC ANISOTROPY

M. Rotter[1], M. Doerr[1], A. Lindbaum[2], M. Loewenhaupt[1], B. Beuneu[3]

[1]Institute für Angewandte Physik (IAPD), Technische Universität Dresden, D-01062 Dresden, Germany
[2]Institut für Festkörperphysik (IFP), Technische Universität Wien, A-1040 Wien, Austria
[3]Laboratoire Léon Brillouin, CEA-CNRS, Saclay, 91191 Gif sur Yvette Cedex, France

What does happen, if the major source of magnetic anisotropy - the crystal field - is switched off ? Is there any other important source of anisotropy or will the system be magnetically isotropic despite its crystalline structure? These questions can be addressed by investigating Gadolinium (Gd) compounds by magnetic diffraction experiments.

Gd has a very large spin moment, but no orbital moment in its ground state ($L=0$), and therefore it is not sensitive to the crystal field. The isotropic interactions (such as RKKY exchange interactions etc.) dominate the magnetic properties and lead to ordering temperatures of more than 100 K for a large number of Gd compounds. The small but finite magnetic anisotropy of the $L=0$ rare earth compounds is topic of various speculations about it's origin: crystal field and exchange effects coming from higher multiplets, or dipole interaction? These sources of anisotropy can be tested by comparing models with experiments.

One of the key factors in such an investigation is the accurate determination of the moment direction in these compounds. Whereas the magnetic propagation is determined by the large isotropic interactions, the moment direction is determined by the small anisotropic interactions. A general treatment of anisotropic interactions has been given in [1] and this model can be directly used for the calculation of the dipolar anisotropy. If the propagation vector **t** of a magnetic compound has been determined from the diffraction data, it is possible to calculate that orientation of the magnetic moments in the ordered state that is favoured by the dipole interaction, and compare it to the experimental one.

However, in practice such an idea suffers a major drawback, because Gd has a very large absorption cross section for neutrons. But the absorption coefficient of Gd depends strongly on the neutron energy. At wavelengths below 0.06 nm, the absorption is small enough to enable an accurate determination of the moment direction by magnetic neutron diffraction experiments, due to the large moment of Gd. Most favourable systems, which can be investigated, are antiferromagnetic compounds.

Because it is installed on a hot-source, the 7C2 diffractometer for liquids of the LLB (neutron wavelength of 0.058 nm) is a powerful tool for such investigations, in spite of its low resolution. We have performed experiments on powdered samples of $GdAu_2Si_2$, $GdAu_2$, $GdAg_2$ and $GdCu_2In$ The absorption to signal ratio was reduced using a hollow cylinder geometry for the sample.
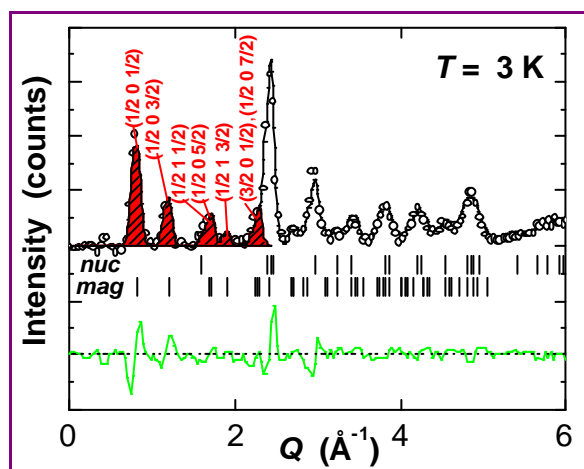
Figure 1. Neutron diffraction patterns of $GdAu_2Si_2$ at T= 3 K. Black line: calculated spectrum, green line: difference between calculated and measured intensity. The positions of nuclear peaks and the magnetic satellites with strong intensity are indicated by the vertical bars.

To give an example we discuss $GdAu_2Si_2$ in more detail. $GdAu_2Si_2$ orders (fig. 2) antiferromagnetically at the Néel Temperature $T_N = 12$ K [2]. Diffraction patterns were taken at 25 K and 3 K (fig. 1). The pattern at 25 K in the magnetically disordered state can be indexed according to the tetragonal $ThCr_2Si_2$ structure. At 3 K the best fit is obtained for a propagation vector $\mathbf{t} = (1/2\ 0\ 1/2)$ and a Gd moment of 6.2 μ_B/Gd oriented parallel to [010], i.e. perpendicular to the propagation vector. The influence of the classical dipole interaction was estimated by a calculation of the Fourier transform of the dipole interaction at the propagation vector $\mathbf{t}$. The largest eigenvalue corresponds to the moment direction [010], in agreement with the diffraction experiment

Taking the results of the 7C2 measurements as a basis, the model has been applied to a large number of other Gd systems using available data from literature. In most cases the observed magnetic anisotropy can be attributed to the dipole interaction. So our experiments indicate that in Gd systems all other interactions are isotropic to a very high degree of accuracy and that the small dipolar interaction determines the anisotropy of these systems. This is true for ferromagnets as well as for antiferromagnets. It is remarkable, that although the magnetic anisotropy of Gd compounds is much smaller than that of other rare earth compounds, it can be predicted with high accuracy from first principles.
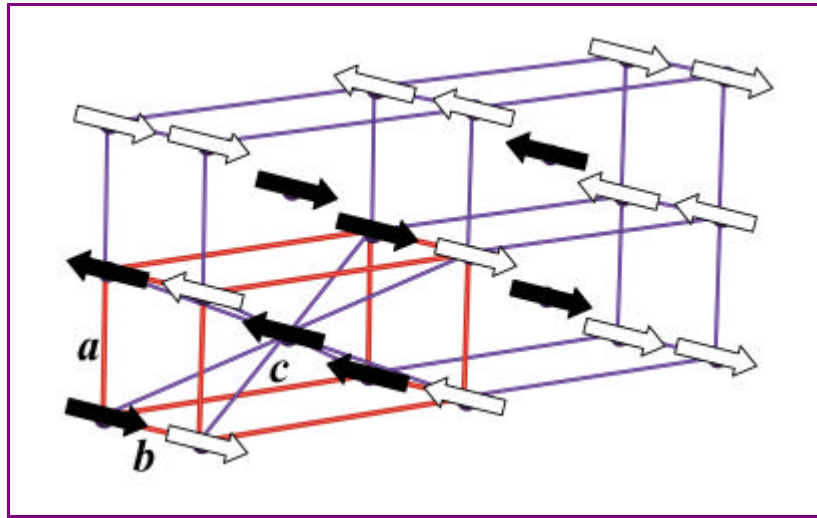
Figure 2. Magnetic unit cell of $GdAu_2Si_2$. Domain with the propagation $\mathbf{t} = (1/2\ 0\ 1/2)$ and magnetic moments parallel to [010] (due to the tetragonal symmetry there exist two domains). For clarity we show only the Gd sublattice.

References
[1] M. Rotter, M. Loewenhaupt, M. Doerr, A. Lindbaum, H. Michor, Phys Rev. B 64 (2001) 14402
[2] R. Mallik, E. V. Sampathkumaran, Phys. Rev. B 58 (1998) 9178

PHOTOINDUCED MOLECULAR SWITCHING STUDIED BY POLARISED NEUTRON DIFFRACTION

A. Goujon[1], B. Gillon[1], A. Gukasov[1], J. Jeftic[2], Q. Nau[1,2], E. Codjovi[3], F. Varret[3]

[1] Laboratoire Léon Brillouin (CEA-CNRS), CEA-Saclay, 91191 Gif-sur-Yvette cedex, France
[2] Laboratoire Ecole Nationale de Chimie de Rennes (ENSCR), UMR CNRS 6052, Av. du Général Leclerc, Campus de Beaulieu,35700 Rennes.
[3] Laboratoire d'Optique et de Magnétisme de Versailles (LMOV), CNRS-Université de Versailles UMR 8634, 45 Avenue des Etats Unis,78035 Versailles.

The design of molecules that could be utilised for information storage is one of the main challenge in molecular material science and optical switching is one of the most intense aeras of interest in memory molecules.

Spin crossover solids represent a promising example of photo-switchable materials, studied for future applications as optical memories or numerical displays [1]. They contain an octahedrally coordinated transition metal ion with the $3d^n$ electronic configuration and can cross over between a low spin (LS) and a high spin (HS) state. The flip between the two states usually occurs with a temperature change, under pressure or under light illumination. Spin crossover compounds containing the Fe^{2+} ion have a LS and a HS spin states characterized by spins of S=0 (diamagnetic) and S=2 (paramagnetic). Photo-excitation at low temperature, with a suitable light wavelength, can provide a switching of the system to a photoindcued metastable state having an extremely long lifetime at low temperatures. Therefore the effect is called Light Induced Excited Spin State Trapping (LIESST).[2] The photo-process involves, either a metal to ligand charge transfer, or d-d transitions. For typical Fe^{2+} compounds, absorption bands for the LS$\rightarrow$HS process are located around ~500 (Metal Ligand Charge Transfer), 550 (d-d) respectively. The reverse process (HS$\rightarrow$LS) occurs by irradiation at ~750 nm, with a lower efficency, due to branching ratio 4:1 for the direct and reverse processes, respectively.

Polarised neutron diffraction is a powerful tool to study the magnetisation densities in crystals and has never been applied so far to the study of photo-induced magnetic states. Figure 1 shows the new experimental setup designed to carry out "in situ" photo-excitation experiments, we have developed for this purpose. The photo-switching process of $[Fe(ptz)_6](BF_4)_2$ compound was observed by polarised neutron diffraction measurements (PND) as shown on Figure 2. The moment of 4.05(7) $_B$

on the iron site (with ^{2} = 5.11) obtained by refinement is very close to the theoretical value of the Fe^{2+} moment at saturation (S=2). This evidences a complete photo-transformation of the crystal.
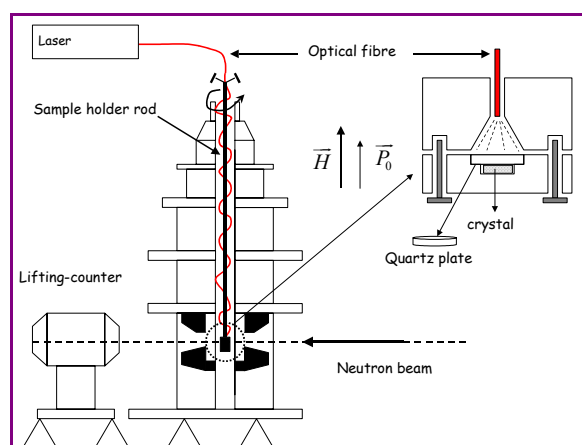
Figure 1 Schematic experimental setup of the polarized neutron diffractometer. In the inset, the sample holder allowing light irradiation is sketched. P_0 corresponds to the neutron polarisation direction .
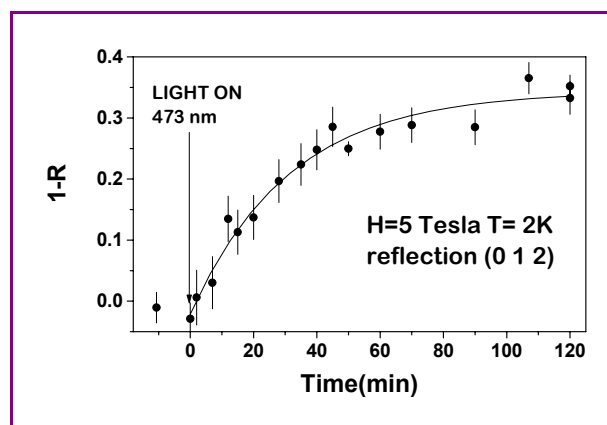
Figure 2 Kinetics of the photo-excitation of $[Fe(ptz)_6](BF_4)_2$. at 473 nm, 2 K, 5 T. Flipping ratio of (1 0 2) reflection with the magnetic field parallel to the [001] direction as a function of time. The first point is measured before illumination and corresponds to a reference point. The solid line is a guide for the eyes.

In Figure 3, the temperature dependence of the magnetisation in the photo-excited state of the crystal, measured under different fields, is displayed. Experimental curves were well fitted with a model that takes into account the magnetic anisotropy due to crystal field and spin-orbit coupling on the ^5D state of high spin Fe^{2+} in trigonal symmetry . For each field and on warming the sample up to 70 K, the relaxation of the excited electronic state is also observed at ~ 55-60 K.
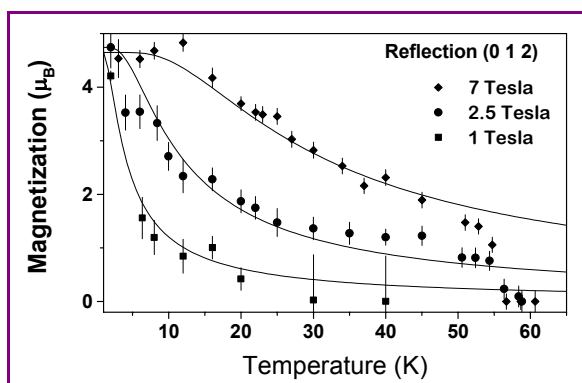
Figure 3   Magnetic data for the thermal relaxation decay, in the dark, of the photo-excited state, created by illumination at   = 473 nm, P = 3 mW/cm^{-2}, t = 1 h 30, recorded for different values of the magnetic field : 1, 2.5, 7 T. The temperature sweeping rate is ~ 0.1 K/min. Solid line is computed using the static Ising model

A data set of flipping ratios, of 67 strongest unique reflections has been recorded for the photoexcited electronic state at 2K and 5 Tesla. The magnetic structure factors of all measured reflections were obtained using   the F_N derived from X-ray diffraction structural parameters.The distribution of magnetisation density in the unit cell was reconstructed from the $F_M(\mathbf{Q})$ data, using a multipole model refinement. The radial expansion and the first monopole population were refined for the Fe and N atoms. No significant density was

observed in the refinement procedure on the nitrogen atoms. The photo-induced magnetisation density is presented in Figure 4 and Fe^{2+} magnetic form factor have been obtained
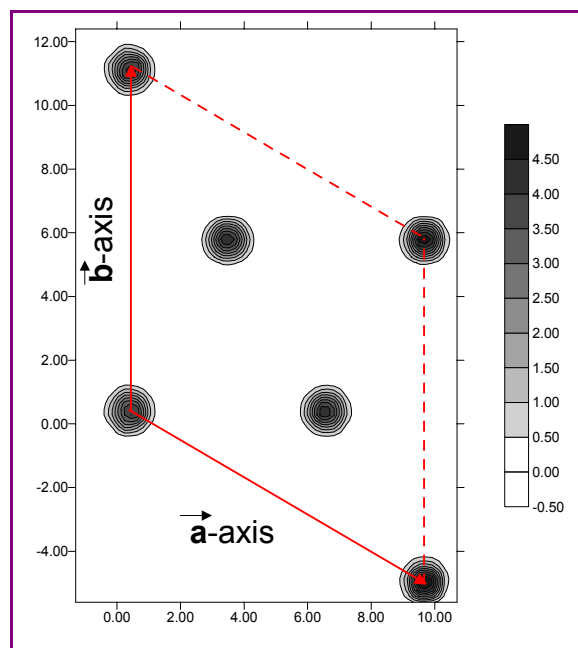
Figure 4. Reconstructed magnetisation density map of the photo-induced state of $[Fe(ptz)_6](BF_4)_2$ at 2K, 5T, projected along the c-axis.

The large possibilities of PND in providing information on the magnetic coupling scheme, the spin density distribution and spin delocalisation effects could be useful for other photo-magnetic crystals. PND investigations of photoinduced state could reveal to be very informative in a variety of systems, including cyanometalate-based magnets,[3] spin crossover complexes [4], diluted magnetic semiconductors[5], doped manganites[6], and spinel ferrite films   where photoinduced magnetic effects have been evidenced.

References
[1] Kahn O., La Recherche **262** (1994) 160.
[2] Decurtins S., Gütlich P., Hasselbach M. K., Spiering H., and Hauser A., Inorg. Chem. **24** (1985) 2174.
[3] Sato O., Iyoda T., Fujishima A., and Hashimoto K. , Science **272** (1996) 704.
[4] Ogawa Y., Koshihara S., Koshino K. , Ogawa T. , Urano C. , and Takagi H., Phys. Rev. Lett. **84** (2000) 3181.
[5] Koshihara S., Oiwa A., Hirasawa M., Katsumoto S., Iye Y., Urano C. , Takagi H., and Munekata H. ,
      Phys. Rev. Lett. **78**(1997) 4617.
[6] Matsuda K., Machida A., Moritomo Y., and Nakamura A. , Phys. Rev. B **58** (1998) 4023.

CREATION AND OBSERVATION OF POLARISATION DOMAINS: A NEW TOOL IN SANS

E. Leymarie, H. Glättli

Laboratoire Léon Brillouin (CEA-CNRS), CEA-Saclay, 91191 Gif sur Yvette

Due to the strong spin dependence of thermal neutron scattering on protons, the scattering length density can be changed appreciably by polarising the protons in materials which contain hydrogen at sufficient concentration . By the method of dynamic nuclear polarisation (DNP) large positive and negative proton polarisations can be established in organic solvents like glycerol-H_2O mixtures, ideally suited as solvents for biomolecules, or in toluene, a standard solvent for polymers. In the past uniform proton (and deuteron) polarisations were used to change the scattering contrast between parts of a sample with different hydrogen density [1,2].

In the DNP method the thermal equilibrium polarisation of dilute paramagnetic centres is transferred to nearby nuclei by microwave irradiation close to the electron paramagnetic resonance (EPR) frequency, taking advantage of the electron-nucleus dipolar interaction. This interaction falls off with the third power of the distance between electron and nuclear moments, so nuclei close to a paramagnetic centre are polarised first while far away (bulk) nuclei rely on spin diffusion to reach equilibrium in a reasonable time. A very useful property of DNP is the fact that either positive or negative polarisations can be selected by an appropriate choice of the irradiating microwave frequency.

The large polarisations of the paramagnetic centres are generally obtained in fields of a few teslas at liquid helium temperatures. This implies the use of frozen samples.

For times that are short compared to spin diffusion the DNP process can create polarisation gradients. They are too short-lived, of the order of seconds, to collect SANS spectra with sufficient precision in one polarisation cycle.

We devised a time resolved acquisition scheme which allows the addition of the corresponding time frames of many identical cycles in a stroboscopic way [3]. The principle of the method is to switch the microwave frequency periodically from positive to negative polarisation.

As an example fig. 1 shows the SANS spectra at different times during the whole cycle of positive and negative polarisation obtained from a sample of 98% deuterated solution containing 5×10^{19} protiated Cr^V complexes/cm^3 [4].
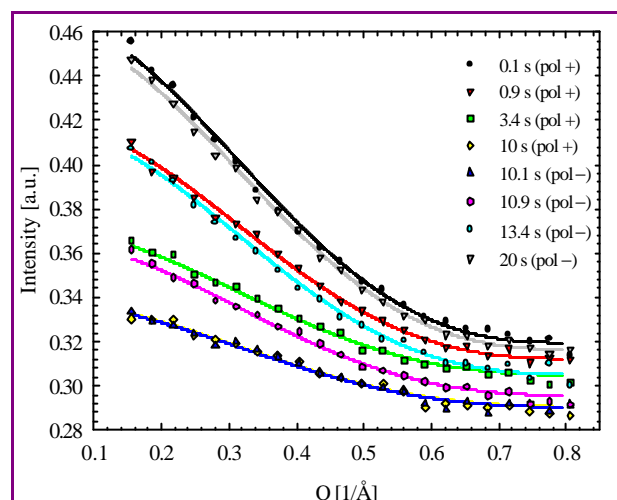
Figure 1. Time-dependent SANS

In this particular sample the scattering length density of the solvent is very weakly dependent on polarisation, so that the coherently scattered neutron intensity depends only on the polarisation of the 20 protons of the Cr^V complexes. Their polarisation could thus be inferred by fitting the SANS spectra of each time frame with a model function for the paramagnetic complex. NMR measurements, insensitive to these close protons, recorded simultaneously the evolution of the bulk proton polarisation.

The difference in the time-evolution of the polarisation between close and bulk protons shown in fig. 2 reflects the mechanism of DNP: a strong initial gradient develops due to a fast polarisation of the protons close to the paramagnetic centre which then spreads out to the bulk with a slower rate.

Polarised proton domains have been observed around several different paramagnetic centers (EHBA-Cr^V, "waxy"DPPH) and in different solvents (glycerol-water with up to 12% ^1H and polystyrene). Different cycling schemes, creating different initial conditions have also been used.
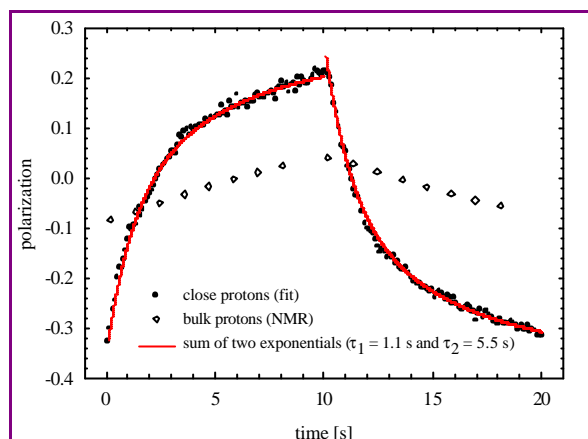
Figure 2. Close proton polarisation deduced from the SANS fit and bulk proton polarisation recorded by NMR

They all confirm the existence of transient polarization domains around paramagnetic centres. These observations open the possibility to increase strongly and selectively the contrast for neutron scattering from paramagnetic centres. For example, the scattering contrast of the 20 protons of the Cr^V complex polarised to 50% in a non-polarised protiated solvent would be two orders of magnitude larger than the magnetic scattering of the complex alone.

It could be possible to locate paramagnetic centres in macromolecules, like *e.g.* relatively stable radicals appearing in biologically active intermediates of enzymes (provided they can be frozen-in at low temperatures). By appropriate spin labelling it could also be possible to investigate selectively details of the structure of macromolecules. Preliminary results have been obtained from catalase samples containing tyrolsyl radicals.

Site selectivity in still another way could be obtained in samples containing several species of paramagnetic centres. Owing to their different EPR frequencies, polarised proton domains will only be established around those centres tuned to DNP.

All experiments have been performed on the PAPOL polarised neutron SANS instrument using our polarising set-up and at PSI and ILL (D22) with a similar PSI equipment in collaboration with scientists from PSI, ILL, IBS and TU Munich.

References

[1] R.Willumeit, N. Burkhardt, G. Diedrich, J. Zhao, K.H. Nierhaus and H.B. Stuhrmann, J.Mol.Struct. **383**, (1996), 201
[2] M.G.D. van der Grinten, H. Glättli and M. Pinot, Neutron News **6**, (1995), 18
[3] E.Leymarie, thèse, Université de Paris Sud, (2002)
[4] B. van den Brandt, H. Glättli, I. Grillo, P. Hautle, H. Jouve, J. Kohlbrecher, J.A. Konter, E. Leymarie, S. Mango, R. May, H.B. Stuhrmann and O. Zimmer, Europhys.Lett., **59,** 62, (2002)

POLARISED NEUTRON REFLECTOMETRY FOR GMR SENSORS OPTIMIZATION

M. Pannetier[2], T.D. Doan[2], F. Ott[1], S. Berger[2], N. Persat[3] and C. Fermon[2]

[1]Laboratoire Léon Brillouin (CEA/CNRS), CEA-Saclay, 91191 Gif sur Yvette, France
[2]DSM/DRECAM/SPEC, CEA Saclay, 91191 Gif sur Yvette, France
[3]OnStream MST B.V. Lodewijkstraat 1, 5652 AC Eindhoven, The Netherlands

The optimisation of multilayer stacks for magnetic sensors and more sophisticated spin electronics devices will strongly benefit from the precise knowledge of the magnetic properties of each layer with their behaviour as a function of the applied field. Polarised Neutron Reflectometry (PNR) allows very precise vectorial measurements of magnetic moments but that technique suffers from its relatively low intensity. Polarised neutron reflectometry with polarisation analysis (PNRPA) has proved to be a useful tool to probe in-depth vectorial magnetic profiles [1] and can be used for selective hysteresis loops [2]. We present results obtained on GMR spin valves. We show how PNRPA allows to determine with a high precision, the thickness and magnetic moment configuration and reveals the mechanism of reversal of the soft magnetic layer. This piece of information has permitted the optimisation of very low noise GMR sensors.

GMR sensors description

The studied GMR spin valve has a rather standard composition : SiO2 / Ta(5) / NiFe(3.7) / CoFe(1.2) / Cu(2.4) / CoFe(2.4) / MnPt(35) / Ta(10). The soft layer (NiFe(3.7) / CoFe(1.2)) can rotate in a field of several Oe as the hard layer (CoFe(2.4)/MnPt(35)) is blocked for fields larger than 1T.

The GMR is built with an easy axis of the soft layer (created by an applied external field during the growth) perpendicular to the hard axis. Figure 1 shows SQUID measurements on a 9x10mm square sample. This sample has been chosen among others because it exhibits a larger coercivity of the soft layer and allows us to separate well the two directions of the varying field.

The GMR effect with current flowing parallel to the layer is increased when the thicknesses of the different layers are smaller. However, a too small NiFe layer gives rather bad GMR spin valves [6]. This GMR exhibit a reasonable effect of 9.18% and a very low 1/f noise. 1/f noise of our optimised GMR sensors is lower in the most sensitive part than in previous works [5]. The reason for the good behaviour is the absence of domain formation during reversal process independently of the direction of the hard layer. In the presence of domains, 1/f noise can be several order of magnitude larger.
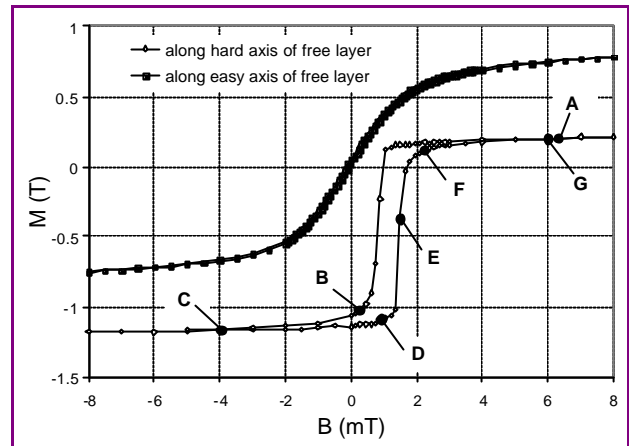
Figure 1. SQUID measurements of the spin-valve GMR01. The anti-ferromagnetic layer is aligned perpendicular to the easy axis of the free layer.

Neutron reflectivity results

In order to follow the magnetic configuration as a function of the magnetic field, we have used the procedure described in reference [2]. A first measurement has been performed in a magnetic saturating field. The hard and soft layers are aligned. Spin-flip reflectivity is then very low due to the absence of non collinear magnetic moments.
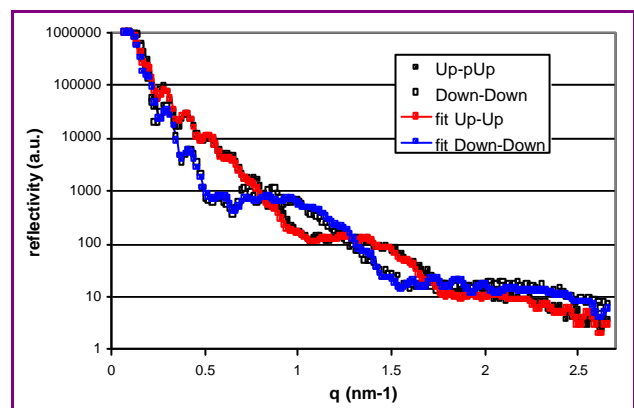
Figure 2. Reflectivity of the system GMR01 in a field of 15mT. The curves given correspond to an anti-ferromagnetic arrangement of the two CoFe layers (point A of figure 1). Black squares : R++, white squares R--, best fit in black line.

The reflectivity of the system in this magnetic state is given in figure 2. Table 1 summarises the parameters obtained from the fitting of the different reflectivity curves. We measure a very low roughness ($< 0.5\,\mathrm{nm}$ RMS). We have then followed the magnetic configuration as a function of the applied magnetic field. The reflectivities have been measured for a small set of angles as a function of the applied magnetic field (see figure 3a).

Then, using the parameters deduced from the saturated state, these reflectivities have been adjusted by varying a single parameter: the magnetic direction of the soft layer. It appears during the fit that a homogeneous magnetic configuration in the NiFe layer cannot account for the measured reflectivities.
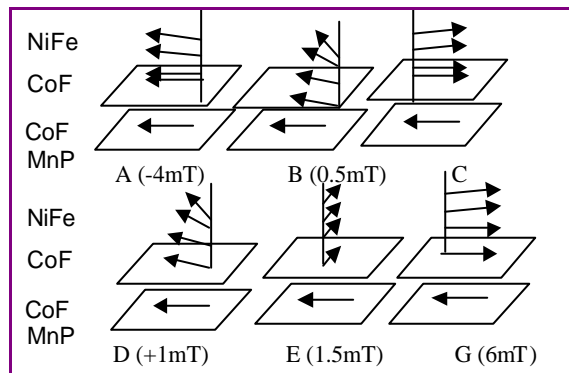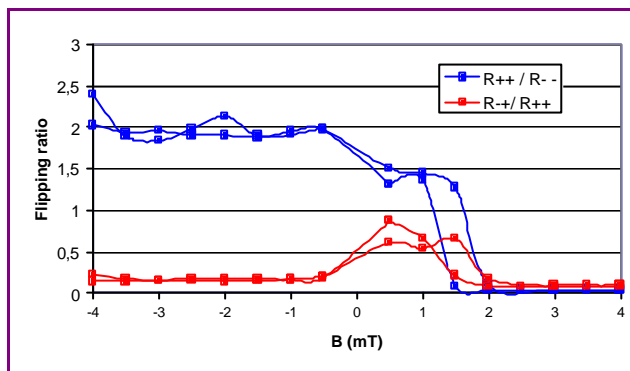
Figure 3 : (a) evolution of the reflectivity R^{++}/R^{--} and R^{+-}/R^{++} (x10) at $q=0.53\,\mathrm{nm}^{-1}$ as a function of the applied magnetic field; (b) schematics of the evolution of the magnetisation direction of the three magnetic layers as a function of the applied magnetic field. The letters refer to the position on the hysteresis loop (see fig. 1).

One needs to consider that a small magnetisation rotation with respect to the CoFe layer occurs inside the NiFe layer. The fit of the curves have been made by cutting the NiFe layer into 3 homogeneous layers of 1.06 nm. The limited intensity in the neutron experiments does not allow a better precision of the NiFe rotation.

The evolution of the magnetic configuration of the GMR system is given in figure 3b. The small rotation of the NiFe, almost non visible in the magnetisation curve, is clearly revealed by the neutron reflectometry curves.

Even at 8 mT, the free layer appears to be not fully aligned with the external magnetic field. This effect appears clearly on the SQUID measurements under 6mT, (points A and C on figure 1) but after A and C a small rotation still exists which is non detectable by SQUID measurements. The effect of that rotation is to induce a coherent rotation of the free layer, beginning from the bottom (Ta layer) to the top (CoFe layer) during the reversal. This effect avoids any domain formation and therefore leads to low frequency magnetic noise in the sensitive region of the GMR. The maximal angle of rotation of the magnetisation in NiFe is fixed by a competition between the anisotropy and the exchange. This gives a rotation of about 0.5° for 0.1 nm (like in NiFe domain walls) and then about 25° for the total NiFe layer in reasonable agreement with the maximum rotation observed in the layer (30°± 5°). Off-specular neutron scattering did not reveal the presence of magnetic domains. The reflectivity values are also adjusted by using the full nominal moments of the layers suggesting that there is no significant domain formation even in unpatterned layers.

Conclusion

Through the particular case of the optimisation of 1/f noise of GMR sensors by avoiding domain formation, we have shown how precise can be the determination of the magnetic configuration using PNRPA even on present sources. Very small rotations of magnetic moments in a specific layer can be determined allowing an in depth understanding of the magnetic evolution of the system under an applied field. The building of third generation neutron sources like SNS will allow us to gain about two order of magnitude in flux and then achieve depth resolution of about 0.2 nm-0.4 nm even in rather complex system with several magnetic layers.

References
[1] S.J. Blundell et al, Phys. Rev. B **46** (1992) 3391.
[2] C. Fermon et al, Physica B **241-243** (1998) 1055.
[3] J.M.Slaughter et al, J. Appl. Phys. **85** (1999) 4451.
[4] H.T. Hardner et al, IEEE Trans. Mag. **35** p2592 (1999), D.S. Reed and al, IEEE Trans. Mag. **37** p2 M. Xiao. IEEE Trans. Mag. **36** (2000) 2593.

SPIN-WAVE IN LAYERS AND HETEROSTRUCTURES

B. Hennion[1] and W. Szuszkiewicz[2]

[1]Laboratoire Léon Brillouin (CEA-CNRS), CEA-Saclay, 91191 Gif-sur-Yvette cedex, France
[2]Institute of Physics, Polish Academy of Sciences, AI. Lotnikow .3246, 0,2-68 Warsaw, Poland

There is a renewed interest raised on diluted magnetic semiconductors, because of potential applications in the field of spintronics. These systems are basically obtained by the substitution of cations by Mn^{2+} in semiconductors based on II-VI compounds. They have the zinc blende (ZB) structure, and present magnetic properties depending on their composition. Superlattices obtained by sandwishing magnetic layers and non-magnetic spacers may be obtained in a large range of composition and thickness.

The understanding of the magnetic properties of these systems have given rise to a lot of experimental and theoretical works. An appealing suggestion is to measure the spin-wave dispersion of a parent compound (MnS, MnSe, or MnTe) to deduce the dominant exchange interactions and anisotropies. Unfortunately, these compounds have no stable ZB structure and only recently, molecular beam epitaxy (MBE) gave the opportunity to get ZB MnTe as a pure system or as layers inside heterostructures. This means quite small available sample volumes, but the progressess realized on triple-axis spectrometers (TAS) allowed us to carry out spin-waves measurements on such systems, as reported here.

MBE-grown MnTe

Below $T_N \approx 65$ K, MnTe becomes a type-III antiferromagnetic (AF) [1]. This is expected in face-centered-cubic magnetic compounds when dominant nearest and next-nearest neighbors exchange are both antiferromagnetic.
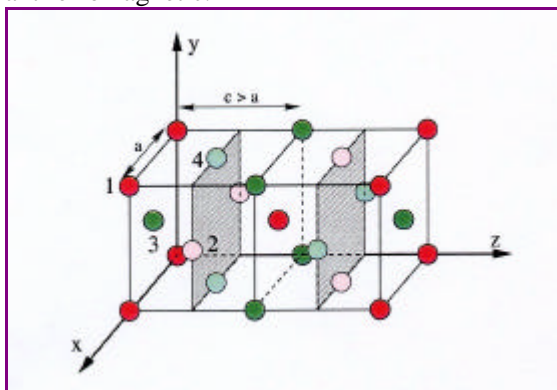
Figure 1. Magnetic structure of AF-III MnTe. Only positions of magnetic Mn atoms are shown. Spins **1** and **3** are antiparallel, as are spins **2** and **4**. When the structure is collinear, spins **1** and **2** are parallel, while in the non-collinear structure proposed by Keffer spins **1** and **2** are perpendicular.

The magnetic transition is of first order and associated to a tetragonal lattice distortion, with c > a. The magnetic cell may be defined as a body centered tetragonal cell, with a doubling of the nuclear cell along c. As seen on figure 1, the structure consists of a stacking of AF planes perpendicular to the c axis, with an arrangement such as A B -A -B. The existence of equivalent axes for the elongation leads to nuclear and magnetic domains. The strain due to may the mismatch between the MnTe layer and the buffer layer (ZnTe or CdTe) interposed on the GaAs substrate, yields inequivalent domain populations.

Several issues have been addressed concerning the magnetic properties of ZB MnTe: 1) Collinearity of the structure: Taking a Mn moment of an A plane, the resultant interactions of the Mn moments of the B planes is null. Hence, any canting angle between sublattices A and B is allowed, up to 90 degrees as proposed by Keffer for β-MnS. 2) Exchange interactions: all exchanges are super-exchanges via Te anions. Theoretical calculations suggest that distant neighbors up to the fourth ones should yield significant contributions. 3) Anisotropy: a single-site anisotropy should be present to force the spin direction in the plane. But no significant dipolar terms are expected. Moreover, the non-centrosymmetry of the structure allows anisotropic exchange, such as the Dialoshinski-Moriya exchange, so inter-site anisotropy has to be considered.
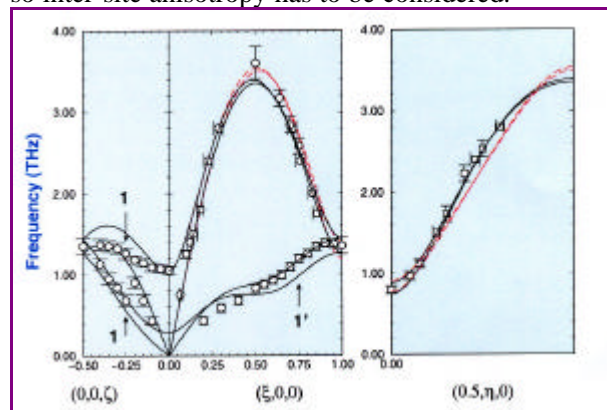
Figure 2. Spin-wave modes of MnTe measured at T $\approx$ 15 K, with calculated curves discussed m Ref. 2.

Samples, up to 6 μm thick, have been obtained at the Institute of Physics of Warsaw (Poland). With a surface of about 3 cm^2, this corresponds to a sample volume of about 1.8 mm^3, but the maximum volume of a magnetic domain was about 0.7 mm^3.

Inelastic neutron scattering measurements have been carried out on the former 1T TAS (before its move on 2T) and on the new 2T design. The dispersion measured at low temperature are reported in Fig. 2, together with calculated curves deduced from a model Hamiltonian used to describe the system. Details on the measurements and the data analysis may be found in Ref. 2.

The main conclusions may be summarized as it follows: 1) The observed spin-wave dispersion is only compatible with a collinear or a very weakly canted structure. 2) Exchange interactions up to the fourth neighbours have to be considered and numerical values have been deduced from the measurements. 3) A planar single-site anisotropy may account for the spin-wave gap at the origin, but induces a mode-splitting along the Brillouin zone, too large when compared to the experiment (see Fig. 2). 4) A Dzialoshinski-Moriya term does not provide a good answer to describe the inter-site anisotropy. Anyhow such an anisotropy is clearly needed for a better account of the experimental results.

Furthermore an unusual damping, illustrated on Fig. 3, has been observed when increasing the temperature. The explanation of such a behavior is still to be found. It might be a consequence of the large frustration inherent to the type-III AF structure when departing from its fundamental state, or to an unusal coupling with the crystalline lattice, as all magnetic exchanges are mediated by Te cations.
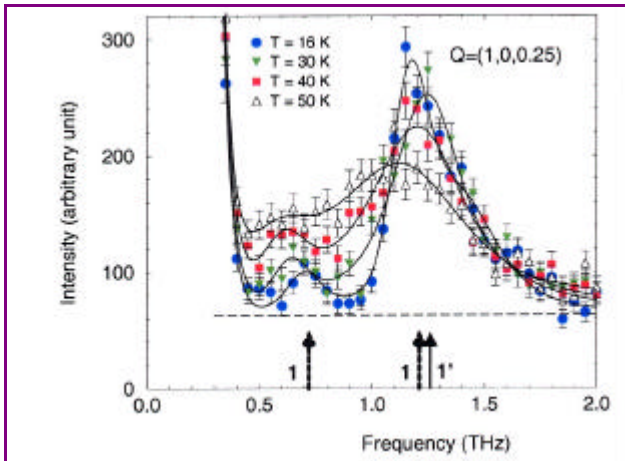
Figure 3. Temperature dependence of the scattering measured at Q=(0.25,0,1). Domain effects superimpose points **1** and **1'** marked in Fig. 2.

MnTe/ZnTe superlattices

At low temperature, each MnTe layer still presents the AF-III structure. A long-range coherence between MnTe layers, through the non-magnetic spacer, is observed up to a ZnTe thickness of about 20 Å. This is not expected for this kind of hetero-structure. Superlattices MnTe(m)/ZnTe(n), where m and n are the number of monolayers in a layer, have been provided by the Institute of Physics of Warsaw. Two series, with m=15 and n=3,4, or 5 and with m=20 and
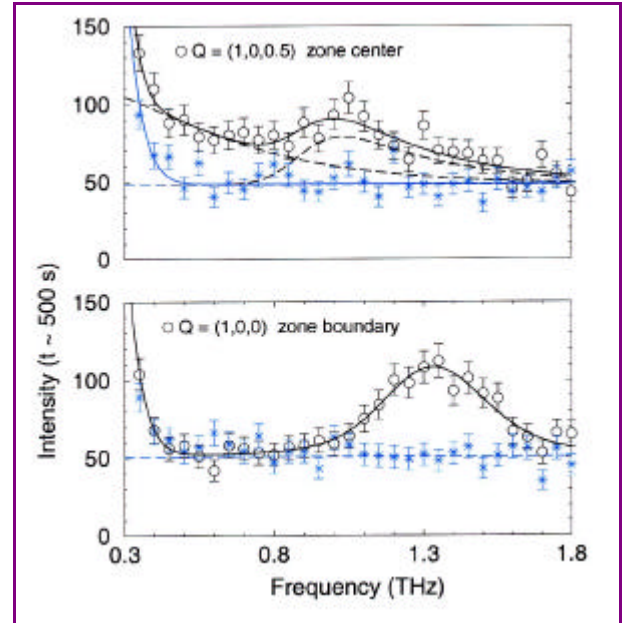
Figure 4. Zone center (top) and zone boundary (bottom) measurements evidencing spin-wave excitations in MnTe(20)/ZnTe(6). Star symbols correspond to background measurements obtained after a 90 degrees rotation of the sample.

n=4,6,8, or 10, have been investigated. Diffraction measurements confirmed a coherence up to $\approx$ 1200 Å for the 15-3 sample, but still of $\approx$ 350 Å in the 20-6 sample, the interlayer distance being $\approx$ 3.2 Å. The most surprising is that this coherence implies the preservation of the phase between MnTe layers through the non-magnetic ZnTe layers, whatsoever the number of monolayers in the layers. The thickness of about 1 μm of the samples corresponded to an overall magnetic volume of about 0.25 mm^3. On the new 2T TAS, we nevertheless succeeded to observe the spin-wave modes in the Q-direction corresponding to a propagation along the stacking axis of the superlattice. Measurements at the zone center and boundary are reported in Fig. 4. Magnetic excitations have been observed in the whole intermediate range. Their analysis is in progress.

References

[1] T. M. Giebultowicz, P. Klosowski, N. Samarth, H. Luo, J. K. Furdyna, and J. Rhyne, Phys. Rev. B **48** (1993) 12817.
[2] B. Hennion, W. Szuszkiewicz, E. Dynowska, E. Janik, and T. Wojtowicz, Phys. Rev. B **66** (2002) 22442

MAGNETISM AND SUPERCONDUCTIVITY

POLARISED GRAZING INCIDENCE DIFFRACTION AS AN OPTION ON EROS FOR THE STUDY OF THIN MAGNETIC FILMS

T.-D. Doan, F. Ott, A. Menelle

Laboratoire Léon Brillouin (CEA-CNRS), CEA-Saclay, 91191 Gif-sur-Yvette cedex, France
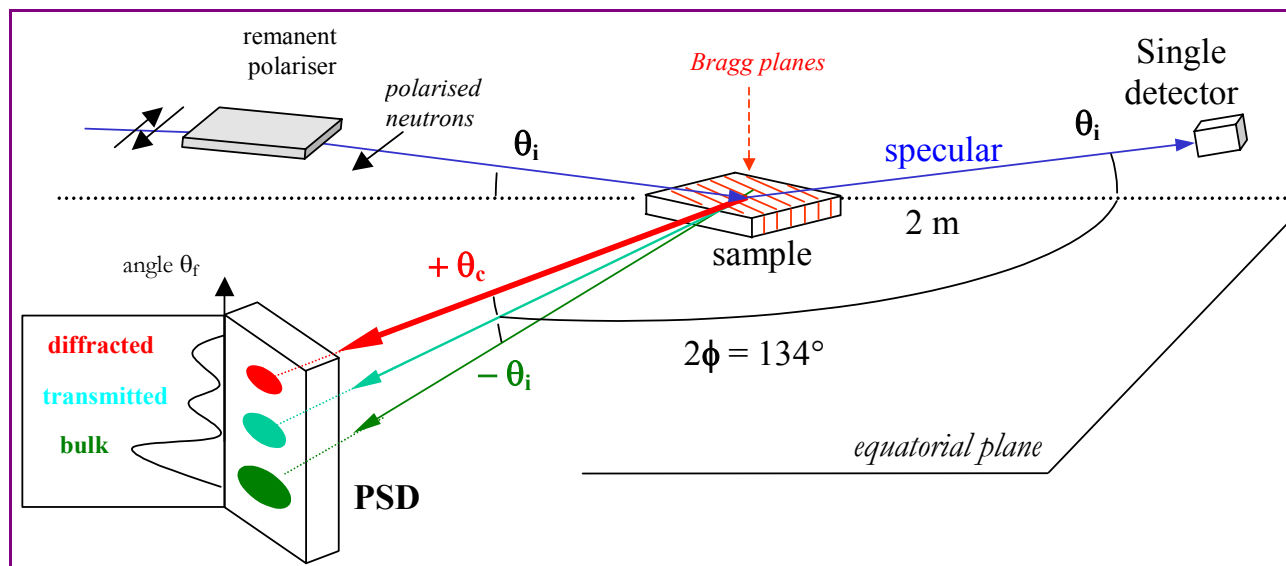
Figure 1. Experimental setup for polarised GID

A surface diffractometer has been recently installed as an option at the LLB on the reflectometer EROS. This new instrument is dedicated to the study of the surface crystallographic and magnetic structure of thin films.

The diffractometer can work in three modes i) in full guide spectrum (Laue-type configuration), ii) in Time of Flight and iii) in monochromatic beam. This configuration are unique and permits an easy sample alignement procedure.

Compared to the reflectometry setup several add-ons were developed for the grazing inicidence diffractomer. The add-ons include a compact goniometric table, a remanent polarizer, a monochromatic mirror, a sample horizontal slit (varying from 20 μm to 1 mm), a sample holder with a permanent magnetic field applied in various in-plane directions and a linear PSD.

Electronics were also added to control the different setup elements. The whole experimental is sketched in Figure 1.

Hence the instrument is designed to provide a polarised beam neutron. The sample in mounted horizontally on a goniometric table

The diffraction signals are detected by a PSD placed in the equatorial plane at a fixed angle 2ϕ. According to the Bragg's law: $\lambda = 2d_{hkl} \sin\phi$ (as the angle ϕ is fixed) the useful wavelength is selected by the in-plane cell parameters of the sample (d_{hkl}). First experiments were applied to a epitaxial thin film of $La_{0.7}Sr_{0.3}MnO_3$ (LSMO) deposited on $SrTiO_3$. The sample is 20nm thick and its surface is 1cm^2. The LSMO compound is ferromagnetic at room temperature and the thin film magnetic moment was measured by reflectivity at 1 μB per unit cell.

The alignment of the sample is performed using the Laue configuration and then the diffracted wavelengths are identified in a Time of Flight measurement. In our case the diffraction signals of the LSMO compound are expected at d_{200}=0.39nm which corresponds to a diffraction wavelength of 0.7nm.
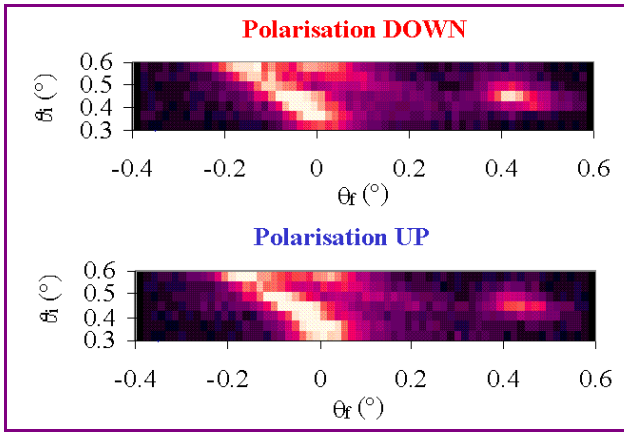
Figure 2. Intensity observed in a linear scale on the PSD as a function of the incident angle (θ_i) and the output angle (θ_f).

Figure 2 shows the signals observed on the PSD for up and down neutron polarizations in linear scale at l=0.7nm in the θ_i-θ_f plane.

At the starting incident angle θ_i=0.3° one can observe the diffraction due to the substrate, this signal is observed for all θ_i values. As the incident angle is increased the diffraction signal from the film (noted Reflected) arises ($\theta_f \sim 0.41°$) which is in a good agreement with the expected value for the critical angle (θ_c). The film diffraction signal is maximum at the critical angle and as the incident angle increases its intensity is strongly decreased. For $\theta_i > \theta_c$ a third feature is observed and it corresponds to the transmitted signal (noted Transmitted). Its angular position is narrowing the substrate signal as the incident angle increases.

A cut at θ_i=0.4° ($\sim\theta_c$) is shown in Figure 3 to explicit the magnetic contrast. A clear difference in intensity is observed as function of the neutron polarization. The magnetic contrast defined as the ratio $I_{(DO)}/I_{(UP)} \sim 1.7$.
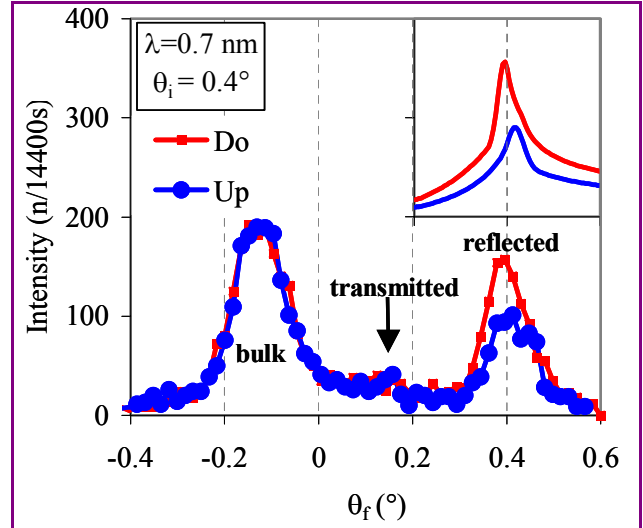
Figure 3. Measured intensity as function of the neutron polarization for θ_i=0.4°. Inset shows the calculations for the magnetic contrast (see text).

Numerical simulations were developed under Delphi in order to calculate the theoretical intensity expected for the reflected signal. The result of these calculations is shown as an insert in Figure 3. The magnetic contrast is well reproduced. One can note that the measured signal width is larger than the simulated one. This feature is under investigation but could not be explained by instrumental or sample divergences.

As a conclusion the grazing incidence neutron diffractometer has shown the feasibility of this technique applied to the study of thin magnetic films. This is the first result of such a measurement on very thin magnetic oxide film. Further improvements of the instrument will include a monochromatic polarizer and 2D PSD. The instrument is included in the further intrumental development plan of the LLB (CAP2010).
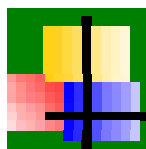
3 - MATERIALS SCIENCE

Materials science is a scientific field at the crossroads of physics, chemistry and engineering sciences, which aims at understanding how parameters such as chemical composition, atomic structure and microstructure determine the macroscopic properties of complex solid systems (alloys, ceramics, composite materials, polymers, geological materials...). The scientific repercussions of this work have short-term consequences on the applications and interest industrial research.

Neutron radiation proves to be an ideal probe to analyse the structure of many materials because of the weak absorption of neutrons, allowing analyses on large volumes and in complex or extreme conditions (temperature, loading...), and because of the advantageous neutron-matter interaction to differentiate some chemical elements. The activity in materials science developed at the LLB are focussed on the analysis of the residual stresses including an approach with industrial needs, but also a fundamental character in particular through the analysis of the mechanical behaviour of micro-heterogeneous materials, the study of crystallographic textures, the analysis of structural heterogeneities, the mechanisms of martensitic phase transitions and the phenomena of precipitation as well as ageing in metal alloys.

1. RESIDUAL STRESSES

The residual stresses present in a material have a considerable influence on its mechanical properties, such as hardness and mechanical resistance, tenacity or fatigue strength. Neutron diffraction is a powerful tool to determine in a non-destructive way the internal stresses in a massive crystalline material. The principle of the technique is the use of the crystal lattice as a strain probe at the atomic scale, allowing to map the strain distribution with a submillimeter space resolution. The stresses are then calculated from the measured strains, applying the linear elasticity laws. At the LLB, the "DIANE" (G5.2) diffractometer installed on the cold neutron channel G5, is dedicated to stress measurements. It has been built in collaboration with INFM (Italy). The stress activity developed at the LLB, at the border of technological interest studies and of research in the field of physical metallurgy, is led in several directions:
- Studies or expertises, in relation with problems encountered by the industrialists;
- Mechanics of heterogeneous materials;
- Development of the peak broadening analysis.

The activity of LLB in Engineering Sciences has significantly increased since the last years. Concerning the residual stresses, several industrial problems were studied, in general within the framework of contracts, or by the means of European programs (in particular TRAINSS).

TRAINSS network and residual stress in metal-matrix composites
(M. Ceretti, R. Levy, A. Menelle, LLB ; A. Lodini, University of Reims Champagne-Ardenne)

Among the main **industrial collaborations** of the 2001-2002 period, let us mention the work carried out with SNECMA. This study concerns Ti-SiC blings considered for replacing the discs of compressors by SNECMA Moteurs. In this composite material, the residual thermal stresses, resulting from the differences in thermal expansion coefficient between the two phases, can have significant consequences during in-service operation. Neutron diffraction makes it possible to separately determine these stresses in each phase of the composite, and in-depth in a non-destructive way on the whole ring. The measurements were performed on this component just after its elaboration and after fatigue tests at 20°C. They showed that the Ti matrix presents, on all the thickness, a homogeneous state of stresses in tension and that the SiC reinforcement is in compression (490 ± 40 MPa and -920 ± 80 MPa respectively for the circumferential stress measured after the elaboration). After the fatigue test, a decrease of the residual stress level is observed for the two phases (360 ± 30 MPa and -660 ± 60 MPa, respectively for the Ti matrix and the SiC). After a fatigue test at higher temperature (450°C, 800MPa, 100 000 cycles), the residual deformations are two times lower than just after the elaboration.

TRAINSS was a European network of the Brite-Euram III program (1998-2001), implying several neutron sources and universities, and intended to train industrialists to the use of neutron diffraction for internal stress determination. Within this framework, specific problems submitted by the SNCF and PSA-Peugeot-Citroen were studied at the LLB. The SNCF was interested by the influence of the residual stresses on the crack propagation at the interface between the wheels and their axis, caused by oligocyclic fatigue in rotational bending. An experimental set-up was developed implying an entry hole to decrease the absorption of the incident neutron beam during the measurements. The measured strains at the wheel-axis interface are in agreement with the predictions of calculations carried out by finite elements. The work performed in the frame of TRAINSS should be extended and broadened to the synchrotron radiation within the 6th EU Framework Program Integrated Project IMPRESS ("Improved safety and reliability through applicable neutron and synchrotron strain scanning"), currently in fulfilment.

*Residual elastic strains in natural Quartzite samples ("**highlight**")*

Since several years, neutron diffraction has been used to study the residual elastic strains and the crystallographic textures in quartzite samples which are relevant for the **understanding of the thermomechanical history of geological materials** (J. C. Guézou, Université Cergy-Pontoise), see "***Highlight***").

*Mechanical properties of heterogeneous materials (see also the two related "**highlights**")*
(M. Ceretti, R. Levy, A. Menelle, LLB ; A. Lodini, University of Reims Champagne-Ardenne)

The diffraction technique gives elastic strain values averaged on the diffracting volume, but the materials can present heterogeneous strains between grains (different phases or crystallographic orientations) or in the grains (fluctuations). The grain heterogeneities are considered as "phases" with different mechanical behaviours. The experimental data analysis needs the use of scale change methods such as the well-known homogenisation method. The comparison between experimental and theoretical results allows to validate a model and to determine the effective properties of micro-heterogeneous materials.

 These approaches constitute a field of research presently under intense development because of the expected applications; they lead to a better description of the material's mechanical behaviour laws and constitute simultaneously an invaluable tool for new materials development. From its high penetration depth in matter and the possibility of distinguishing the various phases, the neutron probe is an ideal tool for a structural study of heterogeneous materials such as polycrystals with coarse grains (heterogeneity of plastic strain), composites with metal matrix, multiphase materials… Several studies of fundamental character have been performed at LLB to understand the mechanical behaviour of such **heterogeneous materials** :

- Experimental residual stress analysis in both phases of a metal matrix composite Al/SiC submitted to various types of strains, has allowed to determine the necessary input physical parameters and to **validate a self-consistent elastoplastic model**, which was shown to give a very accurate prediction of the mechanical properties of the material (see "***Highlight***").
- In collaboration with LMS (J. Crépin, D. Caldemaison, Ecole Polytechnique, Palaiseau, France) and LPMTM (O. Castelnau, N. Letouze, University of Villetaneuse), the inter and intragranular elastic strain distributions have been investigated in a Dual-Phase Steel. This material exhibits an anisotropic elastic local behaviour and presents under load a heterogeneous strain (between the two different phases but also into a phase). "In situ" measurements, in the elastic range, have been realized adapting the loading machine of LMS. The measured Bragg peak displacements and their broadening allowed determining the mean strain of different crystalline orientations and the variance respectively. The data will be compared with a self-consistent estimation.
- A recent study concerning the microstrain investigation in single crystal nickel base superalloys exposed to thermal fatigue, has been performed in order to determine the strain state in gamma prime precipitates and in gamma matrix after different numbers of thermal cycles (J. Zrnik, P. Jencus, Slovakia; P. Lukas, Czech Republic).
- The accommodation of the intergranular strain incompatibilities caused by plastic deformation and/or thermal loading can lead to a field of heterogeneous elastic strain. Neutron diffraction experiments realized on the diffractometer "6T1", allowed to **analyse the residual elastic microdistortions for various crystallographic orientations** in a Zr alloy and to select the most precise theoretical model (N. Letouzé et al, LPMTM and SRMA) (see "***Highlight***").

2. CRYSTALLOGRAPHIC TEXTURES

Crystallographic texture (preferential orientation of the grains) is one of the parameters describing the microstructure of a polycrystalline material, which controls partly its mechanical properties. In metal alloys, texture appears during solidification, then changes during stages of working (rolling, wiredrawing) and finally during the recrystallization. The understanding and the control of texture during the thermomechanical treatments or annealings are necessary to **optimise the material mechanical behaviour**. Neutron diffraction is the best technique to determine the crystallographic texture of massive polycrystalline specimens (~ 1 cm^3), in the form of a crystalline orientation distribution function. Its use is in particular necessary in the case of large grains materials (few mm^3) frequently met after primary or secondary recrystallization, for which the diffraction of conventional X-rays is not applicable. The LLB has dedicated the **6T1** 4-circles diffractometer to texture measurements. The texture studies are carried out usually in close collaboration with the "Laboratoire de Physicochimie de l'Etat Solide" (LPCES, Orsay University), where complementary techniques are performed: local texture and microstructure analyses by EBSD (Electron Back Scattering Diffraction) and by TEM (Transmission Electron Microscopy) as well as numerical simulations of the microstructure evolutions.

Recrystallization mechanisms and stored energy distribution
(M.H. Mathon, C.H. de Novion, LLB; T. Baudin, LPCES, Orsay University)

Within the framework of the **recrystallization mechanisms** study in various materials performed at the LLB in collaboration with the LPCES (Orsay), a method coupling the crystallographic texture and plastic microstrain analysis, both measured on the diffractometer "6T1", was developed. During a plastic deformation, part of the deformation energy is stored in the crystal lattice in the form of dislocations. This energy is one of the main driving forces of the recrystallization and its knowledge is very important for the understanding and the simulation of the texture evolution during the primary recrystallization.

The experimental procedure, based on the **Bragg peaks broadening analysis** measured for many crystallographic orientations describing a regular grid on the different {hkl} pole figures, allows to determine a **stored energy distribution function** and then to know the deformation energy stored by each crystallographic orientation. This kind of measurement was validated on the Fe-50%Ni alloy used in industry for its magnetic properties (transformers) and it was then extended to other materials (copper, duplex steel,...) and deformations (torsion,...).
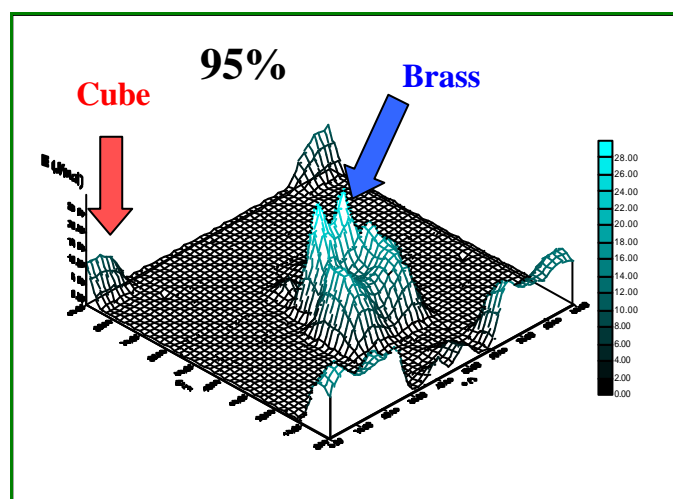
Figure 1. 3D view of the $\varphi_2=0°$ section of the stored energy distribution function for the 95% cold-rolled Fe-50%Ni alloy. The stored energy is higher in the "Brass" ({110}<112>) orientation grains (around 18 J/mol) than in the "cube" ({100}<001>) orientation grains (around 8 J/mol).

In the **Fe-50%Ni alloy**, for a reduction ratio lower than approximately 60%, the primary recrystallization texture is similar to that of deformed specimens. For higher reduction ratios, it develops a strong "cube" component {100}<001>, the volume fraction of which is around 80% in the 95% cold rolled sample. The experimental determination of the stored deformation energy highlighted that the crystals presenting "cube"

crystallographic preferential orientation store less energy than those presenting the rolling ("Brass" copper component) preferential orientations (see Figure 1). The difference increases with the rolling rate, furthering for the strong rates the growth of the "cube" orientation grains. In contrast, for the weak deformations, the variation of energy between the "cube" texture and the other components being insufficient, all the orientations can grow simultaneously and thus the texture tends towards an isotropic texture.

A large part of the crystallographic texture activity was focussed on the following studies: recrystallization mechanisms in various materials (FeNi, two-phase alloys, etc.), phase transformation effect on textures evolution in an industrial titanium alloy, correlations between crystallographic textures and thermomechanical history in geological materials (see the previous paragraph and the related "Highlight"). Let us quote, in particular, a fundamental study of the deformation and recrystallization mechanisms in an austeno-ferritic steel, undertaken in collaboration between the LPCES, the Institute of Metallurgy and Science of Materials of Krakow (Poland) and the LLB. The neutron diffraction experiments allowed to estimate successfully the stored energy levels in each phase according to the rolling reduction rate (0, 40 and 80%). The stored energy increases with the reduction rate and the values of stored energy appear larger for the γ-phase than for the α-phase. Concerning the ferrite, it is shown that the components inside the γ-fiber ({111} <uvw>) present a higher stored energy than the components included in the α-fiber ({hkl}<110 >). All these results are in good agreement with microstructural observations and stored energy evaluation (by calorimetry and TEM observations) performed on single-phase materials, especially ferritic steels.

Recrystallization mechanisms in industrial copper wires: "OPEFiC" project
(M.H. Mathon, S. Jakani, C.H. de Novion, LLB; T. Baudin, A.L. Etter, LPCES, Orsay University)

Recently, the "textures" activity was marked, in 2001, by the start of "**OPEFiC**", a research project partly subsidized by the French Research Ministry, including three laboratories (LLB, LPCES, LPMTM of Villetaneuse University) and two French producing copper wire rod companies (SCCC, SLC). The main objective of this project is to study the residual impurities (S, Pb) effect on the deformation and recrystallization mechanisms in order to understand the wire ductility decrease observed after thermomechanical (wiredrawing followed by heating) treatments. The understanding of the various metallurgical phenomena inherent in the continuous casting and rolling processes should allow an optimisation of manufacture conditions and of the choice of the raw material according to the final wire use.

3. STUDY OF PHASE TRANSITIONS, HETEROGENEITIES, PRECIPITATION AND AGEING

The studies of heterogeneities and of precipitation phenomena are integrated in various themes and are primarily based on Small Angle Neutron Scattering (SANS) experiments. These studies cover a large number of subjects and are the matter of collaborations, in particular with the "Laboratoire de Chimie du Solide Minéral" (Nancy University) concerning the ageing of Pb-Ca-Sn alloys used in the Pb accumulators, and with the Ecole des Mines (Albi) on the effect of a heat treatment and of cyclic plasticity on the precipitation sequence in a steel. Let us quote also the work of the Austrian CRG team on the 3-axis machine G4.3 that is detailed at the end of this paragraph.

Ageing behaviour of martensitic materials under irradiation
(M.H. Mathon, C.H. de Novion, LLB; Y. de Carlan, A. Alamo, J. Henry, CEA/SRMA)

These last years, many experiments were devoted to the study of ageing and of microstructural evolutions under neutron irradiation or thermal ageing in **materials of nuclear interest**. The nuclear reactor constitutive materials, exposed to a neutron flux and/or to high temperatures for very long durations, can present, with increasing time, a progressive degradation of their dimensional or mechanical properties related to a microstructural evolution (swelling, embrittlement due to a new precipitated phase, irradiation-induced specific defect clusters...). It is then necessary to control these microstructural evolutions to be able to **predict the in-service behaviour** of the materials. In this context, SANS presents often advantageous contrasts between the matrix and the precipitates. Moreover, for ferromagnetic materials, additional information about the precipitate chemical composition is extracted from the magnetic scattering.
Recent SANS studies at the LLB were focused on **martensitic materials** which are candidates for the internal structure of future generation reactors (such as fusion or advanced high temperatures reactors) or

spallation sources, because of their remarkable resistance to swelling and their adequate mechanical properties at relatively high temperatures. These include conventional commercial 7-12% Cr steels, reduced activation materials and oxide reinforced materials (ODS).

Conventional and Reduced Activation Martensitic steels have been the subjects of a detailed work for several years. This work allowed to precise the conditions and the **kinetics under irradiation of the phase separation** of the ferrite into two isomorphous body centred cubic (b.c.c.) phases, one Fe-rich (α phase) and the other Cr-rich (α' phase), which is partly responsible for **hardening** and **embrittlement** of the material at relatively low temperature (< 400°C) and moderate dose ($\approx$ 1 displacement per atom (dpa)) (see "Highlight").

The 9Cr-1Mo martensitic steels are candidate materials for the spallation sources. In these materials, the formation of a significant quantity of helium can induce a degradation of the mechanical properties. The helium effect has been studied in EM10 and T91 commercial martensitic steel samples implanted with 0.5 at% helium. The microstructural analysis was performed by TEM and SANS. **Helium bubbles** were detected in both materials implanted at 250 and 550°C and bubble size distributions as well as number densities were determined. Furthermore, the SANS experiments showed that these bubbles are close to thermodynamic equilibrium, i.e. their internal gas pressure is balanced by the surface tension. Based on the microstructural results, it is shown that the high degree of hardening of specimens implanted at 250°C is due to the high density of tiny helium bubbles.

The materials reinforced by oxides dispersion, usually called **ODS (Oxide Dispersion Strengthened)**, have a vast applicability because of their excellent mechanical resistance at medium and high temperatures. They are elaborated by mechanical alloying starting from the components in the form of elementary or alloyed powders. Within the framework of nuclear applications, ODS-based Fe alloys are considered within the international community as potential candidates for any structure subjected to high neutron damage at high temperature (400-700°C) and under constraint. Indeed, the b.c.c. structure of ferrite ensures material a resistance to swelling under irradiation, and the dispersion of oxides improves the mechanical properties (creep, ….) at high temperatures. SANS experiments allow to characterize finely the nanometric oxides distribution in the matrix at various stages of the development process, but also after thermal ageing and under irradiation. In this work, several Fe-9Cr ODS martensitic steels were characterised. It has been shown that the austenite <=> ferrite /martensite phase transformation has no effect on the size distribution of the oxides (Y_2O_3) when the material is cycled in temperature. On the other hand, neutron irradiation at 325°C does not induce any modification of the oxides population up to 5.3 dpa, but involves the formation of chromium-rich b.c.c. α' precipitates in the ferritic matrix (see figure 2).
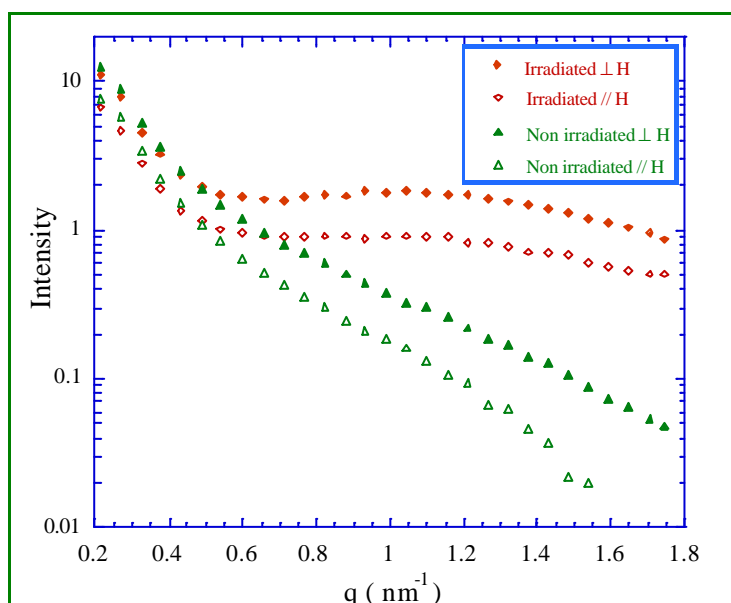
Figure 2. Scattered intensity measured perpendicular and parallel to the applied magnetic field on a non-irradiated and an irradiated (2 dpa at 325°C) ODS martensitic alloy.

Helium damage in long aged metal-tritium systems: Ta, Y and Sc

M.Prem (LLB and Universitaet Wien, Austria), Gerhard Krexner (Institut f. Experimentalphysik, Universitaet Wien, Austria)

Helium damage due to tritium decay in metals is considered as one of the major technical challenges in the construction of future fusion reactors ("first-wall problem"). Continuous helium production induces complex defect structures due to helium clustering and bubble formation with increasing helium content. Earlier studies on bcc Ta were continued and complemented by investigations on hcp yttrium and scandium. Polycrystalline samples of tantalum, yttrium and scandium were loaded with tritium concentrations of about ten atomic percent and the evolution of several Debye-Scherrer lines with respect to position, shape and intensity was investigated repeatedly over a time range covering 10-15 years. These high-resolution measurements were done on the triple axis spectrometer G43 (VALSE). Changes in the line shapes with increasing helium content can be interpreted in terms of a steadily growing number of induced lattice defects: The produced helium atoms cluster and form bubbles entailing increasingly strong lattice strains which finally give rise to the formation of dislocation loops in the host lattice. At later stages an interconnected dislocation network develops which broadens the Debye-Scherrer lines. Tritium on interstitial sites expands the host lattice thus leading to shifts in the lattice parameter. The lattice damage is strongly anisotropic in the hexagonal systems (Y-T and Sc-T) and reflects their elastic properties. A somewhat different behaviour was observed in an yttrium sample cooled to liquid nitrogen temperature immediately after the charging process and kept at this temperature over several years.

Martensitic phase transitions in pure Lithium

M.Prem, LLB and Universitaet Wien, Austria; Gerhard Krexner, Wolfgang Pichl and Maciej Krystian, Institut für Materialphysik, Universitaet Wien, Austria.

The martensitic phase transformation of Li at low temperature is characterized by a complicated phase diagram exhibiting a coexistence of several close-packed phases with the bcc matrix, large thermal hystereses and a number of precursor phenomena. At 80K a rhombrohedral 9R phase (space group R3m) is formed on cooling. On heating, it transforms into an fcc structure at about 100 to 120K while the fcc-bcc reverse transformation occurs only at about 180K. Experimental and theoretical work by the investigators indicates that, contrary to common belief, fcc is the true equilibrium phase of Li at low temperatures and that the 9R phase is only formed as a consequence of geometrical constraints that inhibit direct nucleation of fcc from bcc.

The orientational relationships between bcc matrix and several variants of the 9R phase were investigated in partly transformed Li single crystals on the spectrometer G4.3. Perfect agreement between calculations based on the crystallographic theory of martensite and the experiment was found within the resolution of the instrument. After the formation of the fcc phase the evolution of both the fcc and 9R phase was studied in thermal cycling experiments between 5K and 120K on heating and cooling.

In a small-angle scattering experiment on G5.4 the formation of martensite nuclei induced by small uniaxial deformations in the undercooled bcc phase of Li was investigated. A special deformation cryostat was constructed which allows well-controlled uniaxial in-situ compression and mounting of the oxidation-sensitive Li crystals in a glovebox under protective atmosphere. A uniaxial compression of 3% at 120K leads to two anisotropic peaks in the scattering pattern showing the presence of particles whose size is in the range of 25Å and which are distributed in the (001) plane normal to the compression axis. The scattering pattern remains stable over a wide temperature range even on heating and is indicative of the formation of small martensite embryos which may explain anomalies observed, e.g. in mechanical properties and diffusion experiments well above the transition temperature.

MATERIALS SCIENCE

ELASTOPLASTIC MODEL APPLIED TO THE EVALUATION OF RESIDUAL STRESSES IN METAL MATRIX COMPOSITES.

R. Levy-Tubiana[1], A. Baczmanski[2], M. Ceretti[1], A. Lodini[1,3]

[1]Laboratoire Léon Brillouin (CEA-CNRS), CEA-Saclay, 91191, Gif sur Yvette, France
[2]Faculty of Physics and Nuclear Techniques, Academy of Mining and Metallurgy, 30-059 Krakow, Poland
[3]LACM, Université de Reims Champagne-Ardenne, UFR Sciences, 51100 Reims, France

Modern technologies require materials with an unusual combination of properties which cannot be achieved in conventional alloys, ceramics or polymeric materials. To expand on the range of conventional properties, a variety of composite materials have been developed that possess properties superior to each of the component phases; they are elaborated by introducing a reinforcement, usually a ceramic one, into a metal or an alloy. An increasingly important application for Metal Matrix Composites (MMCs) is as reinforcements in structural components that can be used at medium and high temperatures. However, when MMCs are fabricated at high temperatures and subsequently cooled to room temperature, residual stresses are induced in the composite due to the mismatch of the thermal expansion coefficients between the matrix and the reinforcement. These internal stresses can have several consequences for the mechanical behaviour of the component and thus their evaluation is of fundamental interest.

In the present work, the experimental evolution of residual stresses induced by thermal treatment followed by different types of elastoplastic deformation in an aluminium alloy (Al 2124) matrix reinforced with silicon carbide has been studied. To this end the neutron diffraction method (particularly convenient for the study of multi-phase or composite materials, because it allows the strains to be measured in depth independently in each phase of the material) was applied and data analysed using a self-consistent elastoplastic model, facilitating the identification of different types of stresses. In a mean-field approximation, the behaviour of a crystallite embedded in a homogeneous matrix with mean elastoplastic properties can be modelled. Using a self-consistent model (described below), the strains measured by diffraction can easily be predicted as the average for the volume of crystallites for which the Bragg relation is fulfilled.

Two bars were machined from the quenched plate. One bar was then plastically deformed using the four-point bending technique to a maximum compressive surface strain during loading of 1.1% and a residual plastic compressive strain of 0.5%.

For these samples the stresses were analysed using the neutron diffraction method and elastoplastic self-consistent model. A similar bar was prepared in order to take strain measurements using the 'in situ' bending test.

a) Self-consistent model

In this work, the calculations have been performed using the formalism proposed by Berveiller and Zaoui [1] and Lipinski and Berveiller [2]. This formalism was first applied to composite polycrystals (Al/SiC$_p$) by Corvasce et al. [3].

The calculations using the model are performed on the macro-scale (where the average strains and stresses determined by neutron diffraction are defined) and on the grain-scale, in which the behaviour of each crystallite under local stress is analysed. On this grain scale, plastic deformation occurs due to slips on the crystallographic planes. During plastic deformation, some physical phenomena such as multiplication of dislocations and evolution of their spatial distribution inside the grain influence the mechanical behaviour of the grain, which leads to the hardening of slip systems, generation of internal (residual) stresses by plastic incompatibilities, changes of the crystal orientation of the grain, or modification of the grain shape.

b) Validation of the model

In a simulated simple tensile test, the lattice elastic strains were calculated independently for Al and SiC phases. The average strain values in each phase, corresponding to those measured by diffraction, were determined from the elastoplastic model.

The theoretical results were compared with the strains measured in each phase by diffraction for the "in situ" bent samples (Figure 1). In modelling, the Al and SiC single crystal elastic constants were used respectively for both phases of the composite. Purely elastic properties were assumed for the SiC component, while the plastic properties of the Al matrix were varied in order to find the point of best agreement between the measured and theoretical strains (see Figure 1). The optimal model parameters of plastic deformation for Al (i.e.: τ_o - critical shear stress, H - rate of work

hardening and A- hardening anisotropy) have been calculated. It should be stated that the theoretical values of τ_o and H could be affected by the residual stresses created by quenching [4]. In this case, both parameters should be treated as effective parameters defined for an equivalent material representing the Al matrix.
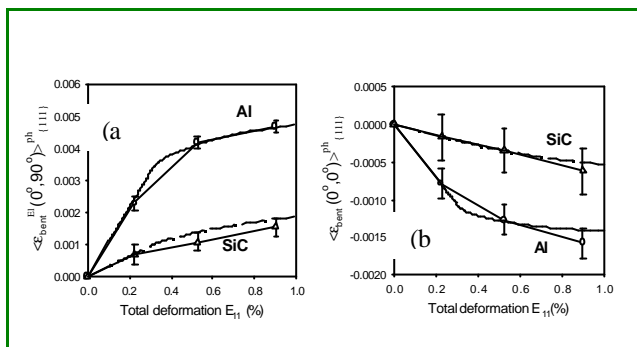
Figure 1. Elastic lattice strains measured 1 mm below the upper surface of the Al/SiC$_p$ bar subjected to bending. The theoretical (line) and experimental (points) evolutions of phase strains in the longitudinal (a) and transversal (b) directions of the sample as functions of the total tensile strain applied are compared.
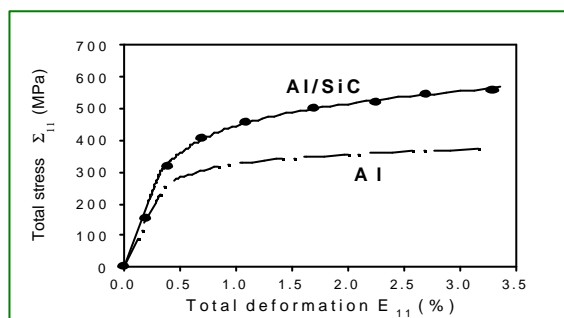
Figure 2. Mechanical test (points) compared with the model results (continuous line) for Al/SiC$_p$ composite. Additionally, the model prediction (dashed line) for single phase Al is shown. The same model parameters as in Figure 1 were used for prediction.

Simultaneously, the calculated total stress vs total strain for the composite was compared to the results of the experimental mechanical tensile test (Figure 2). In this case the macroscopic quantities were calculated as the volume average for all the composite grains.

As shown by Figures 1 and 2, an excellent degree of consistency between the experimental data and model results was obtained for both the neutron diffraction and the simple tensile test on Al/SiC$_p$ composite bars submitted to a plastic deformation. Such a high level of consistency was obtained simultaneously for three different thermal treatments when the plastic parameters of only one component (Al) were modified. Moreover, in the elastic range, the single crystal elastic constants were used as the input data for the model, and no free parameters were optimised.

This proves that the elastoplastic self-consistent model gives a very accurate prediction of the relation between macrostresses and the elastic strains (and stresses) measured for the two phases in the elastic and elastoplastic ranges of deformation. Additionally, the tensile test for single phase Al matrix was predicted using the model parameters (see Figure 2).

In conclusion, this work has allowed to validate the self-consistent elastoplastic model and to determine the model data input physical parameters necessary to predict the mechanical behaviour during plastic deformation of a composite. The parameters characterising the mechanical properties of the Al-metal matrix and the Al/SiC$_p$ composite obtained by the model were found in good agreement with the literature data [5] referring to an Al alloy with the same thermal history than the composite.

These results were part of an article published in Materials Science and Engineering A341(2003) 74-86.

References
[1] M. Berveiller, A. Zaoui, *J. Mech. Phys. Solids*, **106**, (1984), 295.
[2] P. Lipinski, M. Berveiller, *Int. Journ. of Plasticity*, **5** (1989) 149.
[3] F. Corvasce, *Prévision du comportement thermomécanique des composites à matrice métallique*, Ph.D. Thesis, Université de Metz, 1989
[4] L.C. Davis and J.E. Allison, *Metall. Trans.* **24A,** (1993) 2487
[5] L.F. Mondolfo, *Aluminium Alloys: Structure and Properties,* Butter Worths, London-Boston, 1976

MATERIAL SCIENCE

RESIDUAL STRAINS AND CRYSTALLOGRAPHIC TEXTURES IN NATURAL QUARTZITES : TOWARDS AN UNDERSTANDING OF THE THERMOMECHANICAL HISTORY OF ROCKS

J.C Guézou[1], T. Baudin[2], M. Ceretti[3], M.H. Mathon[3], R. Penelle[2]

[1]Département des Sciences de la Terre, Université de Cergy Pontoise, 95031 Cergy, France
[2]Laboratoire de Physico-Chimie de l'Etat Solide, Université de Paris Sud, 91405 Orsay, France
[3]Laboratoire Léon Brillouin (CEA/CNRS), CEA-Saclay, 91191 Gif-sur-Yvette, France

Quartzites are nearly monomineral polycrystalline quartz-rich rocks, very common in the upper crust of the earth, and which have generally supported a complex deformation path at medium or high temperature. They show a great variety of microstructures (grain shapes, sizes and arrangement) and preferential crystallographic orientations (textures) of the quartz grains, and contain also small contents (a few percent) of a brittle second phase (e.g. feldspath or epidote mineral). Both the microstructure and the texture of quartz grains contain informations on the history of the rock deformation.

Due to the difficulty in conducting deformation tests, numerical simulations of the texture have been performed with the experimental residual elastic strain tensor.

The crystallographic texture and the complete residual elastic strain tensor in the quartz phase have been measured by neutron diffraction at the LLB on several quartzite samples, collected in Spain (betic zone) [1] and Turkey.

In order to precise the deformation mechanisms during geological processes, a large set of samples has been collected for many years, and the microstructures as well as the textures have been characterized and discussed.

Two main texture components [*] (plus a random fraction), determined either by the harmonic method or by discrete and component methods, have been clearly identified in all the samples: $\{-1\ 2\ -1\ 0\}<-1\ 0\ 1\ 0>$ and $\{-1\ 1\ 0\ -1\}<-1\ -1\ 2\ 0>$. These components have been further examined with the features of the various types of microstructures, and linked with specific proportions of grains considered respectively deformed and recrystallized. This result is in agreement with the textures of deformed and annealed hexagonal titanium and zirconium alloys.

On figures. 1b and 2 are shown repectively the texture and microstructure of two areas, B (recrystallized) and A (deformed), of a stretched quartzite vein (Fig. 1a), collected in a shear undulation in Turkey.
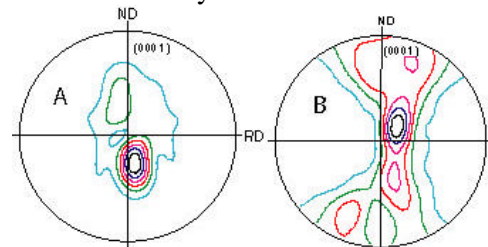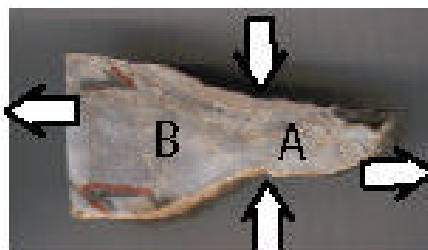
Figure 1. a) Macroscopic sample   b) Pole figures (neutron diffraction)
(RD is the lineation direction and ND is the normal to the foliation plane)
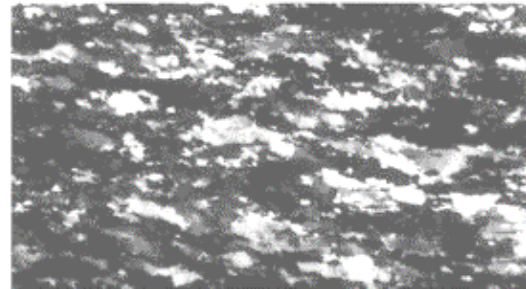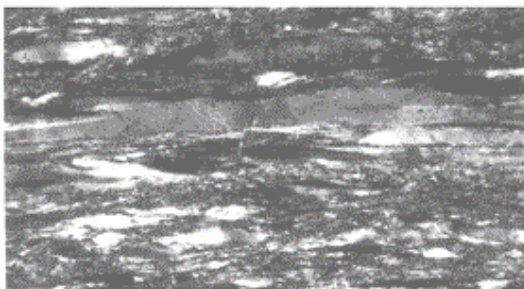
Figure 2. Microstructure of samples A (left) and B (right)

The measured residual elastic strain tensors are given below for the A and B samples depicted in Fig. 1a:

Sample A: $[e] = \begin{bmatrix} -88 & -7 & -7 \\ -7 & 110 & -30 \\ -7 & -30 & 17 \end{bmatrix} \times 10^{-6}$ **Sample B:** $[e] = \begin{bmatrix} -38 & -28 & -14 \\ -28 & -6 & -7 \\ -14 & -7 & 12 \end{bmatrix} \times 10^{-6}$, error $\leq 20 \times 10^{-6}$

The largely recrystallized samples (e.g. sample B) do not show significant residual strains. In the samples containing a strong proportion of non-recrystallized deformed grains (e.g. sample A), the experimental strain values are very low in comparison to those generally measured in deformed metal samples; however, they are significant and allow one to perform texture simulations using a VPSC model (see below). Local measurements show some heterogeneity of the sample deformation. In some cases, the measured strains appear associated to the presence of brittle second phase grains.

A numerical simulation of the deformation texture, based on a visco-plastic self-consistent (VPSC) modelisation applied to anisotropic polycrystals *[2]*, has been performed. The calculation assumes a single-phased material, with an isotropic initial texture, with well-known slip systems and critical shear stresses. However, one does not know anything *a priori* about the plastic strain tensor to apply.

The main hypothesis made here is that the measured residual (elastic) strain tensor, which likely results from the accommodation of plastic incompatibilities between the quartz matrix and the precipitates (brittle secondary phases), is a memory of the plastic strain tensor undergone by the material during its history. Applying this plastic strain tensor (derived from the measured residual elastic strain tensor by reversing the sign of the trace components and setting the trace to zero) to the quartz crystallites in the VPSC model, one obtains simulated pole figures (corresponding to the deformation textures) consistent with those measured by neutron diffraction (compare Fig. 3 to Fig. 1b left).

Usually, modelisation of rock textures is made assuming *a priori* models for the strain tensor. In the present work, this is the first time that a complete "realistic" strain tensor is experimentally determined, and allows to reproduce the experimental pole figures.

In future, this work should be extended by the study of natural quartzites deformed in laboratory conditions, in order to confirm the correspondance of the residual elastic strain tensor with the slip system and the plastic strain intensity deduced from macro and microstructures observed *in situ*.

$\begin{bmatrix} 0.8 & 0.0 & 0.0 \\ & -1.0 & 0.3 \\ & & 0.2 \end{bmatrix}_{e = 1.0}$
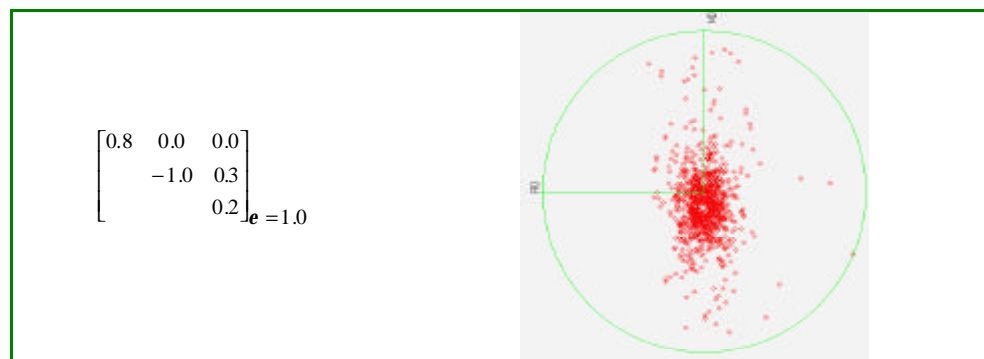
Figure 3. VPSC simulation of the deformation texture of quartzite with a complete strain tensor derived from residual elastic strain tensor measurements. Comparison of the {0001} pole figure of a typical deformed sample (sample A of Figure 1, characterized by the {-1 2 -1 0}<-1 0 1 0> texture component) with the simulated one.

(*) The texture components of rhombohedral structure quartz grains are identified by their crystallographic plane { } and direction < > preferentially parallel to the macroscopic shear plane ("foliation plane") and direction ("lineation direction") of the rock, deduced from the morphology of the grains and other markers of the deformation.

References

[1] J.C. Guézou, T. Baudin, M. Ceretti, M.H. Mathon, R. Penelle, J. Neutron Research 9 (2001) 357.
[2] R.A. Lebensohn and C.N. Tomé, Acta Metall. Mater. 41 (1993) 2611.

HETEROGENEITY OF RESIDUAL STRAINS IN PLASTICALLY DEFORMED ZIRCONIUM ALLOYS

N. Letouzé[1], R. Brenner[1], J. L. Béchade[2], M.H. Mathon[3], O. Castelnau[1]

[1]LPMTM, UPR 901, Université Paris 13, Av. J.B. Clément, 93230 Villetaneuse, France
[2]DEN/SRMA, CEA-Saclay, 91191 Gif-sur-Yvette, France
[3]Laboratoire Léon Brillouin (CEA-CNRS), CEA-Saclay, 91191 Gif-sur-Yvette, France

Zirconium polycrystalline alloys widely used in the nuclear industry, especially as cladding tubes and guide tubes for Pressurized Water Reactors (PWR), behave like an heterogeneous material during plastic deformation, because they are made of grains with soft and hard crystallographic orientations. This behaviour is mainly due to the hexagonal close-packed (h.c.p) structure which induces a very large local plastic anisotropy [1].

Two complementary ways are undertaken to investigate the heterogeneity of residual strains in plastically deformed zirconium alloys: experimentally using diffraction techniques (X-ray and neutron diffraction), and numerically with a modelling approach using homogenisation techniques.

✓ On one hand, diffraction gives a statistical analysis of average elastic residual strains and of their fluctuations in the investigated volume (the whole sample volume in the case of neutron diffraction). These mechanical parameters can be extracted respectively from the position and the shape of the peak.

✓ On the other hand, volumic residual strains can also be predicted by homogenisation techniques, providing that the (non-linear) local mechanical behaviour and the microstructure of the material is known. For polycrystals, the self-consistent scheme (the stresses and the strains are not considered as homogeneous between all the phases) is well adapted owing to the approximate random microstructure [2]. However, the extension of the self-consistent scheme to non-linear behaviour is only approximate.

Comparison between elastic strain maps obtained by neutron diffraction experiments performed on 6T1 at the LLB and by a thermo-elasto-visco-plastic self-consistent model have been performed. An example of (0002) pole figure for a Zircaloy-4 specimen deformed by creep at 400°C in tension up to 5% is given Figure 1. One can see on Figure 2 the good agreement between the experimentally determined residual strains obtained for different orientations in the (0002) pole figure defined by their tilt angle χ and rotation angle φ (open circles) and the micromechanical modelling calculation (affine self-consistent scheme, continuous line)
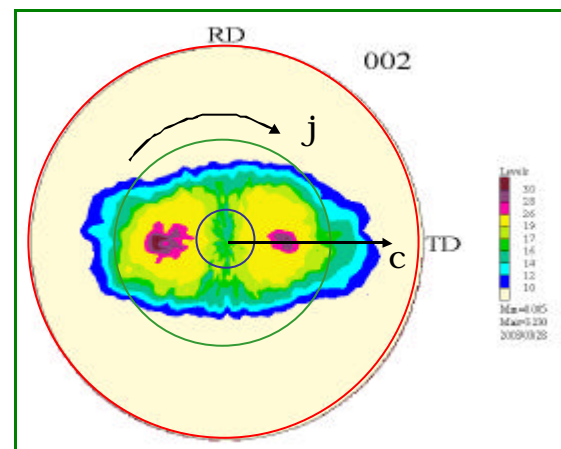
Figure 1. (0002) pole figure measured on a Zircaloy-4 sample deformed by creep at 400°C in tension up to 5% (RD is the rolling direction and TD is the transverse direction)
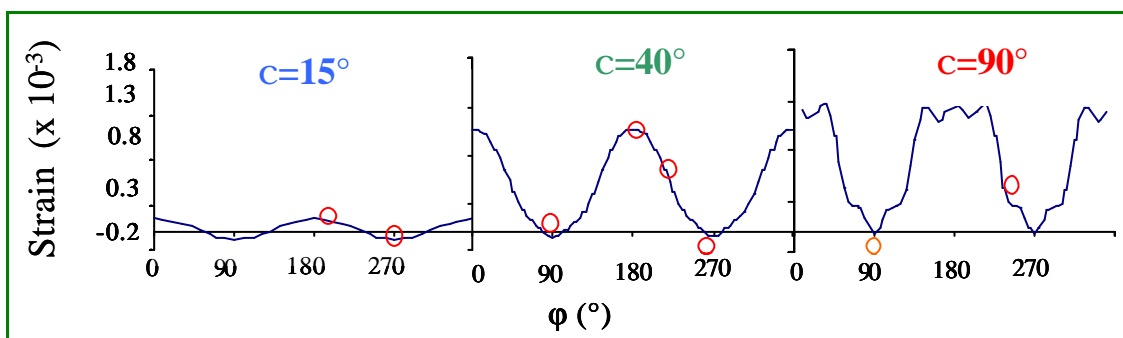
Figure 2. Strain map after thermal creep for different χ angles.

The results obtained show also how diffraction data can be used for the validation of the scale transition model [3] used in the frame of homogenisation methods.

These methods make it possible to estimate or bound the effective behaviour of heterogeneous materials starting from the statistical description of the microstructure (texture) and the knowledge of the mechanical behaviour of the constituents (in this work, we label "phase" a set of grains with the same orientation). They also allow to estimate the intra- and inter-phase fluctuations of the mechanical fields. So the comparison of experimental and calculated strain maps using different non linear approaches, is a promising way for determining the best linearisation procedure.

Figure 3 gives an example of the influence of the linearisation procedure on the prediction of the residual elastic strain for different orientations. In this case, viscoplastic simulation has been performed, using Zircaloy-4 real texture with thermal creep loading in tension at 127 MPa stress level. We used the secant and affine Self Consistent schemes (2 ways of linearization assuming both inhomogeneity of stress and strain) as well as Reuss (stress homogeneity) and Taylor (strain homogeneity) bounds to calculate the phase average stress. Focusing for a particular orientation, here for example at $\chi=55°$, significant differences between several polycrystals models are shown.

One main result is that the Reuss model does not predict any residual strain around the principal orientation (at $\chi=55°$), which is absolutely not realistic. The secant formulation is closer to the prediction of the Taylor bound, whatever χ angle is, the Taylor formulation showing a strain level 10 times higher, for example at $\chi=55°$, and the affine one a strain level 2 times lower compared to the secant formulation. Finally these large discrepancies between different linéarisation procedures would be enough to select the best one when experimental data will be acquired and compared too.

In conclusion, we have shown that neutron scattering provides a volume measurement of the elastic strain distribution in polycrystals on a plastically deformed Zircaloy-4 specimen. Taking into account that the experimental data can be compared rigorously to the results of homogenisation schemes, they may be used for a reliable determination of the local constitutive relation ; this process is a good way for determining the best linearisation procedure in the case of non linear behaviour.

An application to creep loading shows an excellent agreement with the prediction of the **affine self-consistent scheme** for non linear elasto-viscoplasticity (see figure 2). To our knowledge, this result is the first validation of the affine linearisation procedure at a ?nest scale than the macroscopic one.
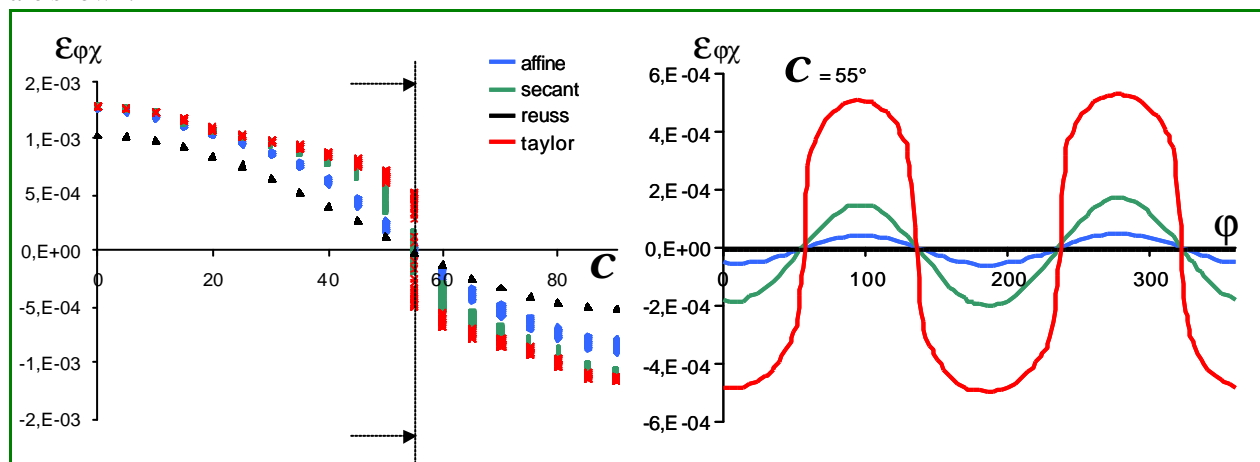
Figure 3. Evolution of the residual strains calculated with several polycrystal models and comparisons for a particular orientation at $\chi=55°$.

References

[1] Brenner R. PhD thesis, Université Paris XIII, France 2001.

[2] Castelnau O, Béchade J-L, Brenner R, Chauveau T, Bacroix B, et al. in: Miannay D, Costa P, François D, Pineau A., editors. Advances in mechanical behaviour, plasticity and damage, Proc EUROMAT 2000 Tours, France (2000), pp. 911–916.

[3] Letouzé N, Brenner R, Castelnau O, Béchade J-L, Materials Science Forum **404-407** (2002) 735.

IRRADIATION-INDUCED HARDENING OF MARTENSITIC STEELS CANDIDATES FOR FUTURE GENERATION NUCLEAR REACTORS

M.H. Mathon[1], Y. de Carlan[2], G. Geoffroy[3], X. Averty[4], A. Alamo[2], C.H. de Novion[1]

[1]Laboratoire Léon Brillouin (CEA-CNRS), [2]DEN/SRMA, [3]DSM/LSI, [4]DEN/SEMI
CEA/Saclay, 91191 Gif-sur-Yvette, France

Martensitic steels with 7-12 wt% Cr are candidates for the internal structures of future generation nuclear reactors or spallation sources, because of their remarkable mechanical properties and resistance to swelling; but they suffer from radiation hardening and embrittlement below 400°C, even at moderate doses. In order to promote their use, it is necessary to understand the evolution of their microstructure and its relationship with the degradation of mechanical properties during irradiation.

The unmixing of the b.c.c. Fe-Cr solid solution below 600°C into two isomorphous phases, Fe-rich (α phase) and Cr-rich (α' phase), observed in thermally-aged alloys with Cr content between 10 and 90 at.%, is an important feature of the binary Fe-Cr equilibrium phase diagram (see Fig. 1). The phase separation occurs at the nanometer scale and induces hardening of the solid solution. α' has also been observed in martensitic/ferritic steels by Transmission Electron Microscopy (TEM) after thermal ageing or neutron irradiation at 400-550°C for Cr content above 13 wt%, but up to now not at lower temperatures (300°C), even after long irradiation (up to 40 displacements per atom (dpa)).

In fact, Small-Angle Neutron Scattering (SANS) is much more powerful than TEM or X-ray scattering to study the α-α' phase separation, because of the large difference between the neutron coherent scattering lengths of Fe and Cr. Also, the A ratio of the magnetic and nuclear SANS contrasts between matrix and particles gives information on the chemical composition of the particles.

In the present study [1], nine martensitic steels with various chemical compositions have been investigated: four Reduced Activation (RA) materials from AEA-Culham, UK (LA4Ta, LA12LC, LA12TaLC and LA13Ta), a low Cr content RA material supplied by JAERI, Japan (F82H), and four "conventional" commercial steels (EM10, HT9, T91 and MANET II). The materials were irradiated in the OSIRIS (CEA, Saclay) or in the HFR (NRG, Petten) reactors at temperatures of 250, 325 and/or 400°C, for doses of 0.7, 2.4 and/or 2.9 dpa.

The neutron scattering experiments were performed at room temperature at the LLB on the PAXY small-angle instrument, under a saturating magnetic field (= 2 Tesla) perpendicular to the incident neutron beam direction.

The main results of this work are summarized below.

1) In the unirradiated state, all materials show a strong SANS signal due to the $M_{23}C_6$ carbides formed during initial thermal treatment; this $M_{23}C_6$ population does not evolve under irradiation. After irradiation, most samples display a supplementary SANS signal, mainly observed at large q; this shows that a new nanometer-sized precipitation has formed. As example, the increase in SANS signal between the LA4Ta steel (Fe-11Cr-0.7W) sample irradiated 0.7 dpa at 325°C and the as-received sample shows a broad maximum around q ~ 1.1 nm^{-1}. This indicates a spatial periodicity in composition, with a characteristic length $2\pi/q$ ~ 5-6 nm, similar to that observed in the thermally aged Fe-Cr solid solution. Moreover, the A value of the irradiation-induced SANS signal (A = 1.9 ± 0.2) is in agreement with α-α' phase separation of the ferritic matrix. Detailed work on the thermally aged Fe-Cr binary alloy suggests that for the considered Cr concentrations (< 20%), a model of isolated Cr-enriched α' precipitates surrounded by a spherical exclusion volume depleted in Cr is adequate [2].

2) The volume fraction of precipitated α' phase increases with the irradiation dose (e.g. from 0.8% at 0.7 dpa to 3.4% at 2.9 dpa for LA4Ta at 325°C) and as the irradiation temperature is lowered (e.g. from 0.1% at 400°C to 0.6% at 250°C for LA12LC at 2.4 dpa). Up to 2.9 dpa, these parameters have only a weak influence on the average size of α' precipitates (radius ≈ 1.3 nm).

3) On Fig. 2 is indicated, for each steel irradiated for 0.8 dpa at 325°C, the volume fraction of α' phase obtained from SANS analyses, versus the Cr content in solid solution in the ferrite matrix (deduced from THERMOCALC type calculations). Except in the EM10 alloy, this precipitated α' volume fraction increases monotonously with the Cr content in the matrix. The Cr threshold concentration in the ferrite for α-α' unmixing under irradiation, deduced from the SANS results (7.2 at.%Cr at 325°C and 8.3 at.%Cr at 400°C) are found to agree with the

THERMOCALC predictions for the Fe-Cr system (see Fig. 1).
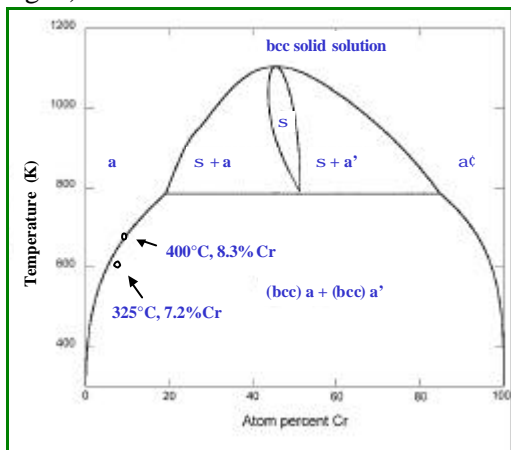
Figure 1. Fe-Cr binary phase diagram calculated from high temperature thermochemical data. Experimental points for the threshold of α' precipitation in irradiated steels deduced from the present SANS study are reported.

Figure 2. α' volume fraction deduced from SANS data after neutron irradiation of 0.7 dpa at 325°C as a function of the Cr amount in the ferrite matrix.

4) The above results show that the precipitation kinetics under irradiation are much faster than during thermal ageing. For the studied materials (Cr content < 20 wt%), the α' phase forms by nucleation and growth process. Two mechanisms can be involved: either (i) an *irradiation-accelerated* mechanism, where the point defect supersaturation allows the achievement of equilibrium much faster than in out-of-pile conditions at the same temperature; or (ii) an *irradiation-induced* mechanism, where the coupling between migrating point defects and solute atoms (Cr) can induce a non-equilibrium state. Experimental evidence exists for a weak binding between vacancies and Cr atoms in the Fe-Cr solid solution; however, our observation that the Cr threshold concentrations in the ferrite for α' precipitation under irradiation are not significantly different from the out-of-pile values obtained from modelisations of the equilibrium Fe-Cr phase diagram (see Fig. 1) suggests that the unmixing is dominated by a simple irradiation-accelerated mechanism.

5) For the materials with the lowest Cr content (F82H and LA13Ta), the SANS signal is unchanged by the irradiation at 325°C up to 0.7 dpa. In the case of F82H (Fe-7.5Cr-2W), a weak increase of the scattered intensity is observed after 3.4 dpa at 325°C.

The A ratio value does not correspond to α' precipitation, but is in agreement with vacancy clusters (A = 1.4). These could be small cavities or dislocation loops which have been observed by TEM in the form of "black dots" [3]. Their number densities deduced from TEM and SANS data ($\approx 3 \times 10^{23}$ m^{-3}) are in better agreement if the defect form factor is assumed to be cavity-like.

5) All the materials studied in the present work show a large increase ($\Delta\sigma_{irr}$) of yield stress after irradiation, ranging from 50 to 275 MPa. No simple correlation appears between $\Delta\sigma_{irr}$ and the chemical composition or microstructural parameters. The contribution of α' precipitates to the hardening of the martensitic steels has been estimated from a study on thermally-aged Fe-20%Cr alloys [4], where it is mainly due to dislocation-shearing of isolated precipitates obtained by nucleation-growth mechanism. This contribution to $\Delta\sigma_{irr}$ ranges from 10-20 to 100 MPa; this is always smaller than the measured increase of yield stress, but represents a significant part of it in the case of the Cr-rich materials: for example, $\approx$ 60-65 MPa compared to measured $\Delta\sigma_{irr}$ values of 100 MPa for LA4Ta and 260 MPa for HT9 irradiated 0.7 dpa at 325°C. However, the main hardening contribution seems to be due to radiation-induced point defects clusters, as the largest yield stress increase at 325°C was found in the F82H irradiated 2.9 dpa, where we observed a vacancy cluster (but no α') contribution to the SANS.

References

[1] This work has been published in M.H. Mathon et al., J. Nucl. Mater. 312 (2003) 236.

[2] F. Bley, Acta Metall. Mater. 40 (1992) 1505.

[3] R. Schäublin, M. Victoria, J. Nucl. Mater. 283-287 (2000) 339.

[4] A. Triki, PhD thesis, Institut National Polytechnique, Grenoble (France) (2 may 1990).
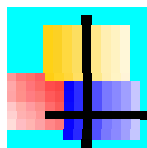
4 - LIQUIDS AND DISORDERED SYSTEMS

Neutron scattering is an essential technique for the study of disordered systems in general and, more specifically for the investigation of structural and dynamic properties of molecular liquids and glasses. This is essentially due to the possibilities of isotopic substitution and of incoherent scattering.

One can realise that there is a very rich variety of experiments in the domain of liquids, glasses and critical mixtures either in bulk form or in confined volumes. They use regularly many of the neutron scattering instruments of LLB: the diffuse scattering diffractometer 7C2, the powder diffractometer G6.1, the small angle scattering instruments, the time-of-flight and spin echo spectrometers.

LIQUIDS: QUANTUM MODES, SUPERCOOLED STATE AND BINARY MIXTURES

Recent studies at LLB focus mostly on properties of liquids under extreme conditions (superfluid or supercooled state, pressure, temperature, critical conditions) or in confined volumes. Because of chemical affinities, in particular the formation of hydrogen bonds between liquids and solid substrates, the local structure of a liquid may be disturbed over distances of two or three molecular layers, inducing specific properties and important consequences in chemical processes. Most of the studies of confined liquids are achieved within a porous matrix and some ambiguity may occur from the superposition of effects due to the interface and due to the size of the pores. Some modern substrates such as carbon and metal nanotubes provide small volumes of diverse shapes where liquids can be confined under well-defined conditions.

Quantum liquid in confinement ("Highlight")

Helium is the prototype of quantum fluid as it is the unique element that stays liquid in normal pressure conditions even at the lowest achievable temperatures. Below the Lambda transition temperature, $T_\lambda = 2.17$ K in bulk, Liquid Helium becomes superfluid with peculiar viscous and thermodynamic properties that have been related to Bose-Einstein Condensation (BEC) but the complex relation between superfluidity and BEC is far from being elucidated.

The confinement of Helium in porous media is expected to decouple the two transitions and may even lead to the inhibition of the Bose-Einstein Condensation due to the reduced dimensionality and disorder. Major efforts were devoted at the LLB to control the thermodynamic state of Helium ^{4}He confined in porous matrices to maximize the confined liquid volume and perform neutron scattering experiments without bulk liquid (Thesis F. Albergamo). Adsorption of Helium in several standard porous systems (carbon nanotubes, Vycor glass and MCM-41) was characterized by thorough isotherm experiments to compare the available porous media, study the capillary condensation and avoid bulk liquid.

Inelastic neutron scattering was performed on time-of flight machines to study the influence of confinement on the elementary excitations and their dispersion curve in the 'Maxon' and 'Roton' regime. The precise control of the adsorption process has even allowed to evidence the peculiar capillary waves, also called "Ripplons", of the precursor wetting films (see the detailed "***Highlight***" thereafter). Modifications in the phonon and roton regime were evidenced and will help to understand the complex relation between the superfluid transition and the Bose-Einstein Condensation.

Supercooled liquid Selenium ("Highlight")

Mode coupling theory (MCT), very successful in the interpretation of the dynamics of viscous liquids, is widely used, even out of its primary domain, probably because of its precise numerical aspects particularly adapted to neutron scattering. Sometimes, it represents simply a good mathematical model of complex systems with a broad relaxation spectrum. In such cases, MCT is used in a phenomenological way and important physical aspects may be bypassed. In some cases, the use of MCT is well adapted and then the information extracted from extensive experiments is very rich.

One of the following highlights details a remarkable study of the dynamics of liquid selenium at temperatures slightly above the glass transition (B. Rufflé and S. Longeville). The quantitative test of MCT

implies normally the analysis of a large time domain covering several orders of magnitude, which implies the use of different spectrometers, as well as a precise evaluation of the structure factor with a high-resolution powder diffractometer.

Binary liquid mixtures

A very innovative experiment concerns the local order in mixtures arsenic-sulphur (M.V. Coulet). The phase diagram of this mixture is particularly interesting and complex. Below a concentration in sulphur of the order of 25% and at high temperature (600°C) there is a miscibility gap.

The study of the structure of the mixture and of the two phases after separation has been done with an automatically driven diaphragm that allows independent measurements in situ from each side of the meniscus. One observes pair correlation functions similar to those of the mixture at 5% or 25% sulphur concentration. At a concentration of 5%, the pair correlation extend to the third neighbours as in As; at a concentration of 25%, it extend to the second neighbours as in Sulphur (Fig. 1).
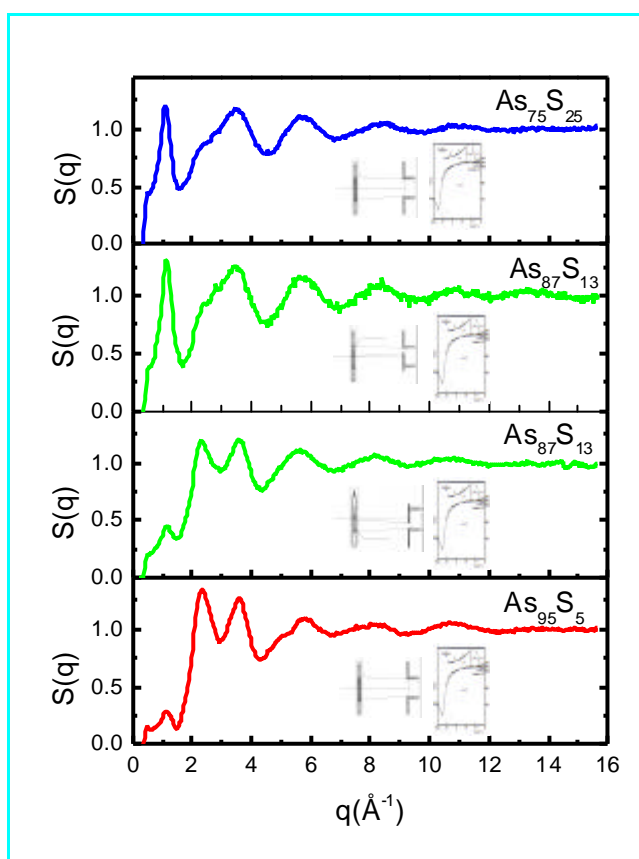
Figure 1. Structure factor of the As_{1-X}-S_X liquid on the borderline of the miscibility gap (bottom red curve x=5 and top blue curve x=25) and in the miscibility gap (x=13 bottom green curve in the dense phase and top green curve in the light phase). Note the similarities between the two top curves as well as between the two bottom curves.

Binary liquid mixtures in confinement (see also the related "Highlight")

In porous media, most of the time, effects due to interfaces dominate those due to pore sizes, what is easily understood if one reminds that the oscillations of the pair correlation function of a molecular liquid extends over distances substantially smaller than the typical size of pores. However, one important exception is the case of mixtures of liquids that phase separate at given conditions of pressure and temperature. At such critical points, the correlation length of concentration fluctuations diverges, even if the extension of local order is not modified. One experiment of neutron scattered at small angles (F. Formisano and J. Teixeira) allowed the characterisation of the structure of two liquids confined in porous silica, at the critical point. The experiment allowed the discrimination between two proposed theoretical models and has interesting applications namely for the industry of oil extraction.

A more recent experiment on the same subject has been performed by S. Schemmel et al (see the detailed "*Highlight*" thereafter). The measurement of the diffusion coefficient by neutron spin echo shows that the microphase separation of the liquid mixture in the porous matrix extends over a large temperature range below the temperature of the phase separation in the bulk mixture.

Solid-liquid interfaces and hydrogen bond lifetime

In other cases, the main purpose is the study of the interactions liquid-solid substrate. In this context, water is by far the more studied liquid, because the interaction can be very different and yield major consequences in many different domains (see for example the Chapter on Life Science).

For example, in the case of silica, hydrogen bonds are formed with silanol groups; their lifetime is much longer than that of intermolecular bonds creating a relatively ordered and stable layer of water molecules at the surface of silica. In contrast, when the solid substrate is hydrophobic, the situation remains not well understood, despite many theoretical studies and computer simulations. The comparison of different hydrogenated liquids allows also the study of the effects due to hydrogen bonds (H. Farman, J.C. Dore and M.-C. Bellissent-Funel).

Always in the domain of structure, several experiments allow the precise evaluation of the molecular arrangement of a solvent around a macromolecule or an ion, as for example, the case of neodymium in diverse solvents (postdoctoral work of B. Belhorma).

Concerning dynamics, most of the experiments make use of the large incoherent cross section of hydrogen atoms to study different molecular motions (self-diffusion, rotations, vibrations). At LLB, the time-of-flight spectrometer Mibémol allows the study of relatively fast dynamics and has been extensively used for the study of the self-diffusion of liquids in confined volumes, already mentioned above.

A problem that remains open and controversial is that of the dynamics of hydrogen bonds. A priori, incoherent neutron scattering, together with NMR, are the best probes to enlighten this problem and establish comparisons with diverse, sometimes contradictory, numerical simulations. A study of the dynamics of the eutectic mixture water - dimethyl sulfoxide (DMSO) allows the separation of the bonds at the vicinity of the acceptor group from that near the hydrophobic methyl groups (J.T. Cabral, A. Luzar, J. Teixeira et M.-C. Bellissent-Funel).

With samples of fully deuterated DMSO, one avoids the large contribution due to the rotation of the two methyl groups and it is then possible to evaluate the diffusion of water molecules and the characteristic lifetime of the hydrogen bonds between water and the oxygen atom of DMSO. It is worth noting that, despite the large mass of the DMSO molecule, this last time is not much longer than that corresponding to bonds between water molecules. Because the study was performed with a eutectic mixture, measurements at very low temperature were possible and demonstrate that the hydrogen bond lifetime has small temperature dependence. This feature is a good argument against several theories of supercooled water that suppose a critical temperature dependence of the hydrogen bond lifetime.

In the same context, a study of the dynamics of water hydrating several polysaccharides (S. Magazù) showed a very rich variety of behaviours. Indirectly, one may understand why trehalose is the more frequent sugar in living organisms that, submitted to extremely low temperatures, can survive.

GLASSES AND DISORDERED SYSTEMS
Concentration modulation in complex silicate glasses

A case rather interesting, also for applications, is that of glasses of complex chemical composition (silicates containing aluminium, magnesium and nitrogen). A tiny change of the amount of additives has large effects on chemical bonding, then mechanical properties (Thesis of S. Deriano, Rennes). This result is important at least in two aspects (Fig.2). First, at the experimental level, the modulation of concentration plays the role of the isotopic substitutions currently used to evaluate the local environment of the atoms of the additives. Even if the method is not completely rigorous, the approximation is very good because the network of silica is only slightly disturbed by the presence of other compounds. Secondly, the determination of very precise distances through the pair correlation function allows their assignment to stable chemical bonds.
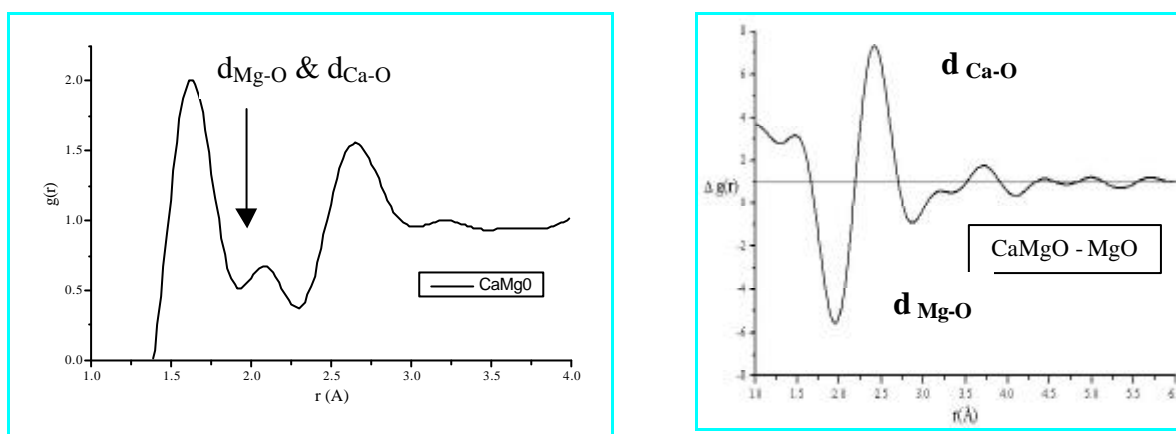
Figure 2. Pair correlation function of the SiO_2-Al_2O_3-CaO-MgO glass (left) and correlation difference (right) with the SiO_2-Al_2O_3-MgO glass allowing to identify the Mg-O and Ca-O distances (d_{Mg-O} ~ 1.99 Å and d_{Ca-O} ~ 2.37 Å).

Small Angle Neutron Scattering (SANS) and complementary techniques (Raman and DSC) were used to characterize the microphase separation of Sulphur-rich glasses at nanometric scale and identify the role of sulphur chains and rings. The metastability of the chains leads to a complex ageing behaviour and changes in the glass transition (see the detailed "***Highlight***", E. Bychkov et al, Université du litoral, Dunkerque).

Influence of a high pressure on the Glass transition ("Highlight")
Finally, the studies of slower motions are achieved in spin echo spectrometers. Some experiments were devoted to the behaviour of viscous liquids, at the vicinity of a glass transition, of biologic macromolecules or at the vicinity of a demixtion point in a confined matrix, as mentioned above.
A particular situation is that of a glass transition of a confined liquid. Confinement changes both the temperature and the width of the transition (see the detailed "***Highlight***", C. Alba-Simionesco et al, Université ParisXI-Orsay).

Polymeric liquids in confinement: anisotropic dynamics of Polypropylene Glycol
To introduce the next chapter on soft matter, let us mention that certainly, there will be in the near future an increasing number of studies of slow dynamics, namely in complex systems.
For example, an important domain, even for applications, concerns polymeric liquids in confined volumes. Polypropylene glycol with variable mass was included in a 2-dimensions porous medium, vermiculite, a clay that forms flat interfaces (J. Swenson and S. Longeville).
Orienting the clay, it is possible to measure the dynamics of the polymer chains either parallel or perpendicular to the interfaces. In the first case, one observes the classical dynamics of a liquid polymer in bulk form, while in the second situation, the dynamics is dramatically reduced. A complete study implies several experiments with polymer chains of different masses.

LIQUIDS AND DISORDERED SYSTEMS

ELEMENTARY EXCITATIONS OF LIQUID ^{4}He IN CONFINEMENT

F. Albergamo[1] , H.R. Glyde[2] , J. Bossy[3]

[1]Laboratoire Léon Brillouin (CEA-CNRS), CEA-Saclay, 91191 Gif-sur-Yvette Cedex (France)
[2]Department of Physics and Astronomy, University of Delaware, Newark, Delaware, 19711 (U.S.A.)
[3]Centre de Recherche sur les Très Basses Températures, CNRS, BP 166, 38042 Grenoble (France)

1. Introduction

Superfluidity Bose-Einstein Condensation (BEC) and extremely well-defined "phonon-roton" (p-r) excitations (full width at half maximum as narrow as 0.1 (μeV at T = 0:8 K) in low-temperature liquid 4He are closely related phenomena. In the bulk liquid, at saturated vapour pressure, they show up together below the so- called λ temperature ($T_s=T_{BEC}=T_\lambda$ =2.17 K).

The superfluid properties (macroscopic in nature) of liquid ^{4}He conned in several porous media have been extensively investigated [1]. It has been found that confinement reduces the superfluidity temperature T_s. The smaller the pore size of the porous media, the further T_s is reduced below T_λ.

From the microscopical point of view, the existence of p-r excitations is considered a proof of BEC. The first measurement of the characteristic phonon-roton excitations of super ^{4}He confined in porous media by inelastic neutron scattering was performed by Coddens et al. [2] in 1994.

The initial goal in these and subsequent measurements was to reveal how confinement and disorder modify the phonon-roton excitations from their bulk ^{4}He values.

Apart from additional weak, relatively broad, side excitations, believed to be supported by denser liquid layers close to substrate surface [3], no major changes have been detected in the microscopical behaviour of the liquid once confined.

1.1. Aim

Two of the possible sources of errors in the above results are:
1. a too large average pore size for the confining medium
2. the presence of bulk liquid helium embedding the porous material and the confined helium sample

A too broad pore size distribution of the confining medium could also non trivially a affect results [4].
We will deal with these points and try to overcome them.

2. Materials

Recently discovered materials as silica MCM-41 seem to provide good confining environments: pores are a collection of bunches of cylindrical pores whose average diameter ranges from 20 Å to 100 Å following synthesis procedure, while pore size distribution has a sharp-peaked shape.

3. Tools

In order to characterize the confined 4 He sample we performed (volumetric-)pressure isotherms using ^{4}He as probe gas. The technique consists in measuring the amount of ^{4}He adsorbed by the porous sample, N_{ads}, at fixed temperature T vs. equilibrium pressure, P. This quantity is obtained by direct subtraction of the residual gas amount at equilibrium, N_{gas}, from the total injected gas amount, N_{inj}.

It is customary to plot results of such a measurement as specific adsorbed amount of matter, n_{ads}, vs. reduced pressure p; these two variables are defined as: $n_{ads} = \dfrac{N_{ads}}{m}$ and $p = \dfrac{P}{P_0(T)}$, where m is the mass of the adsorbing sample and $P_0(T)$ is saturated vapour pressure of the probe gas at temperature T .

The measurements of gas amounts are performed by high accuracy (0.12% on reading) pressure measurements over calibrated (about 0.1% accuracy) volumes. Some features can be extracted directly from the adsorption diagram. In particular, a step in filling at nearly constant pressure in the range $0.1 \leq p \leq 0.9$, is generally associated with the condensation of the probe inside pores into a state very similar to bulk condensed phase. This phenomenon is called "capillary condensation" and occurs in the so-called "mesoporous" materials that is to say, in materials presenting pores whose size ranges from 20 Å to 50 Å. The capillary condensed phase is actually the phase we are interested in: a confined liquid phase. Performing experiments below saturated vapour pressure make us sure that no bulk liquid is sourrounding the confined sample and that all the observed signal is coming from confined ^{4}He.

4. Results

A MCM-41 sample has been provided by University of Mulhouse (France); average pore size is d = (32 ± 3) Å and specific surface is $s \cong 910\ m^2g^{-1}$ as determined by standard nitrogen adsorption measurements and data analysis in the framework of the Barrett, Joyner and Halenda model [5].

We performed ^{4}He pressure isotherms at T = (2.48 ± 0.01)K; results are shown and commented in figure 1; we stress that the sample allows capillary condensation of helium at this temperature. Exploratory neutron scattering experiments have been performed on the MIBEMOL inelastic spectrometer at LLB using an incident neutron wavelenght of 5 Å. Results are shown and

commented in figure 2. The main achievement of these measurements is that they show undoubtly that the inelastic signal generating from confined helium (in the range of exchange energy considered) is mainly due to capillary condensed liquid. This inelastic signal appears to have roughly the same dispersion as expected for the 3D bulk liquid.
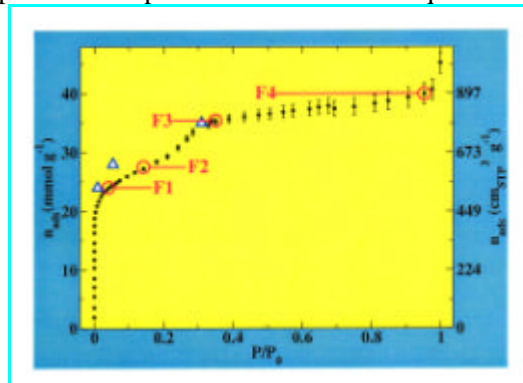
Figure 1. Helium adsorption diagram on a 32 Å A pore diameter MCM-41 sample. Black symbols with error: measured isotherm at $T = (2:48 \pm 0:01)$ K; red circles: selected fillings for neutron scattering experiments; blue triangles: values actually obtained at $T = (1:2 \pm 0:1)$ K while performing a neutron scattering experiment on MIBEMOL (LLB). A large amount of helium (up to $F1 \cong 24$ mmol g^{-1}) is strongly attached to surface being at equilibrium at a tiny pressure; between F1 and $F2 \cong 28$ mmol g^{-1}, some more helium is adsorbed into less favorable adsorption sites, from F2 to F3 $\in 36$ mmol g^{-1}), capillary condensation occurs. At $F4 \cong 40$ mmol g^{-1}, the filling is complete and any subsequent added helium amount is condensed into the bulk phase at $P=P_0(T)$ i.e. $p= 1$.

We then performed an experiment on the IN6 spectrometer (ILL, Grenoble) using an incident neutron wave-length of 4.62 Å. We found that excitations of helium conned into MCM-41 show the same features as in other confining materials. In particular energies and lifetimes of the 3D excitations obtained at filling F3 were the same as the bulk liquid within experimental accuracy. Usual side excitations believed to arise from denser liquid layers close to the substrate surface were detected as well.

The original result concerns excitations supported by the layered liquid (filling F2) that disappear at filling F3 (see Fig.3). This excitation is believed to be a
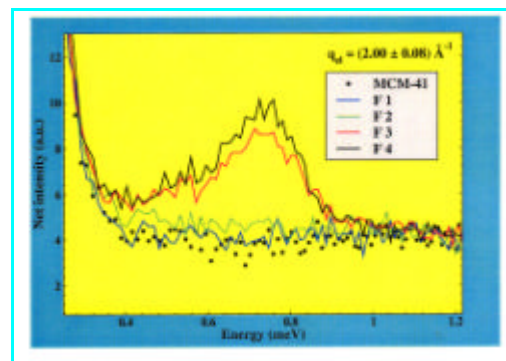
Figure 2. Neutron scattering raw spectra for 32 Å-diameter-pore MCM-41 at selected fillings in helium. Shown spectra have been taken at constant scattering angle; the corresponding value for $q_{el} \equiv q(\omega= 0)$ is $q_{el} = (2:00 (0:08)$ Å^{-1}. We note that the most of inelastic intensity in the range considered is rising from the capillary condensed phase, despite of its relatively small amount. Some intensity could be associated with filling F2.

capillary wave (also called a ripplon) at the liquid-vapour boundary, supported by liquid layered onto the inner cylindrical surface of the pores. These excitations have been already observed in liquid helium layers on a graphite substrate [6]. Upon complete filling of the pores by capillary condensation, the liquid-vapour interface is strongly depressed and the excitation is no more detected. At filling F3, we start detecting typically 3D excitations instead.
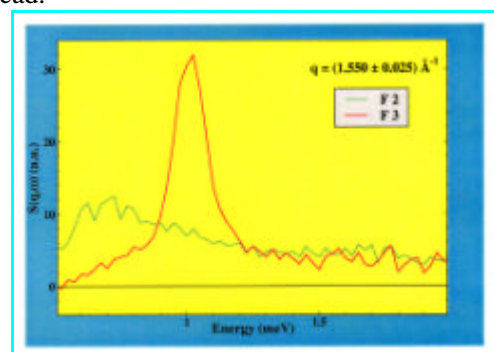
Figure 3. Neutron scattering spectra for 32Å-diameter-pore MCM-41 at selected fillings in helium. Data have been reduced to constant-q scans after subtracting the MCM-41 contribution. An excitation supported by helium at filling F2 appears to be destroyed upon further filling.

References

[1] J. D. Reppy. *J. Low Temp. Phys.*, **87** (1992) 205.

[2] J. de Kinder, G. Coddens, R. Millet. *Z. Phys. B Cond. Mat.,* **95** (1994) 511.

[3] R. M. Dimeo, P. E. Sokol, C. R. Anderson, W. G. Stirling, K. H. Andersen, M. A. Adams. *Physical Review Letters*, **81** (1998) 5860.

[4] R. Maynard, G. Deutscher. *Europhysics Letters*, **10** (1989) 257.

[5] E.P. Barrett, L.G. Joyner, P.P. Halenda. *Journal of the American Chemical Society*, **73** (1951) 373.

[6] H.J. Lauter, H. Godfrin, V.L.P. Frank, P. Leiderer. *Physical Review Letters*, **68** (1992) 2484. 1992.

STRUCTURAL RELAXATION IN SUPERCOOLED SELENIUM

Benoît Rufflé [1] and Stéphane Longeville [2]

[1]Laboratoire des Verres, Université Montpellier II, 34095 Montpellier Cedex 5, France
[2]Laboratoire Léon Brillouin (CEA-CNRS), CEA-Saclay, 91191 Gif-sur-Yvette, France

In the last decade many experiments as well as computer simulations have established that the so-called mode-coupling theory of the glass transition (MCT) [1] is able to give a *qualitatively* correct description of the structural relaxation dynamics of fragile supercooled liquids at least in the weakly supercooled state. In previous works, we have studied the structural relaxation dynamics of a complex oxide glass (Na_2O-Li_2O-$2P_2O_5$) by means of neutron scattering in a broad range of temperature [2]. It has been clearly demonstrated that also intermediate glass formers show features that are in *qualitative* agreement with the predictions of MCT [2,3]. However, starting from the static properties of the system, MCT is able to give a *quantitative* description of the relaxation dynamics of supercooled liquids. In particular it is possible to calculate from the knowledge of the static structure factor $S(q)$ the time dependence of the coherent intermediate scattering function $F(q,t)$. These type of calculations have been done only for very few systems (most are fragile and/or monoatomic *simulated* systems), since they are quite involved even for binary systems [4].
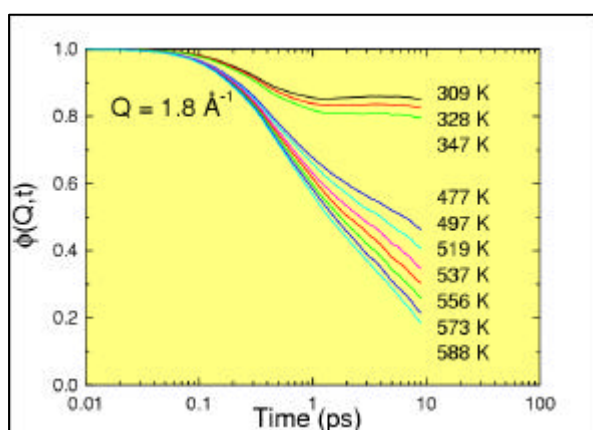
Figure 1. Temperature dependence of the normalized intermediate scattering function of Selenium at Q=1.8 Å^{-1} measured on Mibemol.

The final aim of the reported experiments here is to compare, for the first time, detailed MCT calculations and inelastic neutron scattering experiments on liquid Selenium, a monoatomic system. Selenium is an inorganic polymerlike glass

former of intermediate fragility with a low glass-transition temperature T_g=303 K (T_m=494 K). Due to its predominant coherent scattering cross-section Selenium is a particularly good candidate for neutron spin echo experiments and such an analysis. Fig.1 shows the temperature dependence of the normalized intermediate coherent scattering function $\phi(Q,t)$ measured at the LLB on the time-of-flight spectrometer Mibemol at Q=1.8 Å^{-1}, a value close to the first maximum of the static structure factor. The typical slowing down of the structural relaxation when cooling the liquid from above the melting temperature down to the glass transition temperature is observed. At very short time (~0.1 ps) the correlation functions decay due to the vibrational dynamics. This is followed by a two-step decay: the **b**-regime (~0.1-1 ps) and the structural or **a**-relaxation which is hardly temperature dependent. The gap between 477 K and 347 K corresponds to the temperature range
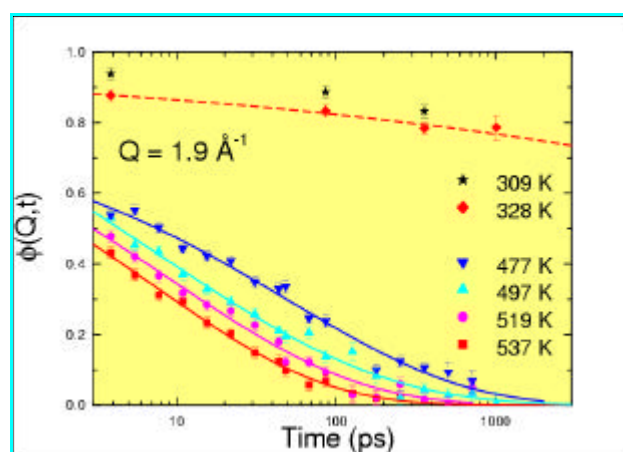
Figure 2. Temperature dependence of the normalized intermediate scattering function of Selenium at Q=1.9 Å^{-1} measured on G1bis.

where crystallization could not be avoided. In order to get in more details the shape of the structural relaxation, its temperature and wavenumber dependence, we have completed the long-time part of some of the TOF spectra with neutron spin-echo data measured on G1Bis at the LLB. Fig. 2 exhibits the temperature dependence of the normalized intermediate coherent scattering

function $\phi(Q,t)$ measured at the LLB on the spin-echo spectrometer G1Bis at a selected Q value, namely $Q=1.9 \, \text{Å}^{-1}$. The solid lines are fits using the usual simple stretched exponential function with all parameters free. In a first analysis all the high temperature spin-echo data, above the crystallization region, are compatible with a common stretch exponent $b=0.5$. However, due to the scatter of data and the limited time-scale of the spin-echo machine, a small temperature and/or wavenumber dependence cannot be excluded. Combining the TOF spectra together with the spin-echo data will certainly make it clear. An efficient way to visualize the Q-dependence of the structural relaxation time with a spin-echo machine is to measure the polarization at selected times t only. As shown for example in Fig. 3 for T=500 K, the data clearly reveal a peak around $1.2 \, \text{Å}^{-1}$, a value close to the position where a small prepeak is detected in the static structure factor of liquid Selenium at high temperature [5]. Assuming a common stretch exponent parameter b, the Q-dependence of the structural relaxation timescale can be estimated from these data and

have been plotted in Fig. 4. The complete time dependence of the solution of the mode-coupling equations in which the full Q dependence is taken into account has been calculated with the experimental static structure factor of liquid Selenium at 531 K [5] as only input (apart particle density). A first result of these mode-coupling calculations is that the shape of the structural relaxation seems to be rather different from the experimental one. The estimated stretch exponent parameter is indeed around $b_{MCT}=0.75\text{-}0.8$ and not 0.5 as found here in these experiments. As recently found for silica [4], the prototype of strong liquids, the mode-coupling equations used could be too simple to describe Selenium. On the other hand the Q-dependence of the calculated structural relaxation timescale, and plotted in Fig.4, clearly reproduces the experimental peak found around $1.2 \, \text{Å}^{-1}$. The detail of the Q-dependence is again far from being perfect probably for the same reason. It has also to be noted that the exact values of the relaxation times cannot be compared at this stage of the analysis.

Figure 3. Q-dependence of the polarization measured on G1bis at T=500 K for selected t values.
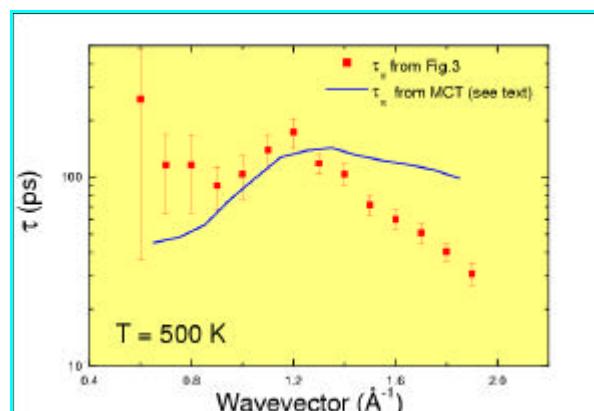
Figure 4. Q-dependence of the a-relaxation time deduced from Fig. 3. The full line is the a-relaxation time Q-dependence deduced from MCT calculations.

References

[1] W. Götze, *J. Phys. Condens. Matter* **10** (1999) A1.
[2] B. Rufflé, C. Ecolivet and B. Toudic, *Europhys. Lett.* **45** (1999) 591.
     B. Rufflé and al., *J. of Non-Cryst. Solids* **235-237** (1998) 244.
     B. Rufflé and al, *Phys. Rev. B* **56** (1997) 11546.
[3] T. Franosch, W. Götze, M.R. Mayr and A.P. Singh, *Phys. Rev. E* **55** (1997) 3183.
[4] F. Sciortino and W. Kob, *Phys. Rev. Lett.* **86** (2001) 648.
[5] R. Bellissent and G. Touraud, J; *Non-Cryst. Solids* **35&36** (1980) 1221.

PHASE SEPARATION OF A BINARY LIQUID SYSTEM IN CONTROLLED-PORE GLASS

S. Schemmel[1], G. Rother[1], A. Brûlet[2], Th. Hellweg[1], G. H. Findenegg[1]

[1]Technische Universität Berlin, Stranski Laboratorium, Straße des 17. Juni 112, 10623 Berlin, Germany
[2]Laboratoire Léon Brillouin (CEA-CNRS), CEA-Saclay, 91191 Gif sur Yvette, France

Binary liquid mixtures separate into two phases of different compositions below a critical solution point. When imbibed in a porous matrix, the phase separation cannot occur on a macroscopic scale but the two coexisting phases form small domains and the dynamics of the growth of these domains is very slow. The interest in the structure and dynamics of phase-separated liquid mixtures in porous materials arises from the increasing importance of mesoscopically disordered systems in materials science [1], but also from applications in separation processes such as liquid chromatography, microfiltration, or the extraction of liquids from porous materials. Many of these applications depend on the flow and diffusion of the liquid in the pores, which in turn are strongly affected by the morphology of the phase separated domains.

A porous medium affects the phase separation of liquid mixture not only by geometrical confinement effects, but also by the preference of the pore surface for one component. In the one-phase region (1?) of the mixture, the latter will cause preferential adsorption, i.e., a concentration profile from the wall into the pore volume. For sufficiently wide pores, the decay length of this profile corresponds to the correlation length ? of fluctuations in the interior of the mixture, but in narrow pores (pore width D < ?) an overlap of the profiles from opposite walls will cause an enhanced adsorption. In the two-phase region (2?) the walls will be wetted, either completely or partially, by the preferred phase, causing either a tube-like or a plug-like morphology of the preferred phase in cylindrical pores [2]. Incipient wetting of the pore walls, manifested by multilayer adsorption, is expected to occur in the one-phase region close to the liquid-liquid coexistence curve in the region in which the preferred component forms the minority component of the mixture.

In order to test some of these predictions, we have studied the structure and dynamics of the binary system iso-butyric acid (iBA) + heavy water (D$_2$O) in a controlled-pore glass (CPG). The mean

pore size of the CPG materials is around 10 nm. Water is preferred by the pore wall in the iBA + D$_2$O system. The phase diagram of this system in the bulk liquid state is shown in Figure 1.
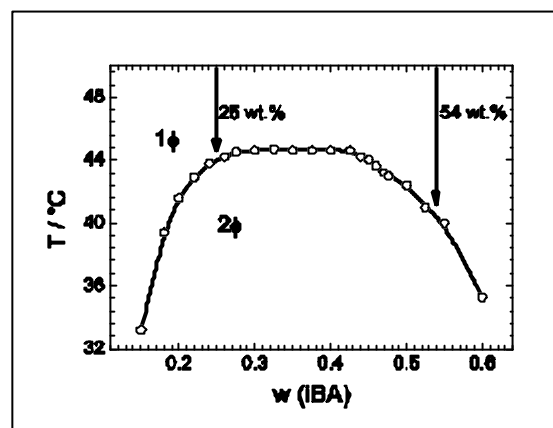
Figure 1. Bulk phase diagram of the binary liquid mixture iBA+D$_2$O. The solid line represents the binodal.

The temperature-induced microphase separation of a water-rich mixture (25 wt.-% iBA) and a water-poor-mixture (54 wt.-% iBA) was studied over a wide temperature range (20 – 70°C), covering both the one-phase and the two-phase regions of the bulk system.

Small-angle neutron scattering (SANS) was used to determine the structure of the liquid mixture in the pores. The scattering data I(q) were analysed by a function I(q) similar to the equation recently proposed by Formisano and Teixeira [3], which is based on a scaling function which represents the correlation peak arising from the quasi-periodic structure of the pore network in CPG, and the contribution from film scattering due to the adsorbed film at the pore interface. Concentration fluctuations in the one-phase region, which are expected to grow in size as approaching the two-phase boundary, are represented by an Ornstein-Zernicke (OZ) function $I(q) \sim q^{-2}$ with a correlation length ?$_C$. Domains of the two phases, separated by sharp interfaces, are described by a $I(q) \sim q^{-4}$ dependent squared OZ expression with a

characteristic correlation length ξ_D. Figure 2 shows the temperature dependences of the correlation lengths (ξ_C, ξ_D) obtained for the 54 wt-% iBA sample.
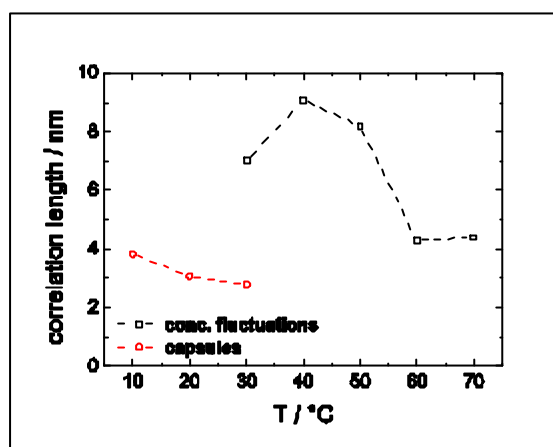
Figure 2. Variations as a function of temperature of the concentration fluctuations ξ_C (□ black) and the two-phases domains ξ_D (○ red) for the 54 wt-% iBA sample.

As expected, the correlation length of the diffuse concentration fluctuations in the one-phase region increases as the phase boundary is approached. A cut off, around 8 nm, is observed: it roughly corresponds to the average pore size diameter. In the two-phases region (T < 30°C), these concentration fluctuations are replaced by the microphase-separated domains of the two phases, which slightly grow in size as one moves deeper into the two-phase region [4].

The dynamics of fluctuations and microphase-separated domains has been investigated by neutron spin-echo (NSE) spectroscopy at the instrument MESS at the LLB. NSE experiments yield the time dependence of the intermediate scattering function $S(q,t)$. They can be fitted by a single-exponential decay, $S(q,t) \sim \exp(-Gt)$, where

G is the characteristic relaxation frequency which is related to the effective diffusion constant of the domains as $D_{eff} = G/q^2$. Figure 3 shows the temperature dependence of D_{eff} for the 54 wt-% iBA-sample. The observed decrease of D_{eff} with decreasing temperature is tentatively attributed to the increase of the size of the concentration fluctuations in the one-phase region and an immobilization of the domains at the pore surfaces in the low-temperature region [5].
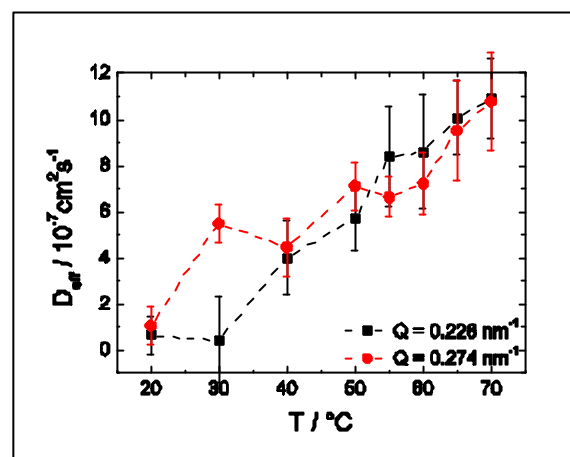
Figure 3. Effective diffusion coefficient as a function of temperature for the 54 wt-% iBA sample. The dashed lines are guides for eyes.

This interpretation is consistent with the results of the SANS study, by which the increase of the concentration fluctuations with decreasing temperature in the one-phase region and the appearance of domains of the two phases at low temperatures have been directly observed.

Both NSE and SANS studies show that the microphase separation of the liquid mixture in the porous matrix does not occur at a sharp temperature but extends over a wider temperature range below the phase separation temperature of the bulk mixture.

References

[1] D.A. Weitz, *MRS Bulletin*, issue on disordered materials, May 1994.

[2] A.J. Liu, D.J. Durian, E. Herbolzheimer, S.A. Safran, *Phys. Rev. Lett.* **65** (1990) 1897; L. Monette, A.J. Liu, G.S. Grest, *Phys. Rev. A* **46** (1992) 7664.

[3] F. Formisano, J. Teixeira, Eur. Phys. J. E 1 (2000) 1; *J. Phys.: Condens. Matter* **12** (2000) A351.

[4] S. Schemmel, G. Rother, G.H. Findenegg, manuscript in preparation.

[5] T. Hellweg, S. Schemmel, G. Rother, A. Brûlet, H. Eckerlebe, G.H. Findenegg, *Eur. Phys. J. E*, submitted.

STRUCTURAL CHANGES IN SULPHUR-RICH BINARY GLASSES

E. Bychkov[1], M. Miloshova[1], M. Fourmentin[1], A. Lapp[2]

[1]LPCA, UMR CNRS 8101, Université du Littoral, 59140 Dunkerque, France
[2]Laboratoire Léon Brillouin (CEA-CNRS), CEA Saclay, 91191 Gif-sur-Yvette Cedex, France

Small-angle neutron scattering, Raman spectroscopy and DSC were used to study structural changes for sulphur-rich AsS_x ($x \geq 1.5$) and GeS_x ($x \geq 2$) glasses. Two structural regions were found in the both systems. (1) Between stoichiometric (As_2S_3 and GeS_2) and 'saturated' ($AsS_{2.3}$ and $GeS_{2.7}$) compositions, excessive sulphur atoms form sulphur dimers and/or short chains, replacing bridging sulphur in corner-sharing $AsS_{3/2}$ and $GeS_{4/2}$ units. (2) Above the 'saturated' compositions at [As] < 30.5 at.% and [Ge] < 27 at.%, sulphur rings and longer sulphur chains (especially in the AsS_x system) appear in the glass network. The glasses become phase-separated with the domains of 20 to 50 Å, presumably enriched with sulphur rings. The longer chains S_n are not stable and crystallise to c-S_8 on ageing of a few days to several months, depending on composition.

Kawamoto et al. [1] were the first who observed two types of sulphur in S-rich GeS_x glasses: (i) insoluble in CS_2 species (sulphur chains), and (ii) soluble in CS_2 species (sulphur rings). Many research groups identified sulphur rings as S_8 using Raman spectroscopy (see, for example, [2]). A simple model was proposed to account for these results. (1) Excessive sulphur atoms, added to the stoichiometric glass (As_2S_3 or GeS_2), transform bridging sulphur into S_2 dimers. At a 'saturated' composition AsS_3 or GeS_4, all structural units ($AsS_{3/2}$ pyramids or $GeS_{4/2}$ tetrahedra) become isolated, i.e., they do not share any longer their corners separated by three (AsS_3) or four (GeS_4) sulphur dimers. (2) Above the 'saturated' compositions at $x > 3$ (AsS_x) or $x > 4$ (GeS_x), the S_8 rings appear in the glass network, evidenced by characteristic vibrations in the Raman spectra and partial glass dissolution in CS_2.

Figure 2. Glass transition temperatures for sulphur-rich GeS_x and AsS_x glasses.

Our Raman spectroscopy results do not support the simple model; in particular, the 'saturated' compositions are clearly different from the predicted ones, AsS_3 and GeS_4. In the AsS_x system, the characteristic vibrations of sulphur rings at 152 and 220 cm^{-1} appear at $x \geq \approx 2.5$. For their germanium counterparts GeS_x, they become visible at $x \geq \approx 3$ (Fig. 1). Nevertheless, the existence of the two suggested composition domains seems to be evident. Only a broad feature at 475 cm^{-1} appears in the spectra of GeS_x in the domain (1) in addition to A_1, A_{1c} and other Raman lines in the 300-450 cm^{-1} range, attributed to Ge-S vibrations in the corner-sharing CS- and edge-sharing ES-$GeS_{4/2}$ tetrahedra [2,3]. The 475 cm^{-1} feature is common to S-S vibrations in all forms of

Figure 1. Raman spectra of sulphur-rich GeS_x glasses.

sulphur from chains to rings, and in the absence of characteristic ring vibrations indicates a chain-like bonding of sulphur species.
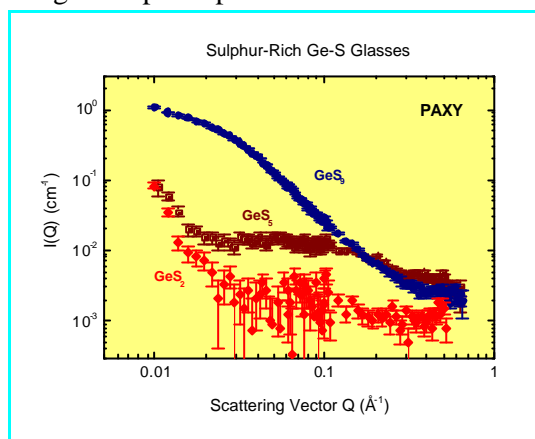
Figure 3. Typical SANS functions for selected GeS_x glasses.

A single glass transition in the domain (1) and a bimodal shape of the DSC traces in the domain (2) for the two binary systems suggests the phase separation. The composition dependence of the glass transition temperatures, T_g, shows also remarkable similarities and differences between the As-S and Ge-S vitreous alloys (Fig. 2). In both cases, the $T_g(1)$ corresponding to either $GeS_{4/2}$ or $AsS_{3/2}$ structural motif decreases with increasing sulphur content but the initial decrease in the domain (1) for the GeS_x glasses ends by a flattening in the domain (2). In contrast, freshly prepared AsS_x alloys exhibit a nearly linear decrease of $T_g(1)$, which extrapolates to -30 °C for pure sulphur, a value characteristic of plastic sulphur, whose metastable structure is a mixture of chains and rings [4,5]. The values of $T_g(2)$ are similar and nearly constant in the both systems. Apparently, they correspond to a glassy phase mostly consisting of sulphur rings. The $T_g(2)$ fraction increases with increasing sulphur content. Typical small-angle neutron scattering functions $I(Q)$ for the selected Ge-S glasses are given in Fig. 3. Homogeneous GeS_2 glass is a weak scatterer, especially at $Q > 0.01$ Å^{-1}. The SANS intensity changes are small in the domain (1). The appearance of the sulphur rings in the domain (2) is accompanied by a characteristic and systematic change in the $I(Q)$. Correspondingly, the SANS intensity increases by two to three orders of magnitude between 0.01 and 0.1 Å^{-1} with

increasing S concentration. A typical size of the second glassy phase varies between 20 and 50 Å. The AsS_x glasses exhibit similar trends, but the structural changes on mesoscopic scale are much less pronounced compared to GeS_x. The stoichiometric glass compositions As_2S_3 and GeS_2 do not show any time-dependent phenomena. Nevertheless, glasses from the domain (2) in the both systems exhibit well-documented ageing. The phase separation becomes more pronounced (Fig. 4), and the T_g increases with time for the S-richest As-S glass compositions. This behaviour needs to be studied in more details.
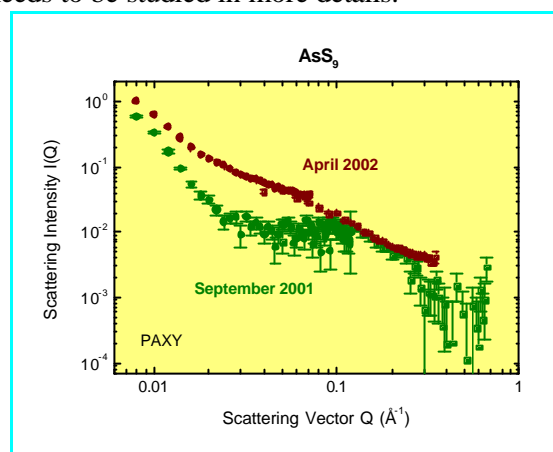
Figure 4. Time-dependent phenomena in the meso-scopic structure for binary glasses in the domain (2).

Quantitative analysis of the Raman data, SANS and DSC indicate that the AsS_x glasses in the domain (2) contain sulphur chains. The above conclusion can explain many observed phenomena. In contrast to the sulphur rings, the S_n chains, where n increases with the S content, are supposed to be inserted in the glass network between the $AsS_{3/2}$ pyramidal units, thus decreasing the network rigidity and T_g in a monotonic manner (Fig. 2). A smaller fraction of the sulphur rings in the AsS_x phase-separated glasses means the reduced SANS intensity, also consistent with the experimental findings. The sulphur chains are not stable neither in crystalline nor in glassy form. Consequently, they would be transformed into the stable c-S_8 form on ageing, giving rise to a number of time-dependent phenomena on mesoscopic (confirmed by SANS) and macroscopic scale (DSC), e.g., a T_g increase caused by the loss or decreasing in length of the inserted S_n fragments.

References

[1] Y. Kawamoto, S. Tsuchihashi, *J. Amer. Ceram. Soc.* **54** (1971) 131.

[2] S. Sugai, *Phys. Rev. B* **35** (1987) 1345.

[3] K. Jackson et al., *Phys. Rev. B* **60** (1999) 14985.

[4] M. Stolz, R. Winter, W.S. Howells et al., *J. Phys.: Condens. Matter* **6** (1994) 3619.

[5] E. Bychkov et al., *13th Intern. Conf. on Non-Oxide Glasses* (Pardubice, Czech Republic, 2002).

LOCAL STRUCTURE AND GLASS TRANSITION OF POLYBUTADIENE UP TO 4GPa

C. Alba-Simionesco[1], A. Cailliaux[1], I. Goncharenko[2], B. Frick[3], L. Willner[4]

[1]Lab. de Chimie Physique, Bât. 349, Université de Paris-Sud, 91405 Orsay Cedex, France *www.lcp.u-psud.fr*
[2]Laboratoire Léon Brillouin (CEA-CNRS), CEA-Saclay, 91191 Gif sur Yvette Cedex, France.
[3]Institut Laue Langevin, BP 156, 38042 Grenoble Cedex 6, France.
[4]Institut für Festkörperforschung, Forschungszentrum Jülich, D-52425 Jülich, Germany.

The glass transition can be induced by decreasing the thermal energy or by increasing the density. The usual way to investigate the glass transition is to cool a sample at ambient pressure, which not only reduces its thermal energy but also increases its density. The viscosity gets very high, the molecular relaxation time increases strongly: when these parameters get bigger than 10^{13}P or 10^3s, the system can not reach equilibrium any more within the experimental time, the melt turns to glass. Let's point out that the glass transition is a kinetic transition, and not a thermodynamic one. Typically the density change during cooling between the high temperature melt and the glass transition temperature T_g is of the order of 6-10% depending on the system. This transition can be observed by many techniques. One of the simplest ones is to follow the density variation and consequently the mean peak position of the static structure factor with temperature: a change of slope occurs at the glass transition. The glass transition is still not fully understood in a fundamental point of view. For instance, it is difficult to disentangle the control parameters of the dynamics: is density or thermal energy mainly responsible of the slowing down of the dynamics occurring at the glass transition ?

It is observed that the characteristic slowing down of the molecular motions, when approaching the glass transition, depends more on thermal energy than on density; at T_g and normal pressure, we have shown that the temperature controls up to 80% of the phenomenon for the simple polymer, the polybutadiene [1] However, the relative importance of thermal energy and density might change if a larger relative density change is imposed by the experimental conditions. For example one can impose a density change of 20–30% by applying high pressure at higher temperature and then the glass transition phenomena might be different with a glass of distinct properties. Furthermore by applying external pressure one can separate the influence of density and thermal energy, and take the advantage of building isochors. These informations are reflected by the changes observed in the static structure factor S(Q) under such conditions.

The main peak of the static structure factor in polymers is expected to be to a large part due to interchain correlations. At constant pressure the effect of increasing temperature on S(Q) results essentially in a shift of the peak position towards lower Q-values. The shift is more pronounced above the glass transition than below, just like one would expect from the different thermal expansion below and above Tg. For deuterated polybutadiene the static structure factor S(Q) was measured previously at several temperatures and moderate pressures, from atmospheric pressure up to 3 kbar, using neutron polarisation analysis of D7 at the ILL with a Niobium liquid pressure cell (from .2 to 2.5 Å^{-1}) [2]. The range of pressure corresponds to a change in local density of about 6 to 10%, equivalent to the change observed at atmospheric pressure from room temperature down to the glass transition (T_g=176K for M_w=8000). Recent experiments up to 4GPa [3], performed on G6.1 at the LLB, in an anvil sapphire cell, show a very good matching between the data obtained at lower pressure with D7 and the ones of G6.1 at the same temperature 295K (see Fig.1a). By these experiments we could extend the observation up to much higher pressures and have observed that the changes of S(Q) with temperature and density affect mainly the Q-region near the first structure factor peak in the melt and in the glassy state as shown in Fig.1b at 160K. The main structure factor peak moves fast to higher Q at low pressures, an obvious sign of increasing local density, and more slowly at higher pressures. These measurements allow to estimate that at an isotherm of T=295K the glass transition should appear in pressure range between 1.2-1.6 GPa, in agreement with calorimetric data (see Fig.2,3).
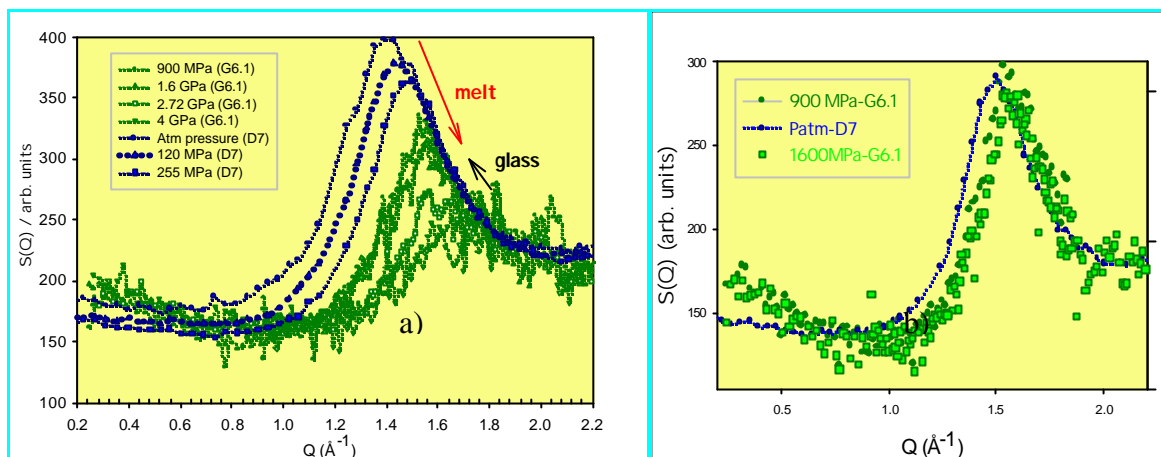
Figure 1. S(Q) of PB as a function of pressure under isothermal conditions: a) at 295K from the melt to the glass; b) at 160K, but the system was quenched from 295K to 160K in order to avoid any pressure gradient.
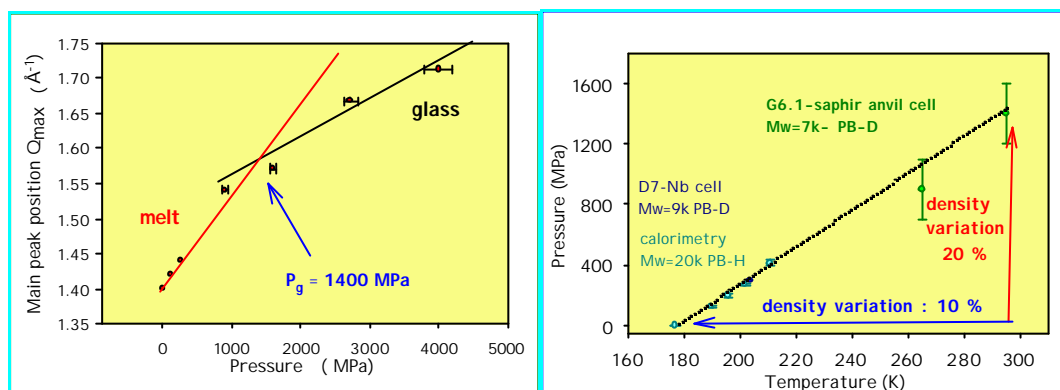
Figure 2. peak position of the first peak in S(Q) as a function of pressure. The arrow shows the glass transition

Figure 3. glass transition line in a P-T phase diagram, with the corresponding density changes. Comparison of data obtained under different conditions

Moreover, we observe that the static structure factor S(Q) does not change along macroscopic isochors which can be determined by calorimetric measurements and P-V-T under high pressure [2,3]. The behaviour of the structure is found to be contrary to the dynamics, where the relaxations observed by the dynamic incoherent scattering law $S(Q,\omega)$ in the ns- to ps-time scale differ strongly along the same thermodynamic path [2]. We conclude that the static behaviour, i.e. S(Q), is dominated by macroscopic density changes, similar to the vibrational excitations in the meV-range.

But the most striking result in figure1 concerns the

height of the peak, which dramatically decreases with pressure; in particular, at 4 GPa, while the system is in the glass region, a tremendous effect is observed. This phenomenon had already been observed in mineral glasses : in the case of SiO_2 and GeO_2, the coordination number of Si and Ge was found to increase with pressure. In our case, when local density increases, the voids size decreases(inducing a lower contrast), and the inter and intra-chain distances tend to match, leading to a more homogeneous system. This point will be discussed in the future with the changes of the Boson peak observed after densification.

References

[1] Ferrer M-L, Kivelson D., Alba-Simionesco C., Tarjus G., *J. Chem. Phys*. **109** (1998) 8010.

[2] Frick B., Alba-Simionesco C., Anderse, K. Willner L. (2003) *Phys.Rev E*, in presse (May).

[3] Cailliaux A., Alba-Simionesco C., Frick B., Willner L., Goncharenko, I., *Phys.Rev.E* (Rapid Comm.), **67** (2003) (010802).
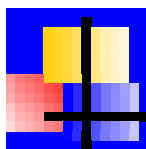
5 - SOFT MATTER AND BIOMATERIALS

This report presents a combination of work from the Soft Matter group own research and work from external users; one can see a kind of synergy, since there are common trends, interactions and collaborations with users in the field. The activity involves SANS, Neutron Reflectivity, and to a lower extent Neutron Spin Echo, Light Scattering (in the lab). It covers the field of colloids, self-assembling surfactants, nanoparticles and polymers, our strongest field of expertise.

One, two and many component systems:
A common trend in Soft Matter focus on studies of complex systems, combining two or more components, which can be observed separately due to the wide range of neutron scattering length densities (through deuteriation in particular). This is the case for polymers systems mechanically reinforced by nanoparticles fillers, vesicles with membranes stabilised by polymers but also for the rising theme of polyelectrolytes with proteins.

Rheological properties, thin films and biomaterials:
In many of these systems, we are interested in mechanical or rheological properties, prompting structural studies under deformation, in other words Rheo-SANS. Leaving the bulk case, neutrons are also very appropriate for analysing confined systems: chains confined in porous media, or in ultra-thin polymer films. Further down to the two-dimensional case, we used Neutron Reflectivity. After former studies of liquid – air interface of thermo-sensitive polymers solutions (PNIPAM, Methyl Cellulose), and of solid-solid interdiffusion profiles between polymer layers (incl. polymer network, in relation with adhesion), we focus here on layers used to capture DNA oligonucleotides at the surface of biochips.

Modelling and Instrumentation:
Work on Instrument or Methods, new Very Small Angle spectrometer (J. Oberdisse), Time resolved nuclear polarization observed by DNPA. (H. Glättli, thesis E. Leymarié, collaboration with PSI, Switzerland), are detailed in other Chapters, as well as Modelling of the complex associations encountered in nanocomposites (see section 5.2).

POLYMER OBJECTS FROM NOVEL SYNTHESIS ROUTES AND ASSOCIATIONS
New polymer architectures:

Beyond what has been imagined by their creators, new architectures in polymer science have definitely to be characterized and neutron scattering is a tool of excellence in the field.

Copolymers:
A first external work is **_highlighted_** in this report: it concerns polypeptide-polybutadiene copolymers, which can form vesicles which shape depends on the nature of the aqueous solvent, pH, salt content etc.
Collaboration S. Lecommandoux, F. Checot, LCPO Bordeaux and A. Brûlet, J.P. Cotton, LLB.
Branched polymers:
Several works concern **bottle-brush branched polymers**. Some promising results have already been obtained by grafting living polymer chains of polystyrene (PS) on an already existing backbone of Polyvinylether (PCVE), as done by Schappacher and Deffieux (LPO, Bordeaux).
Macromonomers:
An on going project is the polymerisation of a molecule, Norbornene, on which is grafted a PS chain, which therefore form a "macromonomer" (Y. Gnanou, V. Herroguez, thesis S. Desvergnes*)*. The polymerisation consists in opening a ring (Ring Opening metathesis), the strength of the reaction being able to connect together macromonomers of different nature (e.g. PS branch and polybutadiene branch).

The shape of bottle-brushes crosses over from spherical shape to rod-like and eventually worm-like shape when increasing the ratio of the backbone length (i.e. the degree of polymerisation DP) to the branch length as illustrated in Figure 1 below. The work on PCVE-based grafted bottle-brush showed that, due to the high grafting density of PS, the persistence length is much higher for the backbone of the grafted polymer than for the non-grafted backbone alone. We are also interested in measuring how the lateral polystyrene chains are elongated, using in all those situations appropriate labelling and contrast conditions.
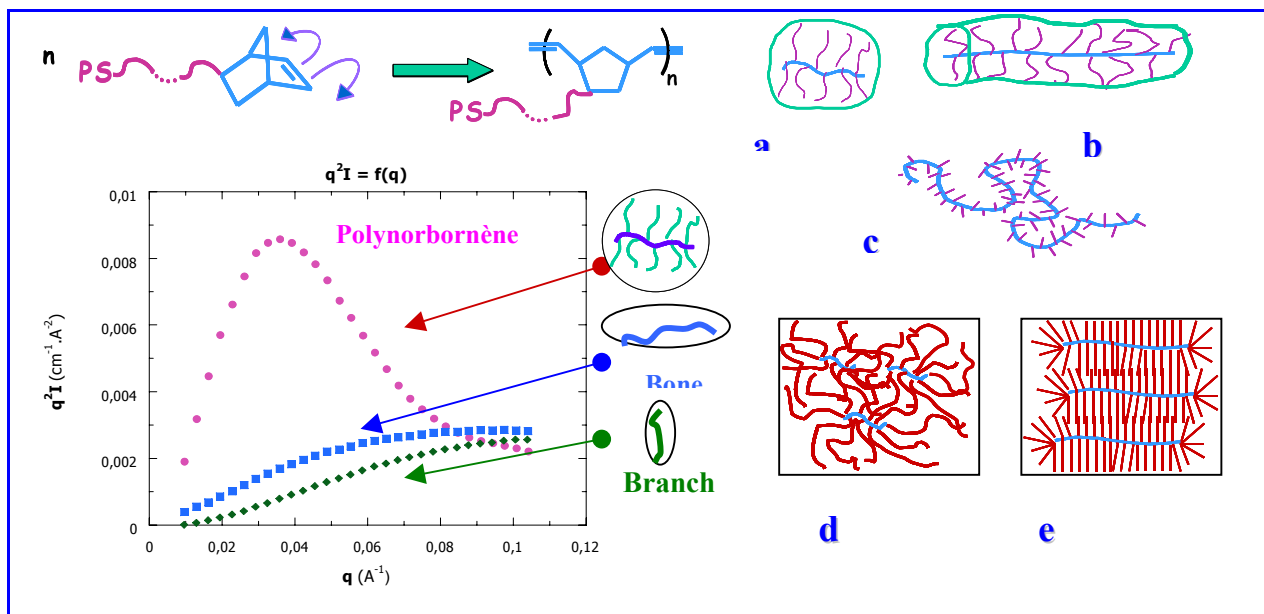
Figure 1. Polymacromonomers. Above, left : a " macromonomer" comprises a polystyrene chain (purple) linked to a Norbornene molecule (blue); this molecule becomes a unit of the backbone after polymerisation by opening the Norbornene ring. Right: depending on the relative length of the backbone (blue) and of the branch chains, the conformation will evolve from a) a sphere to b) a rod and finally to c) a wormlike chain. These objects, depending on their shape, will d) interpenetrate or e) entangle.

Below, left: scattered intensity I (q^2I vs q representation used here) from either the branch or the backbone alone (continuously increasing curve towards a plateau characteristic of a random walk), or from the whole bottle-brush (maximum evidencing the more compact structure similar to the one of a star).

Complex associations and self-assembling systems:

Other complex systems in soft matter take great advantage of the possibilities of labelling using contrast variation, in particular self-assembling surfactants. Instead of pure chemical synthesis, one can create new polymeric objects by association with some molecules, like polyrotaxane introduced through successive rings of cyclodextrines (see "***highlight***" M. Van Der Boogaard et al).

Similar systems explored by the Evry associated team (L. Auvray, G. Gueguan), display a scattering law characteristic of a rodlike shape (I~1/q). This section is also illustrated by two other highlights:

A first highlight is about an external work on complexation by cryptates of the counterions of the micelles. (see "***highlight***" P. Baglioni, C. Gambi and J. Teixeira)

The second highlight concerns an LLB internal work on lipid vesicles extruded though calibrated pores. Variation of the elastic modulus and bending modulus of the membrane (by adding polymer for example) can be followed. (see "***highlight***" L. Auvray, thesis S. Guyon, 2002)

Synthesis of nanocomposites and polymer-coated silica particles:

After grafting of chains **on** silica (J.C. Castaing at LLB, 1995), our new route initiate grafting **from** the nanoparticle surface. Polycaprolactone has been "grafted from" silica via Ring Opening Polymerisation (ROP) for the first time (G. Carrot, with Ph. Dubois, Mons, B). Atom Transfer Radicalar Polymerisation (ATRP) developed also by G. Carrot (first with J.P. Vairon, B. Charleux, Ch. Macromoléculaire, Jussieu) has been applied to platinum nanoparticles (with H. Perez, DRECAM).

Our largest effort is now focussed on silica particles: the collaboration with Rhodia Silica Systems aims at the mechanical reinforcement of rubber. Combining chemistry and SANS (A. El Harrak, thesis started in October 2001), we are following step by step the effect of functionalisation and polymerisation on the colloidal stability of the nanoparticle suspension (see Figure 2).
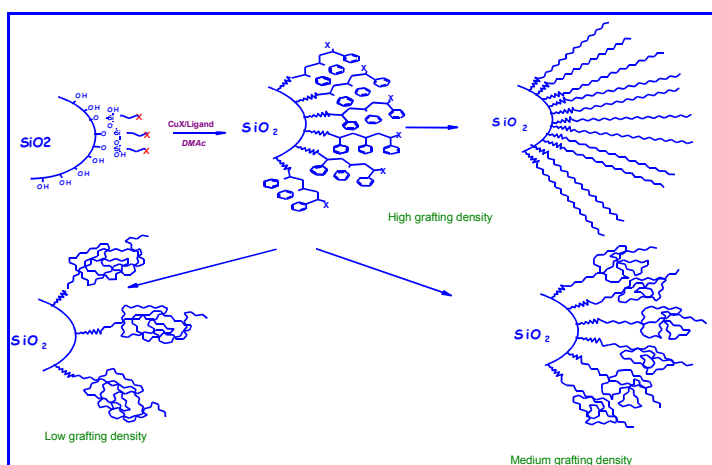
Figure 2. Synthesis of polymer-grafted silica nanoparticles at the surface of which chains are grown ("Grafting from"). The grafting density can be controlled by the polymerisation processes.

SOFT MATTER UNDER CONSTRAINT
Rheology of nanocomposites
Nanocomposites described just above are also studied using rheological measurements and SANS under strain. The effect of stretching has already been studied for nanocomposites polymer/silica materials: they were first made by mixing aqueous suspensions of polymer beads – called polymer latex, with aqueous colloidal silica, drying and letting filmify. *J. Oberdisse*, after careful control, characterisation and modelling of the controlled degree of aggregation, has established the systematic correlation between the structure and the mechanical reinforcement factor (Figure 3).
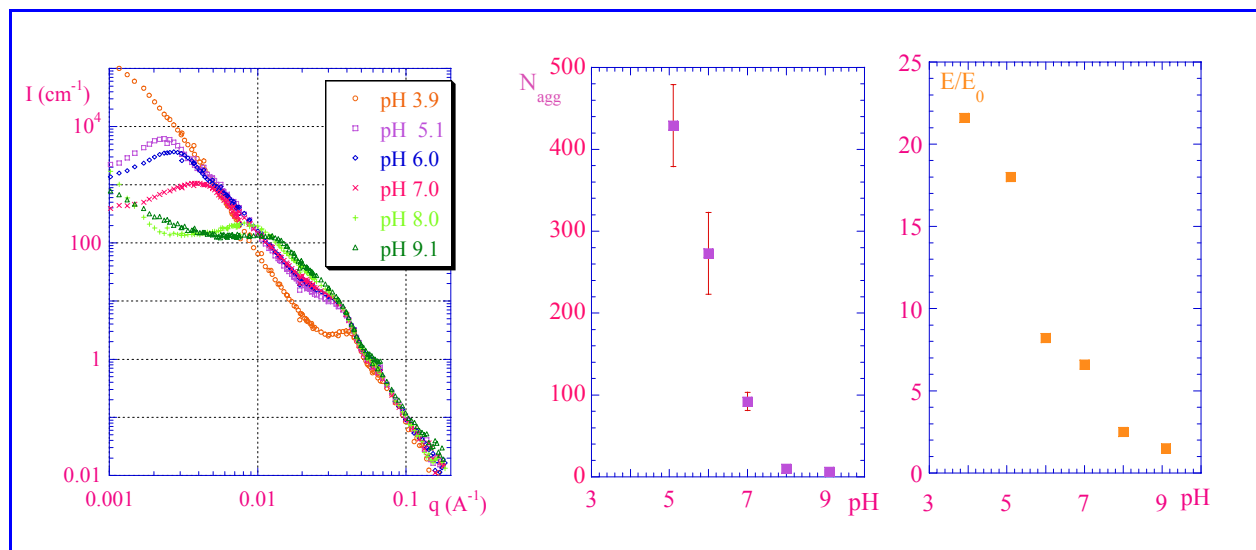
Figure 3. Reinforcement in nanocomposites. Left : Plot of SANS scattered intensity I(q) vs q in log-log scales, for nanocomposites latex-silica filmified from silica plus latex suspensions at different pH (between 3.9 and 9.1, see different colours). Centre : Aggregation numbers extracted from the analysis of the scattered intensity (abscissa of the maximum), vs pH of synthesis. Right : Reinforcement of Young modulus as a function of pH.

The increase of the Young modulus can be very high (100) for large aggregates, indicating steric interactions. The effect of deformation has been modelled.

The effect of in situ silica precipitation in PolyDiMethylSiloxane (PDMS) networks has been studied in coll. with ICSI, Mulhouse (B. Haidar, P. Ziegler, thesis O. Spyckerelle).

Rheo-SANS studies of polymers:

In situ shear is also well developed in polymers. It concerns polymer solutions in two cases:

First, copolymers (B. Hamley, K. Mortensen, Cranbury-Rhodia team, and Pau team (J. Peyrelasse, J François, thesis C. Perreur) with A. Lapp).

Second, shear-induced concentration fluctuations in Semi-dilute polymer solutions (thesis I. Morfin, with P. Lindner, ILL, and F. Boué,) coupling SANS with SALS measurements (with T. Hashimoto, Kyoto). This last study showed the progressive arise of fluctuations gently enhanced along the flow in a first stage (good solvent), then coupled to phase separation close to the bad solvent regime in a second stage, which make them visible by eye. In good solvent, we measured the form factor of a sheared single chain in solution in the Couette, at very high shear ($\gamma'.\tau > 5$).

Results are compared to recent theories of partial disengagement from the tube, the only possibility to explain the shear plateau observed.

Rheology of liquid-crystalline polymers and shear-induced nematic transition:

The shear-induced nematic re-entrant transition has been found for the first time and characterized in two series of comb-like liquid crystalline polymers (LCP): phase diagrams and "plateau" constraints were determined as a function of temperature and compared to theory and related results in giant micelles.

The most striking results come from combined observation of chain conformation by SANS under shear, optical birefringence and rheology (coll. with ESPCI). Starting from the isotropic phase, a shear induced transition has been observed towards a nematic state, which is different from the static one obtained by magnetic field orientation, since both the backbone and mesogenes are parallel to velocity (Figure 4).

For one kind of LCP polymer, striking oscillations are observed in rheology, coming either from complex viscous flows and elastic domains or from sliding-adhesion phenomena at the Couette cell walls.

L. Noirez with V. Castelletto, postdoc, thesis C. Pujolle, 2002.
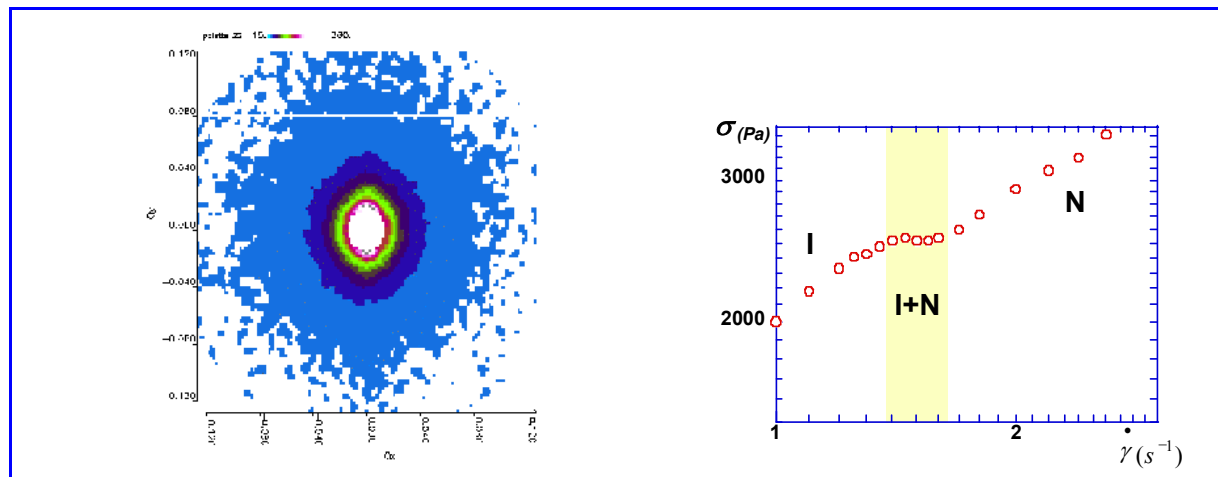
Figure 4. Liquid Crystalline Polymer chain under shear. Left : S.A.N.S from LCP inside a Couette cell, in the plane ($\vec{V}$, $\vec{Z}$) where $\vec{Z}$ is the neutral axis of the shear (PAXY SANS spectrometer at LLB, wavelength 8Å, sample-detector distance 2m). The velocity axis is horizontal. The elliptical shapes are due to the anisotropy of the chain form factor at $T>T_{NI}$ in the shear induced nematic phase; the large symmetry axis of the chain is parallel to velocity Right : Mechanical response of a liquid crystalline polymer melt to a simple shear : stress vs shear rate at $\Delta T=5°C$ above $T_{NI}=110°C$, the nematic-isotropic transition temperature. The yellow zone enlights the stress plateau corresponding to the coexistence of isotropic and shear induced nematic phase. For each point, a delay of 1000s was applied before measurement in order to reach a steady regime.

Liquid crystalline polymers have been also studied under pressure, using neutron high penetrability through many materials. Using a special pressure cell, the different phases of LCP can be observed.

G. Pépy, L. Noirez.

Confined polymers, thin films and porous media:

Confinement, finally, was also studied. Chains trapped in a **Vycor porous glass** are visible inside the nanochannels, since Vycor can be masked by using a D_2O/H_2O mixture also suitable for Zero Average Contrast (ZAC) investigation of the polyelectrolyte chain form factor (L. Auvray, coll. J. Lal, Argonne). Chains dynamics under these conditions are under studies.

Concerning thin films of polymers, measurements of the form factor of chains confined in **a layer as thin as 10 nm**, (Cotton, Brûlet, Boué) are planned for completion of previous studies in the field.

Fuel cell operation observed in situ by SANS:

A last important study under solicitation, completely oriented towards technology application, is the study of a **Nafion** (sulfonated Teflon) **fuel cell** under working conditions (see ***"highlight"*** by G. Gebel et al).

PHYSICOCHEMISTRY OF BIOLOGICAL OBJECTS

Biology related chemical physics problems, finally come as the rising field of activity in soft matter. A first type of biomaterials concerns complex molecules that can be extracted from living systems, e.g. for agro-industry, like Methylated Cellulose, a water-soluble derivative of cellulose. Its complex solution phase diagram (gel formation/phase separation due to temperature balance between methyl groups hydrophobicity and H bonds) has been explored on a very large q range, using SANS, Static, Dynamic and Small Angle Light Scattering (M. Delsanti, SCM), and finally Neutron Reflectivity at air interface, correlated with tensiometry measurements done at INRA Nantes.

Thesis S. Guillot 2001, D. Lairez, M. Axelos, L.T. Lee.

Biochips

Biochips correspond to a second type of biomaterial, closer to biotechnology. Our collaboration with Biomérieux (L. T. Lee, F. Boué, A. Menelle, F. Cousin, with B. Cabane, Paris, and C. Pichot and A. Teretz, UMR Biomérieux-CNRS) shows the potentiality of Neutron reflectivity to characterise successive layers in bio-chips: first the silanisation step, second bounding of proteins or of polymer used to link a third layer of DNA oligonucleotides used to capture the DNA targets in the solution deposited on the chip. The whole system realised with the Biomérieux UMR, mimics a biochip.
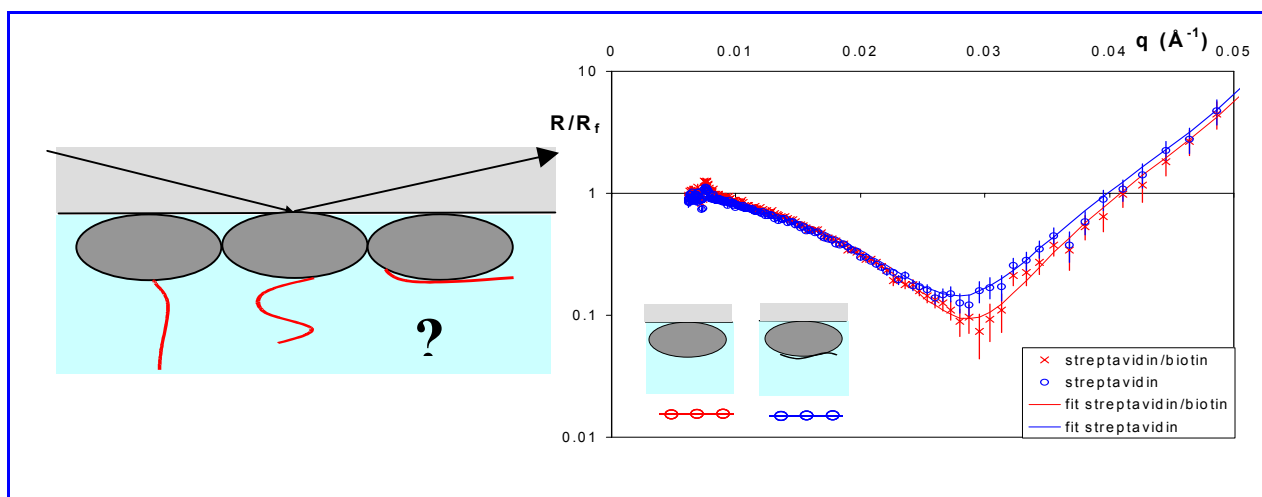
Figure 5. Neutron reflectivity R vs q (represented as divided by the Fresnel reflectivity for a single interface) of a silicon wafer silanised and coated with a layer of streptavidin, on which a biotine layer will in turn adhere.

Polyelectrolytes and DNA:

A **natural polysaccharide**, hyaluronane, has also been studied on a purely physicochemical point of view, to serve as **a model semirigid Polyelectrolyte**. In this case where the intrinsic persistence length is large, the OSF law for the electrostatic part of the chain rigidity is observed for the first time in a covalent polymer (OSF stands for Odijk, Skolnick and Fixman).

The electrostatic part of persistence length L_e is seen to vary as the **square** of the Debye screening length (κ^{-1}, which varies with ionic strength I as $\kappa^{-1} \sim I^{-1/2}$). This is in contrast with direct measurements of the form factor of polyelectrolyte chains in semi-dilute solutions (Zero Average Contrast technique) for

flexible totally charged chains (Sodium Polystyrene Sulfonate, NaPSS), which showed that the total persistence length L_p varied as κ^{-1}, or even at a lower power (expressed as a function of I, this was giving $L_p \sim I^{-1/3}$, instead of $L_p \sim \kappa^{-1} \sim I^{-1/2}$). (see *__"highlight"__* of E. Buhler and F. Boué)

The latter variation was confirmed (E. Dubois O. Vidal, post-docs) at the lowest concentration possible and in presence of multivalent co-ions, introduced by addition of salts. At high concentration, multivalent cations bridge the chains; actually even the structure factor, which displays interactions between chains, is surprisingly different from the (PSS)Na one (collaboration with J. Combet and M. Rawiso).

To finish with polyelectrolyte solutions, let us quote finally studies of DNA strands, in particular the presence of plectonemes (see *__"highlight"__* by J. van der Maarel et al, Leyden, with A. Lapp).

Proteins mixed with polyelectrolytes:

A last biotechnology-oriented study illustrates how SANS is a good tool for mixed systems (O. Vidal, F. Cousin, F. Boué). We have studied mixtures of negatively charged polystyrene sulfonate with positively charged Hen Egg White Lysozyme (pH 4). In the demixed regions of the phase diagram, we observe different morphologies (turbid suspension, solid precipitates, gel) to which we can associate a corresponding structure of aggregates viewed by SANS : closely joined protein in compact aggregates, or looser ones. The phase diagram shows also a solubility range, in which the association is strongly different, related to protein partial unfolding (see figure 6).
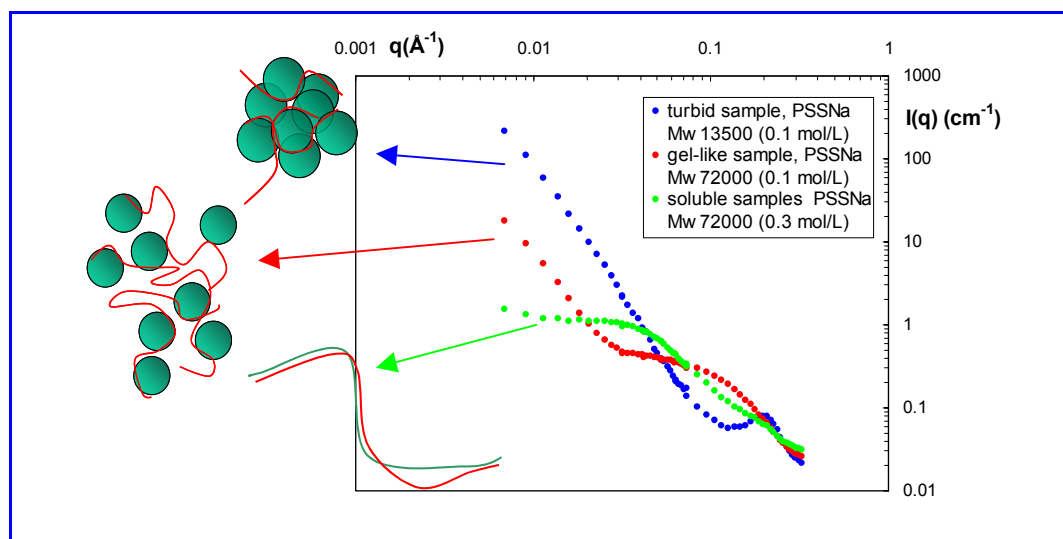
Figure 6. Complexes of polyelectrolytes (sodium polystyrene sulfonate, NaPSS) associated with proteins (lysozyme) : the drawings represent compact aggregates, loose aggregates, and the case where the protein is unfolded, as can be drawn from the aspect of the scattering curves.

We reach here the border with the biology Chapter, where are described related works such as the structure of lignin films probed by neutron reflectivity (B. Cathala), SANS studies of protein denaturation, as well as the diffusion of enzymes through a biopolymer gel, gelatine (G. Fadda, thesis, D. Lairez, and J. Pelta, Univ. Cergy – Pontoise).

SOFT MATTER AND BIOMATERIALS

SELF-ASSEMBLY OF PEPTIDE-BASED DIBLOCK RODCOIL COPOLYMERS : FROM MICELLES AND VESICLES TO NANOCAPSULES

F. Chécot[1], S. Lecommandoux[1], A. Brûlet[2], Y. Gnanou[1], H.A. Klok[3]

[1]LCPO-CNRS-ENSCPB, Université Bordeaux 1, 16 av. Pey Berland, 33607 Pessac, France.
[2]Laboratoire Léon Brillouin (CEA-CNRS), CEA-Saclay, 91191 Gif sur Yvette Cedex, France
[3]MPI for Polymer Research, Ackermannweg 10,D-55128 Mainz, Germany.

The self-assembly of block copolymers is used to create functional materials with nanoscopic dimensions, structural complexity, and/or hierarchy without any additional process required. The so-called "supramolecular" structures that can be obtained and their properties are essentially controlled at the molecular level by the right choice of the block copolymer (in our case block length ratio, chemical composition, entropic constraints, specific interactions…).

Recently, we synthesized a series of diblock copolymers consisting of a rod-like polypeptide-block and a flexible polymer block [1]. These rod-coil type block copolymers are of potential interest as building blocks for the development of novel self-assembled materials [2]. The rod-coil transition undergone by the peptide-block, due to a change in the secondary structure, can provide the molecular basis for stimuli-responsive materials; i.e. the supramolecular organization and properties of these materials can indeed be manipulated by specific variations of temperature, pH or ionic-strength. Even if these amphiphilic rod-coil molecules have been intensively studied in bulk [1,2], we focused in this work on the solution properties of polybutadiene-b-poly(γ-L-glutamic acid) PB-b-PGA diblocks. A series of compounds have been synthesized in order to vary rod-like block volume ratio (Figure 1).

The aggregation behavior of these block copolymers have been investigated by means of fluorescence spectroscopy, dynamic (DLS) and static (SLS) light scattering, transmission electron microscopy and small angle neutron scattering (SANS). The diblock copolymers were found to form well-defined spherical micelles and vesicles in water, depending on the ratio of the hydrophilic peptide block to the hydrophobic polybutadiene one. By combining all these experimental techniques, we have been able to fully characterize the essential features of this system, in term of size, shape and their modifications as a function of stimuli applied (temperature, pH, ionic strength…) Figure 2 represents two characteristic examples of SANS data obtained from block copolymer micelles (Figure 2a) and vesicles (Figure 2b).

A series of experiments was then carried out to demonstrate that the size of these micelles and vesicles can be reversibly manipulated as a function of both pH and ionic strength [3] For instance, the hydrodynamic radii R_H of the vesicles measured by DLS were found to vary from 100nm to 150nm depending on the pH of the aqueous solutions (Figure 3a). Even at high NaCl concentrations, where all the charges are effectively screened, pH-induced changes in the polypeptide secondary structure can be used to reversibly vary the dimensions of aggregates (see figure 3). Compared to other polyelectrolyte-based block copolymers, this PB_{40}-b-PGA_{100} copolymer exhibits an unique feature, which is the capability of its polypeptide block to fold into a compact and well-defined secondary structure as confirmed by circular dichroïsm measurements. Furthermore, by using the 1,2-vinyl double bonds present in the polybutadiene block, we demonstrate that the morphology of such a system can be covalently fixed and a transient supramolecular self-organized aggregate transformed into a permanent "shape-persistent stimuli-responsive" nanoparticle [4].

Finally, these nanoparticles, nanocapsules or polymersomes may be suitable for a number of applications including the encapsulation and/or the release of hydrophilic as well as hydrophobic active species, sensors for nano-devices, and other applications in cosmetics, paints or lubricants...

Figure 1. Schematic representation of the peptide-based diblocks under study.

Figure 2. SANS intensity I(q) as a function of q for (a) micelles formed by the PB_{48}-b-PGA_{114} in water at pH=12. The blue full line curve is the form factor of a sphere of an average radius of 70Å with a LogNormal distribution with a sigma=0.15 (represented in the inset) [5], (b) vesicles of PB_{40}-b-PGA_{100} in water at pH=4 and 12. Static light scattering intensities are added in the low-q range to the SANS data.

Figure 3. (a) Hydrodynamic radius R_H as a function of NaCl concentration and pH. (b) Schematic representation of the peptosome and its change in size as function of pH due to a coil to α-helix secondary structure transition in the peptide part.

References

[1] (a) S. Lecommandoux, M. F. Achard, J. F. Langenwalter, H.-A. Klok, *Macromolecules* **34** (2001) 9100.
    (b) H.-A. Klok, J. F. Langenwalter, S. Lecommandoux, *Macromolecules* **33** (2000) 7819.
[2] H.-A. Klok, S. Lecommandoux, *Adv. Mater*. **13** (2001) 1217.
[3] F. Chécot, S. Lecommandoux, Y. Gnanou, H.-A. Klok, *Angew. Chem. Int. Ed.*, **41** (2002) 1339.
[4] F. Chécot, S. Lecommandoux, H.-A. Klok, Y. Gnanou, *Eur. Phys. J. E*, **10** (2003) 25.
[5] Modelisation done with the help and in collaboration with J. Oberdisse (LLB).

SYNTHESIS OF INSULATED MOLECULAR WIRE : CONFORMATION OF A POLYROTAXANE (SEMI-CONDUCTING-POLYMERS COMPLEXED INSIDE SHEATHS OF CYCLODEXTRINS) : DETERMINATION OF THE MASS AND THE NUMBER OF CYCLODEXTRINS PER DIMER.

M. van den Boogaard[1], P.van't Hoff[1], P.F. van Hutten[1], A. Lapp[2], C.Marques[3] and G. Hadziioannou[4]

[1]University of Groningen,The Netherlands
[2]Laboratoire Léon Brillouin (CEA-CNRS), CEA-Saclay, 91191 Gif sur Yvette cedex, France
[3]Laboratoire de dynamique des fluides complexes (LDFC), Strasbourg France
[4]Laboratoire d'ingénieurie des polymères de haute technologie (LIPHT), ECPM, Strasbourg, France

*One of the focuses of our laboratory is to synthesize insulated molecular wires by using semi-conducting polymers complexed in insulated sheaths of **b**-cyclodextrins.*

The most promising synthesis in which a polythiophene (semi-conducting polymer) is complexed in β-CD sheath is pictured below:
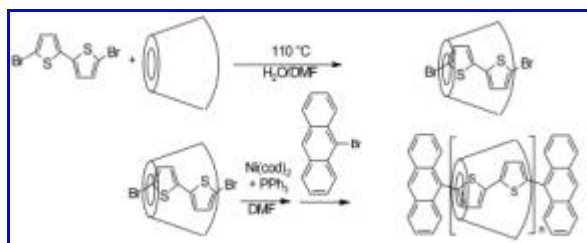
We have isolated the complex, polymerized it[1] and then selected the molecules which are soluble in water. We have characterized these wires with MALDI TOF which is a mass spectrometer using a laser to ionize a matrix containing our sample, and small angle neutron scattering performed at LLB in 2001-2002.

MALDI TOF measurements (figure 1) only yield the mass of the polymer chain because cyclodextrin molecules are destroyed by the ionization of the laser. From this analysis, it is apparent that we have synthesized a **water soluble** polythiophene with a **degree of polymerization of 24**. It is interesting to note that usually polythiophene is not soluble in any solvent beyond a polymerization degree of 6.

To gain additional information about the size, shape and mass of the molecular wire, we performed neutron scattering measurements at LLB (exp. N° 6205) (figure 2). We fit the data from SANS measurements of this PT-Pr with a cylindrical model with the following dimensions: diameter 8.3 Å, length 75 Å. To be soluble in water, the polymer must be complexed in a cyclodextrin sheath. It will be interesting to estimate the number of cyclodextrins that contribute to the sheath.

By calculating the polyrotaxane mass from SANS experiments and extrapolating to q = 0, we have learned that some β-CD escaped from the polymer during the polymerization resulting in a Polyrotaxane composed of 24 thiophene units complexed in only 7 β-CD. To confirm this hypothesis, we then fit the experimental data with a polyrotaxane model composed of a 24 monomer units complexed in 7 β-CD [2].

We are now confident that the polyrotaxanes contain less than one cyclodextrin per dimer of thiophene. This information, obtained via SANS is a major contribution to our understanding of the solubility of the wire and the doping necessary for upcoming measurements of the conductivity of this insulated molecular wire. In the future, this type of measurement will help us to control the degree of insulation of the wire, which is fundamental to measurements of conductivity.
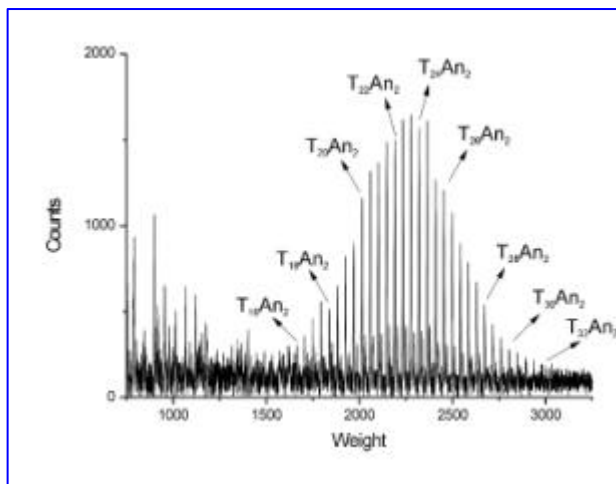
Figure 1. Maldi-TOF spectrum of the polythiophene polyrotaxane in a Dithranol matrix..
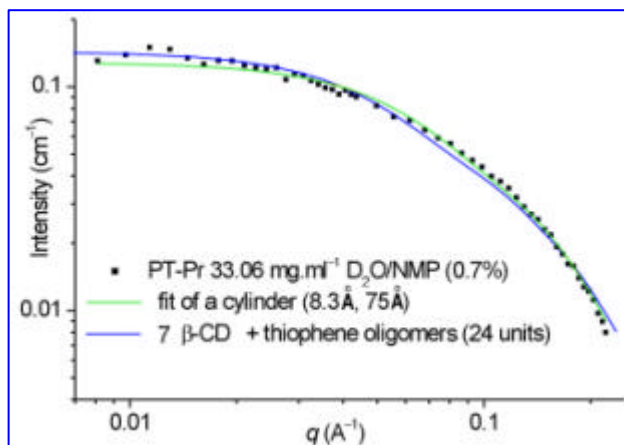
Figure 2. Small angle neutron scattering measurements on polythiophene polyrotaxane.
We can reach the number of cyclodextrin by extrapolating the mass at q=0 and by fitting with models

References

[1] T. Yamamoto, A. Morita, Y. Miyazaki, T. Maruyama, H. Wakayama, Z.-H. Zhou, Y. Nakamura and T. Kanbara, *Macromolecules,* 25, (1992) p. 1214

[2] M. van den Boogaard, P.van't Hoff, P.F. van Hutten, A. Lapp, C.Marques and G. Hadziioannou, *Synthesis and characterization of insulated molecular wires,* to be published

[3] M. van den Boogaard, PhD dissertation **2002**, University of Groningen, NL, *Cyclodextrin-containing supramolecular structures,* http://www.ub.rug.nl/eldoc/dis/science/m.van.den.boogaard/

MICELLE COUNTERIONS COMPLEXATION BY MACROCYCLIC LIGANDS

P. Baglioni[1], C. Gambi[1], J. Teixeira[2]

[1]Dept. of Chemistry & CSGI, Florence University, via della Lastruccia 3 – Sesto Fiorentino, I-50019 Florence, Italy.
[2]Laboratoire Léon Brillouin (CEA-CNRS), CEA-Saclay, F-91191 Gif-sur-Yvette Cedex, France.

Ion transport across hydrophobic media, selective binding of ions in different solvents, electron transfer across micellar interfaces, enhancement of the quantum yield in photoionization processes, metal cation extraction, production of potentiometric sensors and ion-selective electrodes, recovery of cations from nuclear waste materials, the use as accelerants for cyanoacrylate instant adhesives, and as antioxidant stabilizers for organic polymers and, more generally, host-guest molecular recognition processes are just some of the most important applications of cryptand and calixarenes cavity-shaped macrocyclic molecules.
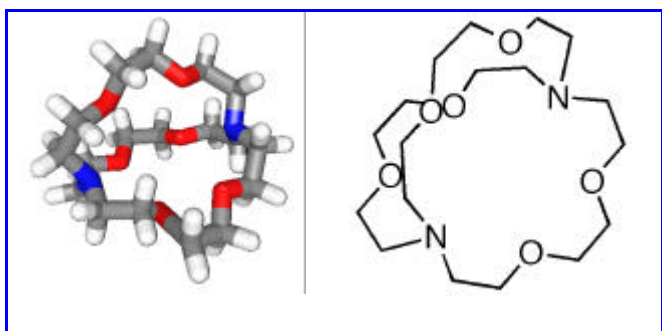
Figure 1. Molecular modeling of the macrocyclic cryptand C222.

In most applications, macrocyclic properties are enhanced by the wide area of supramolecular systems as micelles and microemulsions. The study of the binding of counterions and how they affect the structure of ionic have been already investigated in the past [1-2]. The ligand affinity to complex counterions in solution seems to be the main driving force to significantly change the micellar microstructure and the intermicelle interactions. Lithium dodecyl sulfate (LDS) micelles in aqueous solution have been characterized in the presence of ligands of different type, crown ethers, cryptands, and CESTO molecules [3-4].

In LDS micelles, some SO_4^{-} groups remain unscreened because of the migration of the Li^+ ion toward the bulk water phase, resulting in a net surface charge at the micellar surface. The addition of crown ethers or cryptands leads to important changes in the micellar structure [3-5].

Small-angle neutron scattering (SANS) is a versatile tool for the investigation of these systems.

To characterize the role of C222 addition to SDS aqueous micellar solutions we added to 8% (wt/wt) SDS micellar solution the ligand in a 0.5, 1.0, or 1.5 mole ratio [6].

To study different regions of the system, the C222 location in the SDS micelles and the consequent intermicellar interactions, two systems were investigated:

    (i)   SDS with C222 in D_2O

    (ii)   the same system with deuterated surfactant tail (SDSD)/D_2O

In system (i) the main contrast is between the solvent and the whole micelle, while in system (ii) the contrast is between the interfacial region and the core or the solvent.

The micellar particle structure factor $P(Q)$ has been modeled as a two-shell particle formed of a core containing most of the surfactant aliphatic chains and an interfacial layer containing the surfactant polar headgroups, some CH_2 (or CD_2) groups of the surfactant tail that are close to the polar head, the C222 ligand, and hydration water molecules. The C222 ligand is allowed to be partly located in the micelle and partly in the continuous phase. The interparticle structure factor $S(Q)$ has been calculated assuming an analytical solution for the multicomponent ionic liquid with a mean spherical approximation (MMSA).
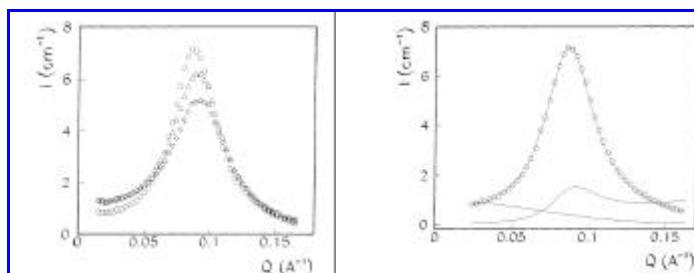
Figure 2. Experimental scattered intensity by SDS aqueous micellar solutions with 8% (wt/wt) concentration for different C222/SDS mole ratios: (O) 0.5 ; (?) 1.0; (open crosses) 1.5.

Figure 3. Experimental curve (O) and fitted curve (continuous line) of the 1.0 C222/SDS mole ratio spectrum of Figure 1. The normalized form and structure factors are also shown.

The fit considered two different possible shapes

(a) **Ellipsoidal model.** Micelles are considered ellipsoidal in shape. The ellipsoidal core of the micelle has a shorter axis equal to the length of

the extended tail of SDS molecule and an external shell around the core.

(b) Polydispersed spheres model. Micelles are considered as polydispersed core-shell spheres, following the Schulz distribution.

The analysis shows that C222 (in spite of its good solubility in water) is partitioned at micellar surface. The ratio C222/SDS increase (from 0.5 to 1.5) is associated to an increase of ligands at the interface (from 40% to 65%). The increase of ligands at the interface produces a decrease of the effective micellar charge from 21 to 12 and of the average aggregation number from 74 to 54. An increase of the shell thickness (from 10 to 12Å) and a decrease of the number of carbons in the hydrophobic core of the micelle (from 12 to 9.5) and of the hydrophobic chain length (18 to 16 Å) are also observed, meaning that the cryptand penetrates below the polar head groups region.
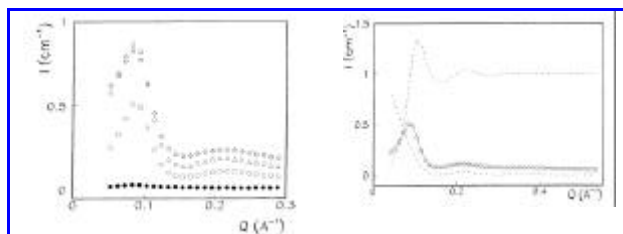
Figure 5. Experimental scattered intensity by deuterated SDS aqueous micellar solutions with 8% (wt/wt) concentration for the C222/SDSD ratios: (O) 0.5; (?) 1.0; (open crosses) 1.5. The full points spec-trum is deuterated SDS without cryptand molecules.

Figure 6. Experimental curve (O) and fitted curve (continuous line) of the 0.5 C222/SDSD mole ratio spectrum of Figure 5. The norma-lized form and structure factors are also shown.

The interaction of cryptand at the micellar surface occurs without any increase of the micellar diameter (55 Å). An increase of the volume fraction of micelles (0.21 to 0.24) is observed, as expected for a macrocycle partitioned at the micellar surface.

The number of solvent molecules at the interface increases from 22 to 29 with the increase of the C222/SDS ratio. The micelles are prolate ellipsoids.

In summary, the analysis shows that the sodium/cryptand complex behaves as a "counterion" that migrates from the bulk solution to the interfacial region of the micelles. Once at the micellar surface, it screens the micelle surface charge, which leads to a reduction of the contact potential and to an increase of the Debye length. A higher interfacial ligand concentration is observed for the deuterated micelles. Therefore, C222 ligand is more efficient in binding the sodium counterion at the micellar surface of deuterated micelles, probably because of a larger hydrophobic repulsive effect than that in the hydrogenated micellar system.

The proposed mechanism of migration of the sodium/cryptand complex from the bulk phase to the micellar surface agrees with a previous study on the adsorption properties of C222 at a charged macroscopic interface studied as a function of the polarization potential and of the ligand concentration[7]. The interfacial adsorption of the C222 ligand has been demonstrated to be driven by the hydrophobic repulsion of the exposed surfaces in the presence of an intermolecular repulsive electrostatic contribution due to sodium cation trapped inside the ligand cage.

We have investigated the most common macrocycles as crown ethers, cryptand, and calixarenes [8-9] as complexing agents for counterions of ionic surfactants (from lithium to cesium, calcium and strontium). SANS has been very powerful in determining the evolution of micelles upon macrocycles addition. Crown ethers, cryptands and calixarenes produce different effects on micelle structure; the evolution of the structure depends on the macrocycle complexing ability and on its location in the micelle. Their use allows the control of the size, shape and charge of ionic disperse systems.

References

[1] Baglioni, P.; Gambi, C. M. C.; Giordano, R.; Teixeira, J. Physica B, 231&214 (1995) 597.

[2] Baglioni, P.; Bencini, A.; Dei, L.; Gambi, C. M. C.; Lo Nostro, P.; Chen, S.H.; Liu, Y.C.; Teixeira, J.; Kevan, L., J. of Phys.: Condensed Matter **6** (1994), A369-A373.

[3] Chen, S.-H.; Liu, Y. C.; Teixeira, J.; Kevan, L., Colloids Surf., A **88** (1994) 59.

[4] Liu, Y. C.; Baglioni, P.; Teixeira, J.; Chen, S.-H. , J. Phys. Chem., **98** (1994) 10208.

[5] Baglioni, P.; Gambi, C. M. C.; Giordano, R.; Teixeira, J., Colloids Surf., A **21** (1997) 47.

[6] Scaffei, L., Lanzi, L., Gambi, C.M.C, Giordano, R., Baglioni,P., Teixeira, J., J. Phys. Chem. B **106** (2002) 10771.

[7] Carla', M.; Gambi, C. M. C.; Baglioni, P., J. Phys. Chem. **100** (1997) 11067.

[8] Capuzzi, G.; Fratini, E.; Pini, F.; Baglioni, P.; Casnati, A.; Teixeira, J. Langmuir, **16** (2000) 188.

[9] Capuzzi, G.; Fratini, E.; Pini, F.; Dei, L.; Lo Nostro, P.; Casnati, A.; Gilles, R.; Baglioni, P., Colloids Surf. A **167** (2000) 105.

EXTRUSION OF VESICLES THROUGH CALIBRATED PORES

S. Guyon, L. Auvray

Laboratoire Léon Brillouin (CEA-CNRS), CEA Saclay, 91191-Gif-sur-Yvette, France

Bilayers made of natural or synthetic lipids are known to be fluid and flexible. The shape fluctuations of giant vesicles or biological cells can be observed directly under an optical microscope but it not easy to study the deformations of these membranes at a more microscopic scale ranging from 1 to a few hundred of nanometers. In order to fill this gap, we have undertaken a series of studies where we probe the mechanical properties of small unilamellar vesicles, whose size varies between 30 and 150 nm, by extruding them through porous membranes with well-defined uniform straight parallel pores. These membranes, known since a long time under the name 'Nuclepore'', are made by chemically etching the latent tracks produced after irradiation of polycarbonate foils by heavy ions (figure 1). They are already used to produce monodisperse vesicles by extruding lipid lamellar phases [1] and a few experimental [2] and theoretical studies [3] of this process have already started.
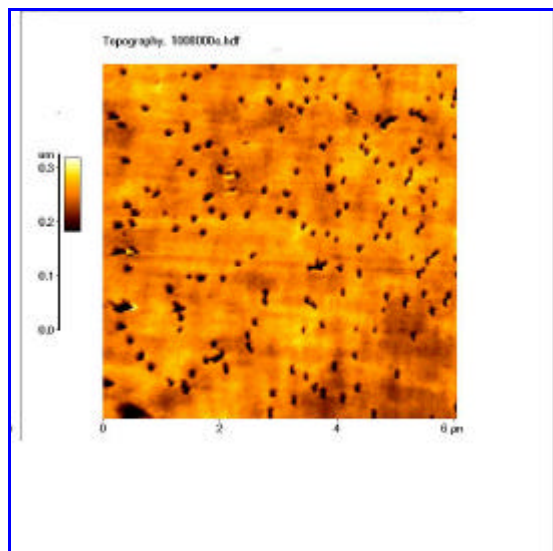
Figure 1. Nuclepore membrane observed by AFM (pore diameter 100 nm).

The studies are made at two levels. At a microscopic level we study the relationship between the flow rate and the pressure that we must apply to extrude the vesicles (figure 2). At a microscopic level, we compare by light and neutron scattering experiments the structure of the vesicles before and after extrusion (Figure 4).
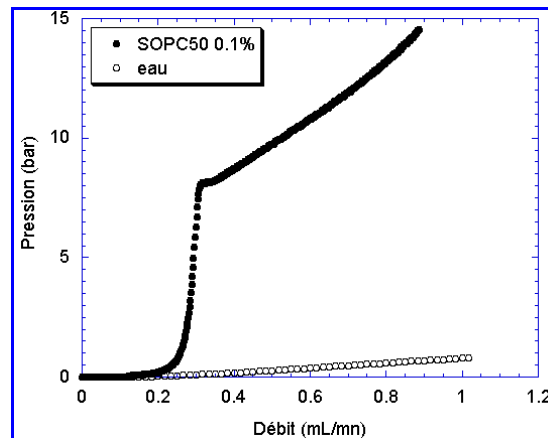
Figure 2. Pressure-flow-rate relationship measured on a porous membrane with a pore radius $R_p = 25$nm, in presence of pure water (empty symbol) and SOPC vesicles (radius 34 nm) (full symbol).

We have focused our studies on the situation where the radius of the vesicles is larger than the radius of the pores. It appears then necessary to vary the applied pressure and the flow rate in a large range. To improve the precision of the measurements we choose to impose the flow rate and measure the pressure with a miniature piezo-resistive pressure sensor. We use either a syringe pump (for low pressure measurements below 1 bar) or a HPLC chromatography pump, enabling us to vary the flow rate between 0.01 and 10 ml/min with a possible pressure range between 0 and 300 bars.

Our main result is visible on figure 2. The vesicles are extruded only if the applied pressure excess a certain threshold, which depends on the vesicles size, pore diameter and lipid composition (figure 3). We expect theoretically two limiting behaviours :

1) for large pore radius R_P, one may possibly deform the vesicles without rupture, increasing only the vesicle curvature energy; this leads to a threshold pressure varying as K/R^3_P where K is the membrane rigidity;

2) for small pores, the vesicles must be stretched in order to enter the pores and break; Laplace's law then lead to a threshold pressure varying as S_l /R_P

where S_l is the lysis tension of the bilayer. This behaviour has already been observed [2].

As shown on figure 3, these two laws interpret rather well the experimental observations,
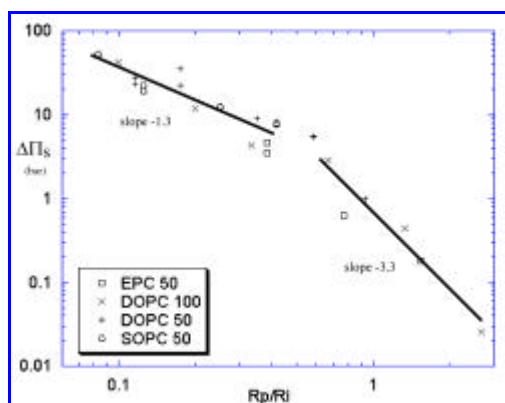
Figure 3. Threshold pressure as a function of the pore size for different vesicles (R_p/R_i is the ratio of the pore to vesicle radius)

We observe on figure 4 showing the neutron and light scattering spectra of surfactant vesicles before and after their passage through different membranes the two main microscopic effects of the extrusion : 1) the diminution of the vesicle radius which shifts the spectra towards the largest q and 2) the vesicles retention which diminishes the value of the scattered intensity in the asymptotic regime. Basically, as shown on figure 5, the pores impose their size.
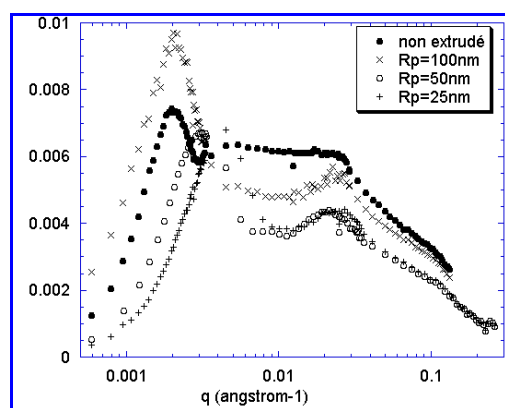
Figure 4. Neutron and light scattering intensity in the representation $q^2 I(q)$ versus q for surfactant vesicles (initial radius 107 nm) extruded through different pores.
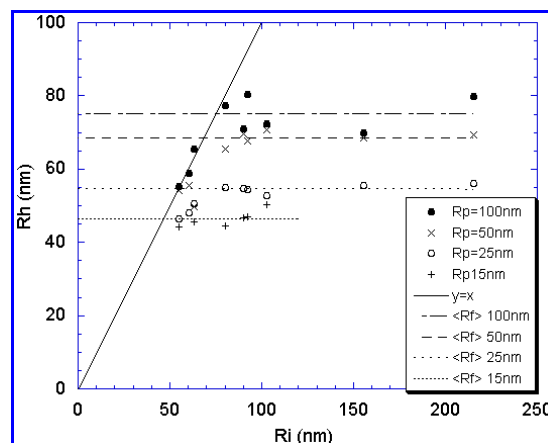
Figure 5. Final radius of surfactant vesicles as a fonction of their initial radius for different pore size.

The size diminution cannot be explained without assuming the rupture of the vesicles, this is confirmed by a direct observation of the liberation of encapsulated fluorescent labels during the extrusion. These fluorescence experiments also confirm the phenomena of vesicles retention and enable us to quantify it.

Finally it was interesting to compare directly the behaviour of small and large vesicles. We thus have observed directly the passage of giant vesicles through micrometric pores made by PDMS moulding at Institut Curie (figure 6). The deformations are very strong even at low flow rate, the vesicle rupture has been observed once.
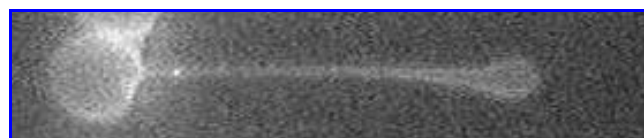
Figure 6. Giant fluorescent vesicles entering a PDMS channel under flow.

References

[1] M.J. Hope, M.B. Bally, G. Webb, P.R. Cullis, *B.B.A.* **812** (1985) 5-65
[2] B.J. Frisken, C. Asmanpatty *Langmuir* **16** (2000) 928-933
[3] R. Bruinsma *Physica A* **234** (1996) 249-270

WATER PROFILE DETERMINATION IN A RUNNING PEMFC BY SMALL-ANGLE NEUTRON SCATTERING.

G. Gebel[1], O. Diat[1], S. Escribano[2], R. Mosdale[2]

[1]DRFMC/SI3M/Groupe Polymères Conducteurs Ioniques
[2]DTEN/SCSE/Laboratoire Hydrogène et Piles à Combustible
CEA Grenoble, 17, rue des martyrs - 38054 GRENOBLE cedex 9, France

A fuel cell is an electrochemical system producing a DC current from two half chemical reactions: an H_2 (the fuel) oxydation at the anode and the reduction of the O_2 at the cathode as indicated in figure 1a. Proton exchange membrane fuel cell (PEMFC) is a cell using a proton conducting polymeric membrane as a solid electrolyte separating both electrodes (and so both gases) and allowing the proton conduction between the anode and the cathode. These membranes require a minimum of water content to exhibit a sufficient conductivity and this water has to be controlled whatever the temperature and current density conditions during the cell operation. Then, the management of the water around the cell and more especially between both electrodes is a major challenge for PEMFC applications. When the cell is operating, water is produced at the cathode. Therefore, under stationary conditions and depending on the current density, an excess of water accumulates at the cathode and has to be removed. Nevertheless, it exists always a water concentration profile across the membrane, which is partially counterbalanced by water back-diffusion and reinforced by water electro-osmosis (see Fig. 1b). This concentration profile can also be reduced using humidified inlet gases especially at the anode.

Several attempts to experimentally determine these profiles during fuel cell operation have been published. However the experimental constraints [1-4] [1-4] lead to operate in conditions, which were not representative of the actual fuel cell operation.
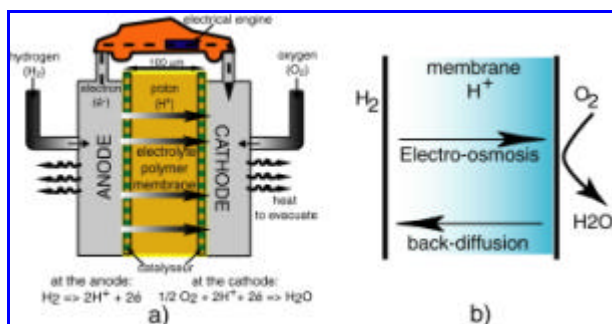
The determination of the water concentration profile across the Nafion[1] membrane and under fuel cell operation can be achieved using small-angle neutron scattering (SANS) technique. Indeed, both the shape and the level of scattered intensities of Nafion spectra are very sensitive to the water content. Moreover, it is possible to use a specially designed fuel cell which is almost transparent to neutrons and allows mainly the observation of the membrane contribution to the SANS spectra. In a previous study, we have demonstrated the feasibility of such experiments but with some poor fuel cell performances due to i) electrodes which were not appropriate (chemically deposited platinum) ii) a cell design which did not allow an optimized gas flow on the membrane and iii) a control of the cell temperature which were non-existent. In the present study, a new bench and a new cell were designed (see Fig. 2) to operate at 80°C and under pressure, to control the gas flow, and to measure the gas outlet humidities.
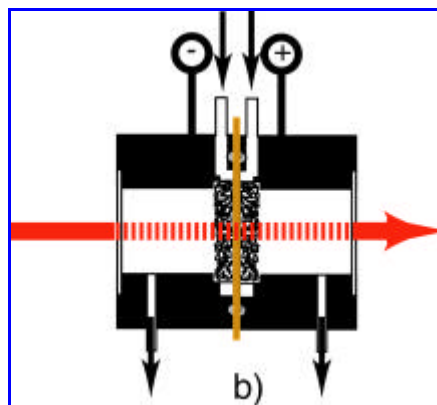
Figure 2. Porous gas distributors and current collectors are either in an titanium/zirconium alloy (48/52) which was grated and sintered or in highly porous steel (90% porosity). Quartz windows were to insure each compartment to be airtight and the transparency to neutrons. The temperature was measured through a thermocouple and adjusted through a temperature controller. Two different types of electrodes were used either a spray (Sm) or a hot pressed Etek® electrode (Etn) on membrane. In the case of Etn electrodes the diffusion layer has been torn away in order to deposit the active layer on the membrane and to avoid the strong scattering of the carbon tissue.

Figure 1. a) Scheme of a fuel cell and b) illustration of the water management in an operating fuel cells

---

[1] Nafion® is a perfluorinated membranes purchased from du Pont de Nemours Company

The experiments (see an example in Fig. 3a) were performed starting from a nearly dry membrane and varying both the current density and the gas stoechiometry in order to determine the kinetics of swelling in addition to the water concentration profiles. Following the different scattering profiles shown in Fig. 3, the membrane was first dried by a flow of dry gases and increasing the temperature up to 80°C. The current density was then increased by step after at least the stabilization of the fuel cell performance and of the SANS spectra (typical steps of current were between 1 and 2 hours). The analysis in term of water concentration profiles is presented in figure 3b.
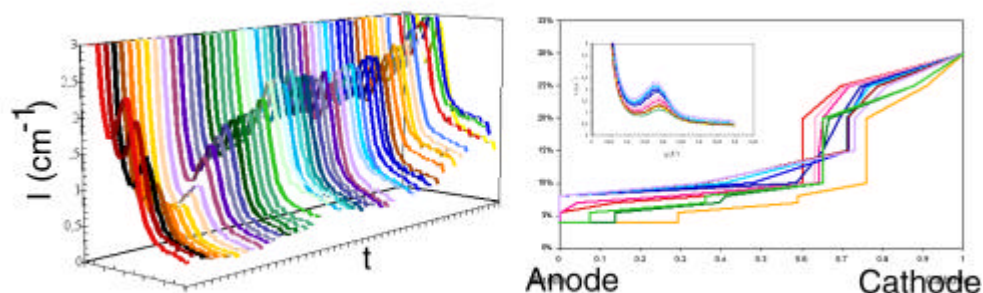
Figure 3. Series of SANS spectra (left) obtained from a Nafion 115 membrane using highly porous gas distributors. The membrane is first dried and then the current density is increased from 0 to 1A/cm^2. Example of a series of experimental data extracted from left. Each curve were fitted (inset) and the corresponding profiles (% of water into the membrane as a function of thickness) are presented (right) for different current densities.

It was shown that it is possible to determine the overall water content of the membrane under operation and to follow its evolution depending on the operating conditions fitting the data using a linear combination of referenced spectra (obtained from membranes at given humidity and placed in similar support and temperature conditions).

The performances and the stability of the fuel cell (polarization curves not shown here) were very good which suggests that the membrane has not to be completely water swollen as it is usually believed. Others experiments indicate that the fuel cell can run with a nearly dry membrane but the operating parameters such as the gas flow, the humidification or the temperature becomes crucial.

References
[1] Watanabe, M.; Igarashi, H.; Uchida, H.; Hirasawa, F. Journal of Electroanalytical Chemistry, **399** (1995) 239
[2] Mosdale, R.; Gebel, G.; Pineri, M. Journal of Membrane Science, **118** (1996) 269.
[3] Bellows, R. J.; Lin, M. Y.; Arif, M.; Thompson, A. K.; Jacobson, D. Journal of The Electrochemical Society, **146** (1999) 1099.
[4] Büchi, F. N.; Scherer, G. G. Journal of The Electrochemical Society, **148**, (2001) 183

PLECTONEMIC STRUCTURE OF TOPOLOGICALLY CONSTRAINED, SUPERCOILED DNA

J.R.C. van der Maarel,[1] S.S. Zakharova,[1] W. Jesse,[1] C. Backendorf,[1] S.U. Egelhaaf,[2] A. Lapp[3]

[1]Leiden Institute of Chemistry, Leiden University, 2300 RA Leiden, The Netherlands
[2]Department of Physics and Astronomy, University of Edinburgh, Edinburgh EH9 3JZ, UK
[3]Laboratoire Léon Brillouin (CEA/CNRS) CEA-Saclay, 91191 Gif-sur-Yvette Cedex, France

Closed circular DNA usually exists in a supercoiled configuration, in which the duplex is wound around another part of the same molecule to form a higher order helix. Supercoiling is utilized in many cellular mechanisms. Here, we explore the extent to which supercoiling controls the compaction of pUC18 bacterial plasmid (2686 base pairs) in a liquid crystal [1,2]. For this purpose, the configuration of the superhelix is monitored with SANS through the phase transition.
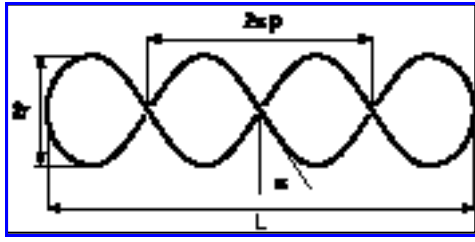
Figure 1. Plectonemic helix with length L, radius r, pitch p and opening angle a.

The topological constraint is characterized by the linking number deficit ΔLk, which is the number of turns the duplex is turned before closure to form a ring. ΔLk is conserved and is distributed among writhe Wr and excess twist ΔTw exerted on the duplex according to $\Delta Lk = Wr + \Delta Tw$. For a right-handed, regular supercoil without end loops, Wr is proportional to the number of crossings n when viewed perpendicular to the superhelical axis $Wr = -n \sin a$, with the pitch angle a as in figure 1. It is convenient to define the normalized length $2L/l$, with l being the length of the DNA molecule. From integration along the contour follows

$$2L/l = p\Big/\left(p^2 + r^2 \right)^{1/2},\qquad (1)$$

if the end loops are neglected. The pitch angle a is given by

$$\tan a = p/r = \left(2L/l\right)\Big/\left(1 - \left(2L/l\right)^2\right)^{1/2} \quad (2)$$

and the writhe reads

$$Wr = -lp\Big/\left(2p\left(p^2 + r^2\right)\right). \qquad (3)$$

The *local* structure of the superhelix is fully characterized by p and r. These parameters determine a, Wr and $2L/l$.

In our experiments, the range of momentum transfer q exceeds L^{-1} by at least an order of magnitude. In this high q-range, the scattering is sensitive to interference over an extent on the order of r and p and effects of overall flexibility and/or branching of the supercoil are beyond observation. We can accordingly use the high-q approximate form of the form factor of a regular superhelix

$$P(q) = \frac{p}{qL}\Bigg[J_0^2(qr) + 2\sum_{k=1}^{ap/2} J_{2k}^2\left((q^2 - 4k^2/p^2)^{1/2} r\right)\Bigg], qL \gg 1 \qquad (4)$$

Note that $P(q)$ is sensitive to the DNA density per unit length projected on the superhelical axis L^{-1}. However, for $qr \gg 1$ and $qp \gg 1$ the scattering is essentially given by a single strand of the superhelix, which is proportional to the density per unit contour length l^{-1}. In both regimes, the form factor displays the characteristic q^{-1} scaling for rodlike particles, but the prefactor drops from L^{-1} to l^{-1}. Our data do however not comply with such idealized structure as depicted in figure 1. Accordingly, we have assumed a Gaussian distribution in r with standard deviation s_r. It is also assumed that a is constant, which implies that p is proportional to r with a proportionality factor given by equation (2). Interactions among supercoils are accounted for in the second virial approximation and the total scattering function takes hence the form

$$S(q) = NP(q)\Big/\left(1 + 2A_2 r P(q)\right), \qquad (4)$$

with N the number of bases, A_2 the second virial coefficient and r the DNA density.
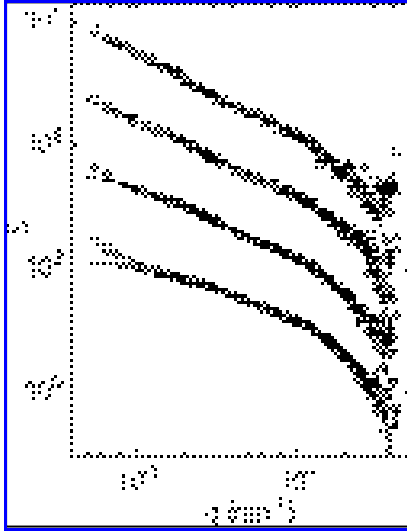
Figure 2. Structure factor S vs momentum transfer q for 3 (Δ), 6 ($\Diamond$), 11 ($\Box$) and 27 (o) g DNA/dm^3 in 0.05 M NaCl.

Due to the presence of a significant distribution in r and p, the structure factors do not exhibit strong oscillatory behaviour. They do show however, the anticipated q^{-1} scaling and the drop in prefactor from L^{-1} to l^{-1} with increasing q. The plectonemic structure is most clearly demonstrated in figure 3, where the structure factors are normalized in a way that they go to unity at high q. The normalized structure factor extrapolates to $2l/L$ for $q \rightarrow 0$ and in the absence of interactions. In the fit procedure, we have optimized r, its distribution width s_r, a and A_2. The other parameters are derived through equation (2) and standard variance propagation. Note that the margins are not related to error, but rather to variation in molecular shape.
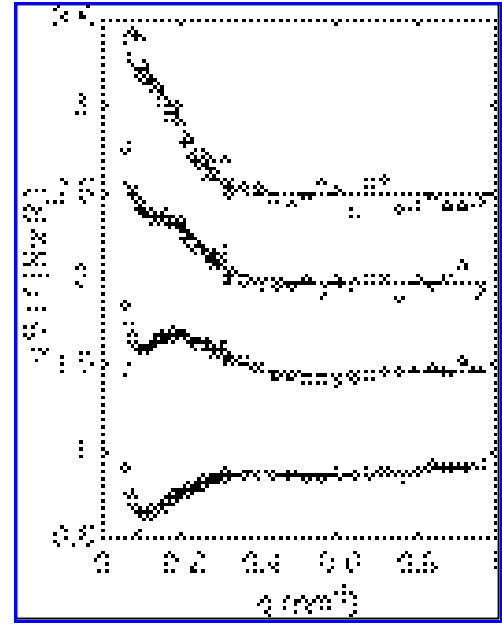
Figure 3. As in Figure 2, but for the normalized structure factor. Lines represent a fit with parameters in table 1. To avoid overlap the data are shifted along the y-axis.

With increasing concentration through the phase transition, r and p are seen to decrease significantly. Because of the (near) constancy of a, Wr decreases and the number of superhelical turns increases ($Wr = -n \sin a$). According to the fact that the sum of the excess twist and the writhe are conserved, this decrease in Wr should be compensated by a positive twist exerted on the duplex if ΔLk is conserved. Apart from the change in physical size of the supercoil, the associated increase in molecular free energy is of great importance in controlling the phase boundaries.

Table 1. Parameters resulting from the fit of the structure factor to the scattering data. Note that the margins are related to a variation in molecular shape.

c (g/dm^3)	r (nm)	p (nm)	α(°)	$2L/l$	Wr	A_2 (10^6 nm^3)
3	10±4	21±9	65	0.91	-6±3	-
6	9±5	14±7	57	0.84	-7±4	0.55
11	8±4	13±7	59	0.86	-9±5	1.22
27	5±3	6±4	52	0.79	-14±10	1.92

References
[1] Zakharova S S, Jesse W, Backendorf C, Egelhaaf S U, Lapp A and van der Maarel J R C, Biophys. J. **83** (2002) 1106
[2] Zakharova S S, Jesse W, Backendorf C and van der Maarel J R C, Biophys. J. **83** (2002) 1119

IONIC STRENGTH DEPENDENCE OF THE PERSISTENCE LENGTH OF A NATURAL MODEL SEMIRIGID POLYELECTROLYTE : AGREEMENT WITH THE OSF MODEL.

E. Buhler[1], F. Boué[2]

[1]Centre de Recherches sur les Macromolécules Végétales-CNRS, UPR 5301, Joseph Fourier University, BP 53, 38041 Grenoble Cedex 9, France
[2]Laboratoire Léon Brillouin (CEA-CNRS), CEA-Saclay, 91191 Gif-sur-Yvette cedex, France

Hyaluronan is a bacterial polysaccharide, hyaluronan (poly[(1→3)-*b*-D-GlcNAc-(1→4)-*b*-D-GlcA]). It belongs to a class of water-soluble linear polysaccharides (helical structure), bearing charges in water, which can be called semirigid polyelectrolytes. This means that apart from electrostatic effects, the chain backbone is locally stiff enough to correspond to an intrinsic persistence length L_0 much larger than one monomer (of mass 400 g/mol and length 10.2 Å) [1].
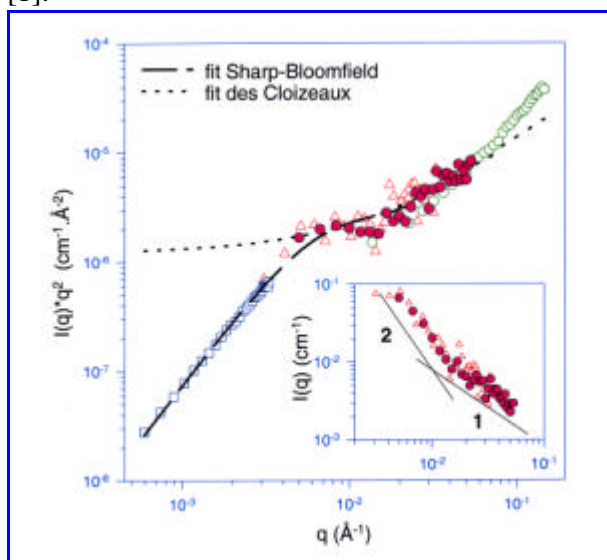
Figure 1. Kratky plot: variation of Iq^2 with q (combined SLS ( ) and SANS (Δ, $\bullet$, and O)) in high ionic strength solution. The log-log representation of the scattered intensity, I, versus q is shown in the insert (SANS). [NaCl]=0.1 M and c=1.5×10^{-3} g/cm^3. The solid line fits the wormlike chain model.

When electrostatic repulsions between the charges along the semirigid chain in aqueous solutions are not screened, they will tend to make even larger the local rigidity and increase the global size of the polyion. An additional electrostatic persistence length, L_e, due to electrostatic repulsions increases the effective persistence length, L_0. Then, following the simplest model, the total persistence length L_T is [2]

$$L_T = L_0 + L_e \qquad (1)$$

The total persistence length L_T would represent the effective rigidity of the polyelectrolyte as the sum of two contributions: the intrinsic persistence length L_0 of the corresponding uncharged chain and the electrostatic persistence length L_e, which would depend on the screening, i.e., on ionic strength due to external salt concentration. In our case, L_0 is easily larger than L_e (at least for external salt concentration larger than 3×10^{-3} M), a situation for which Odijk[1], and Skolnick and Fixman[2], found

$$L_e = \frac{\kappa^2}{4\kappa^2 l_B} \qquad \text{(OSF relation)} \qquad (2)$$

(in absence of condensation, which is the case here) where l_B=7.13 Å in water is the Bjerrum length and κ^{-1} is the Debye-Hückel screening length related to the concentration of the counterions $(\kappa^2 = 4\pi l_B c_f$ in dilute polyelectrolyte solutions).

Using SANS, **we have shown that hyaluronan, a natural product is a model semirigid polyelectrolyte, as good as a synthetic one** when it is well purified and controlled, a know how of CERMAV laboratory. Moreover **we have checked the Odijk law for the first time for a covalent polymer** t our knowledge (it was observed already for composite giant micelles).

In this aim, we have first directly determined the chain conformation at high ionic strength, where Le is naught. We have been able to fit SANS data to the "wormlike" chain model[3,4] (Figure 1). The scattered intensity crosses over, when decreasing q, from a q^{-1} rod variation to a q^{-2} as predicted for a wormlike chain; the analysis yields the backbone, intrinsic, persistence length: L_0=86.5 Å.

Then we have worked at low ionic strength. In this case, we have not been able to measure the whole form factor at low q

because, conversely, intensity crosses over from a q^{-1} to a q^{-4} variation, characteristic of polymer associations(Figure 2). But the larger q measurements allow to claim that the q-1 range is extended at low q (Figure 2 again). This means that L_e is increased ; we find the increase to be at least the amount predicted by OSF, this being the highest predicted by theory. This lower bound at low ionic strength, plus all values measured at

different ionic strength I fits the OSF law, $L_e \sim \kappa^{-2} \sim I^{-1}$ (Figure 3).
Conversely, for the flexible polyelectrolyte case, studied in LLB[5], led to $L_e \sim \kappa^{-1} \sim I^{-1/2}$ or even a lower exponent of I ($I^{-1/3}$). Accepting the failure of OSF law for very flexible chain[6-8] reconciliates the results.
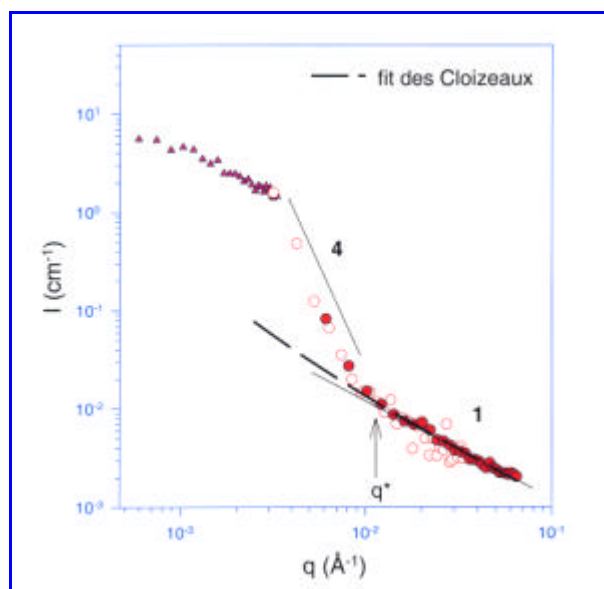
Figure 2. Variation of the scattered intensity with q (SLS ($\blacktriangle$) and SANS ($\circ$, and $\bullet$)) in low ionic strength solution: [NaCl]=10^{-3} M and c=1.5×10^{-3} g/cm^3.
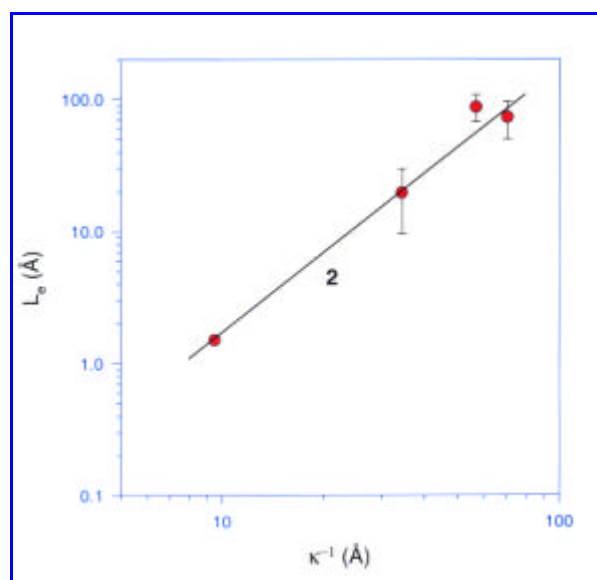
Figure 3. Dependence of the electrostatic persistence length on the Debye screening length. For [NaCl]=0.1 M, we used L_e=1.5 Å (cf OSF eq 2).

References
[1] T. Odijk, *J. Pol. Sci., Polym.* Phys. **15** (1977) 77.
[2] J. Skolnick, M. Fixman, *Macromolecules* **10** (1977) 944.
[3] P.Sharp, V.A. Bloomfield, *Biopolymers* **6** (1968) 120.
[4] J. des Cloizeaux, *Macromolecules* **6** (1973) 403.
[5] Spiteri, Boué, Lapp, Cotton, *Physical Review Letters* **77** (1996) 5218.
[6] J. L. Barrat, J. F. Joanny, *Journal de Physique II* **4** (1994) 1089.
[7] R.Everaers, A.Milchev, V.Yamakov, *European Physical Journal E*, **3** (2002).
[8] T. T. Nguyen, B. I. Shklovskii, *Physical Review E*, **66** (2002)
[9] E. Buhler, F. Boué, *European Physical Journal E*, accepted 2002
[10] E. Buhler, F. Boué, *Macromolecules*, submitted 2002

6 - LIFE SCIENCES

The research activities in Life Sciences at the LLB are in full expansion. They focus on two main fields of interest: the conformation of proteins in solution and the relationship between structure, dynamics and function of biological systems.

Protein folding
The understanding of protein folding remains one of the major goals of biology. This requires, at least, a detailed structural characterization of both the folded and the unfolded states. The structure of proteins and their solvent interactions can be modified by temperature, pH or chemicals. The application of hydrostatic pressure to a protein solution also provides a controlled manner to alter these physical properties. Thus, characterisation of the denatured states of proteins is important for a complete understanding of the factors stabilising their folded conformation.

  Whereas X-ray crystallography or NMR allows this for native proteins, only few techniques can provide precise information about the mean conformation of flexible denatured states. Among these techniques, small-angle scattering, of either neutrons or X-rays, is a very powerful tool giving structural information at low and medium resolution. Complementary information from circular dichroïsm, fluorescence and differential scanning calorimetry is used.

Dynamics and function of biological systems:
Biological macromolecules (e.g., proteins, lipids, DNA) share a structural complexity that is also reflected in a complex dynamic behaviour. At physiological temperatures, internal motions in proteins are partly vibrational and partly diffusive. The description of internal diffusion in proteins is complicated by the variety of existing motions. They involve groups of atoms undergoing a plethora of continuous or jump-like diffusion. Neutron spectroscopy permits the investigation of motions in a very broad time range from 10^{-14} to 10^{-7} seconds (time of flight, backscattering, spin echo techniques). Because of the large incoherent cross section of hydrogen nuclei (about 40 times larger than the cross section of other elements) and the fact that hydrogen atoms are distributed "quasi-homogeneously" in the biological macromolecule, this technique is a powerful tool for the study of all internal motions.

The strategy developed at the LLB is to combine the neutron results with that of light scattering and NMR and to compare them with that of Computer Molecular Dynamics (CMD) simulations. This strategy offers a unique opportunity to validate potential of MD simulations and get a detailed knowledge of protein dynamics. Dynamics of water that plays an essential role in biology becomes also accessible on a detailed way. CMD simulations are analysed with theoretical laws developed for polymeric systems, from which geometry of motions and distribution of relaxation times of various parts of the protein are obtained.

But first of all, let us present the work done at LLB on the structure and dynamics of biological membranes.

MEMBRANES: LIGNIN FILMS, PHOSPHOLIPID BILAYERS AND MEMBRANE PROTEINS
Neutron reflectivity studies of lignin films from plant cell wall
The cell wall of common plants is made of two interpenetrated polymer networks, lignins (phenolic polymers) and polysaccharides. Neutron reflectivity, combined with H/D contrast variation method, has been very powerful to study the first stage of lignin films on a solid surface. The distribution of the phenolic polymer within the polysaccharidic network has been determined (see "***highlight***", B. Cathala et al).

Studies of phospholipid membranes
A recent activity concerns the collective dynamics of hydrated phospholipid bilayers of DLPC. The short wavelength density fluctuation of DLPC bilayers close to full hydration has been studied below and above the main transition temperature by inelastic X-ray scattering techniques at the ESRF. The dispersion relation of the high frequency sound mode has been constructed for the first time (Fig. 1). The marked softening of the excitation near k=14 nm^{-1}, corresponding to the lipid chain-chain correlation peak in the structure factor,

in the L_α phase implies prevalent occurrences of short-wavelength in plane motions of lipid chains that might be of importance for transportation of small molecules across membranes.
Collaboration M.-C.Bellissent-Funel, S.H. Chen, MIT
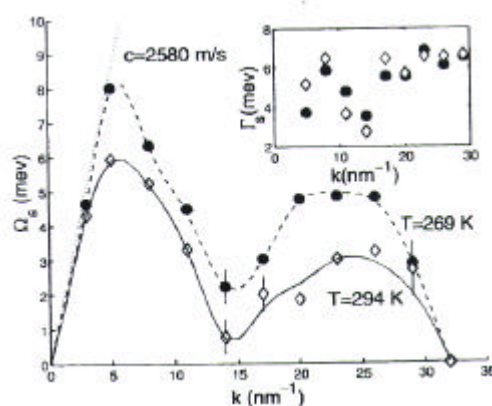
Figure 1 : Sound dispersion and damping (inset) for hydrated DLPC at two different temperatures.

Internal dynamics of the membrane mediated photosynthetic apparatus from purple photosynthetic bacteria.
The experimental work implied: (i) Large-scale preparation of H/D-exchanged RC, RC-LH1 and LH2 pigment-protein complexes. (ii) Quasi-elastic neutron scattering experiments were undertaken. (iii) Structural studies of these same proteins (in detergent or native membrane) by electronic absorption and Raman spectroscopies under applied hydrostatic pressure were made as a prelude to neutron scattering experiments. (iv) SANS measurements on LH1 subunit called B820 established that the structure is a dimer of two single membrane-spanning polypeptides with non-covalently attached bacteriochlorin molecules.
Compared to previous studies of detergent-isolated RC-LH1 in full solution (Thesis of S. Dellerue, 2000), in a lipid environment, the internal dynamics is more restrained. In collaboration with the University of Tartu, Estonia, electronic absorption and pre-resonance FT-Raman spectra for the RC, LH1 and LH2 proteins show that the proteins are still intact at pressures where globular proteins, such as lysozyme, are generally denatured. Thus, we have established the pressure parameters that will enable us to develop inelastic neutron scattering of membrane proteins. To this end, this protein system provides an important contribution to the overall understanding of the inherent differences between integral membrane proteins and globular proteins.
Postdoctoral work of A. Gall, Collaboration B. Robert (DBJC), M.-C. Bellissent-Funel

CONFORMATION OF PROTEINS IN SOLUTION
Influence of molecular weight
The refolding of a high molecular weight protein, fibronectin, has been studied for the first time by SANS. The tentatives to refold fibronectin have led to collapsed but still badly refolded conformations. This shows that efficient folding of high molecular weight nascent proteins depends on assistance of molecular chaperones. The study of *in vitro* refolding assisted by such molecular chaperones should be of great interest but has not been considered up to now (see "*highlight*", D. Lairez and J. Pelta).

Influence of high hydrostatic pressure on hydrated myoglobin
Pressures up to 300 MPa have been applied to azidometmyoglobin. The structural change cannot be observed by SANS experiments. The isothermal compressibility has been obtained in a pressure range that is not accessible by commercial densimeter, limited to 100 Mpa (see "*highlight*", C. Loupiac et al).

Influence of secondary structure on denatured states obtained by heat or guanidinium chloride
Different proteins, such as yeast phosphoglycerate kinase (PGK), β-casein and apo-neocarzinostatin (NCS) were completely unfolded by guanidinium chloride (GdmCl). Small angle neutron scattering (SANS) spectra from these denatured proteins were recorded at wave number transfers Q ranging from 0.006 to 0.4 Å^{-1}.
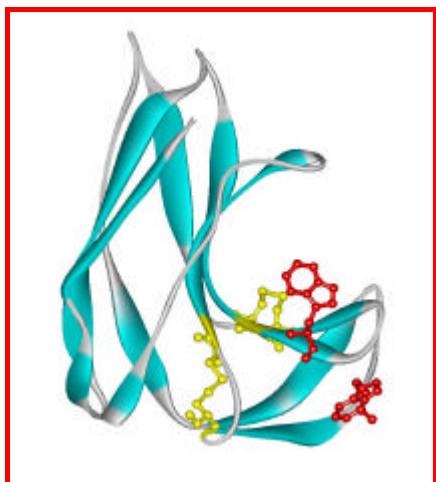
Figure 2. The Neocarzinostatin (NCS) displays a folding pattern typical of a large family, the immunoglobulin fold. NCS belongs to a family of antitumour proteins of bacterial origin that contain a labile chromophore. The protein component, apo-neocarzinostatin is a 113 amino acids protein with two short disulfide bridges, located within different loops. Its structure consists of a seven-stranded antiparallel β-sandwich.

Among the previous proteins, NCS (Fig.2) is the only one that can be denatured by heat without aggregating. Scattering from thermally unfolded NCS was also measured.

The randomness of the final protein states depends on the denaturing conditions. In very concentrated GdmCl solutions, excluded volume interactions are generally present. This means that all the amino acids are fully solvated and repel each other at large distances. As a result, the configurational space available to the polypeptide chain is restricted. On the contrary, at 78°C NCS behaves as an ideal chain. Such a behaviour, which can also be observed at moderate GdmCl concentrations, is prerequisite to folding. These properties of unfolded proteins can be directly inferred from the variation of the forward scattered intensity as function of protein concentration. Using Pedersen's description of semi-flexible polymers chains important structural parameters can be inferred from the scattering profiles.

STRUCTURE-DYNAMICS-FUNCTION RELATIONSHIP IN BIOLOGICAL SYSTEMS
a) *Dynamics of proteins in their native state*
The proteins are representative of the following biological functions: Photosynthesis (soluble proteins, C-Phycocyanin, and membrane proteins, RC, LH2 and RC-LH1); Calcium/magnesium regulation (Parvalbumin); Oxygen-carrying (Myoglobin, Haemoglobin); Enzymatic catalysis (Aspartate transcarbamylase, ATCase); Antibiotic function (Neocarzinostatin, NCS)

Influence of concentration on the diffusion process of myoglobin and haemoglobin
In biological systems such as cells, biological reactions become limited by protein diffusion. To understand oxygen assisted protein diffusion, a detailed study of myoglobin and haemoglobin diffusion in very concentrated solutions has been undertaken. In this case, neutron spin-echo spectroscopy provided a very fruitful and unique tool to study diffusion of protein solution on length scales corresponding to the centre-of-mass distances. In fact, dynamic light scattering experiments are impeded by strong absorption by the heme and multiple scattering. For the first time, *in vivo* haemoglobin diffusion from red blood cells has been studied, using the new spin echo spectrometer MUSES. For myoglobin and haemoglobin, the diffusion coefficient is reduced by a factor of 25 when going from dilute solutions to physiological concentrations. *(see "**highlight**", S. Longeville and W. Doster).*

Influence of hydration on the internal dynamics of globular proteins
Powders at different hydration levels, as well as solutions, were investigated by incoherent quasielastic neutron scattering. In particular, the quasielastic component of the spectrum reveals dynamic aspects related to diffusive motions that might be functionally important by participating to the general flexibility of the protein. From these components, one has inferred that diffusive motions of protein protons occur within a confined volume and that about 25% of the protons in the protein are involved in short-time (MIBEMOL, 10 ps time range) diffusive motions. These protons belong to the surface residues of the protein. The same findings are obtained for hydrated powders of Parvalbumin, solutions of ATCase and haemoglobin (postdoctoral work of C. Loupiac), at the same 10 ps time scale. At higher resolution (IN13, 100 ps time range), backbone motions are observed (see '**highlight**", J. M. Zanotti et al). Analysis of MD simulation leads to similar results (Thesis of S. Dellerue, 2000) and see also the chapter on modelling.

Influence of trehalose on the internal dynamics of globular proteins

Anhydrobiosis is a well-known phenomenon in nature. Several organisms and plant have been found to be able to survive periods of extreme external stresses such as high or low temperatures or periods of extreme drought. Among protecting agents, trehalose has the highest effectiveness to stabilise and protect biomaterials against denaturation caused by external stresses. Neither the protecting mechanisms of trehalose nor its highest effectiveness are clear. A first model, called the "water replacement theory", suggests that trehalose molecules can replace hydration water, and prevents in this way denaturation of the biomolecule. The other model (Angell's theory) focus on the fact that trehalose has an especially elevated glass transition temperature and may form a glassy structure in which the biomaterial gets embedded. This would slow down or even suspend all dynamical processes that could lead to degradation.

We studied the dynamics of a C-phycocyanin protein (CPC) by neutron scattering techniques and investigated the influence of the presence of trehalose molecules on the protein dynamics, on a time-scale from some pico- to several nanoseconds. The C-phycocyanin protein, commercially available in protonated and deuterated forms, is particularly suited for these studies (Thesis of I. Köper, 2002).

The intermediate scattering function of hydrated CPC powder has been compared with that of a hydrated powder when deuterated trehalose is added to water. In the latter case, one observes a slowing down of dynamics of the protein by one to two orders of magnitude. Addition of trehalose to the protein affects only slightly the geometry of movements, thus giving no evidence for direct interactions between the sugar and the protein [3], in agreement with Angell's theory.

(Collaboration I. Köper, M.-C. Bellissent-Funel, W. Pétry (Munich)

b) *Dynamic transition associated with thermal denaturation of neocarzinostatin (NCS)*

A complete understanding of protein folding requires the physical characterization of both native and denaturated state and evaluation of the thermodynamic parameters of the system. This involves obtaining information concerning the structure and dynamics of proteins denatured under various conditions.

We have studied the picosecond dynamics of NCS in solution during heat-induced denaturation, by quasi-elastic neutron scattering (MIBEMOL, resolution 96 µeV). Figure 3 shows the Elastic Incoherent Structure Factor (EISF) obtained for each temperature. The EISF decreases at high Q as the temperature increases, which suggests that the fraction of immobile hydrogen atoms p decreases as temperature increases.
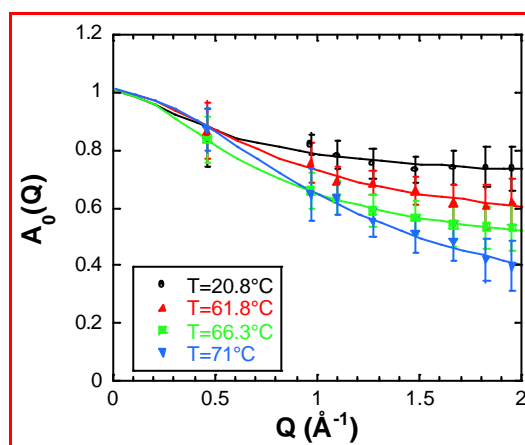
Figure 3. Elastic Incoherent Structure Factor (EISF) of NCS at all investigated temperatures. The lines are the fit, considering a fraction $(1-p)$ of particles diffusing inside spherical confinement volumes with Gaussian distributions.

We found that p decreased by 30% between 20.8 and 61.9 °C, whereas the protein retained its native conformation, and then underwent a more abrupt decrease when the protein starts to unfold. The latter decrease in p to the small value of 0.09 at 71°C shows that almost all the protons in the protein were mobile at the half transition temperature.

The internal dynamics of the native fold at 21°C is consistent with diffusive motions arising from the side chains of the polypeptide loops external to the protein core. These side chains are free to move and to explore a large space. If the temperature increases to 61.8°C, just below the heat denaturation transition, the backbone of NCS become more flexible and the β-sandwich residues less constrained. Evidence for this change is provided in particular by the increasing number of protons with detectable diffusive motions. If the

temperature is the increased to the half-transition temperature, almost all the protons in the protein acquire the ability to diffuse locally. These results show an important aspect of the relationship between structure and dynamics in protein folding (Thesis of D. Russo, 2000).

c)   Role of hydration water

The dynamics of hydration water has been studied in assemblies of identical small peptides. A chain of five alanins has been hydrated, at various levels of hydration, providing with 1 to 25 water molecules. The neutron quasi-elastic experiments allowed us to accessing the dynamics of water molecules that is limited to rotational motions acting to breaking hydrogen bonds. However, the H-bond lifetime remains 3 to 4 times longer than that between molecules in bulk water. The diffusion becomes less confined when the level of hydration increases. This study must be extended to chains containing about twelve monomers and giving rise to two turns of alpha helix.

Collaboration D. Russo (postdoctorant, Berkeley), P. Baglioni (Florence), J. Teixeira.

AN OPENING TO MEDECINE AND MEDICAL APPLICATIONS

Cancer Borotherapy:

First experiments have been carried out in order to elucidate the mechanisms at the molecular level of the radiolysis of ADN during the Boron Neutron Capture Therapy, used for the reduction of cancerous tumours. The results are very encouraging and promising (see "***highlight***", M. Charlier and E. Sèche).

Enzymatic degradation of gelatine gels as a model of tumour dissemination mechanism:

In vivo, proteins are often organized in a gel state, i.e. an elastic solid of macromolecules swollen by a large amount of solvent. On one side, gelation is involved in many biological processes such as blood coagulation or wound healing. Conversely, the transition from a solid gel to a liquid is also important mainly for the extracellular matrix (ECM) behaviour that constitutes a physical barrier isolating organs and regulates cell behaviour.

In tumour dissemination, invasive cells must solubilise the ECM and express for that up to 15 different proteolytic enzymes, especially metalloproteinases (MMP). These proteinases differ by their specificities and reaction mechanisms; moreover, the ECM composition and organisation are tissue-dependent. In spite of these peculiarities, in all cases cell invasion implies a similar process that requires the enzyme-catalysed degradation of the ECM. Beyond the complex biochemical processes involved at a molecular level, the understanding of the degradation mechanisms is crucial to inhibit or slow down the cell invasion.
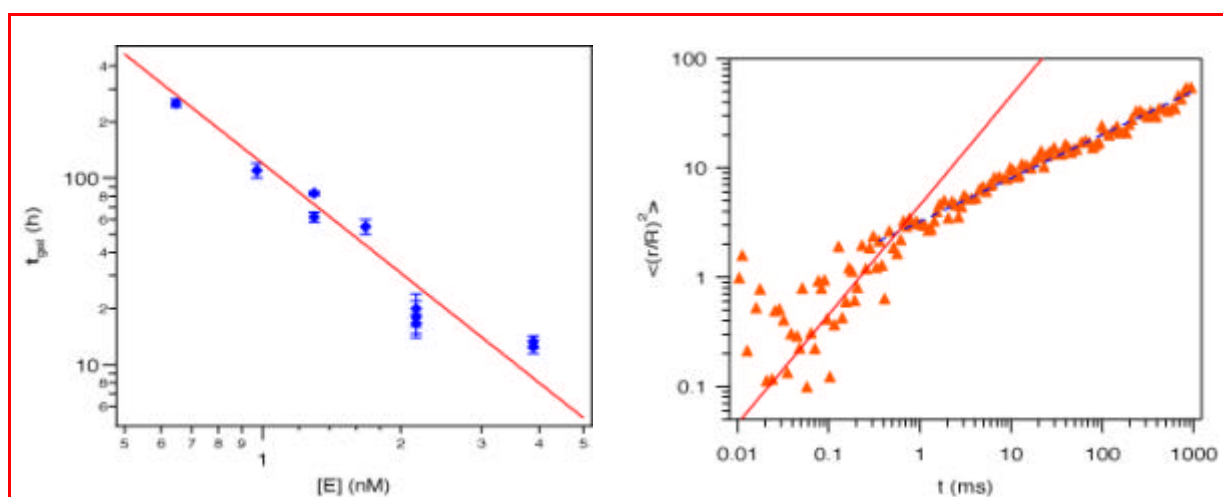
Figure 4. Variation of the gel proteolysis time, t_{gel}, on enzyme concentration, [E]. The straight line has a slope in Log-Log equals to -1.95±0.15.

Figure 5. Reduced mean square displacement of thermolysin in the gel deduced from FCS measurement. The full line accounts for the diffusion of thermolysin in water. The dotted line corresponds to the power law $<(r/L)^2>=(3.2\pm0.1)\ t^{0.40\pm0.01}$ with L the apparatus characteristic length (~ 400 nm)

Thermolysin catalysed degradation of gelatine gels has been considered as a model system to study the ECM solubilisation. Gelatine is a denatured collagen, and thermolysin is a Zn-metalloproteinase from Bacillus thermoproteolyticus, which is an analogue of MMP and displays the same basic mechanism.

A gel degradation rate varying as the square of the enzyme concentration has been observed (Fig. 4), whereas an ordinary Michaelis-Menten mechanism would lead to a linear behaviour. The thermally induced motion of enzymes in the gel has been measured by two-photon fluorescence correlation spectroscopy (FCS) and identified as being anomalously slow (Fig. 5). These experimental results have been interpreted from a theoretical point of view in terms of an anomalous diffusion-controlled mechanism for the gel degradation that should be inherent to the enzyme activity (Thesis G. Fadda, 2002).

IN13 CRG at the ILL and GDR 'Fonction et Dynamique des Macromolécules Biologiques'

In collaboration with IBS (Grenoble) and INFM (Italy), the LLB has participated to the creation of the IN13 CRG, at ILL. Because of its unique characteristics (resolution 8 μeV, $Q_{max} = 5 \ \text{Å}^{-1}$) this backscattering instrument allowed us to fill a gap between time of flight and spin echo instruments. However, a limiting factor of this instrument is the low flux, especially when one likes to do energy analysis of the spectra.

The Department of Life Sciences of CNRS has renewed on January 2003 (for four years) the GDR-1862 entitled 'Fonction et Dynamique des Macromolécules Biologiques' (Director: M.-C. Bellissent-Funel, Co-Director: J. Parello). In the frame of the GDR successful activities have been undertaken: opening workshop of the GDR, (February 2001, Saclay), workshop *"Catalyse Enzymatique, Dynamique Moléculaire et Réactivité"* (January 2002, ICSN) and thematic school *"RMN-Neutrons"* (November 2002, Saint-Rémy-lès-Chevreuse).

Recently, it has been decided to create the "DYNBIO" group, under the impulse of M.-C. Bellissent-Funel and G. Zaccai, the purpose of which is to inform biologists about the potential of neutrons to accessing dynamics (but also conformation) of biological systems. In the post genomic area, one is aware that proteomics will be central to the functional genomics efforts. In the field of proteomics, neutrons can be decisive to solving conformations of big biological assemblies.

B. PERSPECTIVES

During the coming years, the fruitful strategy applied to C-phycocyanin will be extended to other systems. In order to get a full landscape of the dynamics of biological systems in relation with their function, it is necessary to do experiments at different energy or time resolutions. For this purpose, efforts will be devoted to get samples fully and specifically deuterated.

  Membrane proteins are good candidates for that, but some soluble proteins are also envisaged. The development of studies of conformation and internal motions of membrane proteins such as aquaporins, is foreseen, thanks to the new biologist researcher at LLB, S. Combet-Jancenel.

Combined with the proposed strategy, MD simulations will be performed to access a detailed knowledge of the protein dynamics in terms of relaxation times and geometry of motions of various parts of proteins (domains, backbone, side chains, etc). This will be done in close collaboration with G. Kneller and K. Hinsen (Orléans).

Finally, studies of conformations of big biomolecular assemblies (TAT membrane proteins) for which the crystallographic structure is not known are of interest and planed in collaboration with T. Granjon and B.C. Berks (Oxford).

LIFE SCIENCES

FIRST STAGE OF GROWTH OF LIGNIN FILMS ON A SOLID SURFACE

Bernard Cathala[1], Fabrice Cousin [2], Alain Menelle [2]

[1]INRA/URCA, Equipe Parois et Matériaux Fibreux, CRA, 2 Esp R. Garros, BP 224, 51686 Reims Cedex, France.
cathala@reims.inra.fr
[2]Laboratoire Léon Brillouin (CEA/CNRS), CEA-Saclay, 91191 Gif-sur-Yvette cedex, France

Lignins are natural polymers occurring in plant cell walls and represent, after cellulose, the most abundant polymer in nature. These phenolic polymers are embedded in a polysaccharide network composed of cellulose and hemicellulose. As a consequence, plant cell wall is a heterogeneous and composite structure containing several types of polymers differing in their chemical structure and macromolecular organisation. Its complex architecture is still under investigation.

It is now well established that lignins are polymerised in a polysaccharidic medium. Accordingly the structure of the plant cell wall can be considered as two interpenetrated networks: one composed by phenolics polymers, i.e lignins, and the other by polysaccharidics polymers. One of the main difficulty of studying interpenetrated networks is to determine the **organisation of both polymer networks in the vicinity of the wall**.

In order to gain a better understanding of the lignification process, we design a chemical architecture that mimes such process and choose to use neutron reflectivity to study the system. This technique allows the determination of each polymer surface organisation at the nanoscale level. The discrimination between the two polymers is performed by deuteration of one polymer. Taking advantage of the difference in neutron length density between deuterium and hydrogen, specific information will be obtained on both polymers. The architecture is described on figure 1 : a silicon wafer is grafted with polysaccharides (pectins) and peroxidase (enzyme which catalyse the polymerisation) via a spacer – amino propyl arm. Then DHPs (dehydrogenation polymer models lignin) are polymerised at the wafer surface, either from hydrogenated monomers, either from deuterated monomers. The resulting structures were studied by neutron reflectivity to determine the organisation of the phenolic polymer grown within the polysaccharidic structure.
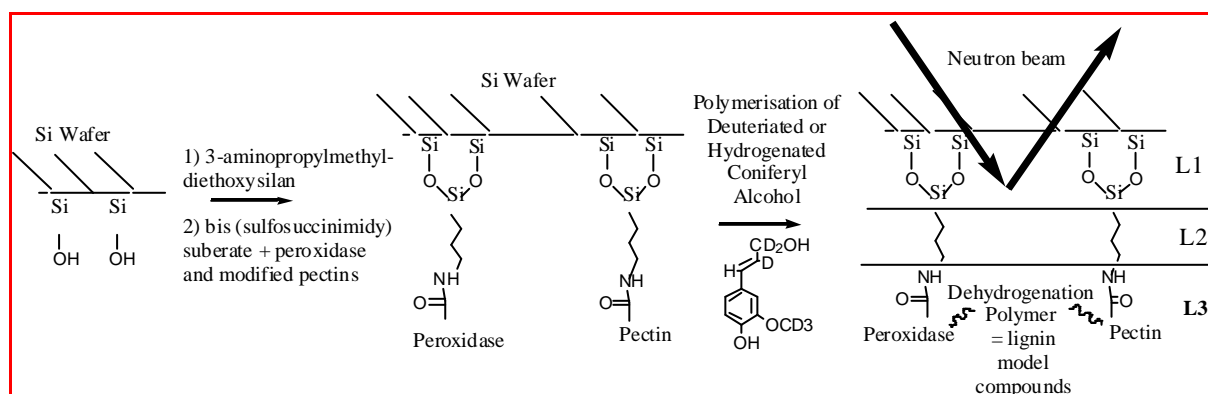
Figure 1. Grafting of the Silicon Wafer and polymerisation of Coniferyl alcohol.

Polymerisation was first performed with hydrogenated monomers in D_2O allowing the determination of the overall organisation of both polymers at the surface. This will give us the total amount of polymer in each layer, without knowing the specific percentage of each polymer. The reaction was then achieved using deuterated

monomers in a mixture D_2O/H_2O (44%/56%) which have roughly the same neutron length density than the pectin and the peroxidase. In this last case, the neutrons reflectivity becomes only sensitive to the deuterated lignin monomers which allow the examination of their location within the blend.

Experimental reflectivity spectrum were recorded for twelve hours and fitted by model reflectivity curves calculated by the standard optical method (figure 2). Best fits between the calculated and experimental spectra were obtained by minimizing χ^2. A three layer model which can be represented according to the scheme reported in the figure 1 was used (L1:silicium oxide, L2: spacer –amino propyl arm, L3: peroxidase/pectin/DHPs). The width and densities of these three layers are resumed in table 1.

In the experiment without matching, the layer 3 consists of a very dense layer. In the second experiment where signals of all components except DHPs are matched, the layer 2 has an apparent volume fraction of 0 : the DHPs are thus all located in L3 which correspond to the peroxidase and pectin layer. Thus, the L2 layer is mainly formed of pectin and peroxydase. The polymerisation of DHPs only occurs in the last layer L3. It can be deduced that the polymerisation stop the diffusion of the lignin monomer within the L2. This result evidences an important process in the lignin polymerisation within the cell walls : it is an even process starting from the outer part of the wall to the inner part. Polymerisation is only able to proceed in the buffer direction and not on the wafer side.
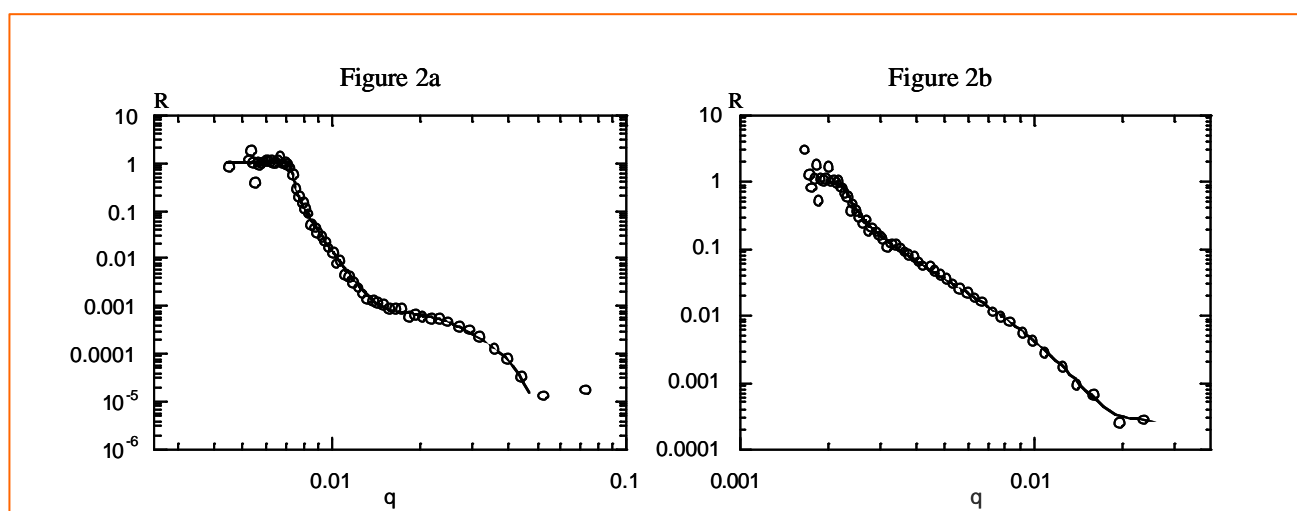
Figure 2. experimental reflectivity spectra (circle) and fit (straight line) for H coniferyl alcohol polymerisation (figure 2a) and for D coniferyl alcohol (figure 2b).

Table 1. Thickness and volume fraction fitted using a the three layer model.

	H Coniferyl alcohol		D Coniferyl alcohol	
	Thickness (Å)	Volume fraction	Thickness (Å)	Volume fraction
L1	15	0,8	25	0,7
L2	45	0,22	60	0
L3	40	0,7	55	0,3

Conclusion
In this preliminary experiment we have designed a new model architecture of the lignin polymerisation. We have shown that using neutrons reflectivity and isotopic effect, we are able to determine the distribution of phenolic polymer within the polysaccharidics network. Future work will be focused on the study of the influence of the structure of the pectins (molar mass, level of methylesterification) on the final structure of the DHPs network. Other physicochemical parameters will be also studied.

REFOLDING OF A HIGH MOLECULAR WEIGHT PROTEIN: SALT EFFECT ON COLLAPSE

D. Lairez[1], J. Pelta[2]

[1]Laboratoire Léon Brillouin (CEA-CNRS), CEA-Saclay, 91191 Gif-sur-Yvette cedex
[2]ERRMECe, Université de Cergy-Pontoise, BP 222, 95302 Cergy Pontoise cedex

The understanding of protein folding is a challenge for biologists. Proteins function are determined by their three dimensional structure and many diseases are linked to protein misfolding. Small globular proteins, generally refold spontaneously to their correct functional conformation after removal of the denaturing agent. Based on folding landscapes, in which the protein conformation moves on a minimum free energy pathway from unfolded conformations to a unique refolded and globular state, theoretical models have been proposed and computer simulations performed. For large or multidomain proteins ($>10^5$ g/mol), the number of possible conformations is beyond the scope of such approaches. Even so, this apparent complexity would allow to benefit from progresses in polyampholytes scaling theories. To a certain extent, the behaviour of a high molecular weight protein should be simpler than expected.

We have studied the refolding of fibronectin (a multidomain protein of the extracellular matrix, M=5.3 10^5 g/mol) once unfolded with 8M-urea and urea slowly removed by dialysis at pH=7.4 and at two different ionic strengths. In dilute (C=8 10^{-3} g/cm^3) and salt containing solutions, measurement leads to the protein form factor $P(q)$ as a function of the scattering vector q (see Fig.1).
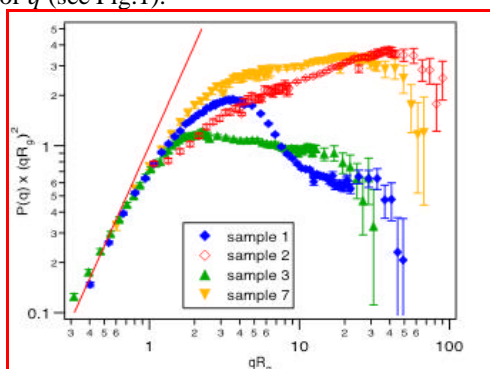
Figure 1. $P(q)(qR_g)^2$ vs. qR_g for samples in salt-containing solution. 1: "native" fibronectin; 2: unfolded fibronectin; 3: "refolded" in salt-containing solution; 7: "refolded" in salt-free solution and added salt after refolding. Radius of gyration R_g are equals to 153±2, 300±10, 88.5±3.5, 220±5 Å for samples 1, 2, 3 and 7, respectively. The largest values of R_g are measured by static light scattering.

Native fibronectin was known to be made of 56 domains which have been mainly identified as resistant to proteolysis. We have shown [1] that native fibronectin adopts the statistical conformation of a flexible string of 56 globules of 25 Å radius each. In 8M-urea solution the protein is unfolded and swells as a linear polymer in good solvent. Data are nicely fitted

using the form factor of a swollen chain of 1250 statistical segments of 13.2 Å each (see Fig.2).
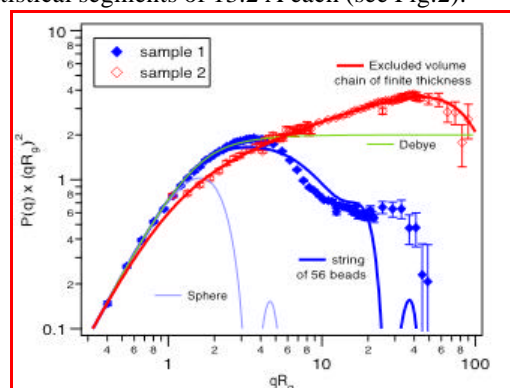
Figure 2. Form factor of the "native" and unfolded fibronectin. The full lines correspond to the theoretical expectation for a sphere, a string of 56 beads, a gaussian chain with infinitely small monomer (Debye function), and a swollen chain with a finite thickness.

As urea is removed, fibronectin collapses as proved by the deacreasing radius of gyration. From polyampholytes theory [2], in the case of neutral polyampholytes, electrostatic interactions reduce to the attractive term between charges of opposite sign, that can be included within an effective two-body volume interaction term. The chain is expected to collapse in a globule with an internal concentration resulting from a balance between attractive two-body and repulsive three-body interactions. The former need a minimum volume (or distance) to be significant, meaning that small chain segments remain gaussian, whereas the overall chain collapses at large length scale. The globule density is governed by the added salt concentration and scales as the screening length, κ_o^{-1}, of electrostatic interactions. Without added salt, the globule density is governed by the polyampholyte charge concentration. In the case of non neutral or asymmetric polyampholytes in salt-free solution, polyelectrolyte like repulsions distort the shape of the collapsed globule at large length scales. A cigar-shape rather than a spherical conformation minimizes the free energy [3]. However, the cigar-shape is unstable and splits into smaller spherical globules linked by narrow strings [4] leading to a "necklace" conformation. Depending on the net charge of the chain (long range repulsions), on the solvent quality and on charge asymmetry (short range attractions), cascade of transitions is expected between necklace conformations of various numbers of beads [5]. Our SANS data interpretations are guided by these expectations that qualitatively explain our results.

Our key observation [6] is the following: as urea is slowly removed from the solution, fibronectin does not recover its native conformation and two different collapsed conformations have been clearly identified depending on the added salt concentration.

For collapse driven at physiological ionic strength, data are accounted for using Monte-Carlo simulations to compute the form factor of a chain made of 1250 statistical segments confined in a sphere of radius R_c (Fig.3). Our results prove unambiguously that the chain in salt-containing solution collapses at large length scales ($r > x$) but remains gaussian at small length scales ($r < x$). The globule embodies a large quantity of solvent compared to the compact situation. The volume fraction of protein inside the globule is found to be $f^* = 0.3 \pm 0.1$. The "blob" size x, below which the chain remains gaussian is found of the order of 33 Å.
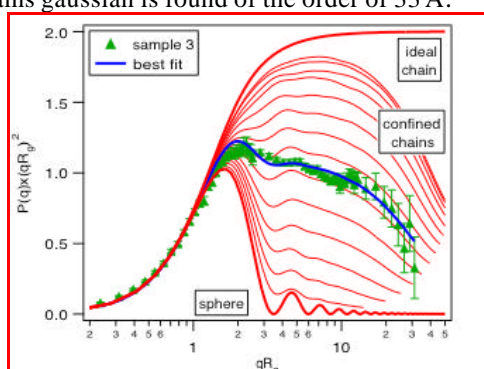
Figure 3. $P(q)(qR_g)^2$ vs. qR_g for fibronectin "refolded" in salt-containing solution (points) compared to confined chains (lines). From the top to the bottom, the lines correspond to: Debye function; confined chains with radius of confinement, R_c from 260 to 35 Å; compact sphere. The line fitting the data corresponds to $R_c = 139 \pm 15$ Å.

For collapse driven in salt-free solution (sample 6), in view of the globule density measured in salted solution, one expects a fully collapsed and compact globule split into a "necklace" conformation. However, in order to access the form factor, salt was added after the collapse stage. Then the form factor shows that the badly refolded protein is not globular but displays both a coil-like and open conformation at large length scales and a local high density area, i.e. exactly the reverse situation as in salted solution. Data are accounted for using either a model of a star polymer with a dense core (the best fit gives 2 arms) or a model of a Gaussian chain scattered with small globules (the best fit gives 1 globule). In both models the local high density area is found to extend over 20 Å. Although the conformation of the collapsed protein in salt-free solution (sample 6) was not unambiguously determined, the analysis of the

high q behaviour and of the interaction peak pleads in favour of a necklace conformation (partly dissolved by salt addition) that may be reminiscent of the native structure.
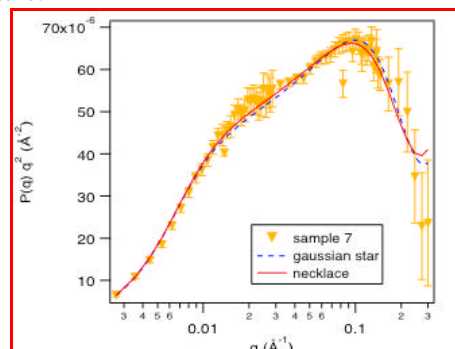
Figure 4. $P(q)\ q^2$ vs. q for the "refolded" protein in salt-free solution and salt added after refolding (sample 7). The solid and dashed lines correspond to a gaussian chain scattered with small globules (best fit gives 1 globule) and a gaussian star with core (best fit gives 2 arms), respectively.
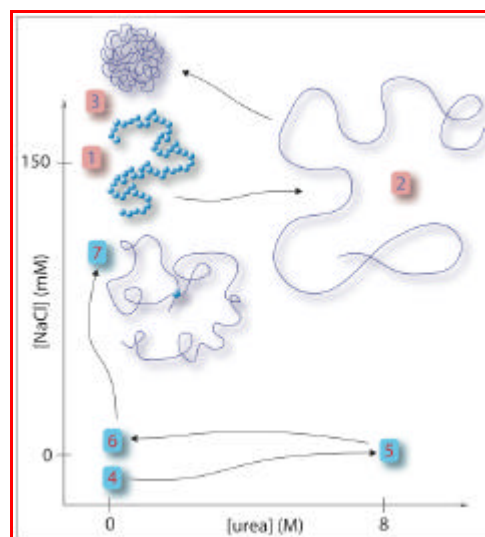
Figure 5. Conformation of fibronectin and sample history.

Although samples 1, 3 and 7 are at the same pH and ionic strength, fibronectin displays three different conformations. Two of these samples are not at the equilibrium. As a high local density may favour quenched and metastable states, it can reasonably be assumed that samples 1 and 7 are not at equilibrium. For the native conformation, this is quite puzzling and opens biological questions, mainly concerning *in vivo* 1) the possible sequential refolding of the newly translated and nascent fibronectin; 2) the assistance of molecular chaperones.

References

[1] J. Pelta, H. Berry, G.C. Fadda, E. Pauthe, D. Lairez, *Biochemistry*, **39** (2000) 5146.

[2] P.G. Higgs, J.-F. Joanny, *J. Chem. Phys.*, **94** (1991) 1543.

[3] A. Dobrynin, M. Rubinstein, *J. Phys. II France*, **5** (1995) 677.

[4] Y. Kantor, M. Kardar, *Phys. Rev. E*, **51** (1995) 1299.

[5] A. Dobrynin, M. Rubinstein, S. Obukhov, *Macromolecules*, **29** (1996) 2974.

[6] D. Lairez, E. Pauthe, J. Pelta, *Biophysical J.*, **84** (2003) 3904

MEASUREMENT OF THE ISOTHERMAL COMPRESSIBILITY OF HYDRATED MYOGLOBIN BY SMALL-ANGLE NEUTRON SCATTERING

C. Loupiac[1], M. Bonetti[2], S. Pin[3], P. Calmettes[1]

[1]Laboratoire Léon Brillouin (CEA-CNRS), CEA-Saclay, 91191 Gif-sur-Yvette cedex, France
[2]Service de Physique de l'Etat Condensé, 91191 Gif-sur-Yvette cedex, France
[3]Service de Chimie Moléculaire, DSM/DRECAM, CEA de Saclay, 91191 Gif-sur-Yvette cedex, France

The isothermal, k_T, and adiabatic, k_S, compressibilities are important quantities because their values give an estimate of the magnitude of the different type of movements in a system. k_S is proportional to the amplitude of longitudinal phonons whereas $(k_T - k_S)$ is proportional to that of the diffusive motions associated with heat diffusion. Therefore the measurement of the isothermal compressibility of a protein provide information on the amplitude of its internal density fluctuations. These fluctuations may modulate its function.

Proteins are also sensitive to pressure. For instance binding of a ligand to a protein is affected by pressures lower than 400 MPa. Furthermore protein denaturation and unfolding may occur at higher pressures. The effects of pressure on hemeproteins have been the subject of numerous investigations. Optical absorption, fluorescence, Fourier-transform infrared, Raman, and nuclear magnetic resonance spectroscopies, and laser flash photolysis have all shown that pressures near 300 MPa leads to subtle local rearrangements of the protein structure and that some intermediate states preceding unfolding probably appear. Therefore is it important to determine whether the modifications observed at the level of the active site of myoglobin (Mb) and the reorganization of the secondary structure are related to a change in the tertiary structure of the protein.
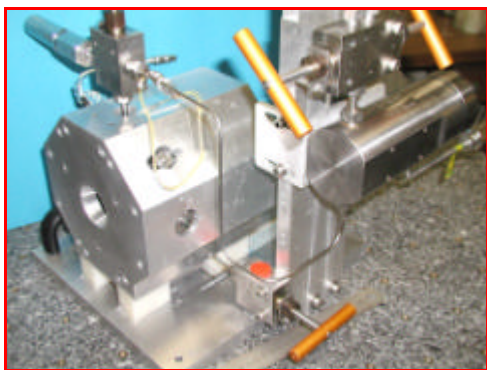
To this end small-angle neutron scattering (SANS) experiments were carried out at room temperature on pD 6.6 solutions of horse heart azidometmyoglobin (MbN$_3$) at pressures up to 300 Mpa [1]. The measurements were performed using various concentrations of MbN$_3$ in order to determine the second virial coefficient of the protein solution and the actual radius of gyration of the protein. The results shows that the interactions between the macromolecules are always strongly repulsive, even if their magnitude decreases with increasing pressure, whereas the radius of gyration of the protein remains constant. This indicates that the compactness of MbN$_3$ is not significantly altered by pressures up to 300 MPa. However it is possible that a molten globule forms at the highest pressures. This structural change cannot be observed by means of SANS experiments [2].
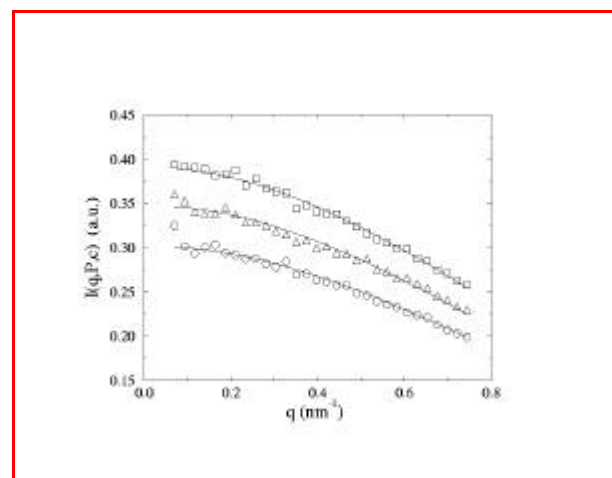
Scattering spectra I(q,P,c) of MbN$_3$ at p^{2}H 7, as a function of the wave-number transfer q. The measurements were performed at 20°C. The protein concentration at atmospheric pressure (0.1 MPa) was c(0.1) = 11.7 mg cm^{-3} and the pressures, P, were: 54 (?), 154 (?), and 302 Mpa (?). Fits of the Guinier approximation to the data are shown as full lines.

Taking advantage of the pressure-induced contrast variation of the protein these experiments allow the partial specific volume, v_p, of MbN$_3$ to be accurately determined as a function of pressure. It is found that $v_p = (0.741 \pm 0.003)$ cm^3 g^{-1} at atmospheric pressure and that its value decreases by about

5.4% at 300 MPa. In this pressure range the isothermal compressibility of hydrated MbN$_3$ is found to be $(1.6 \pm 0.1)\ 10^{-4}$ MPa^{-1} at about 20°C. Therefore, hydrated MbN$_3$ is about two to three times as incompressible as light or heavy water at the same temperature.
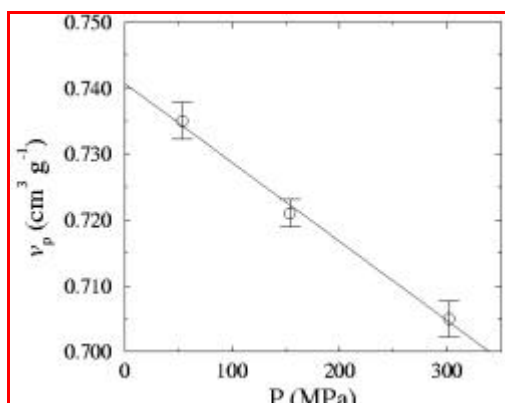
Densimetry would have seem to be the simplest way to measure the isothermal compressibility of a protein. However the only suitable commercial densimeter available today does not allow such measurements to be carried out at pressure higher than 100 Mpa. SANS allows much higher pressures to be reached with a comparable accuracy on the partial specific volume measurements. A new high-pressure cell has already been tested at pressures up to 1 Gpa, pressure at which water freezes at room temperature. It is going to be used in future experiments on proteins.

References

[1] C. Loupiac, M. Bonetti, S. Pin and P. Calmettes, *Eur. Jour. Biochem.* **269** (2002) 4731.

[2] D. Russso, D. Durand, P. Calmettes and M. Desmadril, *Biochemistry* **40**, (2001) 3958.

in-vitro AND *in-vivo* DIFFUSION OF PROTEINS IN CROWDED SOLUTIONS :

S. Longeville [1], W. Doster[2]

[1] Laboratoire Léon Brillouin (CEA-CNRS), CEA-Saclay, 91191 Gif-sur-Yvette cedex
[2] Technische Universität München, Physik Department, James Franck Strasse 1, D-85747 Garching

The interior of living cells is a complex, crowded environment, composed of a large number of molecules including proteins at high concentration. The respective volume fractions range up to 0.4. Under these conditions protein-protein interactions play a central role. The question is raised whether this environment could affect some physical, chemical or biological properties. A particular interest has been devoted to the study of diffusion mechanism in highly concentrated protein solutions, with the aim to address the question of transport properties and the possible diffusion limited kinetics of biochemical reactions. A particular aspect concerns the transport of small molecules like oxygen by protein diffusion. The transport of oxygen from the lung to muscle cells is performed by hemoglobin tightly packed in blood cells. Hemoglobin must catch the oxygen near the cell membrane. Thus the transport depends on a delicate balance between two opposing factors : High protein concentrations in the cells, which will enhance the quantity of stored oxygen, and crowding, which will depress the speed of oxygen carriage because strong protein interactions dramatically decrease hemoglobin mobility. In fact an optimum concentration for the oxygen flux is observed [1].

One central goal of our project is to clarify the question, whether the mobility of different components in a living cell can be understood based on their intermolecular interactions. To this end we studied the diffusion of myoglobin and hemoglobin molecules in-vitro, as a function of their volume fraction at concentration and temperatures corresponding to the physiological conditions. We also studied hemoglobin diffusion directly inside red blood cells.

As a first step, we perform a structural analysis of the solution, based on SANS data (small angle neutron scattering) and the molecular form factor measured on dilute protein solutions. The spectra were recorded as a function of the concentration corresponding to volume fraction ranging from F~0.05 and F~0.4. After some preliminary data treatment and background correction the measured quantity is accurately describable by the function,

$$I(Q) = F v_p (\Delta\rho)^2 . F(Q).S(Q)$$

F is the volume fraction of the protein, v_p is the volume of the molecules $(\Delta\rho)^2$ is the coherent scattering length density contrast of the molecules with respect to the solvent in cm^{-1}. F(Q) is the normalized experimental molecular form factor and S(Q) the structure factor. The spectra were refined using the

renormalized mean spherical approximation calculation (RMSA), the resulting experimental points and structure factor calculations are shown on figure 1.

In this theory, a Yukawa tail is used to account for the electrostatic potential, 3 parameters are relevant for this description, the Debye length L_D, the radius protein (assumed to be spherical) and the absolute protein charge. As can be seen on figure 1 reasonable description of the structure factor can be obtained over all refined concentrations with a diameter $\sigma_p \sim 32\pm2$ Å and the charge $|Z_p|\sim1.7\pm0.2$ e, L_D was computed from salt concentrations.
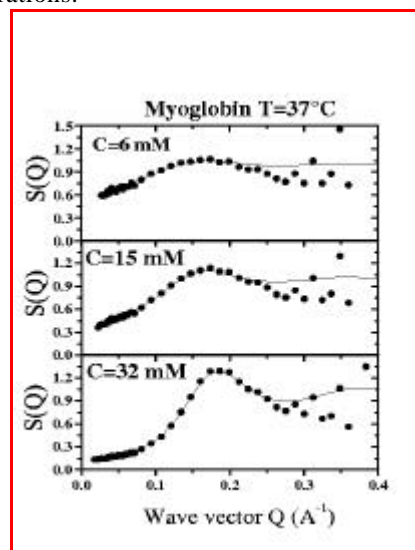
Figure 1. Structure factor S(Q) deduced from SANS data analysis (full circle). The lines are the results of the refinements using RMSA analysis (see text) .

In the second step we measure the time dependence of protein diffusion on the scale of the intermolecular distance using neutron spin echo spectroscopy. The spatial resolution provides insight into mechanistic aspects : How does the diffusion coefficient behave in the vicinity of the intermolecular structure factor maximum, where the interaction is most pronounced? How is hydrodynamic interaction between proteins affecting diffusion?

The Intermediate Scattering Function (ISF) was measured on the medium wave vector G1bis in the range of Q=0.05-0.3 $Å^{-1}$ and on IN15 for smaller Q values down to Q=0.02 $Å^{-1}$. Over the wave vectors and concentration under investigation the time decay doesn't seem to show any departure from the single exponential behaviour. The ISF was refined using I(q,t)~exp(-Γt) with D(q)=Γ/q^2 D(q) is an apparent diffusion coefficient [2].
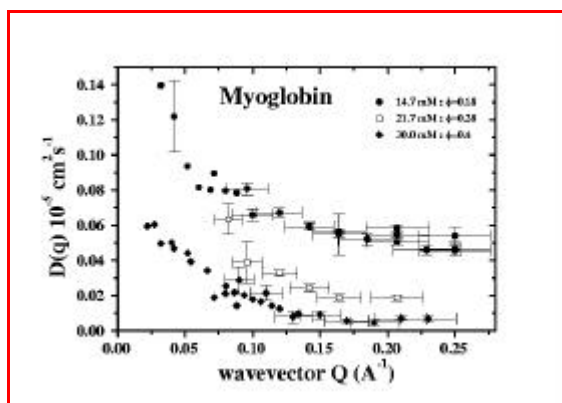
Figure 2. Apparent diffusion coefficient D(q) measured on 3 different myoglobin solutions with volume fraction F=0.18,F=0.28 and F=0.4. The plateau value corresponds to the self-diffusion coefficient.

The coherent scattering length density between protein and solution are strong enough to neglect any other contribution than the protein-protein one. In the wave vector range under investigation, polarisation analysis show that H incoherent scattering can be neglected and D_2O contribute only very little to the scattering intensity. Thus one should include all pair protein-protein contributions in the computation of the ISF and the apparent diffusion coefficient D(q) is similar to the one measured by light scattering. It corresponds to a collective diffusion coefficient, however in a completely different wave vector range. This diffusion coefficient measures the concentration fluctuations relaxations.

The wave vector dependence of the apparent diffusion coefficient D(q) is represented on figure 2 for 3 different concentrations. Whatever the myoglobin concentration the behaviour is similar, D(q) tends to a constant for wave vectors q ~ q*, whereas it present a pronounced increase for q < q*. The asymptotic value of D(q) for high q corresponds to the self diffusion coefficient D_s. We plot on figure 3 the concentration dependence of the self-diffusion coefficient measured on myoglobin.

The figure 4 presents the product D(q)S(q) myoglobin solution with volume fraction F~0.2. D(q) was measured by neutron spin echo spectroscopy and S(q) computed with the appropriate molecular fraction using analytical formulae of the RMSA analysis.
The results can be summarised as follow :
i- using neutron spin-echo spectroscopy one can investigate both individual and collective motions of the molecules over characteristic lengths around the mean interparticle distances,
ii- the reduction of the self-diffusion coefficient from infinite dilution solutions to physiological concentration is of the order of 25 for pure myoglobin and hemoglobin.

iii- Following Ackerson formula D(q)=D_∞H(q)/S(q), and combining structural and dynamical analysis one ca separate the effect of direct interactions (modelled by an hard sphere potential and a Yukawa screened type electrostatic interaction) and indirect (or solvent mediated) hydrodynamic interactions [3].
iv- The hydrodynamic factor H(q) oscillates in phase with the structure factor.
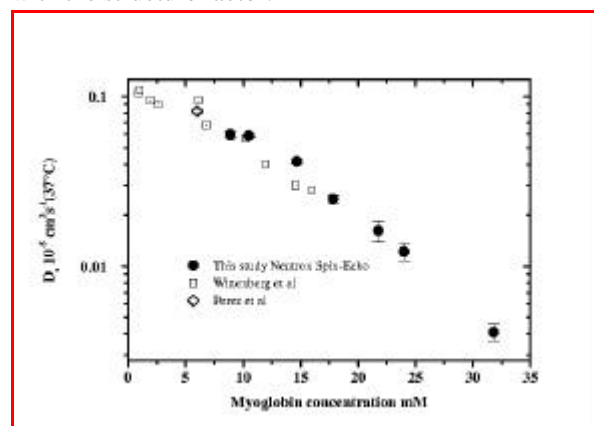
Figure 3. Concentration dependence of the self-diffusion coefficient for myoglobin solution (full circles). The open square correspond to macroscopic measurements by Wittenberg et al which have been corrected for temperature and different in solvent viscosity using Stokes-Einstein relation [2]
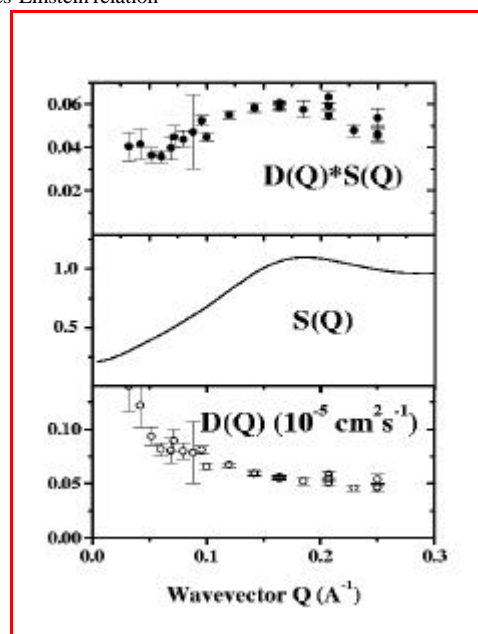
Figure 4. Apparent diffusion coefficient D(Q), structure factor S(Q) and product D(Q).S(Q) for myoglobin solution with a volume fraction F =0.18.

The oxygen transport is under investigation; in particular we focus on the mechanism of oxygen exchanged at the blood cell level with the aim to clarify the relative influences of self and collective motions. Therefore we performed measurements of hemoglobin diffusion directly inside the erythrocites.

References
[1] J.B. Wittenberg, *J.Biol.Chem. 241*(1966) 104-114.
[2] S. Longeville, W. Doster, M. Diehl, R. Gähler and W. Petry, *Neutron Spin Echo Spectroscopy*, *Basic Trends and Applications*, Lecture Notes in Physics, Vol. 601, Eds. F. Mezei, C. Pappas, T. Gutberlet. Springer, Berlin, 2002
[3] S. Longeville, W. Doster, and G. Kali, *Chem. Phys. (*Under press)

INFLUENCE OF HYDRATION AND CATION BINDING
ON PARVALBUMIN DYNAMICS

J.-M. Zanotti[1], J. Parello [2] and M.-C. Bellissent-Funel[1]

[1] Laboratoire Leon Brillouin (CEA-CNRS), CEA Saclay, 91191Gif-sur-Yvette Cedex, France.
[2] UPRES-A CNRS, Faculté de Pharmacie, 15 av. Flahault, 34060 Montpellier, France.

Hydration, internal dynamics and function [1] in proteins are intimately associated. Through its properties of Ca^{2+}/Mg^{2+} exchange, parvalbumin a 11.5 kDa Ca^{2+} and Mg^{2+} binding proteins, is associated with muscle and neuron relaxation. Dynamics of parvalbumin has been previously studied by inelastic neutron scattering and solid-state ^{13}C NMR. It has been shown that the *dynamics of surface charged residues* in the picosecond time range, as seen by neutrons, was *concomitant with the dynamics of the protein backbone,* in the nanosecond time range, as seen by NMR [2]. To definitively check the consistency of our neutron and NMR data, we have extended the previous neutron scattering experiments, to new Q and energy resolution ranges [3].
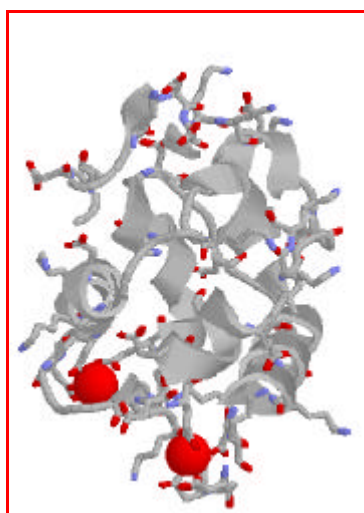
Figure 1. Ribbon representation of parvalbumin (PDB code entry : 1PVA). The two divalent ions Ca^{2+} or Mg^{2+} are symbolised by two black spheres. Charged side chains, lysines, aspartic and glutamic acids, are represented as sticks. As shown by a previous study [2], the localised relaxational dynamics of those surface residues, exposed to the solvent, give rise to the quasi-elastic scattering observed in the ps time range.

In particular, high Q ([1.,5.] $Å^{-1}$) and high resolution (10 μeV) data have been obtained on the thermal backscattering CRG IN13. The data treatment described in reference **[2]** has been applied. EISF obtained for each samples of Ca or Mg loaded parvalbumin hydrated at h=0.27 g_{D2O}/g and h= 0.72 are presented on Fig. 2. In the present high Q range at high energy resolution (10 μeV), a Gaussian distribution of radii has to be taken into account to properly describe the experimental EISF. We assess a fraction of mobile protons and an average confinement radius. The fraction of protons seen as immobile is strongly hydration dependent. At h=0.7, an hydration corresponding to **three water layers around the protein**, on a time scale of 150 ps (R=10 μeV), the protons of almost all (0.94%) the **protein secondary structure elements undergo local relaxational dynamics**. In proteins, the local (steric) environment varies strongly from side-chains to backbone (the compacity is 0.74 in the deep interior of a globular protein). Probably due to the contribution of buried protons experiencing high steric constraints, the average confinement radius decreases from 1.7 Å at 15 ps **[2]** to 1.3 Å on a longer timescale of 150 ps (this work). Interestingly, this characteristic length is not affected by hydration.

For an incoherent system, the Q dependence of the long-time tail of the intermediate scattering function, I(Q,t= ∞)/I(Q,t=0), is the form factor of a confinement volume: the EISF. As shown in Fig.1, at a time scale of 150 ps, accessible with the resolution of 10 μeVof **IN13, NSE** and backscattering experiments show some **very good agreement**. Nevertheless, the comparison between IN13 CRG and IN11 data, showing a significant decrease of the intermediate scattering function beneath the value of extrapolated EISF, suggest that, **on a time scale of few ns, new relaxational modes appear**.
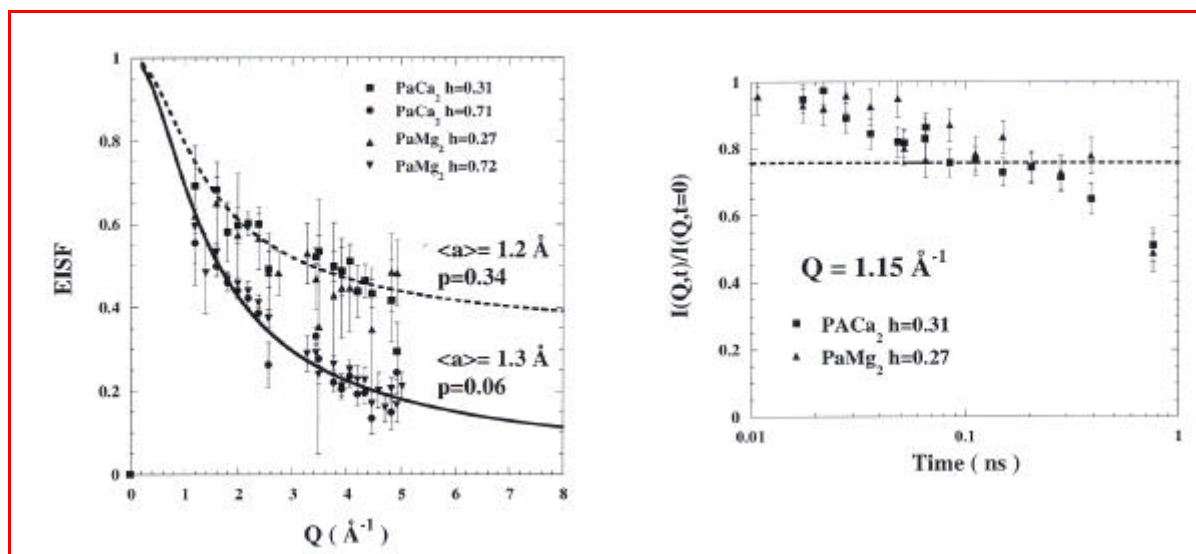
Figure 2. Left) Elastic Incoherent Structure Factor (EISF) of parvalbumin as a function of hydration and divalent ions. Measurements have been performed on IN13 at T=278 K. Dotted and full lines are the fit, for low and high hydration respectively, considering a fraction (1-p) of particles diffusing inside spherical confinement volumes with Gaussian distributions of radii. At each hydration the fitted fraction of immobile protons, p, and the averaged radius <a> are specified. Right: $PaCa_2$ and $PaMg_2$ NSE spectrum obtained on IN11C (ILL) at T=298 K. The dotted line indicates the level of the EISF deduced at Q= 1.15 Å^{-1}, from the parameters extracted from IN13 experimental EISF (Fig.1 left). At a time scale of 150 ps, accessible with the resolution of 10 µeVof IN13, NSE and backscattering experiments show very good agreement. At longer time, the decrease of the intermediate scattering function beneath the value of extrapolated EISF, suggests that relaxational modes, not seen at a timescale of few hundred of ps, appear on the nanosecond time scale.

Conclusion:

No difference has been detected in the dynamics of the calcic and magnesic forms of parvalbumin from ps to ns. The question remains whether there are really no dynamical changes or whether these changes are so local, that they are blurred out by the averaging over all the protein protons.

When increasing energy resolution the strong decrease, nearly to 0, of the fraction of protons seen as immobile, has confirmed that **it is not only the polar side-chains at the surface of the protein** which are primarily affected during the early steps of hydration. Internal non-polar side-chains and **backbone** are also affected. These results and others presented in **[3]** confirm our previous NMR and neutron scattering results that hydration acts on the dynamics of the protein at both local and global levels. This is probably **essential for the biological function** of the protein.

References

[1] J.A. Rupley and G. Careri, *Adv. Protein Chem.*, 41, 37 (1991).
[2] J.-M. Zanotti, M.-C. Bellissent-Funel and J. Parello, *Biophys. J.*, 76, 2930(1999).
[3] J.-M. Zanotti, M.-C. Bellissent-Funel and J. Parello, *Applied Physics A*, 74 : S1277-S1279 (2002).

RADIOLYSIS OF DNA AND PROTEINS BY HEAVY PARTICLES GENERATED BY THE NUCLEAR REACTION ^{10}B(n, **a**)^{7}Li. A STUDY AT THE MOLECULAR LEVEL OF BORON NEUTRON CAPTURE ENHANCEMENT OF FAST NEUTRON RADIOTHERAPY.

Michel Charlier et Édouard Sèche

Centre de biophysique moléculaire, CNRS, rue Charles-Sadron, 45071 Orléans Cedex 2, France

The implementation of boron neutron capture therapy (BNCT) presents some difficulties: the targeting of the boron-bearing drug and the delivery of a substantial flux of thermal neutrons in tumour are problems not yet solved. That is the reason why, some radiotherapists are moving towards a new technique, less satisfying from the theoretical point of view, but more easy to realise: the boron neutron capture enhancement of fast neutron radiotherapy.

During fast-neutron radiotherapy, a fraction of neutrons are thermalised in the irradiated volume by slowing down, as well as scattering by protons of the medium (70-80% water). Thus thermal neutrons are produced inside the tumour, solving by this way the problem of penetration. Targeting of boron can be considered as satisfactory by combining a concentration gradient of boron between tumour and safe tissues, with a very good spatial definition of the irradiation beam (collimator). Computations have shown that, in realistic cases, the dose due to the boron neutron capture in the irradiated volume could be sufficient to sterilise some tumours with sombre prognostic, resistant to γ rays, and difficult to treat using pure fast neutrons, like glioblastoma.

The biological consequences of ionising radiations occur mainly through two pathways. First, the direct effects result from the ionisation of the biological material itself. Second, the indirect effects are due to the chemical attack of the biological material, by the reactive species issued from water radiolysis. These indirect effects are by far the most abundant.

The radiobiological properties of such heavy particles α and Li^{3+} are very different from those of β or γ rays. Their linear energy transfer (LET = dE/dx) in water, that characterises the density of interacting events along the trajectory, is very high: 185 keV / µm in average, compared with less than 1 keV / µm for ^{60}Co γ rays, in fact not for γ rays, but for Compton electrons issued from γ rays interaction with water. (Remind that the mean energy required for water ionisation is 30 eV). The result is that the spatial distribution of the radiolytic events is completely different for γ rays and for both α and Li particles. For the same energy deposition by mass unit of irradiated medium (the dose, in gray (Gy) = 1 J kg^{-1}), the number of particle tracks is considerably smaller in the case of boron neutron capture, but the linear density of events along the trajectory of the particle is considerably greater. The biological implications of the physics of the tracks appear immediately. In the case of boron neutron capture, the mean distance between two radiolytic events (an order of magnitude of 1-2 Å instead of 0.1 µm for γ rays) is much smaller than the size of the target we are studying : DNA plasmid or protein (30-100Å).

Our experiments at the LLB concern the induction of damages in DNA. Supercoiled DNA plasmids in aqueous solution are exposed to a flux of thermal neutrons (white beam on G5-4 line). The neutron fluence, 4.6 x 10^{8} n cm^{-2} s^{-1}, corresponds to a dose rate of 24 Gy min^{-1} for 1 M ^{10}B. The solution contains various concentrations of potassium borate, enriched at 99% in either ^{10}B or ^{11}B (used as reference to account for ? contamination of the beam). The induced DNA chain breaks (SSB as single strand breaks and DSB as double strand breaks) are assayed by relaxation / linearisation of the plasmid. The induction of damages to the bases of DNA is assayed by measuring the excess of strand breaks after enzymatic treatment by endonucleases which are specific of damaged purines or damaged pyrimidines.

The samples (typically 80 µl of DNA solution) are contained in 4 mm diameter thin quartz tubes (NMR type). A special device has been drawn and built to ensure a reproducible centring of the samples in the beam.

Our experiments started on 10th February 2003, and will finish on 31st March. So it is not yet possible to summarise and discuss here the results.

However, a test experiment was made in June 2002. We have shown that DNA single- and double-strand breaks are induced upon thermal neutron irradiation in the presence of ^{10}B, whereas the effects are very

small in the presence of ^{11}B, may be due to the γ contamination of the neutron beam.
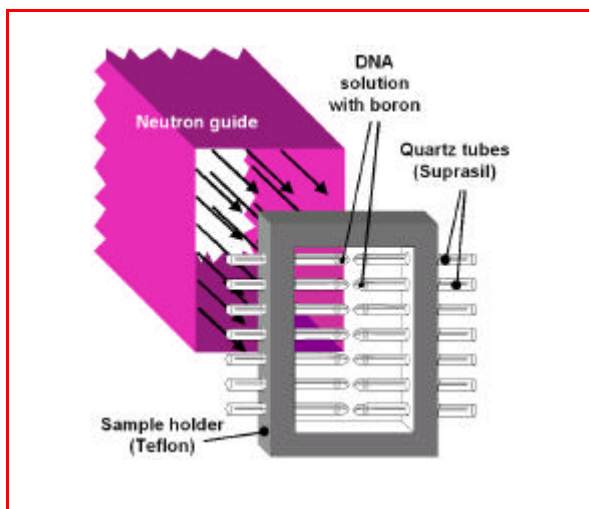
We can make the following remarks :

1 - The dose-response curve depends on the boron concentration. This fact can be explained by the previously observed presence of an impurity in the borate solution, that scavenges with a good efficiency the radicals produced in water. From this point of view, experiments at low boron concentrations are more accurate.

2 - The slope of the dose-response curve for small boron concentrations is smaller than those observed at GANIL with a $^{36}A^{18+}$ ion beam, whose LET is of the same order of magnitude (200 keV / µm). This could be due to a likely overestimation of the dose at the LLB. We do not take into account the scattering of neutrons by protons of water in the samples. Experiments with D_2O could help us to remove this difficulty.
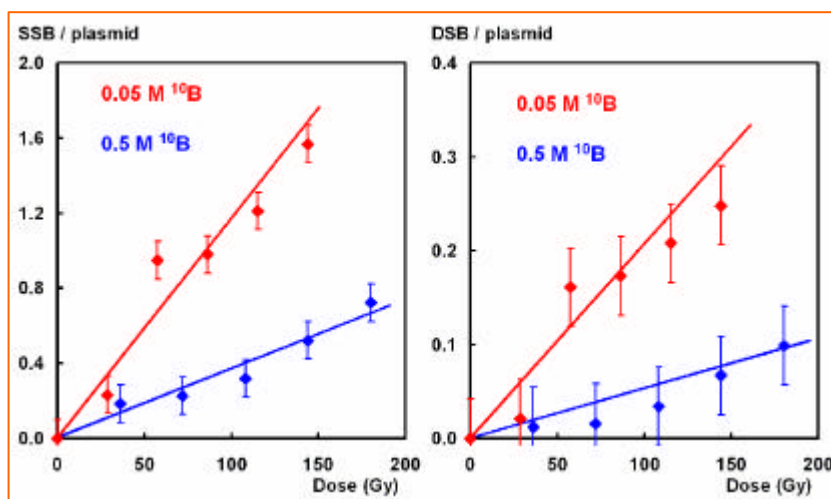
3 - The ratio DSB / SSB is about 0.2 whatever the boron concentration. This very high value (0.02 for γ rays, 0.05 for fast neutrons) is close from that measured for high LET particles. As SSB are easily repaired by repair enzymes in the cells, whereas DSB are considered as major DNA damages, this observation is of real importance for biological and medical applications.
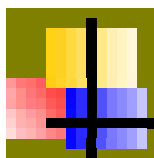
7 - MODELLING

The interpretation of neutron scattering data requires powerful modelling tools. These last years, the understanding and modelling at a finer level has triggered the development of more and more elaborate analysis tools. In this section we present recent development of these numerical tools that have been developed to reduce, model and interpret neutron scattering data.

The capacity of understanding neutron data is strongly correlated with the progress made in various fields of modelling. These modelling efforts can be separated in several categories:
- Understand the physical phenomena at the very deepest level (1-4)
- Accurate modelling of physical systems (SIMBO, CCSL, MOLECULAR DYNAMICS)
- Write fitting programs based on these models (FULLPROF, SIMULREFLEC)
- Develop more efficient fitting methods (CRIME)
- Provide efficient User Interfaces to fitting programs for neutron users (FULLPROF, SIMULREFLEC)

Efforts are being made in all these directions at the LLB.

POLYMERS, COMPLEX SYSTEMS AND BIOLOGY

- *Theory and simulations of ultrafast electronic transfer:*

Electronic transfer is the elementary process of all chemical reactions the dynamics of which can be very fast and very complex at the same time. Ultrafast dynamics can now be studied in details, thanks to the availability of femtosecond laser sources and powerful spectroscopic techniques, complementing the standard neutron spectroscopy that works currently in the Gigahertz-Terahertz regime. The whole bunch of spectacular results starting to emerge call for sophisticated theories and simulations that go beyond adiabatic approximations and thermally activated processes (see "*highlight*" 1).

- *Modelling the SANS from Nanocomposites:*

Data analysis often focuses on prominent features in the Small Angle Neutron Scattering (SANS) spectra, like correlation peaks, power laws, or the Guinier regime. Sometimes, data fitting with analytical expressions can be done, but it is possible only for simple geometries (spheres, rods, etc.). However, the power and flexibility of contrast matching methods can give access to the detailed organisation of selected parts of complex systems. In this framework, new tools to model and interpret SANS data measured on complex nanostructures are being developed (see "*highlight*" 2)

- *Molecular dynamics simulations in Life Sciences:*

An increased effort will also be made in the field of molecular dynamics. A team from the "Centre de Biophysique Moléculaire" will join our laboratory in order to combine in an efficient way Molecular Dynamics and experimental neutron scattering data in Life Sciences. A more detailed description can be found in the following pages (see "*highlight*" 3)
.

Polarised neutron reflectometry

The "Magnetism and Superconductivity" chapter has described the experimental results obtained in the field of polarised reflectometry and has detailed the related technical developments, i.e. the magnetic surface diffraction and GISANS methods. To complement these experimental efforts, a new user-friendly program SIMULREFLEC has been developed for the fitting of polarised reflectivity neutron data, obtained for example on the PRISM reflectometer (see "*highlight*"4)

Crystallography and data reduction in diffraction

- In the field of crystallography, new fitting methods are being developed. The new program CRIME CRYSTALLOGRAPHIC Imaging using Maximum Entropy can be used to reconstruct 3D electron and scattering densities from X-Ray and Polarized/Unpolarized Neutron diffraction data. It provides a very significant gain with respect to the widespread conventional Fourier Imaging. The state of the art of CRIME is illustrated in the following "*highlight*" 5 via two examples pertaining to two typical neutron examples: a spin-density study and a proton density determination. The next pages present the new improvements that have been made in the modelling of magnetic structures by taking into account local magnetic anisotropy.

- Other progress is being made in the modelling of magnetic structure. Two new computing programs, SIMBO and ENERMAG (SEE "*highlight*" 6), provide an invaluable help to interpret experimental magnetic structures occurring in real systems. These programs decipher the crystal structure and the related topology of the magnetic exchange interactions of either well-known or completely new materials and facilitate the detection of new frustrating topologies of interest in magnetism. They allow the possibility of *a priori* predictions about the magnetic ordering in new materials when estimated values of the exchange interactions are available.

- Steady and continuous progresses are also being made in the field of power diffraction. The last FULLPROF version not only allows the treatment of even more complex problems but the user interface has also been improved. Further progress is planned within a European project in which new people, working at ISIS, will collaborate with our team.

Local Magnetic Anisotropy Axes And Atomic Site Susceptibility Tensors In Polarised Neutron Diffraction

A. Gukasov (Laboratoire Léon Brillouin) and P. J. Brown (Institut Laue Langevin)

The anisotropy due to the local environment of magnetic atoms can give rise to the appearance of different magnetic moments on equivalent crystallographic positions when the magnetization is induced in the paramagnetic region by an applied magnetic field. Polarized neutron diffraction provides information about the magnetization density of each individual crystallographic site. Here, the role of the atomic site susceptibility tensor χ_{ij} accounting for the magnetic response of individual atoms to an external magnetic field is discussed. The symmetry of this tensor is very similar to that of the tensor u_j describing the thermal motion of atoms. By analogy with the atomic displacement parameters (ADPs), atomic susceptibility parameters (ASPs) can be introduced [1]. The six independent atomic susceptibility parameters can be determined from polarized neutron flipping ratio measurements and visualized *as magnetic ellipsoids*, which are analogous to the thermal ellipsoids, obtained from ADPs. If the local anisotropy is small these magnetic ellipsoids approximate to spheres with diameters proportional to the induced magnetization. In other cases *anomalous* (elongated or flattened) ellipsoids will occur. The ASPs have been determined in the compound Nd_3S_4 that has the Th3P4 structure. They correspond to strongly oblate magnetic ellipsoids.

Prolate Sm_3Te_4
$\chi_{11} < \chi_{33}$

Oblate $Nd_{3-x}S_4$
$\chi_{11} > \chi_{33}$
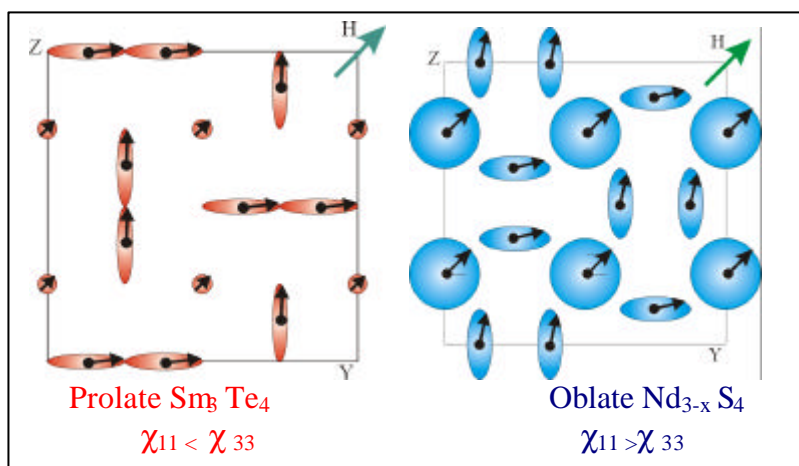
In contrast in the isomorphous compound Sm3Te4 the magnetic ellipsoids are found to be prolate. Hence in the case of Nd_3S_4 the local tetrahedral axis may be thought of as a *local hard magnetization axis* and the moment induced on the Nd site has a tendency to turn away from it if the magnetic field is not parallel to the tetrad axis. Other examples demonstrate that the anomalous elongation of the magnetic ellipsoids can be considered as a precursor of the low temperature magnetic order [2].

[1] A. Gukasov and P. J. Brown. *J. Phys. ; Condens. Matt*. **14** (2002) 8831

[2] A. Gukasov, P. Rogl, P. J. Brown, M. Michalik and A. Menovsky. *J. Phys.; Condens. Matt*. **14** (2002) 8841

Diffraction Data Analysis: CRYSFML, WINPLOTR and FULLPROF

Juan Rodríguez-Carvajal, Lab. Léon Brillouin, CEA/Saclay 91191 Gif sur Yvette Cedex, FRANCE,
Javier González-Platas, Departamento de Física Fundamental II, Universidad de La Laguna Tenerife, SPAIN,
Thierry Roisnel, Lab. de Chimie du Solide et Inorganique Moléculaire, UMR6511, CNRS-Univ. de Rennes I,
Carlos Frontera, Instituto de Ciencia de Materiales de Barcelona (CSIC), Universidad Autónoma Bellaterra, SPAIN

WINPLOTR and FULLPROF

In the last few years we have been working in the development of computing tools for data analysis of powder and single crystal diffraction. The public distribution of the programs **WINPLOTR** and **FULLPROF** [1-3] has allowed the introduction of substantial and progressive improvements, thanks to the feedback from the users. At present, the combination of **WINPLOTR** and **FULLPROF** constitutes one of the most popular Rietveld suites and they are used worldwide for the analysis of powder diffraction data. The treatment of incommensurate magnetic structures is one of the areas of expertise of **FULLPROF** that other programs cannot handle [4, 5].

In last few years many improvements have been performed on aspects of the **WINPLOTR** and **FULLPROF** programs concerned with their user friendliness and the treatment of even more complex problems [2, 3]. The task of improving the programs and creating new tools to simplify their use will be reinforced in the forthcoming future. **WINPLOTR** is a Windows-based application that is presently the most used GUI to **FULLPROF** and cannot be easily ported to Linux or other Unix systems.

A re-arrangement of the code and the use of a new library to access the Windows, or X/Motif, API are needed to make it independent of the platform. This will be done using *Winteracter,* as is the case of **GFOURIER** and **EDPCR**. Improvements in the capabilities of **WINPLOTR** are already continued in an incremental way through feedback with the user community. Concerning the improvement and development of **FULLPROF** itself it is important to emphasize that the program can handle flipping ratio measurements from polarized neutrons. Multipolar and wave-function refinements can now be performed from single crystal flipping ratio data.

An important step in the friendliness for using **FULLPROF** has been the development of **EDPCR** that allows a simple use of the program without knowing all the details of the input control file. Within **EDPCR** stand-alone programs, based in **CRYSFML**, like **BASIREPS**, are accessible with a simple click. There are conversion tools for different formats of crystallographic data and CIF files can be easily imported. A crystallographic calculator will be soon implemented. **EDPCR** is completely interoperable with **WINPLOTR/FULLPROF** through a common hidden file collecting run time events: end of a calculation, modifications of a file by one of the applications, etc.

Programs based in CRYSFML

We have developed a set of FORTRAN 95 modules, Crystallographic FORTRAN Modules Library (**CRYSFML**)[6], which may be used in crystallographic and diffraction computing programs. Modern array syntax and new features of FORTRAN 95 are used through the modules. We take advantage of all object oriented programming techniques. The library is entirely written in a subset of FORTRAN 95 called **F**. Compilers for the **F**-language are publicly available for the most important operating systems [7].

The present **CRYSFML** contains procedures for reading files of many different formats, string utilities for handling the reading in free format, generation and reading of CIF files, mathematical modules, modules for generating space groups from their Hermann-Mauguin or Hall symbols for whatever setting. More generic space groups with non-conventional lattice centring vectors can also be built using user-defined generators. Reflection handling modules may be used for generating reflections in selected regions of reciprocal space and for calculating structure factors, etc.

Public programs using **CRYSFML** are **FOURIER**, **GFOURIER**, **BASIREPS** and **EDPCR**.

These programs work on Windows and Linux and are already distributed from the LLB Web site. The first two programs are dedicated to the Fourier analysis of diffraction data. **EDPCR** is a new (still under development) Graphic User Interface (GUI) to **FULLPROF** input control file of extension PCR. **BASIREPS** is a program for calculating basis functions of irreducible representations of space groups. This program is useful for determining magnetic structures and phonon symmetry analysis.

SIMBO, ENERMAG and data-reduction related programs

We dispose of a set of computing programs based on **CRYSFML** that are not yet distributed publicly in the scientific community. A non-exhaustive list is the following:

- **SIMBO and ENERMAG:** Programs for the analysis of the magnetic topology and classical magnetic energy of an arbitrary crystal structure. A more detailed account of these two programs is given in a separate document of this report.

- **SIMILAR:** Program to make conversion of settings for describing crystallographic structures. It determines automatically the splitting of Wyckoff positions on going from a space group to one of their subgroups. Calculate all the *translationengleiche* subgroups of a space group, co-set decompositions, etc.

- **DATARED:** Program for data reduction of single crystal data. It handles twinning and incommensurate magnetic and crystal structures. At present it can read data provided by several integration programs, in particular several versions of COLL5 (LLB and ILL) and prepares files to be read by **FULLPROF** when using single crystals.

The current tasks in course within the project of developing **CRYSFML** include:

i) The implementation of procedures for calculating, using the Blume equations, the scattered polarisation and intensity of reflections of single crystals when using 3D polarimetry.

ii) The implementation of specialised structure factor subroutines for molecules described in the Z-matrix formalism. The free parameters being the distances, bond angles and torsion angles. This last task is extremely useful for structural analysis, based on powder or single data, of molecular pharmaceutical compounds.

References:

[1] "FullProf.98 and WinPLOTR New Windows 95/NT Applications for Diffraction" Juan Rodríguez-Carvajal and Thierry Roisnel, *Commission for Powder Diffraction, IUCr Newsletter* **20**, (1998).

[2] "WinPLOTR: a Windows tool for powder diffraction patterns analysis" T. Roisnel and J. Rodríguez-Carvajal, *Materials Science Forum* **378-381**, 118-123 (2001).

[3] "Recent developments of the program FullProf", Juan Rodríguez-Carvajal, *Commission for Powder Diffraction, IUCr Newsletter* **26**, 12-19 (2001). The complete FULLPROF suite can be obtained from ftp://ftp.cea.fr/pub/llb/divers/fullprof2k/.

[4] "Magnetic structure determination from powder diffraction. Symmetry analysis and simulated annealing" J.Rodríguez-Carvajal, *Materials Science Forum* **378-381**, 268-273 (2001).

[5] "Magnetic structure determination from powder diffraction using the program FullProf" J.Rodríguez-Carvajal, *Proceedings of the XVIII Conference on Applied Crystallography*, *Ed. Henryk Morawiec and Danuta Stróz, World Scientific*, London 2001, pp 30-36.

[6] "Crystallographic Fortran Modules Library (CrysFML). A simple toolbox for crystallographic computing programs"J. Rodríguez-Carvajal and J. González-Platas, *Acta Cryst.* A**58** (Supplement), C87; see also: *Computing Commission, IUCr Newsletter* **1**, 50-58 (2003), this document is freely accessible via the Internet at http://www.iucr.org/iucr-top/comm/ccom/newsletters/2003jan/.[7]   All free F-compilers can be downloaded from the site: *ftp://ftp.swcp.com/~walt/pub/F*.

See also *http://www.fortran.com* for information about FORTRAN 95 and ELF90.

MODELLING
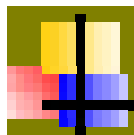
A NONADIABATIC THEORY FOR ULTRAFAST CATALYTIC TRANSFER OF ELECTRONS AT LOW TEMPERATURE

S. Aubry[1] and G. Kopidakis[2]

[1] Laboratoire Léon Brillouin (CEA-CNRS), CEA Saclay, 91191-Gif-sur-Yvette, France
[2] Department of Physics, University of Crete, P.O. Box 2208 71003 Heraklion, Crete, Greece

Electron transfer is a ubiquitous elementary process of chemical reactions[1]. Electron transfer is well described by the standard Marcus theory [2], based on an adiabatic hypothesis, as a thermally activated process with a characteristic energy barrier (figure 1). However, the fastest electron transfer occurs close to the Marcus inversion point characterized by a vanishing energy barrier in a regime where the adiabatic hypothesis breaks down. The need of an improved theory is thus a prerequisite to interpret the fast transfer at low temperature.
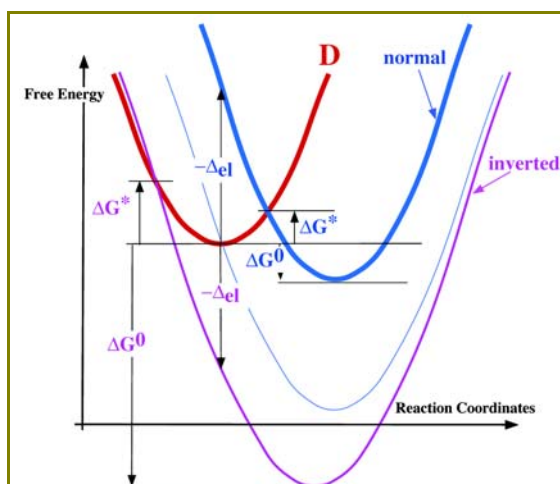
Figure 1. Free energy versus Reaction Coordinates of the system donor-acceptor when the electron is on the donor (top left curve D) or on the acceptor for several redox potentials in the normal regime (top right curve), at the inversion point (middle right curve) and in the inverted regime (bottom right curve). The chemical reaction energy is the distance between energy minima ΔG^0. The energy barrier is ΔG^*. The electronic excitation energy on the donor at fixed reaction Coordinates is Δ_{el}.

We have constructed a quantum model of a weakly interacting electron in a _nonadiabatic_ phonon bath, in a standard tight-binding scheme of the wave functions. The resulting effective equation that describes the tunneling of electrons is a discrete nonlinear Schrödinger equation with damping terms coming from the nonadiabaticity. These damping terms are necessary to dissipate the transfer reaction energy and bring about its irreversibility. The thermal fluctuations of phonons introduce random forces in the effective equation at non-zero temperature.

Far from the inversion point, our model recovers fairly well the main predictions of the Marcus model in the standard situation of thermally activated and relatively slow electron transfer. Close to the inversion point, nonlinear effects liven up as the energy level of a given electronic state depends on its occupation density, modifying the transfer between Donor and Acceptor that was supposed to be resonant. This may induce an energy barrier and in any case to a slowing down of the transfer reaction.

We have already shown in previous works [3] that nonlinear tunneling can occur but it imposes an extra condition on the nonlinearities, stating that electronic states of the two molecules involved in the transfer must stay equal. In this case, the electronic density, initially on the donor molecule interacting weakly with the acceptor molecule in a nonlinear resonance, is going to slowly oscillate between the two molecules (as in the linear case) but the transfer will be done with a variation of the electronic level (not present in the linear case). This nonlinear tunneling of the electron is a coherent nonstochastic quantum process. However, the energy of the transfer reaction is zero and this ideal transfer case is physically marginal.

An acceptor molecule in nonlinear resonance with the Donor cannot accept irreversibly the transferred electron and will be named catalysor for now on in this note because it can induce spectacular catalytic effects to transfer the electron with a positive energy reaction on a third Acceptor molecule that is not initially in resonance with the Donor. The condition is simply that the oscillating electronic level of the Donor-Catalysor system must cross the unoccupied level of the acceptor molecule interacting weakly with the first system (figure 2). This resonance triggers the transfer of the electron from the Donor-Catalysor system to the acceptor molecule.
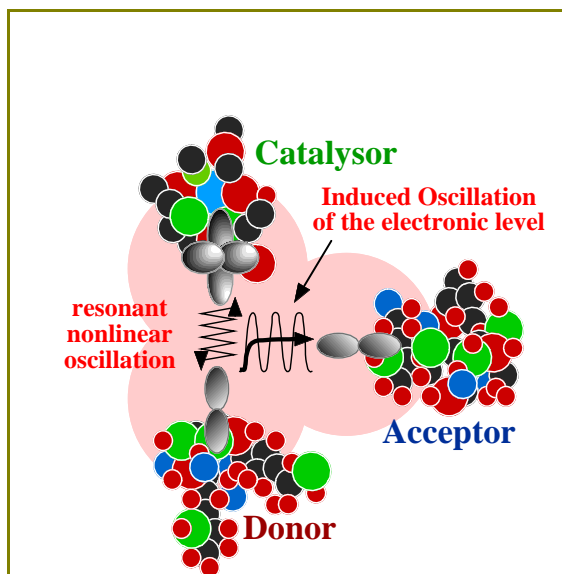
Figure 2. Scheme of a Donor-Acceptor electron transfer induced by a Catalysor. The electron, initially on the donor, oscillates between donor and catalysor, inducing a variation of the energy level. The electronic level resonates with the unoccupied level of the acceptor and the electron is irreversibly transferred with energy dissipation in the phonon bath.

Despite the further loss of the resonance, the reaction energy is dissipated with the charge fluctuations and the electron is irreversibly transferred in its fundamental state on the acceptor. This catalytic effect has been confirmed by numerical simulations of our effective equation of the electron transfer (figure 3) showing the transient passage on the catalysor and the total transfer in picoseconds, an ultrafast process compared to the activated case. The catalytic effect is still efficient at low temperature for cases where the direct transfer donor-acceptor is impossible due to a too high-energy barrier.
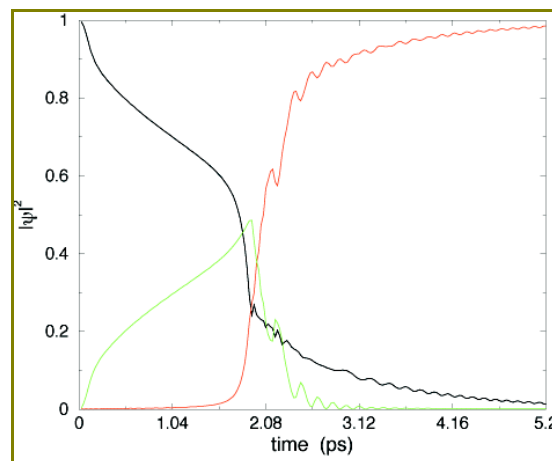
Figure 3. Electronic density as a function of time, on the Donor (in black), the catalysor (in green) and the acceptor (in red) in a realistic example: reaction energy of 0.375 eV, transfer integral of 0.01eV and activation energy around 0.071 eV without catalysor. At zero temperature, the weak coupling with the catalysor induces a partial transfer on it and then a complete transfer on the acceptor.

Our approach can be extended to quantum excitation transfers and shed new light on the molecular logical functions in biochemistry reactions.

The crucial nonlinear resonance in the Donor-Catalysor system may be detuned by very small changes, coming for example from mutations in the biological world, leading to an inhibition of the electron transfer or at least a considerable slowing down. The photosynthetic reaction center of primitive bacteria, heavily studied experimentally [4], displays striking phenomena, qualitatively foreseen by our model.

References

[1] A.M. Kuznetzov and J. Ulstrup, *Electron Transfer in Chemistry and Biology: An introduction to the theory*, Wiley series in Theoretical Chemistry (1999)

[2] R.A. Marcus, *Rev. Mod. Phys*., **65** (1993) 599--610

[3] S. Aubry and G. Kopidakis, Proceeding of "*Localization and Energy Transfer in Nonlinear Systems*", in San Lorenzo de El Escorial, Spain (June 2002)

[4] R.E. Blankenship (2002), *Molecular Mechanisms of Photosynthesis*, Blackwell Science

INTERPRETATION OF COMPLEX SANS SPECTRA : CONTRIBUTION OF NUMERICAL SIMULATIONS

J. Oberdisse[1], J.-F. Berret[2]

[1] Laboratoire Léon Brillouin (CEA-CNRS), CEA-Saclay, 91191 Gif-sur-Yvette cedex, France
[2] Complex Fluids Laboratory, CNRS-Rhodia, UMR n°166, Cranbury NJ 08512, USA

It is well known that the intensity I(q) measured in a SANS experiment does not contain all the structural information of the sample. This is mainly due to the loss of the phase and the incomplete knowledge of I(q) in all q-space. Therefore, data analysis focuses often on prominent features of the intensity, like correlation peaks, power laws, or the Guinier regime. Sometimes, data fitting with analytical expressions can be done, which exist only for simple geometries (spheres, rods, etc.).

Here, we discuss two cases of data recently measured on small angle spectrometers (PAXE at LLB and D11 at ILL) for which specific models of more complex geometries have been developed and successfully applied. The <u>first</u> study investigates the phase behaviour of a mixture of charged-neutral hydrophilic diblock copolymers and surfactant of opposite charge in aqueous solution.
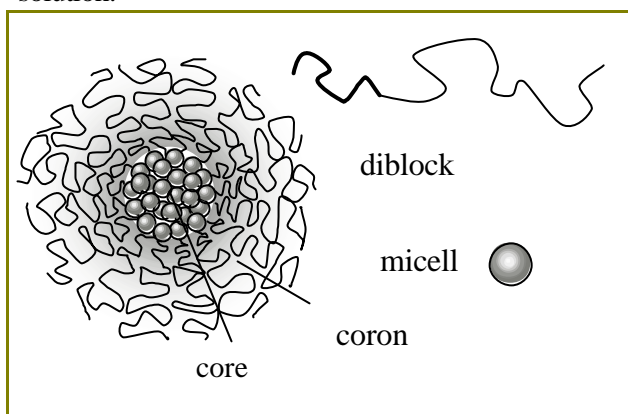
Figure 1. Complex aggregate formed by charged micelles and neutral-charged copolymers.

The data presented here has been obtained in the DTAB/PANa-b-PAM/D_2O system, but very similar features have been found in other systems, e.g. charge-inversed ones. The surfactant forms micelles which attract each other under the influence of the copolymer (bridging), and seem to build a micelle-containing aggregate of well-defined aggregation number [1,2]. This is schematically represented in Fig. 1.

To check the consistency of this picture with the data, we have set up a simple model of micelles in thermal motion inside a sphere, which represents the confinement of the micelles within the aggregate core. This confinement is due to the intermicellar attraction mediated by the charged part of the copolymer. The hairy outer layer of the aggregates, which is made up of the uncharged, hydrophilic part of the copolymer, is thought to prevent the aggregates from infinite growth. An example of experimental and theoretical SANS intensities is shown in Fig. 2 [3].
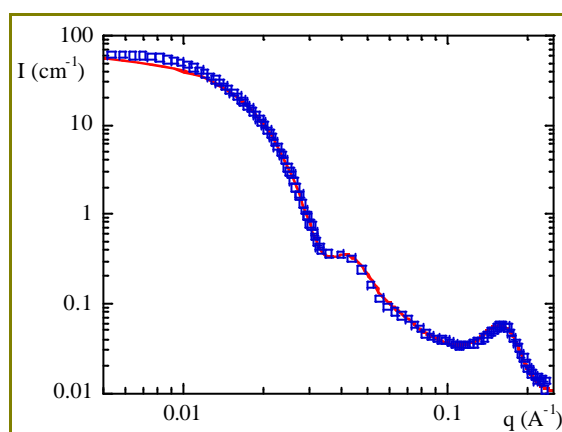
Figure 2. Scattered intensity of a mixture of ionic surfactant (DTAB) and a hydrophilic copolymer (PANa-b-PAM). The solid line is our model calculation (internal volume fraction 50%, hard sphere repulsion between micelles, core radius = 120 Å, Gaussian polydispersity 25 Å). The low-q deviation is due to the interaggregate structure factor, which is not described here.

Note that the size, polydispersity and internal concentration of the aggregate are directly related to the small- and intermediate-angle scattering (signal height and oscillations). The interaction peak at 0.16 Å^{-1} is due to the internal structure of the aggregates. The rather good agreement between model and experiment is a strong hint in favour of our understanding of the aggregate structure at all length scales accessible in SANS.

A <u>second</u> study deals with the fragmented structure of non ionic surfactant (like Triton X-100, or C_nE_m) adsorbed onto colloidal silica beads in water at high pH. It is well-known that build-up of complete bilayers is favored at low pH, due to the possible hydrogen-bonding of the oxy-ethylene headgroups with the surface silanols. At higher pH, the adsorption isotherms indicate reduced adsorption. Up to now, the incomplete layer has always been described in structural studies as a complete layer of lower density [4], although early dynamical results (fluorescence-decay) indicate micellar-type aggregates at the surface [5].

The result of a calculation of a complete layer structure (cf. lower inset) is compared to an experimental SANS-intensity in Fig. 3. In this experiment, the silica has been matched by the solvent [6]. The scattering from the adsorbed layer (dotted line) is predicted to be very high, and has to be reduced by a factor of 5 to fit the experimental data in the intermediate q-range. Then, the high-q scattering is far too low. The reason for its failure at high q is the presence of a lateral organization in the layer. We have studied a simple model (cf. upper inset) which reproduces the scattered intensity quite nicely (solid line) [6]. It is based on the geometrical description of adsorbed micelles, taking the hard-core repulsion between micelles into acount. Given the relatively high volume fraction of silica (some percent), the bead-bead interference term was also included (by RMSA) in this work. As a result, we are able to quantify the shape and degree of ordering of the aggregates adsorbed on the surface.
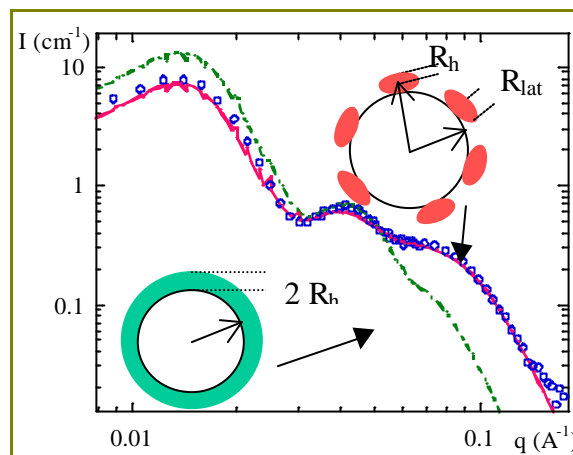
Figure 3. Intensity scattered by a matched silica bead with adsorbed surfactant. The continuous layer model (dotted line, thickness 40 Å) predicts a wrong Porod decay. The solid line is the prediction of our decorated bead model with excluded volume interactions between beads (R_h = 25 Å, R_{lat} = 30 Å, N_{mic}^{av} = 14).

The two examples discussed here show that under certain circumstances (for instance, low polydispersity) structures can be shown to be consistent with experimental data, or on the contrary, be ruled out, by relatively easy and straightforward modelling. If modelling is successful, additional information on sizes, aggregation numbers or polydispersities can be obtained.

References

[1] P. Hervé, M. Destrarac, J.F. Berret, J. Lal, J. Oberdisse, I. Grillo, *Europhys Lett,* **58** (2002) 912

[2] J.-F. Berret, C. Cristobal, P. Hervé, J. Oberdisse, I. Grillo, *Eur. Phys. J. E*, **9** (2002) 301

[3] J.-F. Berret, P. Hervé, O. Aguerre-Chariol, J. Oberdisse, *J Phys Chem*, in press

[4] Grillo, I.; Levitz, P.; Zemb, Th. *Eur Phys J B,* **10**, (1999) 29

[5] Levitz, P.; Van Damme, H.; Keravis, D. *J Phys Chem*, **88** (1984) 2228

[6] Despert G., Oberdisse J., submitted

MOLECULAR DYNAMICS SIMULATION AND NEUTRON SCATTERING FROM PROTEINS

G.R. Kneller[1], K. Hinsen[1] and M.C. Bellissent-Funel[2]

[1]Centre de Biophysique Moleculaire (CNRS UPR 4301),Rue Charles Sadron, F-45071 Orl¥eans Cedex 2, France
[2]Laboratoire Léon Brillouin (CEA-CNRS), CEA-Saclay, F-91191 Gif-sur-Yvette Cedex, France

1 Introduction

Since the early days of Rahman's historic simulation of liquid argon [1], Molecular Dynamics (MD) simulations have become a standard tool for the investigation of the structure and dynamics of condensed matter. The best experimental reference for MD simulation are neutron scattering experiments, since both methods cover the same time and space domains (approximately 0.1 fs – 10 ns, and 1 – 100 Å), and neutrons "see" the atomic nuclei, which are the basic objects in MD simulations.Once agreement between simulated and experimental spectra is found, the simulated trajectories can be analyzed in detail and information not accessible to experiments can be extracted from simulations. This approach is particularly useful for the study of complex molecular systems, such as biological macromolecules. Over the last ten years programs have been developed which allow to simulate and analyze the structure and dynamics of molecular systems an the basis of MD simulation [2, 3].

2 C-phycocyanine

The first example concerns hydrated C-phycocyanin, a light-conducting protein in cyanobacteria. MD simulation and an analytical model have been used to model diffusive motions in this protein. Since the simulation-derived scattering function was found to be in good agreement with experiment, a further analysis was undertaken to find the essential contributions. It is found that the geometry of the atomic motions can be modeled as diffusion in spheres with a distribution of radii that is different for backbone (average radius = 1.1 Å) and side chains (average radius = 2.0 Å). The time dependence follows a stretched exponential behavior, reflecting a distribution of relaxation times. With this description, the average side-chain and backbone dynamics are quantified and compared. The dynamical parameters are also shown to present a smooth variation with distance from the core of the protein. This is reflected in a progressive increase of the mean sphere size of diffusion and in the narrowing and shift to shorter times of the relaxation time distribution. This smooth, "depth-dependent" dynamics may have important consequences for protein function. It may allow local reorganization of the structure for efficient ligand binding without affecting the internal stability [4, 5].

3 Simulation-based modeling

An essential point that should be retained from the last example is that internal protein dynamics is characterized by multi-scale relaxation processes. A model process that is still simpler than diffusion in a sphere, and which describes confined motions as well, is diffusion in a multidimensional harmonic well. Multiscale relaxation is obtained by coupling harmonic oscillators with friction. Such models can give quantitative agreement with full MD simulations, if one considers a coarse-grained scale where each residue is represented by a point [6, 7]. The parameters of the model (force constants and friction coefficients) are obtained from conventional protein force fields and short simulations [7]. Another method to describe multiscale relaxation in proteins is to use the concept of memory functions [8]. Each correlation function, and in particular the intermediate scattering function,

$$I_{coh}(\mathbf{q},t) = \sum_{\alpha,\beta} \overline{b_\alpha b_\beta} \left\langle e^{i\mathbf{q}^T.\left[\mathbf{R}_\beta(t)-\mathbf{R}_\alpha(0)\right]} \right\rangle \qquad (1)$$

obeys an integral equation of the form

$$\partial_t I(\mathbf{q},t) = -\int_0^t d\tau \xi(\mathbf{q},t-\tau)I(\mathbf{q},\tau). \qquad (2)$$

Here $\xi(\mathbf{q},t)$ is the *memory function* which can be interpreted as a generalized friction coefficient. In case of confined motion the memory function equation (2) is applied to $I'(\mathbf{q},t) = I(\mathbf{q},t) - EISF(\mathbf{q})$, where $EISF(\mathbf{q}) = \lim_{t\to\infty} I(\mathbf{q},t)$ is the Elastic Incoherent Structure Factor. When the memory kernel is short-ranged compared to the correlation function $I(\mathbf{q},t)$, the latter becomes a simple exponential. Internal protein dynamics is known to span an enormous range of time scales, ranging from sub-picoseconds to seconds. There is no characteristic time scale for the decay $I'(\mathbf{q},t)$,
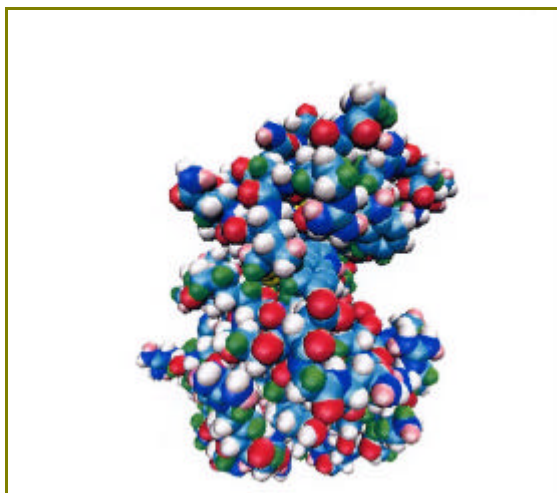
Figure 1. The lysozyme molecule. Each atom is represented by a sphere with the corresponding van derWaals radius.
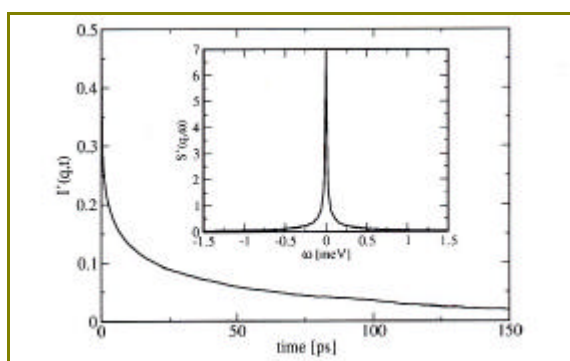
Figure 2. Simulated incoherent intermediate scattering function, $I'(\mathbf{q},t)$, of lysozyme, averaged over 30 momentum transfer vectors with $q = 15\ nm^{-1}$. The corresponding dynamic structure factor, $S'(\mathbf{q},\omega)$, is shown in the inset.

since all internal protein motions are coupled due to the high atomic density which can be higher than in solids. This leads to a non-exponential

decay of $I'(\mathbf{q},t)$, and the corresponding dynamic structure factor, $S'(\mathbf{q},\omega)$, is not a Lorentzian. Fig. 2 shows the simulated incoherent intermediate scattering function of lysozyme (see Fig. 1) at 300 K and normal pressure and the corresponding dynamic structure factor. All functions have been computed from a 1 ns trajectory, using autoregressive modelling of time series [3, 9]. The corresponding memory function is shown in Fig. 3. It can be seen that $\mathbf{x}(\mathbf{q},t)$ has an algebraic long-time tail of the form

$$\xi(\mathbf{q},t) \propto (\beta - 1)\left(\frac{t}{\tau}\right)^{\beta-2}, (3)$$

where $\tau > 0$ and $0 < \beta < 1$. This is a characteristic feature of "fractal dynamics" with long-time memory [10, 11]. We note that the short-time behavior of $\xi(\mathbf{q},t)$ is not well resolved since a coarse-grained autoregressive model with a sampling interval of $\Delta t = 0.4\ ps$ has been used.
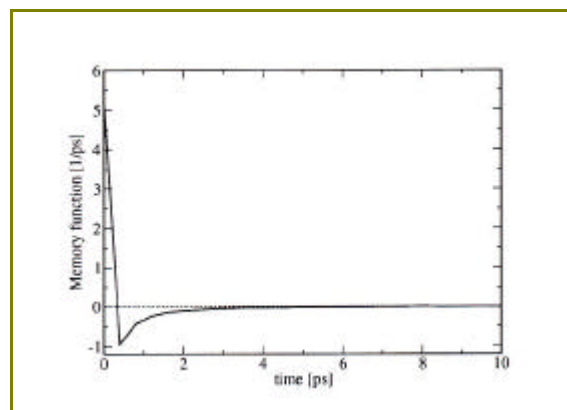
Figure 3. Memory function corresponding to $I'(\mathbf{q},t)$ depicted in Fig. 2.

References

[1] A. Rahman. *Phys. Rev.*, **136**(2A) (1964) 405-411.

[2] G.R. Kneller, V. Keiner, M. Kneller, and M. Schiller. *Comp. Phys. Comm.*, **91** (1995) 191-214.

[3] T. Rog, K. Murzyn, K. Hinsen, and G.R. Kneller. *J. of Comp. Chem.*, **24** (2003) 657-667.

[4] S. Dellerue. PhD thesis, Université Paris Sud, 21 January 2000.

[5] S. Dellerue, A.J. Petrescu, J.C. Smith, and M.-C. Bellissent-Funel. *Biophys. J.*, **81** (2001) 1666-1676.

[6] G.R. Kneller. *Chem. Phys.*, **261** (2000) 1-24, 2000.

[7] K. Hinsen, A.-J. Petrescu, S. Dellerue, M.C. Bellissent-Funel, and G.R. Kneller. *Chem.Phys.*, **261** (2000) 25-38.

[8] R. Zwanzig. *Statistical Mechanics of Irreversibility*, pages 106-141. Lectures in Theoretical Physics. Wiley-Interscience, New York, 1961.

[9] G.R. Kneller and K. Hinsen. *J. Chem. Phys.*, **115** (2001) 11097-11105.

[10] M.F. Shlesinger, G.M. Zaslavsky, and J. Klafter. *Nature*, **363** (1993) 31-37.

[11] W.G. Glockle and T.F. Nonnenmacher. *Biophys.J.*, **68** (1995) 46-53.

SimulReflec

A NEW TOOL FOR THE SIMULATION OF REFLECTIVITY MEASUREMENTS

F. Ott, T.-D. Doan, C. Fermon

Laboratoire Léon Brillouin(CEA-CNRS), CEA-Saclay, 91191 Gif-sur-Yvette cedex, France

In order to provide to the users a frienly interface for modelling polarised neutron reflectivity data we have developed this new fitting program.

This program allows to simulate reflectivity curves and to fit experimental x-rays and neutron data. The incident waves can be either neutrons or p-polarised x-rays. The multi-layer system has to be described by a series of discrete layers which model as accurately as possible the physical system. The layers in this model can be characterised by their thickness, their density, their scattering diffusion length, their magnetisation, the direction of their magnetisation, their RMS roughness, the in-plane correlation length and a critical exponent describing the fractal dimension of the roughness…

The program has advanced convolution possibilities and if necessary can use any arbitrary angular and wave-length distributions. The possibility of fitting Time Of Flight data is also offered.

The calculation is performed using an exact recursive matrix calculation. In the case of polarised neutrons, the program can handle any magnetisation configuration (in or out of plane) and any applied magnetic field (in direction or magnitude). The Zeeman energy splitting effects are taken into account in the calculation. They can lead to large effects in the case of the spin-flip signals.
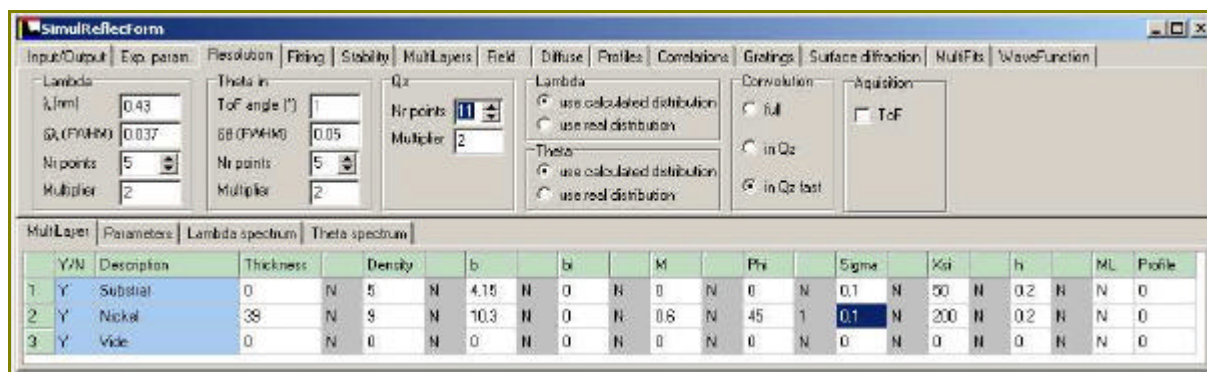
Figure 1. Main interface window for the modelling and simulation of reflectivity data

The figure 1 illustrates the main graphical window used to describe the system being studied. The system is described as a series of discrete layers. In the case of soft matter systems, it is possible to generate smooth profiles. The modelling user interface is coupled with a user friendly plotter (see figure 2).

Beyond simple specular reflectivity data fitting, the program offers some more advanced modules for experienced users. It is for example possible to plot the wave-function amplitudes and phase inside a multi-layer system as well as the reflection and transmission coefficients at each interface. The program also offers some possibilities in the field of off-specular reflectivity and surface diffraction simulations. A "grating" module is under development.
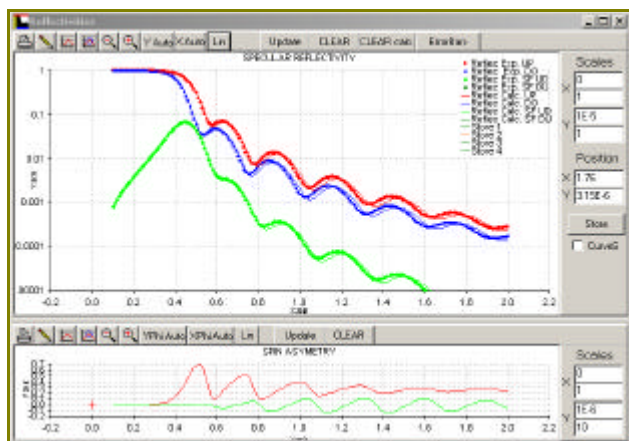
Figure 2. 1D graph window for displaying the experimental data and fits.

It is possible to simulate complex systems such as multi-layers and to include thickness and roughness fluctuations. The possibilty of fitting a two phases system is also available (which may mostly be encountered in the case of magnetic domains for example).
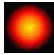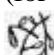
Additionnal modules include :
- An advanced 1D plotter for printing high quality graphics
- An analytical fitting modules (also usable for 2D fits)
- A parser allowing batch processing of data and arithmetic operations on spectra.
- Some utilities such as SLD conversion tools and interface to a SLD database.

The program is developed under the GPL license and can be downloaded at the following address :
www.llb.cea.fr/prism/programs/programs.html
The most recent sources are also provided on the Web. The development is made under Delphi ™. This program can be coupled with its twin brothers :

- **SpectraProcessor** (for data reduction)
- **SpectroDriver** (for data acquisition)
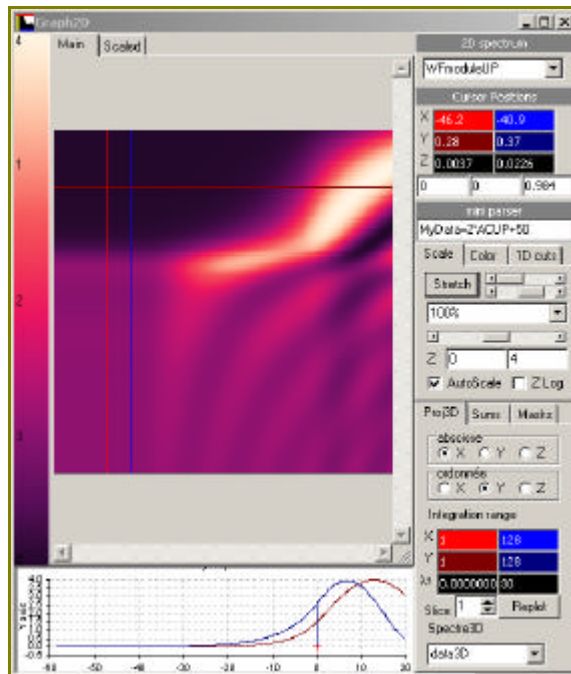
Figure 3. 2D graph window for displaying fits stabilities or wavefunctions amplitudes

CRYSTALLOGRAPHIC IMAGING USING MAXIMUM ENTROPY @ LLB

Robert J. Papoular

Laboratoire Léon Brillouin (CEA-CNRS), CEA-Saclay91191 Gif sur Yvette cedex, France

CRystallographic **I**maging using **M**aximum **E**ntropy (**CRIME**) is used to reconstruct 3D electron and scattering densities from **X-R**ay and **P**olarized / **U**npolarized **N**eutron diffraction data. It provides a very significant gain with respect to the widespread conventional Fourier Imaging. The state of the art of CRIME is illustrated hereafter via two examples pertaining to two typical neutron examples: a spin-density study and a proton density determination.

Either one is borne from experimental data obtained at our flagship hot source single-crystal diffractometers **5C1** [using **P**olarized **N**eutrons, see Fig.1] and **5C2** [using **U**npolarized **N**eutrons and discussed below in some more detail].

A most legitimate worry relates to whether the inappropriate use of Maximum Entropy would still lead to reconstructing spurious features to be mistaken for real Physics/ Chemistry phenomena. This is why the crucial part of *a priori* modelling to produce adverse non-uniform prior densities is emphasized. New features showing up in **CRIME** reconstructions are only deemed reliable if they survive the negative bias induced by the use of plausible advert non-uniform priors, and are considered untrustworthy otherwise.

There are quite a few reasons to go beyond the standard crystallographic procedure, besides reducing the well-known Fourier series truncation errors : **i**) experimental error bars should be taken into account and **ii**) all the available information should be used, such as Fourier components that are either unphasable, overlapped in the case of powder data, or incompatible with a given direction when a 2D projection of the object is sought.

For our most recent results, see:
R.J. Papoular (2002), SCI2002 Proceedings [Orlando,USA], Vol. XVII, pp.313-320.
A. Gukassov et al (2002), Phys . Rev. Lett. **89** 087202
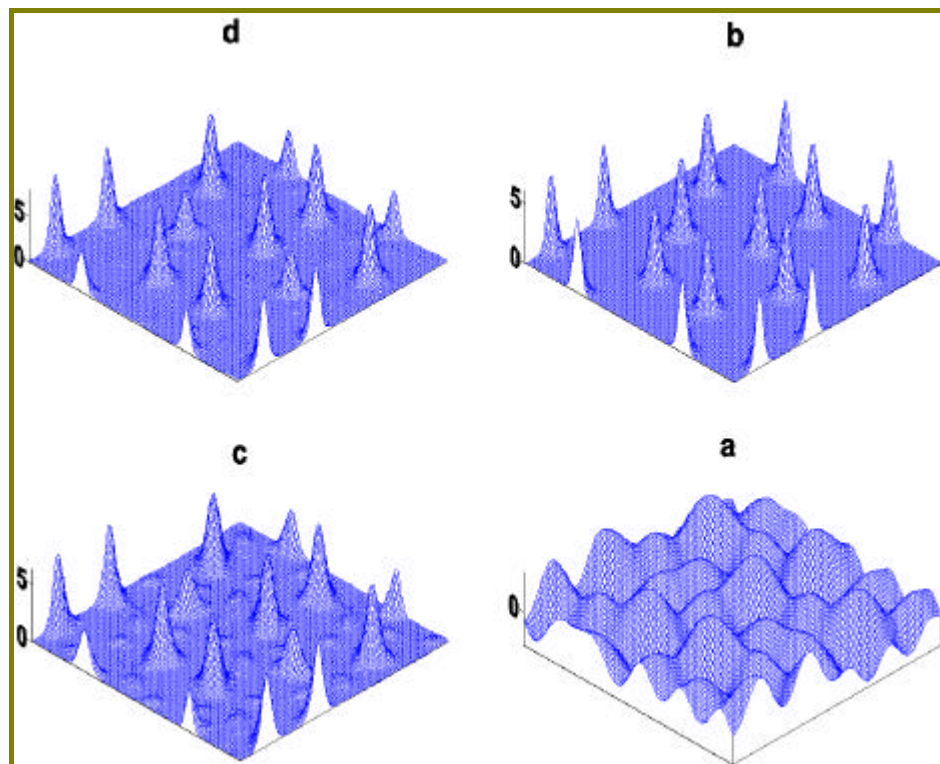
Figure 1. CRIME step by step. **a) Why** : the Standard Fourier map is unusable **b) How** : Use a non-uniform prior density biased against the expected effects [different peaks, new ones**] c) What if :** Using a uniform density prior is not good enough : new effects are now hinted at but may not be reliable **d) What** : using the non-uniform prejudice b) sets it right : there are only two different kinds of peaks. The weakest ones as found in c) are not warranted by the data.

Aspirin and Unpolarized Neutron Diffraction

As expertedly reviewed in a recent book by C.C. Wilson, entitled "*Single Crystal Neutron Diffraction from Molecular Materials*" (World Scientific, 2002), the neutron asserts itself as a unique structural probe to **i)** locate protons accurately, **ii)** quantify their thermal parameters, **iii)** investigate proton disorder. It is thus an exceptional tool to study polymorphism and hydrogen-bond networks in molecular compounds in general, and in pharmaceuticals in particular.

Perhaps surprisingly, using CRIME affects the experimental measurement process. Whereas measuring weak intensities is generally considered a waste of time and neutrons since the related Fourier components do not contribute appreciably to the conventional Fourier maps, it becomes crucial to measure them as well possible if ghosts atoms or ripples are to be avoided in an improved model-free imaging. Complete data sets (down to a certain resolution) become essential. *A first bonus* of using CRIME is the possibly to use a variety of density priors and check the stability of the reconstructed proton density against the latter. As demonstrated below in the case of aspirin, we advocate the systematic use of at least two prior densities : the bi-uniform and the non-uniform backbone one. *A second bonus* is to be able to use Fourier components than cannot be phased reliably using an appropriate model (built from the non-H atoms, and usually derived from a previous X-ray single crystal experiment). *A third bonus* is the further ability of CRIME to tackle the simultaneous reconstruction of the proton density [which is usually negative unless the sample is deuterated] and of the backbone usually positive density.

The use of this two-channel (one positive, one negative) entropy is a logical extension of our previous applications of CRIME to magnetization [Papoular & Gillon, EPL, 1990] and accurate charge densities [Papoular et al, Acta Cryst. A., 1996]

In our recent work initially aimed at studying the methyl group [Schiebel et al , PRL 1999] a single-crystal of aspirin was measured on 5C2 at the Orphée reactor at 15 K. One complete datasets comprising 1050 unique reflections was collected. Model-free imaging of the linking protons between the two molecules of the aspirin dimer [see Fig.2] resolves a controversy : do the protons jump between two possible positions, sit right in the middle of the O-H...O bonds, or preferentially belong to one of the molecules?
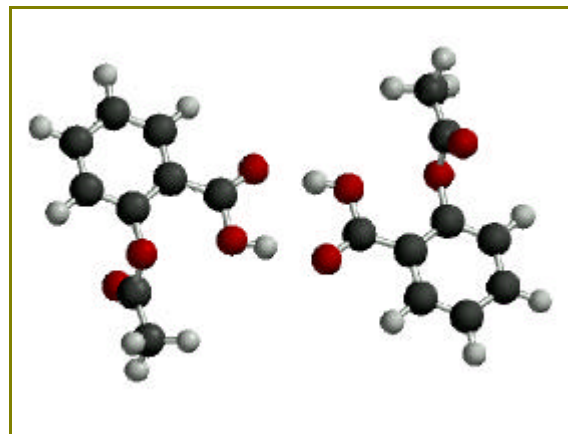
Figure 2. Schematic view of an aspirin dimer

The unambiguous result is shown in figure 3.
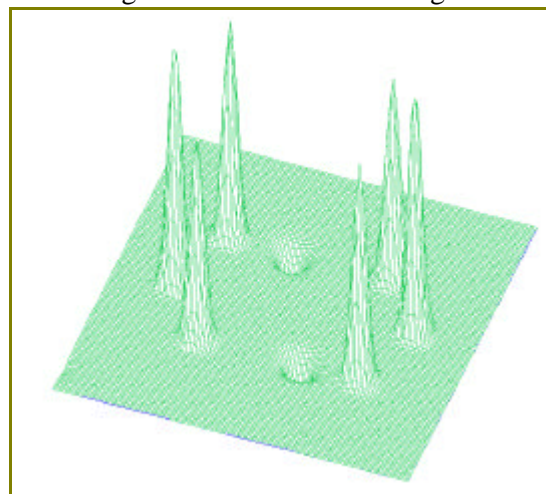
Figure 3. Model-free reconstruction of the protons involved in the carboxylic acid dimer part of aspirin at T= 15 K. The protons appear as holes because their neutron scattering length is negative

SIMBO and ENERMAG:
TWO COMPUTING PROGRAMS FOR ANALYSING THE TOPOLOGY OF EXCHANGE INTERACTIONS AND THE CLASSICAL MAGNETIC ENERGY

J. Rodríguez-Carvajal

Laboratoire Léon Brillouin (CEA-CNRS), CEA-Saclay, 91191 Gif sur Yvette cedex, France

We have developed two computing programs, SIMBO and ENERMAG, which provide an invaluable help to interpret experimental magnetic structures occurring in real systems. The study of the crystal structure, and the related topology of the magnetic exchange interactions of old or new materials, by using these programs facilitates the detection of new frustrating topologies of interest in magnetism. They allow the possibility of *a priori* predictions about the magnetic ordering in new materials when approximate values of the exchange interactions are available.

The program SIMBO analyses the crystal structure of an insulator in terms of super-exchange M_1-X-M_2 and super-super-exchange M_1-X_1-X_2-M_2 paths. In case of intermetallic compounds, or if the user asks for, direct exchange paths are also considered. SIMBO needs as input the list of atom co-ordinates in the asymmetric unit, as well as their ionic charge and the saturation magnetic moment, the space group symbol and the cell parameters. The program uses this information to calculate distance, angles and exchange paths. The user may introduce some constraints concerning the geometry of the required exchange paths in order to limit and eliminate loops of involved shapes.

SIMBO produces, as output, a list of exchange paths and attributes symbols for the different exchange interactions that are also classified as a function of the inter-atomic distances. SIMBO provides also a formal description of the Fourier transform of the isotropic exchange interactions in form of an $n \times n$ matrix, where n is the number of magnetic ions in a primitive unit cell (see below). This information is summarised in a file that serves as input for the program ENERMAG.

The program ENERMAG tries to solve the problem of the first ordered state for a particular magnetic topology and a set of exchange interactions. The first ordered state is obtained in the mean-field approximation, as a function of $\mathbf{k}$, on the surface or at the interior of the Brillouin Zone (BZ), and the exchange integrals, as the eigenvector corresponding to the highest eigenvalue of the Fourier transform of exchange integral matrix [1-4]:

$$\xi_{ij}(\mathbf{k}) = \sum_m J_{ij}(\mathbf{R}_m).\exp\{-2\pi i \, \mathbf{k} \, \mathbf{R}_m\}$$

The indices i,j refer to the magnetic atoms in a primitive cell, $J_{ij}(\mathbf{R}_m)$ is the isotropic exchange interaction between the spins of atoms i and j in unit cells separated by the lattice vector $\mathbf{R}_m$ and $J_{ij}(\mathbf{R}_m)$ includes the spin modules. Our convention for magnetic energy is to take negative J's for anti-ferromagnetic coupling.

The program ENERMAG handles the diagonalisation of the above matrix that is provided by the output file coming from SIMBO. It solves the parametric equation:

$$\mathbf{x}(\mathbf{k}, \mathbf{J}) \, \mathbf{v}(\mathbf{k}, \mathbf{J}) = \lambda(\mathbf{k}, \mathbf{J}) \, \mathbf{v}(\mathbf{k}, \mathbf{J})$$

where $\mathbf{J}$ stands for the given set of exchange interactions $\mathbf{J}=\{J_{ij}(\mathbf{R}_m)\}$, and $\mathbf{k}$ is a vector in the asymmetric unit of the BZ. For a given set $\mathbf{J}$, and no degeneracy, the highest eigenvalue $\lambda_{max}(\mathbf{k}_0, \mathbf{J})$ occurs for a particular $\mathbf{k}_0$, for which the ordering temperature is maximal: $3k_B T_{max}=\lambda_{max}(\mathbf{k}_0,\mathbf{J})$. The corresponding eigenvector $\mathbf{v}_{max}(\mathbf{k}_0,\mathbf{J})$, that may be complex for incommensurate structures, describes the spin configuration of the first ordered state.

The user can give the value of the exchange interaction and study the magnetic energy as a function of $\mathbf{k}$ in the BZ using lines, planes or the whole BZ including special points. Another way of working with ENERMAG is the generation of "magnetic phase diagrams" as a function of the exchange parameters. The program explore, for each point in the J-space, the asymmetric unit of the BZ and detects the value of $\mathbf{k}=\mathbf{k}_0$ for which the ordering temperature is maximal and equal to $\lambda_{max}(\mathbf{k}_0,\mathbf{J})/3k_B$. The eigenvector $\mathbf{v}_{max}(\mathbf{k}_0,\mathbf{J})$ gives the Fourier coefficients of the magnetic structure as a function of the exchange parameters $\mathbf{J}$.

Examples of the use of both programs may be found in references [5-9]. In Figure 1 it is shown the case of the $MFePO_5$ family [5], for which we have studied in detail the topology of the exchange interactions. In figure 2 a part of the phase diagram is shown. The observed magnetic structure is in the area labelled G_M+G_{Fe} (+ - + - ; + - +-).
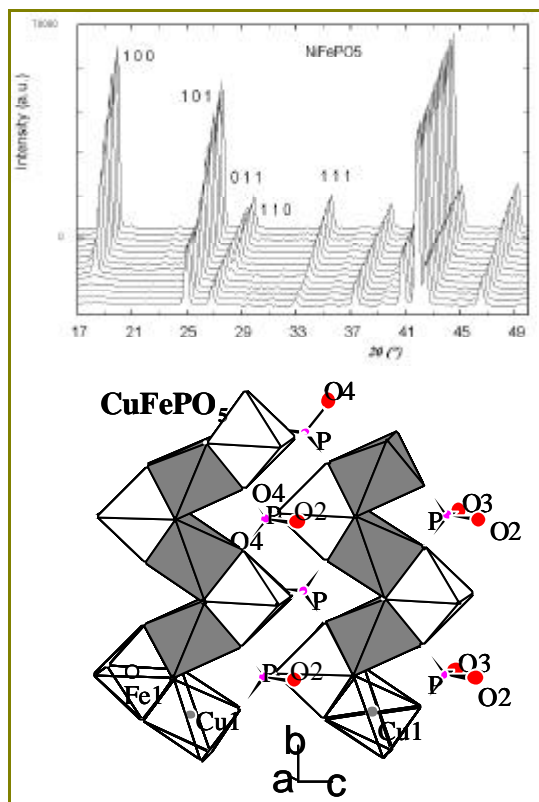
Figure 1. Neutron powder diffraction as a function of temperature for one of the members of the family $MFePO_5$ (M=Fe, Co, Ni, Cu) and schematic view of the crystal structure of the compound M=Cu [5].
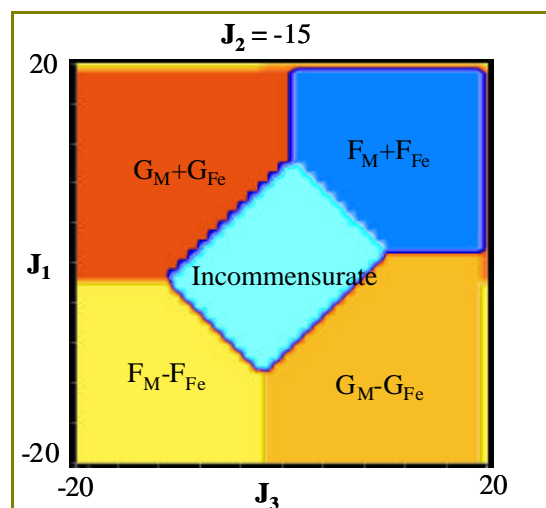
Figure 2. Part of the magnetic phase diagram generated by ENERMAG for the family of compounds $MFePO_5$

At present the most important limitation of the program ENERMAG is that only isotropic exchange interactions are allowed. For the forthcoming development we have devised the implementation of a general tensor for describing the exchange (pseudo-dipolar and Dzyalozinskii-Moriya interactions). This will extend the capabilities of the program to handle explicit spatial components (general $3n \times 3n$ exchange matrix) of the eigenvectors representing the Fourier coefficients of the magnetic structure.

References

[1]   J. Villain, *J. Phys. Chem. Solids* **11** (1959) 303.
[2]   A. Yoshimori, *J. Phys. Soc. Japan* **14** (1959) 807.
[3]   D. H. Lyons and T. A. Kaplan, *Phys. Rev.* **120** (1960) 1580.
[4]   M.J. Freiser, *Phys. Rev.* **123** (1961) 2003.
[5]   N. El Khayati, R. Cherkaoui El Moursli, J. Rodríguez-Carvajal, G. André, N. Blanchard, F. Bourée, G. Collin, and T. Roisnel. *Eur. Phys. J. B* **22** (2001) 429.
[6]   E. García-Matres, J.L. Martínez, and J. Rodríguez-Carvajal. *Eur. Phys. J. B* **24** (2001) 59.
[7]   G. Rousse, J. Rodríguez-Carvajal, C. Wurm, and C. Masquelier.
       Chem. Mat. **13** (2001) 4527.
[8]   Gwenaelle Rousse, Juan Rodríguez-Carvajal, Calin Wurm and Christian Masquelier.
       Solid State Sciences **4** (2002) 973.
[9]   N. El Khayati, J. Rodríguez-Carvajal, F. Bourée, T. Roisnel, R. Cherkaoui, A. Boutfessi, A. Boukhari.
       Solid State Sciences **4** (2002) 1273.
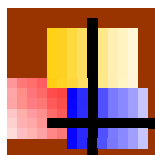
8 - TECHNICAL AND INSTRUMENTAL DEVELOPMENTS

One of the important goals of the LLB activities is the research and development of neutron scattering methods. This topic concerns very different aspects of neutron scattering technique, the increase of the luminosity of neutron spectrometers, realisation of large area position sensitive detectors and development of new approaches in the data acquisition and in the data treatment.

It also includes the development of new sample environment devices, which allow to perform neutron measurements in extreme conditions, for example at low temperatures (down to 80 mK) in high magnetic fields (8 T), and high pressures (4 GPa) applied simultaneously.

A special attention during the last year was paid to elaborate a new instrumentation program, called CAP2010, which summarizes the "roadmap" of future technical and instrumental developments at the LLB for the following 8 years.

Development of spectrometers

Polarised neutron option on the upgraded thermal three-axis spectrometer 2T :

After the enlargement of the beam tube size 2T in 1999, a polarized inelastic neutron option has been installed on the thermal beam triple axis spectrometer 2T. The setup is a standard triple-axis spectrometer with Heusler monochromator and analyzer, similar to that of IN20 and IN22 at ILL, with an incident energy up to about 100 meV. Heusler single crystals have been grown at the ILL. The horizontal and vertical sizes of the monochromator and analyzer, respectively 140x130 mm^2 and 120x100 mm^2, have been chosen to fully make use of the available beam size. Permanent NdFeB magnets, delivering a 1.2 T field, are used to saturate the Heusler magnetization. The magnetic field is applied horizontally on the monochromator, which has a vertical focusing, and vertically on the analyser, which has a horizontal focusing. This combination of curvatures has been chosen as the most effective and hence, the beam geometry for polarized neutron is basically similar to that of the unpolarized beam. The flipping ratios of ~12 so far obtained are encouraging and will be improved in the near future. A preliminary polarized experiment has been performed on high-T_c superconductors: an intensity ratio between the unpolarized and the polarized setups is about ~20. Some improvement is expected from a realignment of the Heusler analyzer, which was found to be non optimal. In any case, with the enlargement of the beam size on the 2T spectrometer the intensity counted in the detector is now comparable to that of the polarized triple axis spectrometers IN20 and IN22 at the ILL.

Bidimensional neutron detectors for the 7C2 spectrometer on the hot source:

The LLB is currently developing micro-strip gas counters (MSGC) based on the charge division principle. These detectors, developed in the frame of the European TECHNI (n° HPRI-CT-1999-50005) contract, are suitable for small area 200×100mm^2 and good spatial resolution (~ 2mm). They rule out the possible mechanical problems related to wire grid detectors by replacing the wires with anode and cathode metal stripes deposited on a glass substrate.

A MSGC consist of a gap chamber filled with high-pressure ^{3}He gas (up to 10 bars) to capture the neutrons and create an electrical charge. The charge amplification is performed by a high electrical field (~1000 V/m) between anodes and cathodes (the amplification gain of about 10^4). This electrical charge is split in two by a resistive line. The position of the neutron is determined by measuring the charge ratio between the two ends of the resistive line. The charge division design has been chosen because of the very low cost of the associated electronics (the number of charge amplifiers is limited to 3.) The gamma discrimination is performed by measuring the total electrical charge collected on the cathodes. At the moment, the largest size available is 200x100mm^2 (see Fig.1). It is limited by the fabrication and the capacitance of the micro-strip glass plate itself. A bidimensional position-sensitive detection can be achieved by using two perpendicular sets of stripes (on the front and on the back of the glass substrates).

Ultra High Vacuum techniques have been used for the design of the detectors casings in order to maintain the purity of the detection gas. This is essential to prevent any deterioration of the metallic anodes stripes and to avoid parasitic signals.
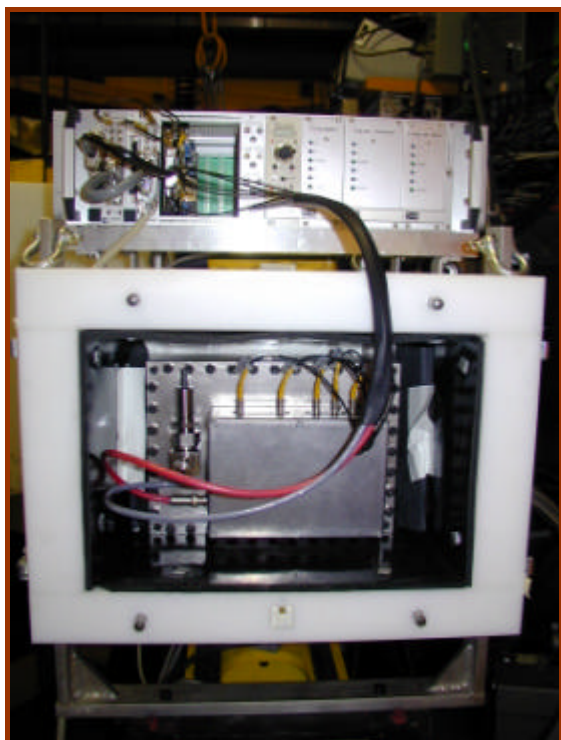
Figure 1. View of 200x100 mm² MSGC detector mounted on 7C2 diffractometer

The electronics is composed of a compact electronic chain including the charge amplification and the charge division calculation, a conversion board with two 12 bits ADC converters, an interface board to communicate with the standard LLB EuroPSD and EuroScaler counting boards.

The speed of the electronics counting rate is limited to 5MHz, but the actual limitation is given by the detector itself (due to the resistance of the charge division line.)

These MSGC can achieve a 1.5-2 mm spatial resolution (see Figure 2). The background noise is 30 counts/min on a 100x200mm² detector.
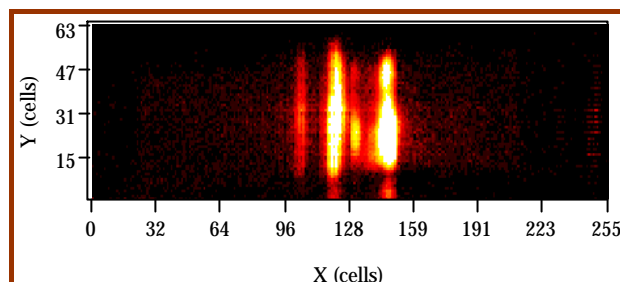
Figure 2. Picture of the reflectivity measured on a grating (right, direct beam; left reflected beams).

The diffractometer 7C2, dedicated to the study of liquids and amorphous systems, is being renewed. The present « banana-type » detector of 7C2 consists of 640 cells covering a scattering angle of 128° and a BF_3 detection gas under atmospheric pressure. It is very stable but has a quite low efficiency (17% at 0.07nm, which is the most commonly used wavelength). This detector will be replaced by a set of 14 2D-micro-strip detectors described above, filled with 15bars of ^{3}He (see figure3).
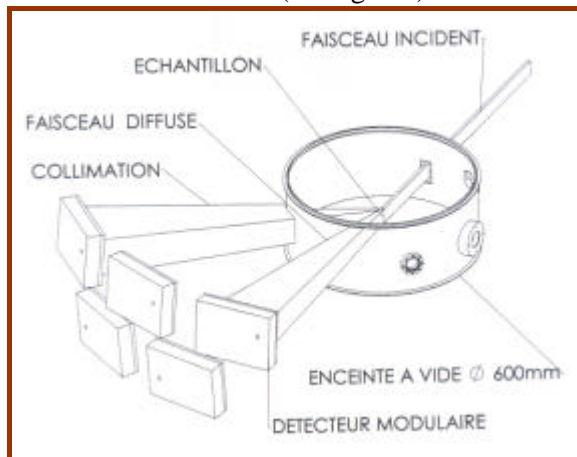
Figure 3. Layout of the 7C2 diffractometer equipped with MSGC detectors.

This high pressure gives a good detection efficiency (~92%) at short wavelengths (0.07nm). Due to the better resolution of such a detector, it can be placed closer to the sample (1m instead of 1.5m), which will result in a larger solid angle for detection. Each detector will have its own collimation system. The detectors will be arranged in such a way that the same angular acceptance as the actual one will be covered. In 2002 one of the micro-strip detector was regularly tested on 7C2, and the collimator for each detection module has been designed and tested. Monte Carlo simulations of the present and the new instruments (using the VITESS program, HMI-Berlin) show that the resolution will be close to the present one.

New spectrometer for nano-objects "TPA":

The very small angle spectrometer **TPA** ('Très Petits Angles') is currently developed on the guide G5bis. Its aim is to cover a q-range from 10^{-4} Å^{-1} up to intermediate angles. It will allow neutron studies of larger objects ($\approx$ 1000 Å), like giant micelles, membranes, biophysical gels, large-scale porosity and precipitation in alloys for metallurgical applications.

The principles of the spectrometer are very close to traditional small-angle machines. In the first design, the collimation is a pinhole-collimation with smaller diaphragms, but more complex collimation devices (lenses, focalization, etc..) are also tested. The detection is 2D. A relatively high pixel definition is necessary for very small-angle scattering, because the maximum length of the spectrometer is limited due to guide hall constraints. The only commercially available detectors with a pixel size smaller than 1 mm are 'image plate' detectors. We have installed a MAR345, with a Fuji plate for neutron-photon conversion and a spatial resolution of 150 microns has been easily achieved. Its major drawback is the high γ-ray sensitivity. The complete instrument is therefore designed in order to minimize background: Monochromatisation is achieved by monochromating $3\theta_c$-mirrors (XENOCS, Grenoble) with 15%-bandwidth. This allows deviating the direct beam and eliminating the γ-ray background from the guide by an appropriate shielding. Moreover, the mirrors replace a mechanical velocity selector, also responsible for a high γ-ray background in the direct beam. The collimators are made of ^{6}Li diaphragms and heavy lead shielding behind the diaphragms, along the neighbouring guide G5 and around the detector is further decreasing the background. Preliminary test runs on the prototype show the feasibility of this spectrometer, and first parts of the final construction plans will be finished these months.

Development of new sample environment

Advanced sample environments have been developed, in particular for **high-pressure neutron diffraction.** In *soft matter and biology*, even modest pressures (<1 GPa) can induce considerable changes in interatomic distances and physical properties. Numerous studies of polymers or proteins (0.3 – 0.4 GPa) have been performed using specialised high-pressure cells (see chapter 4, 5 and 6).

In *solid-state physics*, much higher pressures are generally required to induce significant changes in electronic or structural properties (through *structural* or *valence transitions*, for example).

During the last years, original high-pressure and neutron techniques have been developed at the LLB in order to study magnetic and structural phenomena under very high pressures (>10 GPa) by neutron diffraction. The LLB holds a world record in high-pressure neutron studies: **50 GPa (500 kbar)**. The record measurements were performed on a specialized **high-pressure powder diffractometer "MICRO"** (G6.1) equipped with neutron focusing systems and high pressure cells with sapphire or diamond anvils. On this instrument, very high pressures can be combined with low temperatures (down to 1.4 K). The wide P-T range allowed discovering new physical phenomena, especially in studies of magnetic ordering and phase transitions under pressure. With a new multidetector for "MICRO" currently under tests and a project for replacing of the present G6 guide by a supermirror guide, LLB considers high-pressure studies as a high priority. Recently, ultra-compact pressure cells have been successfully used in combination with a superconducting magnet and a dilution refrigerator. At the single crystal diffractometer 6T2, pressures up to **7 GPa** can be combined with magnetic fields up to **7.5 T** and very low temperatures down to **100 mK** (see Fig.4 on the right).

Figure 4. High-pressure cells with sapphire anvils mounted on a ^{3}He – ^{4}He dilution refrigerator
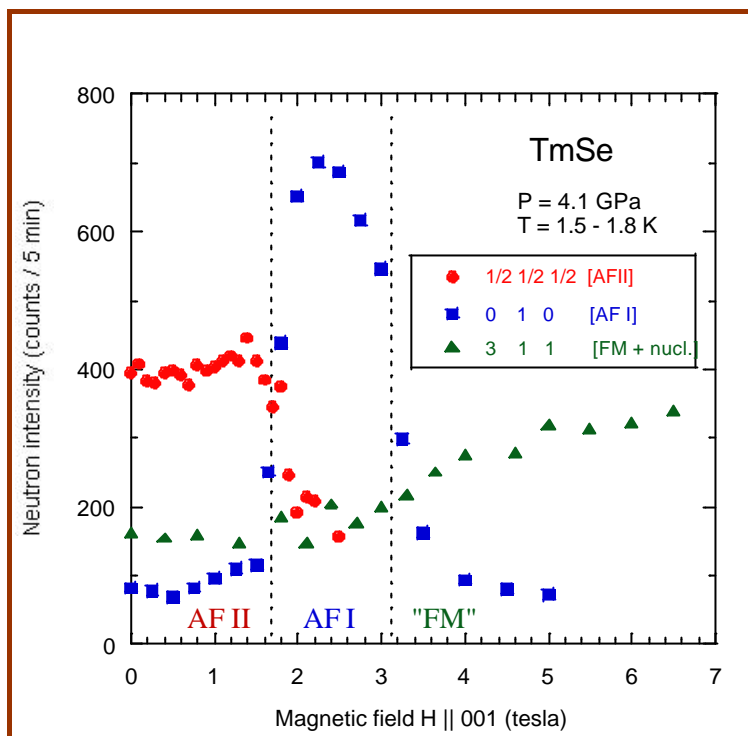
Figure 5

Several examples of neutron diffraction studies curried out under "multi-extreme" conditions can be mentioned, in particular experiments on $CeRhIn_5$ (0.15 K and 0.7 GPa) or a study of the H-P-T magnetic phase diagram of TmSe, shown in Fig.5 above.

Complemented by "medium-pressure" devices (He pressure cell, McWhan-type piston-cylinder cell), the sample environment techniques available at the LLB provide an unprecedented range of thermodynamical parameters for neutron studies.

TECHNICAL AND INSTRUMENTAL DEVELOPMENTS

FRESNEL ZONE PLATES FOR IMAGING AND FOCUSING NEUTRONS

F. Sacchetti[1], M. Altissimo[3], C. Petrillo[3], E. Di Fabrizio[1], S. Colleoni[2], F. Ott[4]

[1]INFM & Dipartimento di Fisica, Università di Perugia,Via A. Pascoli, I-06123 Perugia, Italy
[2]TASC-INFM, Elettra Synchrotron Light Source,Area Science Park, I-34012 Basovizza, Trieste, Italy
[3]INFM & Dipartimento di Fisica, Politecnico di Milano, Piazza Leonardo da Vinci 32, I-20133 Milano, Italy
[4]Laboratoire Léon Brillouin (CEA/CNRS), CEA Saclay, F-91191 Gif sur Yvette, France

The high penetration power of neutrons makes them ideal for non-destructive studies of materials and enables *in situ* measurements of the environment-dependent properties. The requirement of non destructive characterisation tools, coupled to the ability of manipulating the neutron beam in the sub-millimetre scale by novel neutron optics, would make neutron diffraction and imaging a powerful technique in the rapidly evolving fields of biophysics and nano-science research. Here we report on the results obtained in focusing a cold neutron beam by means of two newly developed optical devices, which exploit the Fresnel zone plate (ZP) concept, and have been designed to intercept a large portion of the beam and to minimise flux losses.

Recently innovative applications of neutron radiography and imaging have been presented [1-2], which stimulate the development of novel optical devices for neutron beam focusing [3-6]. Long ago [7], it was demonstrated that a phase reversal ZP can be successfully employed to focus and image a cold neutron beam ($\lambda \approx 20$ Å). It is only in recent times that progress achieved in nano-fabrication has made possible the production of high-efficiency and high-resolution ZPs for focusing of short wavelength x-rays [8] (see figure 1).
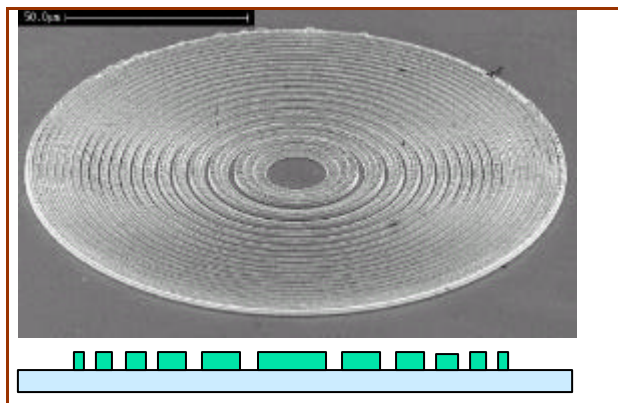
Figure 1 : (top) MEB image of a Fresnel zone plate (bottom) side view of the lens, in blue the Si substrate and in green the Ni rings.

Exploitation of the modern nano-lithographic techniques will give a new impetus to the field of neutron optics while opening challenging possibilities for neutron microscopy.

We have developed two devices characterised by a relatively large aperture and size of the lens, and rather short focal length. The first is a large aperture phase reversal ZP, with 5 mm diameter and 13.5 m focal length at 1.54 Å thermal neutron wavelength. The second is a square matrix, 1 cm^2 surface, consisting of 900 zone plates, 0.3 mm diameter each and 1 m focal length at 3 Å. The matrix is capable of focusing the neutron beam from a point source into 900 small spots. The thickness of the phase shifter (natural Ni) was larger than 3.5 μm, resulting in aspect ratios of ~11 and ~5 for the two devices respectively.

A series of neutron tests was carried out on the monochromatic neutron beam of the TPA diffractometer. The performances of the ZP were measured at $\lambda = 6.85$ Å, which corresponds to focal length of 3 m and a theoretical efficiency of ~ 40%. A 1 mm hole was inserted at 3 m upstream the ZP, so that a parallel beam 5 mm diameter was expected at the image plate detector (0.15 mm resolution), 4 m downstream the lens (Fig. 2).
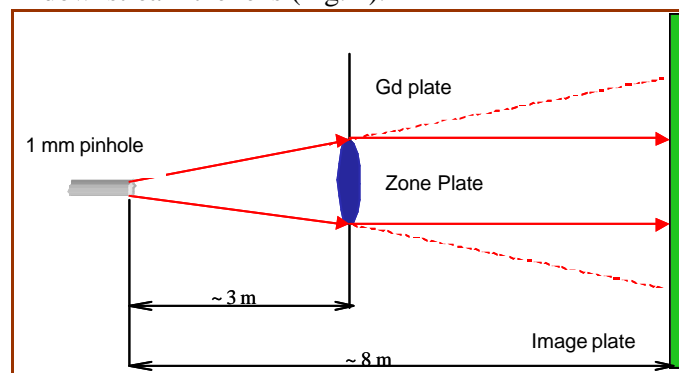
Figure 2 : experimental configuration

The difference between the intensities collected with and without insertion of the ZP is shown in figure 3. The focusing effect is clearly visible and a measured efficiency in excess of 20% was obtained.
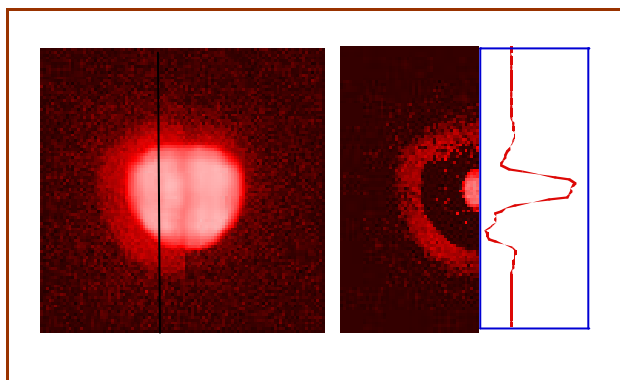
Figure 3. (left) images without and with the lens (right) measurement of Intensity map obtained by taking the difference between the measurement with ZP and without it.

The zone plate matrix (Fig. 4) was tested at $\lambda = 13.7$ Å, with a 0.8 mm pinhole placed at the image position, 23.6 cm from the lens, where 900 spots, 70 µm in diameter each, are formed. In the experimental configuration, a sharp spot is expected without the matrix, whereas a broad image is formed at the detector position when the matrix is in place. This is apparent from figure 5, where the intensity difference is shown.

The present test clearly demonstrates the excellent operation of these new devices which enable an easy focusing of neutron beams at sub-millimetre scale, with potentially useful applications in high-resolution neutron imaging.
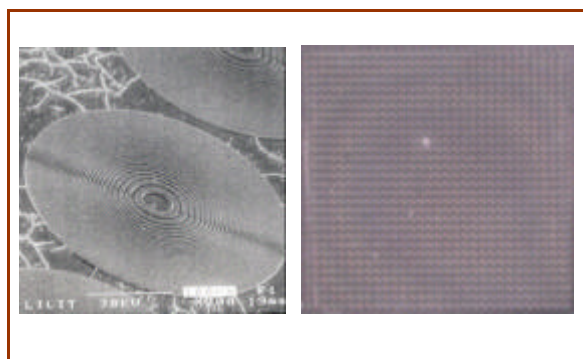
Figure 4. (left) matrix of zone plates (30x30) (right) an individual zone plate. scanning electron microscope image of a portion of the ZP matrix.

Without the lens   *With the lens*   *Difference*
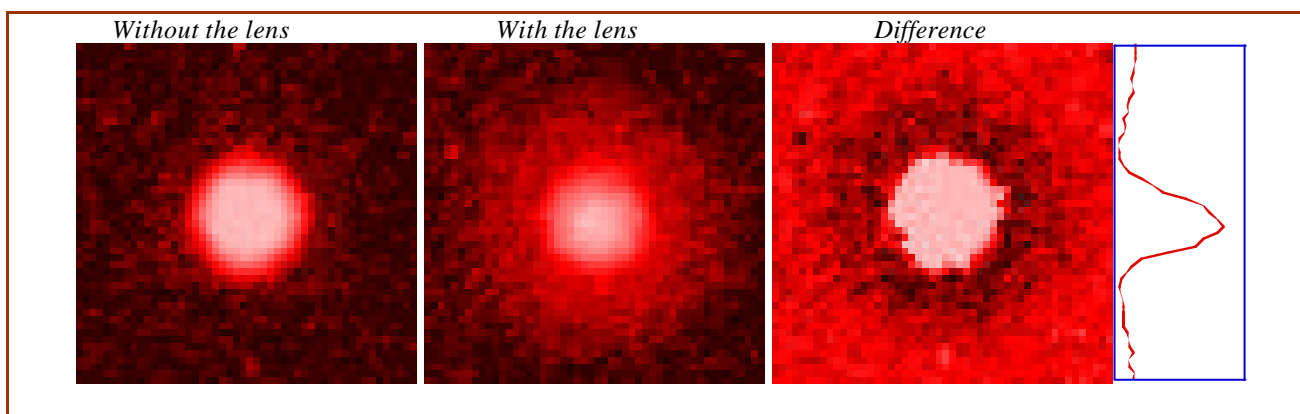
Figure 5: Intensity map obtained by taking the difference between the measurement with the matrix and without it.

References

[1] Aliman, B. E., McMahon, P. J., Nugent, K. A., Paganin, D., Jacobson, D. L., Arif, M., Werner, S. A. Phase Radiography with neutrons. *Nature* **408**, 158-159 (2000).

[2] Masschaele, B., Baechler, S., Cauwels, P., Dierick, M., Jolie, J., Mondelaers, W. First results of micro-neutron tomography by use of a focussing neutron lens. *Rad. Phys. and Chem.* **61**, 623-624 (2001).

[3] Eskildsen, M. R., Gammel, P. L., Isaacs, E. D., Detlefs, C., Mortensen, K., Bishop, D. J. Compound refractive optics for the imaging and focusing of low-energy neutrons. *Nature* **391**, 563-566 (1998).

[4] Kumakhov, M. A. & Sharov, V. A. A neutron lens. *Nature* **357**, 390-391 (1992).

[5] Chen, H., Downing, R. G., Mildner, D. F. R., Gibson, W. M., Kumakhov, M. A., Ponomarev, I. Yu., Gubarev, M. V. Guiding and focusing neutron beams using capillary optics. *Nature* **357**, 391-393 (1992).

[6] Allman, B.E., Cimmino, A., Griffin, S. L., Klein, A. G., Nugent, K. A., Anderson, I. S. & Høghøj, P. Novel optics for conditioning neutron beams. II Focussing neutrons with a "Lobster-Eye" optic. *Neutron News* **10**, 20-23 (1999).

[7] Kearney, P. D., Klein, A. G., Opat, G. I. & Gähler, R. Imaging and focusing of neutrons by a zone plate. *Nature* **287**, 313-314 (1980).

[8] Di Fabrizio, E., Romanato, F., Gentili, M., Cabrini, S., Kaulich, B., Susini, J., Barrett, R. High-efficiency multilevel zone plates for keV X-rays. *Nature* **401**, 895-898 (1999).

Recent progresses in the neutron spectrometry as well as the evolution of scientific topics prevail on the LLB to propose major improvements of several spectrometers both in the guide hall and reactor hall. Beside of this project named CAP2010, the upgrades in progress in the laboratory will continue: MUSES, 7C2 , TPA… (see the introduction of this chapter).

Increasing research in new materials for technical applications has brought new needs of structure determination. In condensed matter physics and chemistry, the role of high resolution powder neutron diffraction becomes more and more important. One priority of LLB is to rebuilt the detection system of the **3T2 diffractometer** in order to achieve both better resolution and higher counting rates. The last upgrade of this spectometer was done in 1997, a new focusing Ge (335) monochromator, which gave an increase of the neutron flux by a factor 4.5. The present project concerns the change of the collimators in front of the detectors to increase the resolution by a factor 2, and the installation of 50 (instead of 20) ^{3}He detectors to cover an angular range of 120° (instead of 57°). Figure 1 shows the schema of the new high resolution powder diffractometer 3T2.
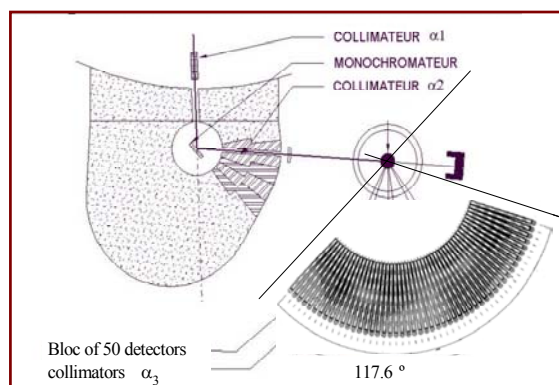
Figure 1. Schema of the project for the high resolution powder diffractometer 3T2.

We also plan to complete the renewal of the **high pressure diffractometer MICRO** on the G6.1 guide, which was recently partly rebuilt to realized original experiments under pressure as high as 100GPa (1Mbar). Pressures up to 51 GPa (510 kbar) are already reached. The replacement of its detector (an old 400 cells banana filled with BF_3

gaz with an angular range of 80°) by a curved linear detector filled with ^{3}He gaz covering a larger solid angle has been decided several years ago. Development of this new detector is still in progress. Increase the pressure up to 1Mbar will require a sample volume reduction. To compensate the intensity loss inherent to this reduction, we will increase the incident beam divergence, i.e. the flux, by changing the nickel coating of the main guide G6 with new $2\theta_c$ super-mirrors, till the monochromator of G6.1. We can then use a better focusing graphite monochromator, especially adapted to the divergence of the new $2\theta_c$ super-mirrors guide.

The **4-circles spectrometer 6T2** (on thermal neutron beam) is actually used at LLB for two kinds of experiments: in its "lifting detector" mode, it is devoted to studies of magnetic structures whereas in its 4-circles configuration, it allows to study the structure of compounds of large unit cell. We would like to shift the 4-circles experiments on the **3T1** channel equipped with an Eulerian cradle. Indeed, as it exists an important demand of single crystal studies, the 3T1 spectrometer could be definitely transformed in 4-circles diffractometer, fully dedicated to single crystal measurements. It could also be equipped in the future with a big two dimentionnal detector.

Another priority is the major modification of the **reflectometer EROS**, spectrometer especially adapted to surface and interface studies in liquid systems. A multi-disc chopper has just been installed instead of the old single chopper : a gain of a factor 2 of the neutron flux is obtained. Still the present limit of the neutron flux on EROS arises from the small beam divergence due to the length of the spectrometer required to obtain a high resolution. Recently, experiments requiring this high resolution have disappeared to the benefit of low reflectivity measurements at large angle, studying small distance. Indeed, the scientific community is now more interested in studies of thin interfaces, from 2 to 10nm. If we compare EROS to the other reflectometers in the world, it appears that to be competitive, it needs to gain a factor 10 to 100 in the neutron flux on the sample. Our solution is to shorten the spectrometer, and first its collimator (see Figure 2).
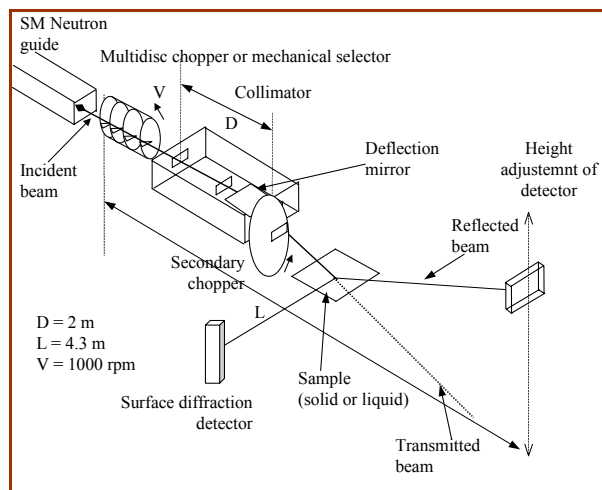
Figure 2. Scheme of the modified reflectometer EROS.

An optimized collimator of 2m length will give an important gain by a factor 10 of the neutron intensity at large angle. More, by putting the detector tube under vacuum, we will gain a new factor 2 on the neutron flux. In the future, a second change should be envisaged: that of the guide. At the moment, EROS is located at the end of a multi-layer guide, G3bis, and thus has few short wavelengths. On a main guide coated with super-mirrors, we would expect an additional neutron flux gain of 4! Two end guide positions are possible: G3 and G6. Whatever the future decisions concerning the new position of EROS in the guide hall, the modifications will keep the options already available on EROS : surface diffraction and off-specular measurements.

Concerning the **time of flight spectrometer MIBEMOL,** the high resolution inelastic scattering spectrometer (in the range 10µeV to 100meV), the comparison of its performances with those of other spectrometers recently built at ILL (Grenoble) or at HMI (Berlin) shows that we shall be soon no more competitive. Then in order to answer to the demand in TOF measurements, we are faced to an alternative. The first solution is the **renewal of MIBEMOL**. It will imply super-mirrors guides associated with vertical focusing method. The disc-choppers will be replaced by choppers with magnetic bearings (in order to increase the rotation velocity of choppers). Such a solution would increase the ratio neutron flux/resolution by a factor 5 or 8. To achieve such a technical solution, another end of guide position instead of that of G6 is necessary. MIBEMOL will have to move on another super-mirror guide to benefit from the whole guide height (15cm)

available for focusing. The second possibility is the construction of a **new time of flight spectrometer, named TDV2**, with a **higher flux and a medium resolution.** This spectrometer could work in two modes, time focusing or energy focusing, as FOCUS spectrometer [1] at PSI (Villigen, Switzerland). The two main elements of such spectrometer are a focusing monochromator (crystals) and a Fermi chopper (see figure 3).
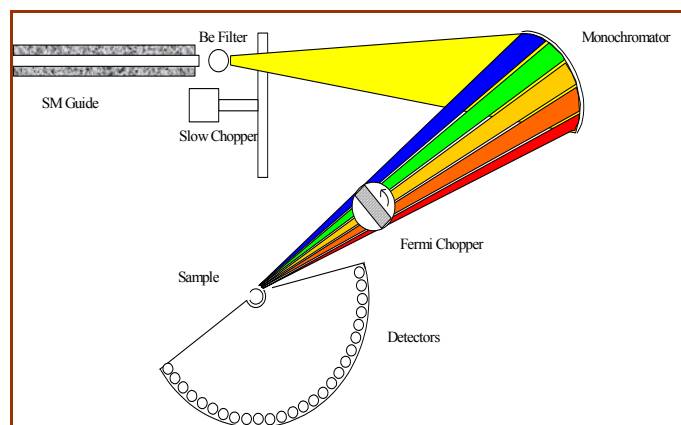
Figure 3. Principles of the project for a new mixte time of flight spectrometer TdV2.

The wavelength distribution of the beam delivered by the monochromator is directly function of the distances guide to monochromator and monochromator to sample. When these distances are equal, the wavelength dispersion is minimum. This mode gives access to a high energy resolution. When they are not equal, the wavelength distribution is large, but the neutron flux is very high and time focusing is possible. The latter technique increases the flux by one order of magnitude compared to multi-chopper spectrometers as MIBEMOL with a comparable energy transfer range, 40µeV to 100meV. This kind of spectrometer is attractive since it offers two possibilities, either a high flux with a low resolution or a low flux with a high resolution. The estimated ratio flux/resolution of TDV2 will be 10 to 15 times higher than that of MIBEMOL (present). For the TDV2 project, the location could be the end of guide position G3, coated with super-mirrors.

Another instrument that we plan to rebuilt is the **polarised neutron diffractometer** (PND) **5C1**. This diffractometer allows to study inter-atomic or inter-molecular magnetic interactions and gives a direct access to the spin density distribution in the unit cell. At present, the only places in the world properly equipped for performing PND ("flipping

ratio measurements") are: ILL (Grenoble) with an instrument D3 (hot neutrons) and D23 (thermal neutrons), and LLB with a dedicated instrument 5C1 (hot neutrons). The measurements of polarised neutron flipping ratios on all these instruments are done by a single counter reflection after reflection, which is quite time consuming. Therefore, any improvement of the instrument which can may decrease the total time of the experiment and improve the accuracy, is of a great interest. The aim of the project concerning the instrument 5C1 is to multiply by a factor 5 (20 for large unit cells) the data collection rate. This diffractometer is characterized by a relatively broad wavelength band $\Delta\lambda/\lambda \approx 10\text{-}20\%$, which could make possible simultaneous measurements of a large number of reflections for each sample orientation if a 2D position sensitive detector (PSD) was available. The procedure of measurements will be slightly different from that of the recent Laue-type diffractometers at ILL, LADI and VIVALDI. The sample will be rotated about the vertical axis and the diffraction images will be recorded for each polarisation state. Moreover, the image plate technique used on Laue-type diffractometers, which provides a large detector area combined with a high spatial resolution, is not suitable in the case of PND, since its electronics can not be switched rapidly to ensure the intensity measurements in two polarization states. Our solution is to use an array of one dimensional position sensitive (resistive) detectors or a two dimensional PSD, with an appropriate electronics allowing to separate the two polarisation channels. In our project of very intense precession (VIP) diffractometer (see figure 4), we rely on the collaboration with ILL, where a new multi-tube detector technology has been developed. Such a technique allows to cover a quite large detection area with a resolution of 1.5x10 mm. Preliminary measurements performed at the 6T2 diffractometer in LLB using a multi-tube detector of dimension 320x320 mm made in ILL show that the spatial resolution of the detector is sufficient for our purpose (see figure 5).
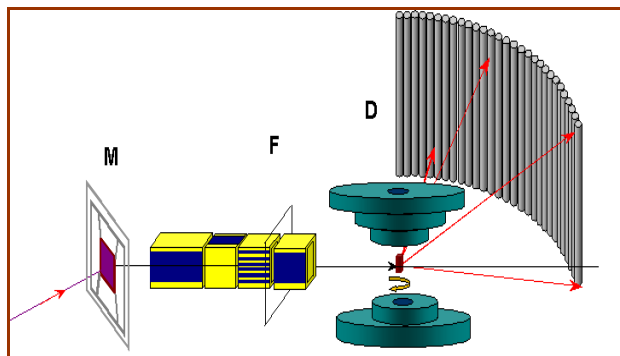
Figure 4. Schema of the polarised neutron diffractometer project on 5C1 , « **V**ery **I**ntense **P**recession diffractometer (VIP diffractometer) ». (M) is the polarizing monochromator (Heusler crystal), (F) is the flipper. Instead of a single detector (D), a new arrangement of 2D multi-tube vertical position sensitive detectors is envisaged.
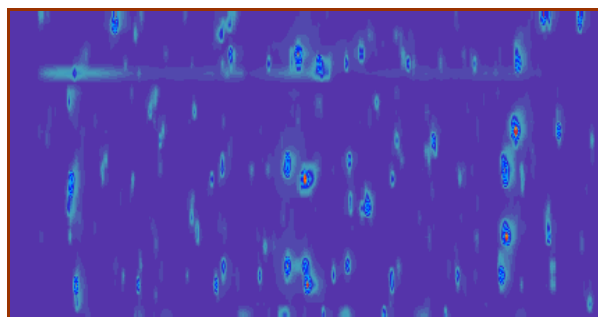
Figure 5. Precession image of the diffraction from the $Sr_{14}Cu_{24}O_4$ single crystal. The image is constructed using 900 frames measured with a step of 0.1°, with the exposition time of 10 seconds. The data collection rate is one order of magnitude higher than with a simple detector.

As a conclusion, all these developments show the will of LLB to enlarge the possibilities of neutron scattering, a tool already useful and determinant to a large research area at the microscopic level (structure and dynamics) in physics, chemistry, biology and materials science.

Reference

[1] J. Mesot, S. Janssen, L. Holitzner and R. Hempelmann, *J. Neutron Research*, **3** , 293 (1996).
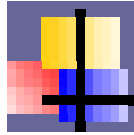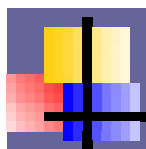
EXPERIMENTAL PROGRAMME AND USER ACTIVITIES

1. Operation of the Orphée Reactor and LLB facility

In 2001-2002, the LLB associates (CEA and CNRS) decided to reduce the operation of the Orphée reactor to 180 days per year (FPED, Full power equivalent days) for budgetary problems. The previous agreement between the two associates (CEA and CNRS) had fixed this number of operating days to 210 days during the previous two year-period, i.e. 1999-2000. In fact, the reactor operation has slightly exceeded these nominal numbers in the past three years, leading to a real availability greater than 100% (see table 1). The Orphée reactor is one of the most recent medium power reactors in Europe and has a very efficient operation.

Year	1995	1996	1997	1998	1999	2000	2001	2002
Reactor Days	215	245	188	218	205	213	186	183
% Availability	94,2	98,2	95,4	99,4	96,8	101,4	103,3	101,6

Table 1. Operation of the LLB-Orphée reactor for the last eight years. The nominal operation was of 245 days up to 1997, of 210 days in 1998-2000 and of 180 days in 2001-2002. The low figure in 1997 is due to the replacement of the zircaloy housing core.

The number of experiments and experiment days performed at LLB in 2001-2002 scaled closely with this 14% decrease of the available beam time, compared to the previous two-year period:
An average of 3642 experiment days in 2001-2002 (3670 exp. days in 2001 and 3613.5 exp. Days in 2002) to be compared with an average of 4074 experiment days in 199-2000 (4196 exp. Days in 1999 and 3953 exp. Days in 2000). The number of experiments decreased also in a smaller proportion: an average of 489 experiments in 2001-2002 (500 experiments in 2001 and 477 in 2002) to compare with an average of 509 experiments in 1999-2000
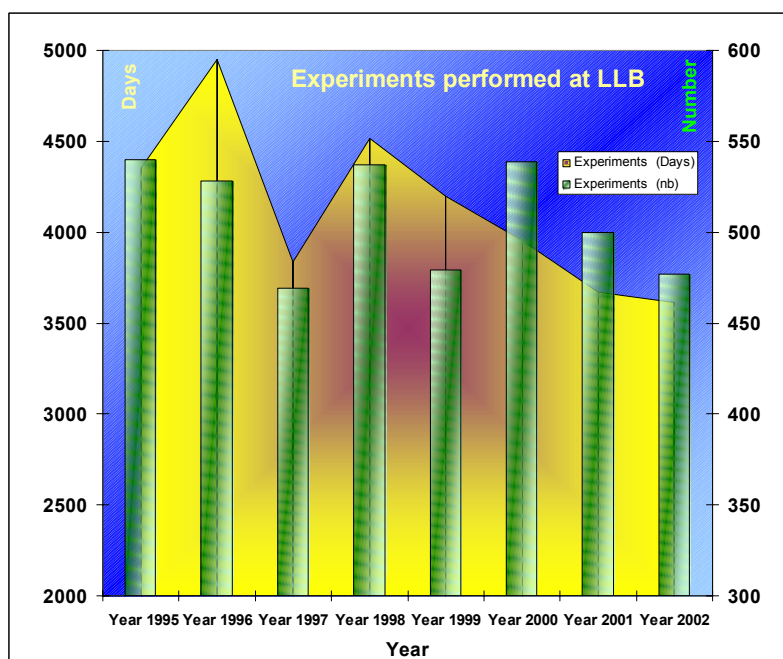
Figure 1. Graph of the number of experiments (green bars and right scale) and experiment days (yellow curve and left scale) performed at LLB-Orphée during the last eight years. The curves followed closely the number of operation days of the Orphée reactor (table 1).

Experiments at LLB are performed on various types of spectrometers. The four main groups are composed of three-axis spectrometers, powder diffractometers, small angle machines and single crystal diffractometers. They delivered more than five hundreds (500) experimental days per year and performed 60-120 experiments each year. The four smaller groups deal with diffuse scattering, quasi-elastic scattering, material science and reflectometry. They deliver around three hundreds (300) experimental days per year corresponding to 20-40 experiments each year.
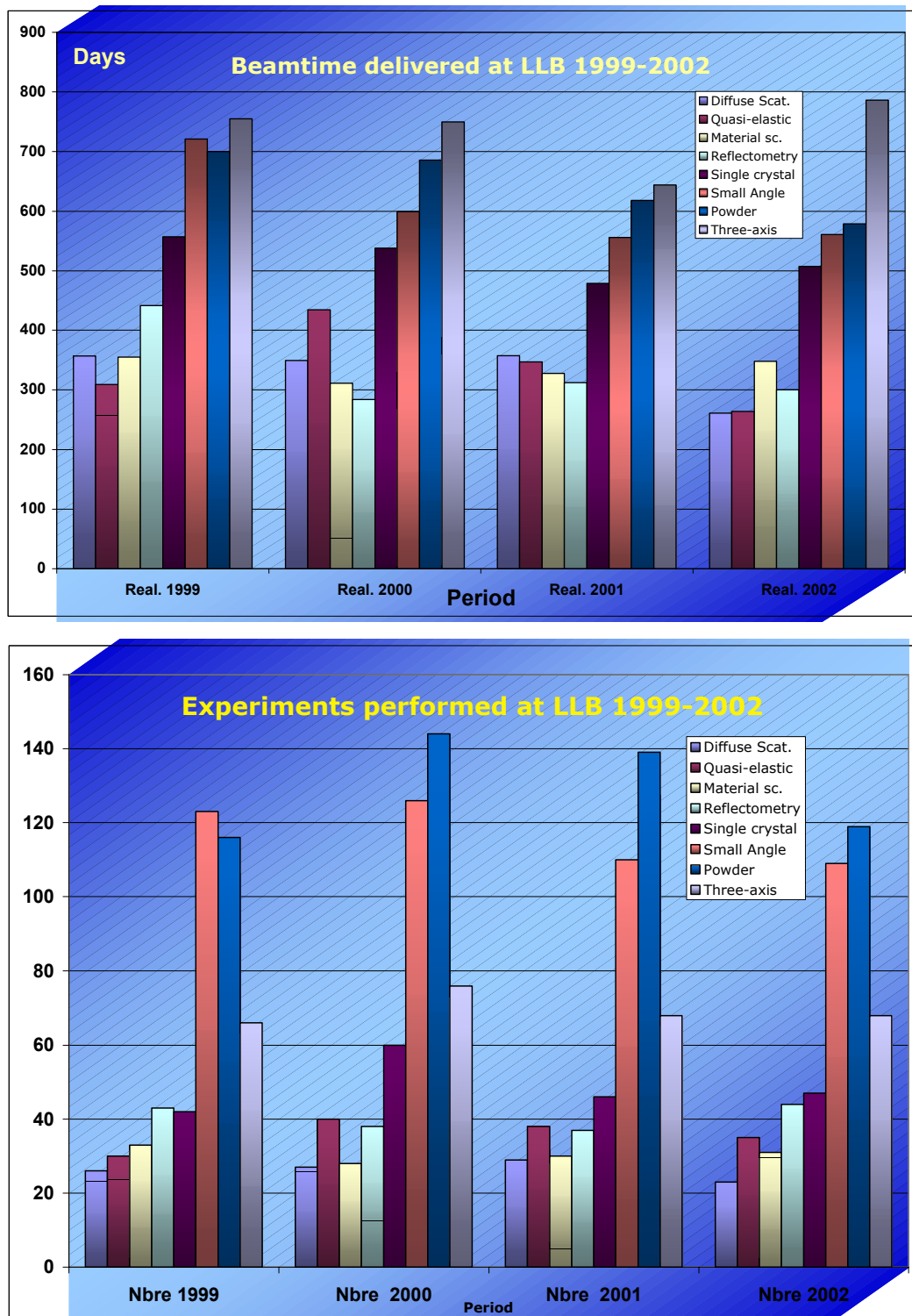
Figure 2. Beam time (upper figure) delivered at LLB-Orphée over the last four (4) years and experiments (lower figure) done in the same period as a function of the instrumental group (listing at the section end).

2. Experimental programme and user activities

Experiments performed at the LLB in 2001-2002 have been realised by French teams coming from all over the country (figure 3 below). The French experiments stand for nearly two-thirds (2/3) of the total beam time delivered during this two-year period. The neutron teams from European and associated countries have benefited of nearly one fourth (1/4) of the total beam time, part of this use being supported by the European support for large-scale facilities (see next sub-section). The rest of the beam time has been used mainly by Russia, PECO countries and for a small fraction by the remaining countries (USA, Japan, Switzerland, …, see beam time allocation subsection for a detailed analysis by countries).
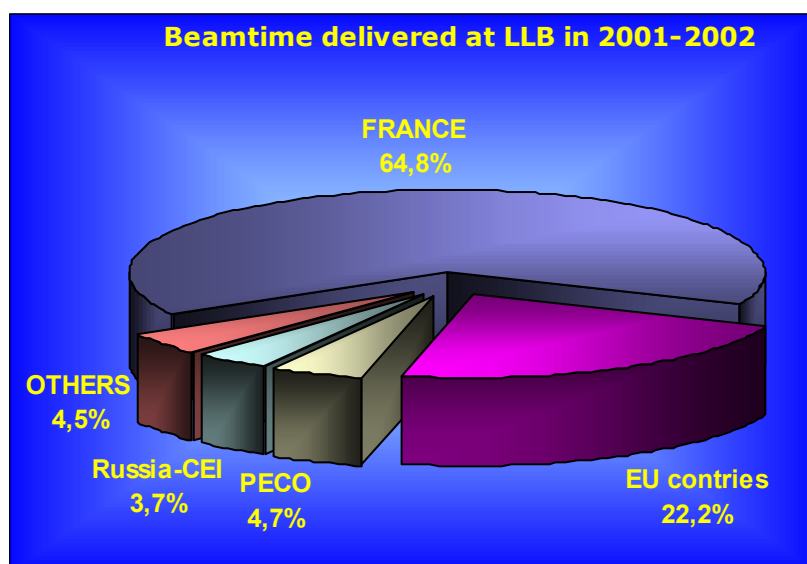
Figure 3. Beam time delivered at LLB-Orphée in 2001-2002 as a function of the nationality of the neutron teams involved (upper graph) and geographical repartition of the experiments realised by French teams (lower graph).

166

3. European access programme

Since 1993, the LLB is a large-scale facility for the transnational access of European users in the framework of the Human Capital and Mobility (HCM, 1993-1997) and Training and Mobility of researchers (TMR, 1996-2000) programmes of the European Commission. In 1999, The LLB applied successfully for the new HPRI European programme opened also to associated countries (e.g. central Europe). The first contract HPRI-CT-1999-0032 started on 1 February 2000 for three years until 31 January 2003, thus covering this two-year report. The initial plan was to deliver five hundred and ten (510) days of beam time for seventy (70) projects involving one hundred (100) individual users. The access really delivered by the LLB during the total three-year period amounted in fact up to five hundred and fifty (550) days of beam time, delivered to ninety-four (94) projects and concerned one hundred and thirty-five individual users coming from EC countries or associated countries. Amongst the ninety-four (94) projects, sixty-three projects came from EC countries and thirty-one projects from associated countries.

The LLB has signed a new contract in 2002, HPRI-CT-2001-0170 for two years until February 2004. This contract will concern one hundred and eighty-five (185) days of beam time for twenty-five (25) projects involving thirty-seven (37) individual users. This second contract will end up the transnational access programme of the FP5 scheme and will be replaced by new contracts in the FP6 scheme. Indeed, the LLB has applied successfully to continue in participating to the transnational access of European users to large-scale facilities in the Neutron-Muon integrated initiative in the forthcoming years.

The LLB is particularly keen to attract new user groups from EC or associated countries and those wishing to apply neutron techniques to novel scientific areas. Researchers wishing to apply under the EC programme can do so via the normal LLB proposal mechanism. The LLB will provide travel and subsistence cost for up to two researchers in an accepted experiment.
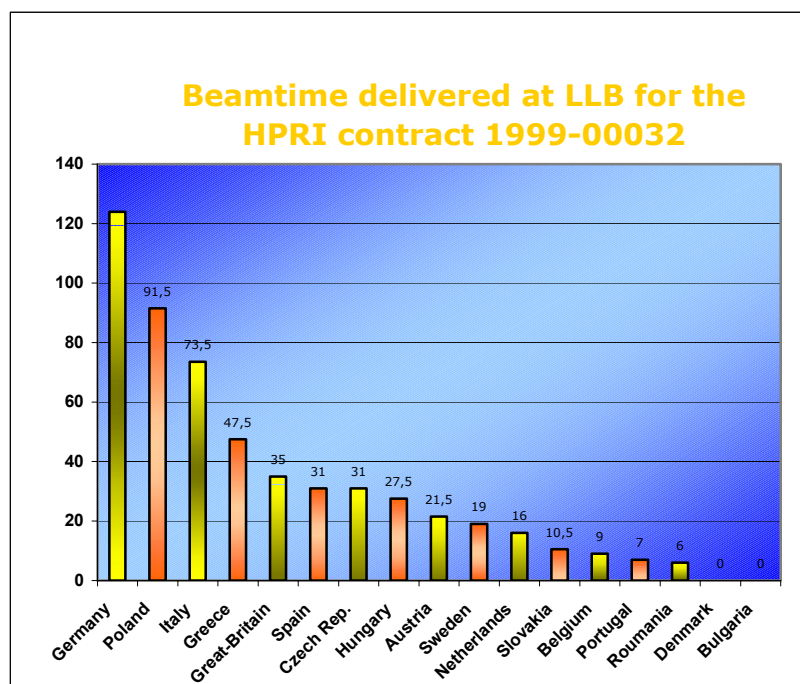
Figure 4. Beam time delivered at LLB-Orphée in 2001-2002 in the framework of the transnational access program supported by the European FP5 scheme for large scale facilities, as a function of the nationality of the neutron researchers invited by the LLB.

4. Selection panel and Beam time allocation

Proposals for experiments are selected and beam time allocations are made through peer review. Review committees of specialists from France and the most parts of European countries have been set up in the following scientific areas:

> Session A for physical chemistry and biology
> Session B for structural studies and phase transitions
> Session C for Magnetism and superconductivity
> Session D for disordered systems and material science.

The relative importance of these four committees of the selection panel at LLB is depicted in the figure 5 below this paragraph. The largest committee of the LLB is the one dealing with magnetism and superconductivity, domain where the LLB expertise is acknowledged worldwide. The three other committees are roughly equivalent in importance and share the rest of the allocated beam time, each of them getting around 20% of the total beam time.

The review committee meet twice a year, some six weeks after the deadline for submission of proposals (1 April in spring and 1 October in fall). Accepted proposals submitted by April receive beam time in the second half of the year and those submitted by October, in the first half of the next year. More detailed information on applications for beam time and deadlines are given on the LLB web site at http://www-llb.cea.fr

There are three different ways of submitting a proposal to the LLB:

- Standard submission of a research proposal, twice a year in Spring and Fall
- Long term research project over three (3) years, twice a year in Spring and Fall
- Fast access procedure for short experiment or test, without time restriction.

Special access for proprietary research and industrial users and firms are considered separately.
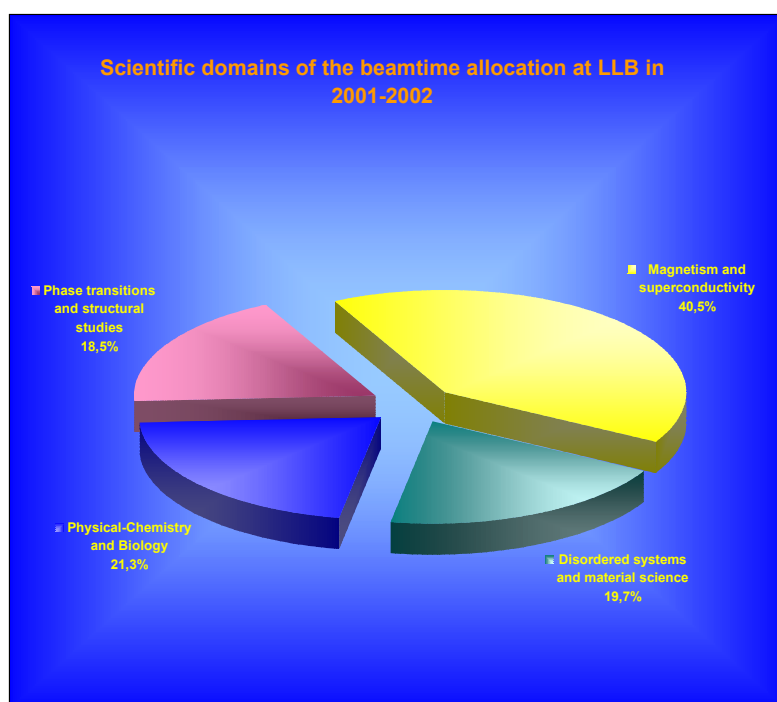
Figure 5. Repartition of the beam time delivered at LLB-Orphée in 2001-2002 amongst the four committees of the selection panel with the corresponding percentage.

 The four review committees of the selection panel of the LLB comprise fifty (50) international scientists (see table) who meet twice a year at the LLB and have the difficult job of assessing the scientific quality and timeliness of submitted proposals and to advise on the allocation of beam time. The four committees report to the direction of the LLB who regulate the beam time allocation.

Overall, the four review committees of the selection panel scrutinised nine hundred thirty-two (932) proposals requesting 8666.5 days of beam time for 2001-2002, out of which seven hundred forty-one (741) proposals received beam time, allocating 5321.5 days on the twenty-five (25) LLB instruments.

The distribution of beam time requested and allocated amongst the different European and other counties is shown in the table 2. Nearly two-thirds of the allocated beam time go to the French proposals covering all domains of science and nearly all regions of France. One fourth of the beam time is devoted to European proposals coming from the major "neutron-wise" countries, i.e. Germany, Great Britain, Spain, Austria and Italy. Half of this European beam time goes to German experiments in long term collaborations, initiated on all instruments and not only on the CRG ones. Collaborations with Austria and Italy suffered with the closedown of the corresponding CRG instruments. On the contrary, the collaborations with Russia and PECO countries are still very active and count for nearly seven percent of the allocated beam time, comparable with the rest of the internationally allocated beam time.

Country	Proposals 2001-2002	Experiments 2001-2002	Beam time asked (days)	Beam time all. (Days)	Beam time asked (%)	Beam time all. (%)
France	520	436	5012.5	3269.5	57.8%	61.4%
FRANCE	520	436	5012.5	3269.5	57.8%	61.4%
Germany	93	82	809	611	9.3%	11.5%
Austria	17	13	165	105	1.9%	2.0%
Italy	20	15	134	75.5	1.5%	1.4%
Great-Britain	23	18	217.5	132	6.9%	5.0%
Spain	10	9	117	71.5	1.6%	2.0%
Others	68	43	511	264	5.9%	5.0%
EU countries	231	180	1953.5	1259	22.5%	23.7%
Poland	24	15	244	113	2.8%	2.1%
Hungary	15	10	128	75.5	1.5%	1.4%
Czech Rep.	6	5	46.5	36.5	0.5%	0.7%
Others	8	6	55	28.5	0.6%	0.5%
PECO	53	36	473.5	253.5	2.6%	2.6%
Russia	50	37	409	196.5	4.7%	3.7%
Ukraine	10	1	215	7	2.5%	0.1%
RUSSIE-CEI	60	38	624	203.5	7.2%	3.8%
United-States	23	21	190	132.5	2.2%	2.5%
Japan	18	12	159	94	1.8%	1.8%
Switzerland	6	5	69	38	0.8%	0.7%
Magrheb	13	8	105	47	1.2%	0.9%
Others	8	5	80	24.5	0.9%	0.5%
Others	68	51	603	336	7.0%	6.3%
TOTAL	932	741	8666.5	5321.5	100%	100%

Table 2. Compilation of the proposed and accepted experiments at LLB by the four series of selection panels done in 2001-2002 with the corresponding beam time demand and allocation in days and percentage for France, the EC countries, PECO and Russia and the rest of the world. The main "neutron-wise" countries have been highlighted.

The LLB is the French national neutron source and one of its primary missions is to deliver neutron beam time to all the French laboratories involved in neutron science. The figure 6 shows the geographical repartition of the French proposals.

Figure 6. Geographical repartition of the experiments realised by French teams (lower graph).

The LLB has kept in 2001-2002 the system of Round Tables and User Selection panels with a spring and fall sessions put in place in 1996. Each session of the Selection Panel comprises typically nine (9) members (3 French members, 3 foreign members and 3 LLB members). The list of the selection panel for Fall 2002 is given at the end of this section.

The Spring session of the selection panel consists of a two-day meeting of the committees at the LLB and for the Fall session, the Selection Panel is preceded by a user meeting, called "Tables Rondes du LLB". This user meeting consists of:
- Invited talks and topical scientific reviews in each committee
- Presentation of recent scientific results of external and internal users (Poster sessions)
- Technical presentations
- And discussion with users.

In the future, It has been decided to discontinue the "Tables Rondes du LLB" that will be replaced by thematic workshops organised in close collaboration with other Large-scale facilities and laboratories from the Saclay Plateau. These workshops will focussed on the major scientific areas of the LLB:

Physical chemistry and biology (Session A)
Structural studies and phase transitions (Session B)
Magnetism and superconductivity (Session C)
Disordered systems and material science (Session D).

5. Instrument operation in 2001-2002

The instrumental operation at LLB in 2001-2002 was smooth and efficient. The major point was the end of the refit of the 2T triple-axis spectrometer with the installation of the full-polarized mode. The LLB has continued in 2001-2002 to upgrade its instrument park, specially on the material science spectrometer G5.2 "Diane", the resonant spin-echo spectrometer G1.Bis "Muses" and the polarised Small Angle Spectrometer G5.5 "Papol". The LLB has progressed in the development of the Very small angle spectrometer TPA and finished the validation tests on the prototype spectrometer. The spectrometer will be built in the forthcoming years. In the near future, the high resolution powder diffractometer 3T2 will be completely rebuilt and upgraded. Upgrade of the time of flight reflectometer G3.Bis "Eros" is also under study and will be rapidly undertaken.

Group	Proposals 2001-2002	Beam time 2001-2002	Session A	Session B	Session C	Session D	TOTAL Alloc.	F_over
Diffuse Scatt.	45	520.0	50.0	7.0	4.0	231.0	292.0	1.78
Quasi-elastic	78	810.0	227.0	44.0	35.0	119.0	425.0	1.91
Materials	44	673.0	0.0	0.0	0.0	366.0	366.0	1.84
Reflectometry	59	635.0	157.5	0.0	186.0	34.0	377.5	1.68
Single crystal	118	1532.0	0.0	327.0	579.0	0.0	906.0	1.69
Small Angle	238	1603.5	679.0	10.5	88.5	131.0	909.0	1.76
Powder	193	1132.0	6.0	217.0	519.0	84.0	826.0	1.37
Three-Axis	154	1736.0	14.0	379.0	742.0	60.0	1195.0	1.45
TOTAL	932	8666.5	1133.5	984.5	2153.5	1050.0	5321.5	1.63

Table 3 Compilation of the proposed experiments at LLB by the four series of selection panels done in 2001-2002 with the corresponding beam time demand and allocation in days by the four committees: Session A stands for physical chemistry and biology, Session B for structural studies and phase transitions, Session C for Magnetism and superconductivity, Session D for disordered systems and material science. Last column displays the overload factor in the eight instrument categories and the global overload factor calculated on the beam time allocation.
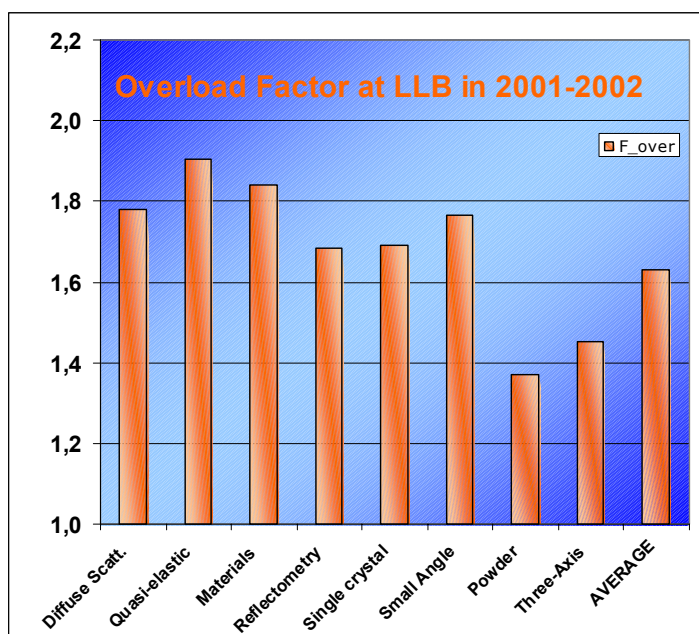
Figure 7. Overload factor of the various instrument groups at LLB 2001-2002 calculated on the beam time demand and allocation.

INITIAL MEMBERSHIP OF THE USERS SELECTION PANEL AUTUMN 2002

SUBPANEL A : Physical Chemistry, Biology

F. Nallet (President)	France	M. Geoghegan	United Kingdom
J. Combet	France	T. Hellweg	Germany
B. Demé	France	P. Mariani	Italy
O. Diat	France	P. Stepanek	Czech Republic
M. Ferrand	France		

SUBPANEL B : Structural Studies, Phase Transitions

T. Fernandez-Diaz	Spain (ILL - France)	H. Boysen	Germany
S. Klotz	France	M. Braden (President)	Germany
M. Latroche	France	J.-M. Perez-Mato	Spain

SUBPANEL C : Magnetism, Superconductivity

C. Dufour	France	J.-L. Garcia-Munoz	Spain
A. Ivanov	Russia (ILL - France)	G. Mc Intyre (President)	Australia (ILL - France)
H. Noël	France	L. Paolasini	Italy (ESRF - France)
		P.G. Radaelli	Italy (ISIS - UK)

SUBPANEL D : Disordered Systems, Materials Science

M. Bee	France	I. Cabaco-Fialho	Portugal
D. Fruchart	France	A. Wiedenmann	Germany
F. Hippert	France		
J.-M. Sprauel (President)	France		

List of LLB instruments scheduled for external users

Powder diffractometers

3T2	"Thermal neutrons" 2-axis (20 detectors) high resolution, mainly for nuclear structure determination
G4.1	"Cold neutrons" 2-axis (multidetector 800 cells) high flux, mainly for magnetic structure determination
G4.2	"Cold neutrons" 2-axis (7x10 detectors) high resolution, for structure determination on polycrystalline samples with large unit cell.
MICRO (G6.1)	"Cold neutrons" 2-axis (multidetector 400 cells) with long wavelength (-5A) and high flux, for the study of very small powder samples (<1 mm'). Very high pressure cell available (40 GPa).

Diffractometers for material science studies

6T1	"Thermal neutrons" 4-circle for texture determination
DIANE (G5.2)	"Cold neutrons" 2-axis for internal strain mapping in bulk samples with spatial resolution ~1 mm^3.

Single crystal diffractometers

5C1	"Hot neutrons" 2-axis with lifting arm, polarised neutrons, magnetic field (8 Tesla) for spin-density maps determination
5C2	"Hot neutrons" 4-circle for nuclear structure determination.
6T2	"Thermal neutrons" 2-axis, lifting arm and 4-circle, mainly for magnetic structure determination. 12 Tesla magnetic field available

Diffuse scattering instruments

7C2	"Hot neutrons" 2-axis (multidetector 640 cells) for local order studies in liquid or amorphous systems. Cryostat and furnace available (1.2K 1300°C).
G4.4	"Cold neutrons" 2-axis (48 detectors, elastic/inelastic discrimination by Time-of-flight technique) for local order studies in single crystals. Furnace available (1400°C).

Small-angle scattering instruments

PACE (G1.1)	"Cold neutrons" (annular detector, 30 rings) for study of large scale structures in isotropic systems (mainly polymers and colloids).
PAXY (G2.3)	"Cold neutrons" (X-Y detector, 128×128 cells) for study of large-scale structures (10 to 500 Å) in anisotropic systems (polymers under stress, metallurgical samples, vortex in superconductors ..).
PAXE (G5.4)	"Cold neutrons" (X-Y detector, 64x64 cells) for multipurpose studies of large scale structures
PAPOL (G.5.5)	"Cold polarized neutrons" with dynamic nuclear polarisation facility

Reflectometers

EROS (G3bis)	"Cold neutrons" reflectometer operating in time-of-flight mode for multipurpose surface studies.
PRISM (G2.4)	"Cold neutrons" reflectometer with polarised neutrons and polarisation analysis for the study of magnetic layers.

Triple-axis instruments

1T	"Thermal neutrons" high-flux 3-axis instrument with focusing monochromator and analyser, mainly devoted to phonon dispersion curves measurements. Very high pressure cell (100 Kbar) available.
2T	"Thermal neutrons" high-flux 3-axis instrument with focusing monochromator and analyser, mainly devoted to spin-waves and magnetic excitations studies (1.5 to 80 meV).
4F1	"Cold neutrons" high flux 3-axis instrument with double monochromator and analyser, mainly devoted to the study of low-energy (15μeV to 4meV) magnetic excitations. Polarised neutrons and polarisation analysis option available.
4F2	"Cold neutrons" high-flux 3-axis instrument for the study of low-energy excitations (e.g. soft modes) or modulated structural studies in single crystals.
G4.3	"Cold neutrons" high resolution and low background 3-axis instrument, mainly devoted to elastic diffuse scattering studies.

Quasi-elastic instruments

MIBEMOL G6.2	"Cold neutrons" high resolution (~15 μeV at 10Å) time-of-flight instrument for the study of low energy excitations, mainly in disordered systems.
MESS (G3.2)	"Cold neutrons" small-angle high resolution spin-echo instrument, for the study of slow dynamics (Fourier time ~40 ns) of disordered matter (movements of large molecules in biology or physical chemistry, relaxation of magnetic moments).
MUSES (G1bis)	"Cold neutrons" large-angle high flux spin-echo instrument for the studies of biological or colloid systems

GENERAL IMPLANTATION OF LLB INSTRUMENTS

Single crystal diffractometers

Powder and liquid diffractometers

Inelastic scattering instruments

Small angle scattering instruments

Reflectometers

Internal use and test instruments
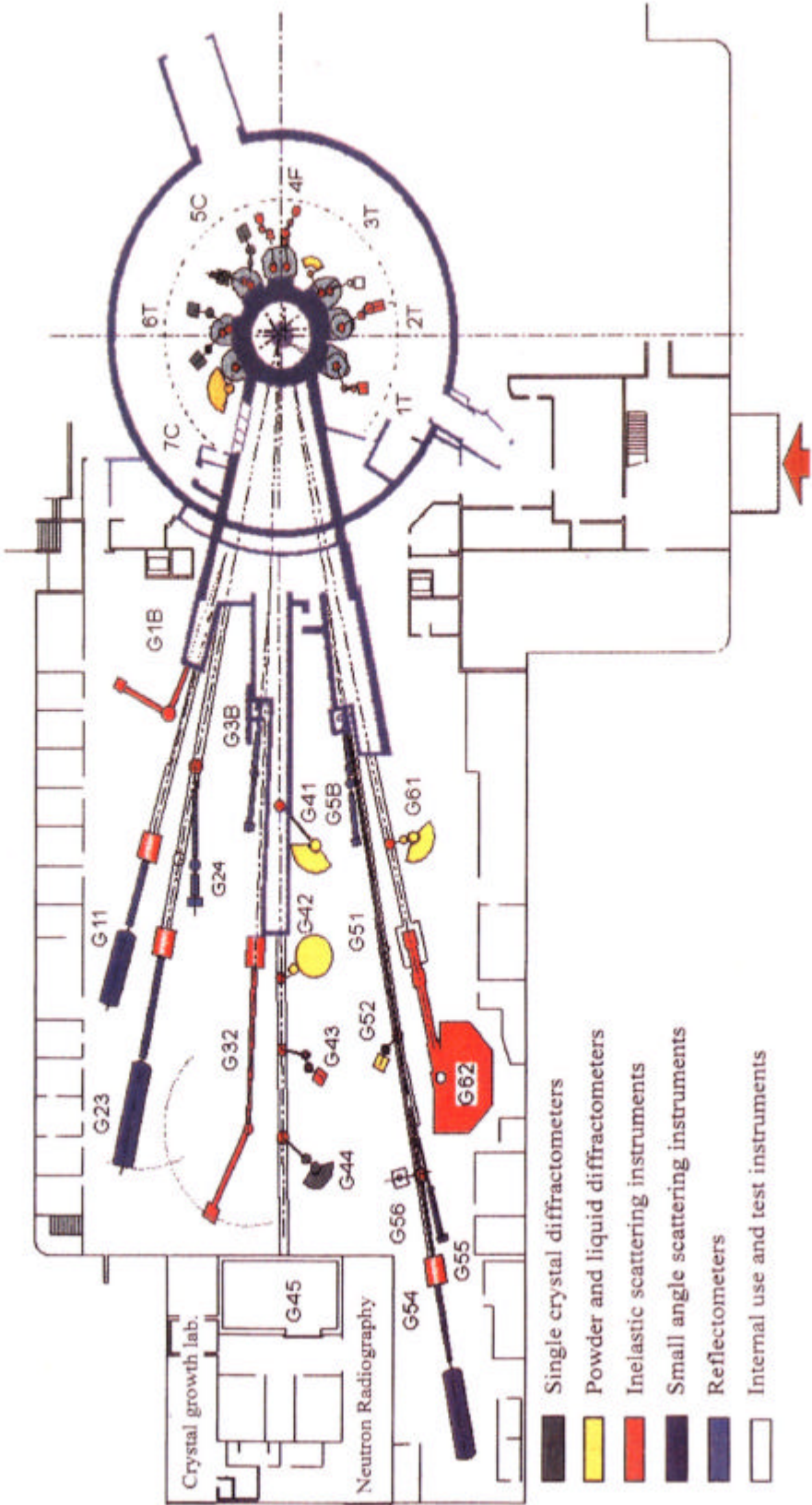
THESARDS de 1999 à 2002

NOM	Directeur de thèse	SUJET	Date de fin de thèse
ALBERGAMO Francesco	M. Héritier	Etude par diffusion de neutrons des propriétés dynamiques de l'hélium liquide confiné dans des milieux poreux	30/11/2001
ALMASY Laszlo	M.C. Bellissent	Structure and dynamics in binary mixtures with limited miscibility. Investigation of aqueous solutions of methyl-substituted pyridines.	28/10/2002
APPAVOU Marie-Sousai	M.C. Bellissent	Influence de la pression sur la structure, la dynamique et la fonction d'un inhibiteur de la catalyse enzymatique, le BPTI.	01/10/2004
AUTRET Cécile	C. Martin	Etude de pérovskites de manganèse à propriétés de magnétorésistance colossale.	06/12/2002
BACRI Guillaume	F. Boué	Etude d'une interface entre deux polymères : relation entre la résistance à la fracture et le profil de concentration.	22/11/1999
BIOTTEAU Gaël	M. Hennion	Etude au moyen de la diffusion élastique et inélastique de neutrons de systèmes pérovskites dopés présentant une magnétorésistance géante.	16/11/2000
BOUIS Frédéric	P. Pfeuty	Etude théorique du modèle de réseau Kondo (fermions lourds et isolants Kondo)	14/10/1999
CADAVEZ PERES Paula Cristina		L'étude du magnétisme des systèmes géométriquement frustrés AMn2Hx. Influence de la pression et des substitutions chimiques.	06/12/2002
CHAPERON Isabelle	M. Duguet	Etudes des réactions de renaturation et d'échange de brin dans l'ADN	31/03/1999
DAOUD-ALADINE Moursidali Aziz	A. Revcolevschi	Etudes par diffraction des corrélations entre magnétisme et structure des perovskites de manganèse à ordre de charges.	20/12/2001
DELLERUE Serge	M.C. Bellissent	Dynamique de protéines membranaires photosynthétiques.	21/01/2000
DESVERGNE Sandra	Y. Gnanou	Nano-objets polymères : de la synthèse aux propriétés, étude par diffusion de rayonnement.	21/01/2005
DURIVAULT Laurence	B. Chevalier	Influence de la composition chimique sur le comportement physique des germaniures ternaires appartenant au système Ce-Ni-Ge. Déterminattion des structures magnétiques.	04/11/2002
EL HARRAK Abdeslam	F. Boué	Nanocomposites polymères/particules dures : synthèse de particules greffées par une bonne dispersion de la charge renforçante	01/10/2004
FADDA Giulia	V. Laretta-Garde	Proteolyse enzymatique d'un gel: microrheologie et mecanisme de degradation".	18/09/2002
FLAMENT Xavier	R. Caudron	Etats métastables correspondant à la nucléation lors de la mise en ordre des alliages.	24/11/2000
FRIEDT Oliver	B. Hennion	Couplage électron-spin-réseau dans les ruthénates.	30/09/2002
GALDEANO Sophie	C.-H. de Novion	Influence des conditions de broyage sur la distribution de nanoparticules magnétiques (Fe,Co) dans une matrice de cuivre.	10/12/2001
GUILLOT Samuel	A.V. Axelos	Structures d'agregations et propriétés interfaciales de la methylcellulose.	12/12/2002
GUYON Stéphanie		Extrusion de vésicules à travers des membranes poreuses calibrées.	12/11/2002
HIRSCHI Karina	A. Lodini	Analyse des contraintes résiduelles et des paramètres microstructuraux par diffraction des neutrons dans un acier inoxydable austénitique.	11/10/1999

THESARDS de 1999 à 2002

JAKANI Saâd	M.-H. Mathon	Etude des mécanismes de recristallisation du cuivre en fonction de la teneur en impuretés résiduelles	07/01/2004
JEAN Bruno	B. Cabane	Les interactions entre polymères associatifs et surfactants : études structurales aux interfaces et en solution.	18/12/2000
KOBER Pascale	F. Moussa	Etude des propriétés magnétiques et structurales des perovskites de Mn à magnétorésistance géante par diffusion de neutrons.	01/10/2004
KÖPER Ingo	M.C. Bellissent	Influence du tréhalose sur la dynamique de la C-phycocyanine : une étude par diffusion quasiélastique de neutrons.	01/07/2002
LATKOVIC Mladen	S. Aubry	Etude des modèles théoriques pour les ondes de densité de charge et de spin dans des composites organiques.	31/12/2000
LE MENN Florence	W. Paulus	Dynamique et désordre du groupe méthyl dans différents composés moléculaires.	12/09/2002
LE TOQUIN Ronan	M. Halet	Etude structurale et magnétique de La2CoO4+delta par diffraction des rayons X (synchrotron) et des neutrons	01/10/2003
LEYMARIE Edouard	H. Glattli	Méthodes de variation de contraste par polarisation nucléaire en diffusion de neutrons aux petits angles. Observation de domaines de polarisation nucléaire par diffusion de neutrons ;	28/11/2002
MORFIN Isabelle	J.-F. Legrand	Structures induites par l'écoulement dans une solution viscoélastique de polymère. Etude par diffusion de neutrons aux petits angles en association avec des techniques rhéooptiques et mécaniques.	17/09/1999
MORGANTE Anna-Maria	S. Aubry	Multibreathers et ondes stationnaires dans des systèmes dscrets non-linéaires.	03/09/2001
PAILHES Stéphane	B. Hennion	Etude par diffusion de neutrons des fluctuations magnétiques dans YBCO dopé au calcium.	01/10/2004
PRIGENT Gilles	R. Bellissent	Distortion de Peierls dans les alliages liquides II-VI et III-V isoélectroniques des semi-conducteurs du groupe IV.	10/12/1999
PUJOLLE Caroline		Identification et étude de la transition isotrope-nématique induite sous cisaillement dans les polymères cristaux liquides.	30/09/2002
RUSSO Daniela	P. Calmettes	Etude structurale et dynamique de l'état natif et des états dénaturés de la néocarzinostatine, par microcalorimétrie différentielle, spectroscopies optiques et diffusion de neutrons et rayons X.	04/11/2000
SAUREL Damien	C. Simon	Séparation de phases dans les manganites à magnétorésistance colossale Pr(1-x)CaxMnO3.	01/10/2005
SHRAMCHENKO Nataliya	R. Bellissent	Localisation des espèces atomiques dans les quasi-cristaux Al-Pd-Mn.	22/10/2001
YAMEOGO Arsène	C. Prioul	Amélioration de la durée de vie des essieux-axes ferroviaires par retardement ou élimination du fretting.	22/07/2004
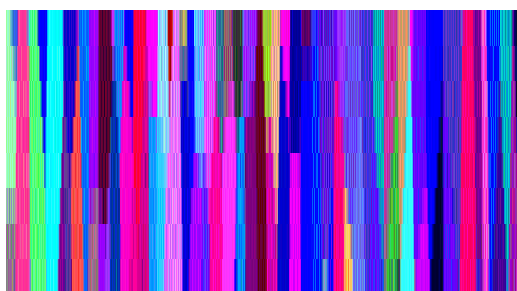
PUBLICATIONS

PUBLICATIONS - 2001-2002
PAPERS PUBLISHED IN SCIENTIFIC PERIODICALS
AND CONFERENCE PROCEEDINGS

1 - STRUCTURES AND PHASE TRANSITIONS

ABAKUMOV A.M., ROZOVA M. G., PAVLYUK B. PH., LOBANOV M.V., ANTIPOV E. V., LEBEDEV O.I., VAN TENDELOO, G., SHEPTYAKOV D. V., BALAGUROV A.M., BOUREE F - Synthesis and crystal structure of novel layered manganese oxide $Ca_2MnGaO_{5+\delta}$
Journal of Solid State Chemistry **158** (2001) 100-111

ALVAREZ-VEGA M., RODRIGUEZ-CARVAJAL J., REYES-CARDENAS J. G., FUENTES A. F., AMADOR U - Synthesis and characterization of new double tungstates $Li_2MII(WO_4)_2$ (M = Co, Ni, and Cu).
Chemistry of Materials **13** (2001) 3871-3875

AUTRET C., RETOUX R., HERVIEU M., RAVEAU B - Charge ordering in a 2D manganite, $Pr_{0.25}Ca_{1.75}MnO_4$
Chemistry of Materials **13** (2001) 4745-4752

AUTRET C., MARTIN C., MAIGNAN A., HERVIEU M., RAVEAU B., ANDRE G., BOUREE F., KURBAKOV A., TROUNOV V. - Destabilization of the cooperative Jahn-Teller effect in $Sm_{0.2}Ca_{0.8}MnO_3$ by Ru-doping.
Journal Magnetism and Magnetic Materials **241** (2002) 303-314

AUTRET, C., MARTIN, C., MAIGNAN, A., HERVIEU, M., RAVEAU, B., ANDRE, G., BOUREE, F. - Strained structure in $Ho_{0.5}Sr_{0.5}MnO_3$
Journal of Solid State Chemistry **165** (2002) 65-73

AUTRET C., ANDRE G., BOUREE F., MARTIN C., HERVIEU M., MAIGNAN A., RETOUX R., RAVEAU B. - Structural and magnetic properties in bidimensionneal manganites
Applied Physics A **74** (2002) S683-S685

BASHIR J., KHAN RTA., BUTT NM., HEGER G**. -** Thermal atomic displacement parameters of SrO
Powder Diffraction **17** (2002) 222-224

BEAURY L., DEROUET J., HOLSA J., LASTUSAARI M., RODRIGUEZ-CARVAJAL J. - Neutron powder diffraction studies of stoichiometric NdOF between 1.5 and 300 K.
Solid State Sciences **4** (2002) 1039-1043

BEDOYA C., MULLER Ch., BAUDOUR J.-L., BOUREE F., SOUBEYROUX J.-L., ROUBIN M.- Ferroelectric-paraelectric phase transition in $PbHf_{0.2}Ti_{0.8}O_3$ studied by neutron powder diffraction
Journal of Physics : Condensed Matter **13** (2001) 6453-6470

BOGICEVIC C., LACOUR F., MALIBERT C., DKHIL B., MÉNORET C., DAMMAK H., GIORGI M.L, KIAT J.M. - Synthesis of nanometric cubic $BaTiO_3$ by using an original chemical route : freeze-drying method
Ferroelectrics , **270** (2002) 57-62

BORDERE S., BOUREE F., CHEVALIER B., ETOURNEAU J. - Magnetic ground states of the tetragonal U_2Fe_2Sn-type structure using an anisotropic RKKY exchange modeling
Journal Magnetism and Magnetic Materials **253** (2002) 15-24

BOULET P., ANDRE G., BOUREE F., NOEL H. - Neutron diffraction studies of the binary uranium stannides USn_2 and U_3Sn_7.
Journal of Alloys and Compounds **329** (2001) 47-49.

BRINKS H. W., RODRIGUEZ-CARVAJAL J., FJELLVAG H., KJEKSHUS A., HAUBACK B. C. - Crystal and magnetic structure of orthorhombic $HoMnO_3$.
Physical Review B **63** (2001) 094411

CADAVEZ-PERES P., GONCHARENKO I.N., MIREBEAU I. - Competing magnetic anisotropies in the mixed rare-earth Laves hydrides
Physical-Review-B- **64** (2001) 094419

CADAVEZ-PERES P., GONCHARENKO I.N., MIREBEAU I., GLADKICH R, MAKAROVA O.L. - Competing ferromagnetic and antiferromagnetic interactions in Laves hydrides
Applied Physics A **74** (2002) S692-694

CAILLEAU H., LUTY T., LEMEE-CAILLEAU M. H., COLLET E., BURON-LE COINTE M., ZIENKIEWICZ E., MOUSSA F. - Pressure tuning of condensation and ordering of charge-transfer strings.
NATO Science Series, II: Mathematics, Physics and Chemistry (2001), 48(Frontiers of High Pressure Research II: Application of High Pressure to Low-Dimensional Novel Electronic Materials), 167-178

CHAPON L., RAVOT D., TEDENAC J.C., BOUREE-VIGNERON F. - How cerium filling fraction influences thermal factors and magnetism in $Ce_yFe_{4-x}Ni_xSb_{12}$
Materials Research Society Symposium Proceedings (2001) 626

CHEVRIER G., NAVAZA A., KIAT J.M., MONTI G.A., ZURIAGA M.J., MARTIN C.A., GUIDA J.A., LANZELOTTI P.L., AYMONINO P.J. - Low temperature phase of strontium nitroprusside tetrahydrate $Sr[Fe(CN)_5NO]\cdot 4H_2O)$ Refinement of the neutron structure at 60K
Journal of Chemical Chemistry **31** (2002) 491-500

CHIPAUX R., ANDRE G., COUSSON A. - Crystal structure of lead tungstate at 1.4 and 300 K
Journal of Alloys and Compounds **325** (2001) 91-94

COLLET E.,., BURON-LE COINTE M., LEMEE-CAILLEAU M.H, CAILLEAU H., TOUPET L., MEVEN M., MATTAUCH S., HEGER G., KARL N. - Structural evidence of ferrielectric neutral-ionic layered ordering in 2,-dimethyltetrathiafulvalene-p-chloranil
Physical Review B **63** (2001) 054104

COLLET E., LEMEE-CAILLEAU M.H., BURON-LE COINTE M., CAILLEAU H., RAVY S., LUTY T., BERAR J.F., CZARNECKI P., KARL N. - Direct evidence of lattice-relaxed charge-transfer exciton-strings
Europhysics Letters **57** (2002) 67-73

COUSTARD J.M., LE TOQUIN R., LEO R., PAULUS W.,COUSSON A. - (E)-5-[Hydroxyimino(phenyl)methyl]-1-methyl-3,4-dihydro-2H-pyrrolium trifluoromethanesulfonate.
Acta Crystallographica, **C57** (2001) 815-816

COUSTARD J.M., LE TOQUIN R., LEO R., PAULUS W., COUSSON A. - (E)-3-Methoxy-3-methylsulfanylisothiochroman-4-one oxime.
Acta Crystallographica, **E57** (2001) 256-257

DAOUD-ALADINE A., RODRIGUEZ-CARVAJAL J., PINSART-GAUDARD L.,FERNANDEZ-DIAZ M.T., REVCOLEVSCHI A. - Zener polaron ordering ion half-doped manganites
Physical Review Letters **89** (2002) 097205

DAOUD-ALADINE A., RODRIGUEZ-CARVAJAL J., PINSART-GAUDARD L.,FERNANDEZ-DIAZ M.T., REVCOLEVSCHI A. - Ordering of ferromagnetic Mn-Mn dimmers vs. Mn^{3+}/Mn^{4+} charge ordering in the $Pr_{1-x}Ca_xMnO_3$ (x $\approx$ .5) perovskites
Applied Physics A **74** (2002) S1758-S1760

DE LAISSARDIERE GT., MAYOU D., SIMONET V., HIPPERT F., AUDIER M., BELLISSENT R - Origin of magnetism in Al-Mn and Al-Pd-Mn quasicrystals., related crystals and liquids
Journal Magnetism and Magnetic Materials **226** (2001) 1029-1031

DEROLLEZ P., GONZALEZ J., HENNION B., FOURET R. - Anharmonic properties of the $AgGaSe_2$ compound.
Physica B **305** (2001) 191-196

DEROLLEZ P., KLOTZ S., LAZEWSKI J., BRADEN M., DKHIL B., KIAT J. M., CALVARIN G., BALDINOZZI G., VAKHRUSHEV S. B., SUARD E. - Local and long range polar order in the relaxor-ferroelectric compounds $PbMg_{1/3}Nb_{2/3}O_3$ and $PbM_{0.3}Nb_{0.6}Ti_{0.1}O_3$.
Physical Review B **65** (2002) 024104

DEROLLEZ P., KLOTZ S., LAZEWSKI J., BRADEN M., HENNION B., FOURET R., GONZALEZ J. - Pressure dependence of acoustic modes in $AgGaSe_2$
High Pressure Research **22** (2002) 283-286

DKHIL B., KIAT J. M - Electric-field-induced polarization in the ergodic and nonergodic states of $PbMg1/3Nb2/3O3$ relaxor.
Journal of Applied Physics **90** (2001) 4676-4681.

DURIVAULT L., BOUREE F., CHEVALIER B., ANDRE G., ETOURNEAU J., ISNARD O. - Magnetic structure of the ternary germanide $Ce_3Ni_2Ge_7$.
Journal Magnetism and Magnetic Materials **232** (2001) 139-146.

DURIVAULT L., BOUREE F., CHEVALIER B., ANDRE G., ETOURNEAU J. - Magnetic ordering in the ternary germanide $Ce_2Ni_3Ge_5$ as studied by neutron powder diffraction
Journal Magnetism and Magnetic Materials **246** (2002) 366-374

DURIVAULT L., BOUREE F., CHEVALIER B., ANDRE G.,WEILL F., ETOURNEAU J. - Magnetic structure of some strongly correlated electron Ce-Ni-Ge systems
Applied Physics A **74** (2002) S677-S679

EL KHALKI A., COLOMBAN PH., HENNION B. - Nature of protons, phase transitions, and dynamic disorder in poly- and oligoaniline bases and salts: An inelastic neutron scattering study.
Macromolecules **35** (2002) 5203-5211.

EL KHAYATI N., CHERKAOUI EL MOURSLI R., RODRIGUEZ-CARVAJAL J., ANDRE G., BLANCHARD N., BOUREE F., COLLIN G., ROISNEL T. - Crystal and magnetic structures of the oxyphosphates $MfePO_5$ (M=Fe,Co,Ni,Cu). Analysis of the magnetic ground state in terms of superexchange interactions
European Physical Journal B **22** (2001) 429-442

EL KHAYATI N., RODRIGUEZ-CARVAJAL J., BOUREE G., ROISNEL T., CHERKAOUI R., BOUTFESSI A., BOUKHARI A. - Magnetic structure and exchange interactions in $CuFe_2(P_2O_7)_2$
Solid State Sciences **4** (2002) 1273-1283

ETRILLARD J., BOURGES PH., HE H. F., KEIMER B., LIANG B., LIN C. T. - Acoustic phonons in the aperiodic layered crystal of $Bi_2Sr_2CaCu_2O_{8+\delta}$
Europhysics Letters **55** (2001) 201-207.

FAUTH F., SUARD E., CAIGNAERT V., DOMENGES B., MIREBEAU I. - Interplay of structural, magnetic and transport properties in the layered Co-based-perovskite $LnBaCo_2O_5$ (Ln=Tb, Dy,Ho)
European Physical Journal B **21** (2001) 163-174

FAUTH F., SUARD E., CAIGNAERT V., MIREBEAU I. - Spin-state ordered clusters in the perovskite $LnBaCo_2O_{5.47}$
Physical Review B **66** (2002) 184421

FRONTERA C., GARCIA-MUNOZ J. L., LLOBET A., ARANDA M. A. G., RODRIGUEZ-CARVAJAL J., RESPAUD M., BROTO J. M., RAQUET B., RAKOTO H., GOIRAN M. - Structural, spin state, and magnetic transitions in $GdBaCo_2O_{5+\delta}$ ($\delta\approx0.5$).
Journal of Alloys and Compounds **323-324** (2001) 468-471

FRONTERA C., GARCIA-MUNOZ J. L., LLOBET A., ARANDA M. A. G., RODRIGUEZ-CARVAJAL J., RESPAUD M., BROTO J. M., RAQUET B., RAKOTO H., GOIRAN M. - Spin state transition: the origin of structural, magnetic and metal-insulator transitions in $GdBaCo_2O_{5+\delta}$ ($\delta\approx0.5$).
Journal Magnetism and Magnetic Materials **242-245** (2002) 751-753.

GARCIA-MATRES E., MARTINEZ J. L., RODRIGUEZ-CARVAJAL J. - Neutron diffraction study of the magnetic ordering in the series R_2BaNiO_5 (R = Rare earth).
European Physical Journal B **24** (2001) 59-70.

GONCHARENKO I. N., CADAVEZ-PERES P., OURNAL I., MAKAROVA O. L - Pressure-induced long-range magnetic order in the frustrated Laves hydride $Tb(Mn_{0.88}A_{l0.12})_2D_{1.04}$.
Europhysics Letters **54** (2001) 807-812.

GUILLOT B., LECOMTE C., COUSSON A., SCHERF C., JELSCH C. - High-resolution neutron structure of nicotinamide adenine dinucleotide.
Acta Crystallographica **D57** (2001) 981-989.

GUILLOT M., El-GHOZZI M., AVIGNANT D., ANDRE G., BOUREE F., COUSSON A. - Magnetic properties of a mixed-valence (III/IV) terbium fluoride KTb_2F_{12}
Journal of Applied Physics **91** (2002) 8519-8521

HENNION B., QUILICHINI M. – An introduction to structure, physical properties, and applications
In « QUASICRYSTALS » Springer Series in Materials Science **55** (2002), Eds J-B. Suck, M. Schreiber, P. Häussler, pp. 436-453
Chapitre 22: Experimental determination of the dispersion of vibrations in monodomain quasicrystalline alloys.

HERNANDEZ-VELASCO J., SAEZ-PUCHE R., HOSER A., RODRIGUEZ-CARVAJAL J. - Low temperature incommensurate magnetic order in R_2BaCoO_5 [R=rare earth]
Applied Physics A **74** (2002) S781-S783

HERNANDEZ O., HEDOUX A., LEFEBVRE J., GUINET Y., DESCAMPS M., PAPOULAR R., MASSON O. – ab initio structure determination of triphenyl phosphite by powder synchrotron X-ray diffraction
Applied Crystallographica **35** (2002) 212-219

HERRMANNSDÖRFER T., FISCHER P., STRÄSSLE T., GONCHARENKO I.N., MATTENBERGER K., VOGT O. - Temperature and pressure dependence of the ordered magnetic U moment of USe
Applied Physics A **74** (2002) S754-S756

HODGES J. A., BONVILLE P., FORGET A., ANDRE G. - First-order transition in frustrated $Yb_2Ti_2O_7$ without long-range order.
Canadian Journal of Physics **79** (2001) 1373-1380

HODGES J. A., BONVILLE P., FORGET A., YAOUANC A., DALMAS DE REOTIER P., ANDRE G., RAMS M., KROLAS K., RITTER C., GUBBENS P. C. M., KAISER C. T., KING P. J. C., BAINES C. - First-Order Transition in the Spin Dynamics of Geometrically Frustrated $Yb_2Ti_2O_7$.
Physical Review Letters **88** (2002) 077204

JOUBERT J.M., LATROCHE M., BOWMAN Jr. R.C., PERCHERON-GUEGAN A., BOUREE-VIGNERON F. - Structural study of the $LaNi_{4.6}Ge_{0.4}$-D_2 system using X-ray and neutron powder diffraction
Applied Physics A **74** (2002) S1037-S1039

KAISER-MORRIS, E., NICOLAI, B., COUSSON, A., PAULUS, W., FILLAUX, F. - 2,6-Dimethylpyrazine at 5 K: a neutron-diffraction study.
Acta Crystallographica, **E57** (2001) 1116-1117.

KAISER-MORRIS, E., NICOLAI, B., COUSSON, A., PAULUS, W., FILLAUX, F. - 2,6-Dimethylpyrazine at 20 K: a neutron-diffraction study.
Acta Crystallographica, **E57** (2001) 1113-1115.

PUBLICATIONS
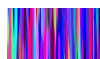
KAISERMAYR M., RENNHOFER M., VOGL G., PAPPAS C., LONGEVILLE S. - Neutron spin-echo spectroscopy for diffusion in crystalline solids.
Physical Review B **66** (2002) 024302

KAMBAS. , KULDA J., PETRICEK V., MCINTYRE M.G., FRENANDEZ-DIAZ M.T., KIAT J.M., PELZELT J. - High pressure structural and dielectric studies of the phase transitions in LTT
Journal of Physics : Condensed Matter**,** **14** (2002) 4042-4055

KIAT J.M., UESU Y., DKHIL B., MATSUDA M., MALIBERT C., CALVARIN G. - Monoclinic structure of unpoled morphotropic high piezoelectric PMN-PT and PZN-PT compounds.
Physical Review B **65** (2002) 064106

KLOTZ S., BRADEN M., KULDA J., PAVONE P., STEININGER B. - Transverse acoustic phonons of GaSb up to 7 Gpa by inelastic neutron scattering
Physica status solidi B **223** (2001) 441-447

KREISEL J., DKHIL B., BOUVIER P., KIAT J.-M.. - Effect of high pressure on relaxor ferroelectrics.
Physical Review B **65** (2002) 172101

KREMENOVIC A., SPASOJEVIC-DE BIRE A., BOUREE F., COLOMBAN P., DIMITRIJEVIC R., DAVIDOVIC M., MIOC U.B. - Structural modifications of dodecatungstophosphoric acid hexahydrate induced by temperature in the 10-358 K range. In situ high-resolution neutron powder diffraction investigation
Solid State Ionics **150** (2002) 431-442

KREZHOV K., SOMOGYVARI Z., MESZAROS Gy. SVAB E., NEDKOV I., BOUREE F. - Neutron powder diffraction study of (Co,Ti)-substituted fine-particle Ba-hexaferrite
Applied Physics A **74** (2002) S1086-S1088

LAFOND A., LEYNAUD O., ANDRE G., BOUREE F., MEERSCHAUT A. - Magnetic properties of $Ln_2Ti_2S_2O_5$ compounds and magnetic structure of $Tb_2Ti_2S_2O_5$.
Journal of Alloys and Compounds **338** (2002) 185-193.

LALIGANT Y., LACORRE P., RODRÍGUEZ-CARVAJAL J. - Powder Structure Determination of Li_2PdO_3: a NaCl structure Type with Turbostratic Effect
Materials Science Forum **378-381** (2001) 632-637

LEFORT R., TOUDIC B., ETRILLARD J., GUILLAUME F., BOURGES P., CURRAT R., BRECZEWSKI T. - Dynamical molecular disorder and diffuse scattering in an alkane/urea incommensurate inclusion compound.
European Physical Journal B **24** (2001) 51-57.

LEMEE N., BOUYANFIF H., DELLIS J. L., EL MARSSI M., KARKUT M. G., DUPONT L., DKHIL B., KIAT J. M. - Pulsed laser deposition of PbMg1/3Nb2/3O3 thin films and PbMg1/3Nb2/3O3/PbTiO3 multilayers.
Journal de Physique IV (2001) **11** (Pr11)
TFDOM 2 International Conference on Thin Film Deposition of Oxide Multilayers Hybrid Structures, 2001), 65-69

LETOUBLON A., DE BOISSIEU M., BOUDARD M., GASTALDI J., HENNION B., CAUDRON R., BELLISSENT R - Phason elastic constants and diffuse scattering in the i-Al-Pd-Mn phase.
Ferroelectrics **250** (2001) 261-264.

LETOUBLON A., DE BOISSIEU M., BOUDARD M., MANCINI L., GASTALDI J., HENNION B., CAUDRON R., BELLISSENT R. Phason elastic constants of the icosahedral Al-Pd-Mn phase derived from diffuse scattering measurements.
Philosophical Magazine Letters **81** (2001) 273-283.

LETOUBLON A., YAKHOU F., LIVET F., BLEY F., DE BOISSIEU M., MANCINI L., CAUDRON R., VETTIER C., GASTALDI J. - Coherent X-ray diffraction and phason fluctuations in quasicrystals
Europhysics Letters **54** (2001) 753-759

LIMOT L., MENDELS P., COLLIN G., MONDELLI C., MUTKA H., BLANCHARD N. - Ga-NMR local susceptibility of the Kagome-based magnet SrCr9pGa12-9pO19: a high-temperature study.
Canadian Journal of Physics **79** (2001) 1393-1399.

LIMOT L., MENDELS P., COLLIN G., MONDELLI C., OULADDIAF B., MUTKA H., BLANCHARD N., MEKATA M. - Susceptibility and dilution effects of the kagome.acte. bilayer geometrically frustrated network: A Ga NMR study of $SrCr_9Ga_{12-9}pO_9$.
Physical Review B **65** (2002) 144447

LIVET F., BLEY F., CAUDRON R., GEISSLER E., ABERNATHY D., DETLEFS C., GRUBEL G., SUTTON M. - Kinetic evolution of unmixing in an AlLi alloy using x-ray intensity fluctuation spectroscopy
Physical Review E **63** (2001) 036108

LIVET F., BLEY F., SIMON J.P., CAUDRON R., MAINVILLE J., SUTTON M., LEBOLLOC'H D. - Static and kinetics of the ordering transition in the $AuAgZn_2$ alloy
Physical Review B **66** (2002) 134108

LOUER D., BATAILLE T., ROISNEL T., RODRÍGUEZ-CARVAJAL J. - The crystallite growth of nanocrystalline Y_2O_3 studied from diffraction lined-profile analysis
Powder Diffraction **17** (2002) 262-269

LUTY T., CAILLEAU H., KOSHIHARA S.-Y., COLLET E., TAKESADA M., LEMEE-CAILLEAU M.H., BURON M., RAVY S., NAGAOSA N., TOKURA Y., ZIENKIEWICZ E., OULADDIAL B. - Static and dynamic order of cooperative multi-electron transfer
Europhysics Letters **59** (2002) 619-625

MAKAROVA O.L., GONCHARENKO I.N., IRODOVA A.V., MIREBEAU I., SUARD E. - Interplay of magnetic and hydrogen ordering in the hexagonal Laves hydrides
Physical Review B **66** (2002) 104423

MANOUN B., EL JAZOULI A., GRAVEREAU P., CHAMINADE J.P. BOUREE F. - Determination and Rietvelt refinement of the crystal structure of $Li_{0.50}Ni_{0.25}TiO(PO_4)$ from powder X-ray and neutron diffraction
Powder diffraction **17** (2002) 290-294

MAURY F., MIREBEAU I., NICOLAS-FRANCILLON M., BOUREE F. - Hole doping by Li substitution and antiferromagnetism in $YBa_2Cu_3O_y$ studied by neutron powder diffraction measurements.
European Physical Journal B **27** (2002) 459-466.

MAURY F., NICOLAS-FRANCILLON M., MIREBEAU I., BOUREE F. - Antiferromagnetism in Li substituted $YBa_2Cu_3O_y$ studied by neutron powder diffraction measurements
Physica C **353** (2001) 93-102

MEINNEL J., COUSSON A., BOUDJADA F., PLAZANET M., MANI M. - Delocalization of methyl groups protons or deuterons in molecular compounds.
Journal of Low Temperature Physics **122** (2001) 257-263.

MENORET C., KIAT J. M., DKHIL B., DUNLOP M., DAMMAK H., HERNANDEZ O. - Structural evolution and polar order in $Sr_{1-x}Ba_xTiO_3$.
Physical Review B **65** (2002) 224104

MENORET C., SPASOJEVIC-DE BIRE A., DAO N.Q., COUSSON A., KIAT J. M., MANNA J.D., HOPKINS M.D. – Chemical bonding in methylidyne complexes : neutron diffraction study on a single crystal of BrW-tplbond.CH(dmpe-d12)2
Journal of the Chemical Society, Dalton Transactions n°19 (2002) 3731-3736

MIREBEAU I., GONCHARENKO I.N., GOLOSOVSKY I.V. - Neutron diffraction in $Ho(Mn_{0.9}Al_{0.1})_2$ under pressure up to 7.8 Gpa : Long-range magnetic order induced by pressure in a frustrated system
Physical Review B (Rapid communications) **64** (2001) 140401

MIREBEAU I., GONCHARENKO I.N., CADAVEZ-PERES P., BRAMWELL S.T., GINGRAS M.J.P., GARDNER J.S. - Pressure-induced crystallization of a spin liquid
Nature **420** (2002) 54-57

MULLER C., VALMALETTE J.C., SOUBEYROUX J.L., BOURÉE F., GAVARRI J.R. - Structural disorder and ionic conductivity in $LiVO_3$: a neutron powder diffraction study from 340 to 890 K
Journal of Solid State Chemistry **156** (2001) 379-389

NAVAZA A., CHEVRIER G., KIAT J.M., BARAN E.J. - Neutron diffraction structure of $Y_2V_{10}O_{28}$ $24H_2O$ at 297 and 60K
Journal of Chemical Crystallography, **30** (2001) 545-555

NAVAZA A., CHEVRIER G., KIAT J.M., BARBEY C. - Contribution of neutron diffraction to the crystal structure determination of 1-hydroxy-1-phosphono-pentyl-phosphonic acid dimethyl ammonium salt
Journal of Solid State Chemistry **167** (2002) 441-445

NICOLAI B., KEARLEY G.J., COUSSON A., PAULUS W., FILLAUX F., GENTNER F., SCHRODER L., WATKIN D. - Structure of manganese diacetate tetrahydrate and low-temperature methyl-group dynamics
Acta Crystallographica B **57** (2001) 36-44

PAULUS W., COUSSON A., DHALENNE G., BERTHON J., REVCOLEVSCHI A., HOSOYA S., TREUTMANN W., HEGER G., LE TOQUIN R. - Neutron diffraction studies of stoichiometric and oxygen intercalasted La_2NiO_4 single crystals
Solid state Sciences **4** (2002) 565-573

PIERRARD A., GREDIN P., DE KOZAK A., VIANA B., ASCHEHOUG P., VIVIEN D., DEROUET J., BOUREE-VIGNERON F. - Structural characterization of $KLa_2F_7 : Nd^{3+}$
Physica Status Solidi B **226** (2002) 329-338

PINSARD-GAUDART L., RODRIGUEZ-CARVAJAL J., DAOUD-ALADINE A., GONCHARENKO I., MEDARDE M., SMITH R. I., REVCOLEVSCHI A. - Stability of the Jahn-Teller effect and magnetic study of $LaMnO_3$ under pressure.
Physical Review B **64** (2001) 064426

PLAZANET M., JOHNSON M.R., COUSSON A., MEINNEL J., TROMMSDORFF H.P. - Molecular deformations of halogeno-mesitylenes in the crystal : structure, methyl group rotational tunneling, and numerical modeling
Chemical Physics **285** (2002) 299-308

QUILICHINI M., PEREZ-MATO J. M., ARAMBURU I., HERNANDEZ O - Polarization-flip transition under electric field in BCCD.
European Physical Journal B **25** (2002) 431-438.

RABILLER P., ETRILLARD J., TOUPET L., KIAT J. M., LAUNOIS P., PETRICEK V., BRECZEWSKI T. - Disorder versus structure analysis in intergrowth urea inclusion compounds.
Journal of Physics: Condensed Matter **13** (2001) 1653-1668

RADULESCU O., JANSSEN T., ETRILLARD **J -** Dynamics of modulated and composite aperiodic crystals - The signature of the inner polarization in the neutron coherent inelastic scattering
European Physical Journal **29** (2002) 385-398

RECKO K., SZYMANSKI K., DOBRZYNSKI L., WALISZEWSKI J., BIERNACKA M., SATULA D., PERZYNSKA K., SUSKI W., WOCHOWSKI K., HOSER A., ANDRE G., BOUREE F. - Magnetism of $UFe_{4-x}A_{18+x}$ (x=<-0.4, 0.4>) intermetallics.
Journal of Alloys and Compounds **323-324** (2001) 531-533.

RECKO K., SZYMANSKI K., DOBRZYNSKI L., SATULA D., SUSKI W., WOCHOWSKI K., ANDRE G., BOUREE F., HOSER A. - Magnetism of the UFe_xAl_{12-x} alloys.
Journal of Alloys and Compounds **334** (2002) 58-67.

REDHAMMER G. J., ROTH G., PAULUS W., ANDRE G., LOTTERMOSER W., AMTHAUER G., TREUTMANN W., KOPPELHUBER-BITSCHNAU B. - The crystal and magnetic structure of Li-aegirine $LiFe_{+}Si_2O_6$: a temperature-dependent study.
Physics and Chemistry of Minerals **28** (2001) 337-346.

RESPAUD M., FRONTERA C., GARCIA-MUNOZ J.L., ARANDA MIGUEL A.G., RAQUET B., BROTO J.M., RAKOTO H., GOIRAN M., LLOBET A., RODRIGUEZ-CARVAJAL J. - Magnetic and magnetotransport properties of $GdBaCo_2O_{5+\delta}$: a high magnetic-field study.
Physical Review B **64** (2001) 214401

REUTLER P., MOUSSA F., HENNION M., WANG F., REVCOLEVSCHI A. - Spin wave anomalies and phonons at low temperature in $La_{0.875}Sr_{0.125}MnO_3$.
Journal Magnetism and Magnetic Materials **242-245** (2002) 689-691.

RODRIGUEZ-CARVAJAL J. - Personal reflections: What is Crystallography ?
Zeitschrift für Kristallographie **217** (2002) 361-362

RODRIGUEZ-CARVAJAL J., DAOUD-ALADINE A., PINSARD-GAUDART L., FERNANDEZ-DIAZ M. T., REVCOLEVSCHI A. - A new interpretation of the CO state in half-doped manganites: new results from neutron diffraction and synchrotron radiation experiments.
Physica B **320** (2002) 1-6.

ROLS S., GONCHARENKO I.N., ALMAIRAC R., SAUVAJOL J.L., MIREBEAU I. - Poligonisation of single-wall carbon nanotube bundles under high pressure
Physical Review B **64** (2001) 153401

ROUSSE G., WURM C., MORCRETTE M., RODRIGUEZ-CARVAJAL J., GAUBICHER J., MASQUELIER C. - Crystal structure of a new vanadium (IV) diphosphate: VP_2O_7, prepared by lithium extraction from $LiVP_2O_7$.
International Journal of Inorganic Materials **3** (2001) 881-887.

ROUSSE G., RODRIGUEZ-CARVAJAL J., WURM C., MASQUELIER C. - Magnetic Structural Studies of the Two Polymorphs of $Li_3Fe_2(PO_4)_3$: Analysis of the Magnetic Ground State from Super-Super Exchange Interactions.
Chemistry of Materials **13** (2001) 4527-4536

ROUSSE G., RODRIGUEZ-CARVAJAL J., WURM C., MASQUELIER C. - A neutron diffraction study of the antiferromagnetic diphosphate $LiFeP_2O_7$.
Solid State Sciences **4** (2002) 973-978.

ROUSSE G., RODRIGUEZ-CARVAJAL J., WURM C., MASQUELIER C. - Magnetic structure of two lithium iron phosphates : A- and B-$Li_3Fe_2(PO_4)_3$
Applied Physics A **74** (2002) S704-S706

SANTUCCI S., LOZZI L., VALENTINI L., KENNY J.M., MENELLE A. - Hydrogen concentration and mass density obtained by X-ray and neutron reflectivity on hydrogenated amorphous carbon nitride thin films
Diamond and Related Materials **11** (2002) 1188-1192.

SANTUCCI S., VALENTINI L., MENELLE A., LOZZI L., COPPOLA R., KENNY J.M. - Ar dilution effects on hydrogen concentration and mass density obtained by X-ray and neutron reflectivity on hydrogenated amorphous nitride thin films
Applied Physics A **74** (2002) S1104-S1106

SCHOBINGER-PAPAMANTELLOS P., RODRIGUEZ-CARVAJAL J., ANDRE G., DUONG N. P., BUSCHOW K. H. J., TOLEDANO P. - Simultaneous structural and magnetic transitions in YFe_4Ge_2 studied by neutron diffraction and magnetic measurements.
Journal Magnetism and Magnetic Materials **236** (2001) 14-27.

PUBLICATIONS

SCHOBINGER-PAPAMANTELLOS P., ANDRE G., RODRIGUEZ-CARVAJAL J., BUSCHOW K. H. J., DURIVAULT L. - Magnetic ordering of $CeNi_{0.78}Sn_2$ and $Ce_3Ni_2Sn_7$ compounds by neutron diffraction.
Journal of Alloys and Compounds **325** (2001) 29-36.

SCHOBINGER-PAPAMANTELLOS P., ANDRE G., RODRIGUEZ-CARVAJAL J., MOZE O., KOCKELMANN W., TUNG L. D., BUSCHOW K. H. J. - Magnetic ordering of $PrCoAl_4$ a neutron diffraction study.
Journal Magnetism and Magnetic Materials **231** (2001) 162-171.

SCHOBINGER-PAPAMANTELLOS P., ANDRE G., RODRIGUEZ-CARVAJAL J., DUONG N. P., BUSCHOW K. H. J. - Multiple competing interactions and reentrant ferrimagnetism in $Tb_{0.8}Nd_{0.2}Mn_6Ge_6$.
Journal Magnetism and Magnetic Materials **231** (2001) 121-134.

SCHOBINGER-PAPAMANTELLOS P., RODRIGUEZ-CARVAJAL J., BUSCHOW KHJ., DOORYHEE E., FITCH AN. - Re-entrant magneto-elastic transition in $HoFe_4Ge_2$: an XRPD study
Journal Magnetism and Magnetic Materials **250** (2002) 225-240

SENAS A., RODRIGUEZ FERNANDEZ J., GOMEZ SAL J.C., GONCHARENKO I. - Pressure-induced antiferromagnetism in TbPt and $TbPt_{0.6}Cu_{0.4}$: a neutron-diffraction study
Applied Physics A **74** (2002) S786-S788

SHRAMCHENKO N., DENOYER F. - The Al-Pd-Mn quasicrystalline approximant ξ-phase revisited
European Physical Journal B **29** (2002) 56-59

SILVESTRE J.P., DAO N.Q., HEGER G., COUSSON A. - Refinement by neutron diffraction of the crystal structure of hydroxyethylidenebisphophonic acid monohydrate : $C(CH_3)(OH)(PO_3H_2)_2.H_2O$
Phosphorous, Sulfur and Silicon and the Related Elements **177** (2002) 277-288

SIMONET V., HIPPERT F., AUDIER M., BELLISSENT R. - Mn/Cr isomorphic substitution in μ $Al_4Mn_xCr_{1-x}$ phase compounds $(0 <= x <= 1)$
Physica B **315** (2002) 187-200

SOMOGYVARI Z., SVAB E., MESZAROS G., KREZHOV K., NEDKOV I., SAJO I., BOUREE F. - Vacancy ordering in nanosized maghemite from neutron and X-ray powder diffraction
Applied Physics A **74** Part 2 (2002) S1077-S1079

SOMOGYVARI Z., SVAB E., MESZAROS GY., KREZHOV K., KONSTANTINOV P., NEDKOV I., BOUREE F. - Nanosize effects on the microstructure of $BaFe_{10.3}Co_{0.85}Ti_{0.85}O_{19}$ hexaferrite.
Journal of Applied Physics **91** (2002) 6185-6187.

STRIDE JA., JAYASOORIYA UA., MBOGO N., WHITE RP., NICOLAI A., KEARLEY G.J. - Hydrogen-bonding in the self-organising system 3.,5-dimethylpyrazole
New Journal of Chemistry **25** (2001) 1069-1072

SZWARC H., GRELL A.-S., MASIN F., TAMARIT J. LL., VAN MILTENBURG J. C., ALLOUCHI H., AGAFONOV V., RODRIGUEZ-CARVAJAL J., CEOLIN R. - The C_{60}, 2S8 solvate: Mysteries and certainties.
Journal de Physique IV: Proceedings (2001) **11** (Pr10), XXVII JEEP, Journées d'Etude des Equilibres entre Phases, (2001) 41-45.

TARASENKO V. F., ALEKSEEV S.B., FEDENEV A.V., GONCHARENKO I. M., KOVAL N.N., OSKOMOV KK.V., ORLOVSKII V. M., SOCHUGOV N.S., SHULEPOV M.A. - Study on IR and UV-laser interaction with metal surfaces.
SPIE-The Inter. Society for Optical Engineering (2002) 4631 (Gas and Chemical Lasers and Intense Beam Applications III) 234-243.

TEJADA-ROSALES EM., RODRIGUEZ-CARVAJAL J., CASAN-PASTOR N., ALEMANY P., RUIZ E., EL-FALLAH MS., ALVAREZ S., GOMEZ-ROMERO P . - Room-temperature synthesis and crystal., magnetic., and electronic structure of the first silver copper oxide
Inorganic Chemistry **41** (2002) 6604-6613

TELLGREN R., ANDERSSON Y., GONCHARENKO I., ANDRE G., BOUREE F., MIREBEAU I. - High-pressure neutron diffraction studies of the magnetic structures of cubic Pd_3Mn, $Pd_3MnD_{0.7}$
Journal of Solid State Chemistry **161** (2001) 93-96

TENAILLEAU C., SUARD E., RODRIGUEZ-CARVAJAL J., CROSNIER-LOPEZ M. P., LACORRE P. - Effect of Mo Doping on the Room-Temperature Structure of Vanadium Sesquioxide.
Chemistry of Materials **14** (2002) 3569-3575.

TOUGAIT O., ANDRE G., BOUREE F., NOEL H. - Neutron diffraction study of magnetic ordering of two binary uranium tellurides U_3Te_5 and U_2Te_3.
Journal of Alloys and Compounds **317-318** (2001) 227-232.

TRAN V.,H., KACZOROWSKI D., TROC R., ANDRE G., BOUREE F., ZAREMBA V. - Magnetic structure of the Kondo UCu_5In
Solid State Communications **117** (2001) 527-530

TRAN V. H., STEGLICH F., ANDRE G. - Antiferromagnetic order with short correlation length and Kondo interactions in U_2PdGa_3 and U_2PtGa_3.
Physical Review B **65** (2002) 134401

ULRICH C., KONDO S., REEHUIS M., HE H., BERNHARD C., NIEDERMAYER C., BOUREE F., BOURGES P., OHL M., RONNOW H. M., TAKAGI H., KEIMER B. - Structural and magnetic instabilities of $La_{2-x}Sr_xCaCu_2O_6$.
Physical Review B **65** (2002) 220507

VAJDA P., ANDRE G. - Commensurate and incommensurate magnetic structures in rare-earth hydrides.
Journal of Alloys and Compounds **326** (2001) 151-156.

VANHOYLAND G., BOUREE F., VAN BAEL M.K., MULLENS J., VAN POUCKE L.C. - Structure determination and refinement of acid strontium oxalate from X-ray and neutron powder diffraction
Journal of Solid State Chemistry **157** (2001) 283-288

VIEIRA L. G., HERNANDEZ O., RIBEIRO J. L., COUSSON A., KIAT J. M., CHAVES M. R., ALMEIDA A., KLOPPERPIEPER A. - Structure of the X-phase of 38% brominated betaine calcium chloride dihydrate.
Acta Crystallographica **B57** (2001) 296-302.

VILMINOT S., RICHARD-PLOUET M., ANDRE G., SWIERCZYNSKII D., BOUREE-VIGNERON F., MARINO E., GUILLOT M. - Synthesis, structure and magnetic properties of copper hydroxysulfates
Crystal Engineering **5** (2002) 177-186

2 - MAGNETISM AND SUPERCONDUCTIVITY

ALEKSEEV P..A., NEFEODOVA E.V., STAUB U., MIGNOT J.-M., LAZUKOV V.N., SADIKOV I.P., SODERHOLM L., WASSERMANN S., PADERNO YU.B., SHITSEVALOVA N. Yu., MURANI A. - Low-energy response and Yb valence in the Kondo insulator YbB_{12}
Physical Review B **63** (2001) 64411

ALEKSEEV P.A., MIGNOT J.M., OCHIAI A., NEFEODOVA E.V., SADIKOV I.P., CLEMENTYEV E.S., LAZUKOV V.N., BRADEN M., NEMKOVSKI K.S. - Collective magnetic excitations in mixed-valence $Sm_{0.83}Y_{0.17}S$
Physical Review B **65** (2002) 153201

ALEKSEEV P. A., MIGNOT J.-M., STAUB U., OCHIAI A., OLUBKOV A. V., BRADEN M., BEWLE R. I, NEFEODOVA E. V., SADIKOV I. P., CLEMENTYEV E. S., LAZUKOV V. N., NEMKOVSKI K. S. - f-Electron excitations in the neutron spectra of mixed-valence Sm1-xYxS.
Physica B **312&313** (2002) 333-335.

ALEKSEEV P. A., MIGNOT J.-M., NEMKOVSKI K.S., KAHN R., SHITSEVALOVA N.YU., BEWLEY R.I., ECCLESTON R.S., CLEMENTYEV E. S., LAZUKOV V. N., NEFEODOVA E. V., SADIKOV I. P., TIDEN N.N. - Yb-Yb correlations and crystal field in the Kondo-insulator YbB_{12}
Applied Physics A, **74** (2002) S662-S664

BIOTTEAU G., HENNION M., MOUSSA F., RODRIGUEZ-CARVAJAL J., PINSARD L., REVCOLEVSHI A., MUKOVSKII Y.M., SHULYATEV D. - Approach to the metal-ins transition in $La_{1-x}Ca_xMnO_3$ ($0 \leq x \leq 0.2$) : magnetic inhomogeneity and spin-wave anomaly
Physical Review B **64** (2001) 104421

BOBROFF J., ALLOUL H, MacFARLANE W.A., MENDELS P., BLANCHARD N., COLLIN G., MARUCCO J.F. - Persistence of Li induced Kondo moments in the superconducting state of cuprates
Physical Review Letters **86** (2001) 4116-4119

BOBROFF J., ALLOUL H, OUAZI S., MAHAJAN A., MENDELS P., BLANCHARD N., COLLIN G., GUILLEN V., MARUCCO J.F. - Absence of static phase separation in the high T_c cuprate $Yba_2Cu_3O_{6+x}$
Physical Review Letters **89** (2002) 157002

BORGES R. P., GUICHARD W., LUNNEY J. G., COEY J. M. D., OTT F. - Magnetic and electric "dead" layers in $(La_{0.7}Sr_{0.3})MnO_3$ thin films.
Journal of Applied Physics **89** (2001) 3868-3873.

BRADEN M., MEVEN M., REICHARDT W., PINTSCHOVIUS L., FERNANDEZ-DIAZ M.T., HEGER G., NAKAMURA F., FUJITA T. - Analysis of the local structure by single crystal neutron scattering in $La_{1.85}Sr_{0.15}CuO_4$
Physical Review B **63** (2001) 140510 (rapid comm.)

BRADEN M., REICHARDT W., SHIRYAEV S., BARILO S.N. - Giant phonon anomalies in the bond-stretching modes in doped $BaBiO_3$: comparison to cuprates manganites and nicklates
Physica C **378-381** (2002) 89-96

BRADEN M., FRIEDT O., SIDIS Y., BOURGES P., MINAKATA M., MAENO Y - Incommensurate magnetic ordering in $Sr_2Ru_{1-x}Ti_xO_4$
Physical Review Letters **88** (2002) 197002

BRADEN M., SIDIS Y., BOURGES P., PFEUTY P., KULDA J., MAO Z., MAENO Y. - Inelastic neutron scattering study of magnetic excitations in Sr_2RuO_4
Physical Review B **66** (2002) 64522

BRADEN M., REICHARDT W.,HENNION B., DHALENNE G., REVCOLESCHI A. - Lattice dynamics of $CuGeO_3$: Inelastic neutron scattering and model calculations
Physical Review B **66** (2002) 214417

DANNEAU R., WARIN P., ATTANE J. P., PETEJ I., BEIGNE C., FERMON C., KLEIN O., MARTY A., OTT F., SAMSON Y., VIRET M. - Individual domain wall resistance in submicron ferromagnetic structures.
Physical Review Letters **88** (2002) 157201

FRIEDT O., BRADEN M., ANDRE G., ADELMAN P., NAKATSUJI S., MAENO Y. - Structural and magnetic aspects of the metal insulator transition in $Ca_{2-x}Sr_xRuO_4$
Physical Review B **63** (2001) 174432

FRIEDT O., BRADEN M., ANDRE G., NAKATSUJI S., MAENO Y. - Neutron-diffraction study of the crystal structure of $Ca_{1.5}Sr_{0.5}R_4$
Applied Physics A **74** (2002) S1627-S1629

GALLAIS Y., SACUTO A., BOURGES P., SIDIS Y., FORGET A., COLSON D. - Evidence for two distinct energy scales in the Raman spectra of $YBa_2(Cu_{1-x}Ni_x)_3O_{6.95}$.
Physical Review Letters **88** (2002) 177401

GILLON B. - Spin distributions in molecular systems with interacting transition metal ions.
Editor(s): Miller Joel S., Drillon Marc. Magnetism: Molecules to Materials (2001) 357-378. Publisher: Wiley-VCH Verlag GmbH, Weinheim, Germany

GILLON B., MATHONIÈRE C., RUIZ E., ALVAREZ S., COUSSON A., KAHN O. - Spin densities in a ferromagnetic bimetallic chain compound : polarized neutron diffraction and DFT calculations
Journal of American Chemical Society **124** (2002) 14433-14441

GOLOSOVSKY I.V., MIREBEAU I., ANDRE G., KURDYUKOV D.A., KUMZEROV Yu. A., VAKHRUSHEV S.B. - Magnetic ordering and phase transition in MnO embedded into a porous glass
Physical Review Letters **86** (2001) 5783-5786

GOLOSOVSKY I.V., MIREBEAU I., MARKOSYAN A.S., FISHER P., POMJAKUSHIN V. Yu. - Neutron diffraction study of the magnetic order in the $Dy(Mn_{1-x}Al_x)_2$ system in the region of a magnetic instability
Physical Review B **65** (2002) 014405

GOLOSOVSKY I.V., MIREBEAU I., RODRIGUEZ-CARVAJAL J., ROISNEL T., MARKOSYAN A.S. - Evolution of the magnetic order in $Ho(Mn_{1-x}Al_x)_2$ system. Neutran Diffraction study.
Journal of Physics : Condensed Matter **14** (2002) 11737-11745

GUIDI M. CESTELLI, ALLODI G., DE RENZI R., GUIDI G., HENNION M., PINSARD L., AMATO A. - Staggered magnetization, critical behavior, and weak ferromagnetic properties of $LaMnO_3$ by muon spin rotation.
Physical Review B **64** (2001) 064414

GUKASOV A., BRADEN M., PAPOULAR R. J., NAKATSUJI S., MAENO Y. - Anomalous Spin-Density Distribution on Oxygen and Ru in $Ca_{1.5}Sr_{0.5}RuO_4$: Polarized Neutron Diffraction Study.
Physical Review Letters **89** (2002) 087202

GUKASOV A., BROWN P.J. - Determination of atomic site susceptibility tensors from polarized neutron diffraction data
Journal of Physics : Condensed Matter **14** (2002) 8831-8839

GUKASOV A., ROGL P., BROWN P.J., MIHALIK M., MENOVSKY A. - Site susceptibility tensors and magnetic structure of $U_3Al_2Si_3$: a polarized neutron diffraction study
Journal of Physics : Condensed Matter **14** (2002) 8841-8851

HE H., SIDIS Y., BOURGES P., GU G.D., IVANOV A., KOSHIZUKA N., LIANG ., LIN C.T., REGNAULT L.P., SCHOENHERR E., KEIMER B. - Resonant spin excitation in an overdoped high temperature superconductor.
Physical Review Letters **86** (2001) 1610-1613

HE H., BOURGES P., SIDIS Y., ULRICH C., REGNAULT L.P., PAILHES S., BERZIGIAROVA N.S., KOLESNIKOV N.N., KEIMER B. - Magnetic resonant mode in the single-layer high temperature superconductor $Tl_2Ba_2CuO_{6+d}$
Science **295** (2002) 1045-1047.

HENNION B., HICKS T. J., SIDIS Y., MIREBEAU I. - The dynamics of transverse magnetic defects in antiferromagnetic $Mn_{90}Cu_{10}$.
Journal Magnetism and Magnetic Materials **226-230** (2001) 512-514.

HENNION M., MOUSSA F., WANG F., MUKOVSKII Y., SHULYATEV D. - Spin wave anomalies interpreted as unusual magneto-vibrational modes in $La_{0.8}Ca_{0.2}MnO_3$.
Physica B **312&313** (2002) 752-753.

PUBLICATIONS

HENNION B., SZUSZKIEWCZ W., DYNOWSKA E., JANIK E., WOJTOWICZ T. - Spin-wave measurements on MBE-grown zinc-blende structure MnTe by inelastic neutron scattering
Physical Review B **66** (2002) 224426

HODGES J. A., SIDIS Y., BOURGES P., MIREBEAU I., HENNION M., CHAUD X. - Antiferromagnetic ordering in a 90 K copper oxide superconductor.
Physical Review B **66** (2002) 020501

IVANOV A. S., BOURGES P., PETITGRAND D., CASALTA H. - High-energy spin dynamics in Pr_2CuO_4.
Journal Magnetism and Magnetic Materials **226-230** (2001) 485-486.

IWASA K., KOHGI M., GUKASOV A., MIGNOT J.M., SHIBATA N., OCHIAI A., AOKI H., SUZUJI T. - Polarized neutron study of one dimensional magnetic response under magnetic field in the charge-ordered phase of Yb_4As_3
Journal Magnetism and Magnetic Materials **226-230** (2001) 441-443

IWASA K., KOHGI MA. GUKASOV A., MIGNOT J.M., SHIBATA N., OCHIAI A., AOKI H., SUZUKI T. - Staggered-field effect on the magnetic-field-induced magnetization of the one-dimensional antiferromagnet Yb_4As_3.
Physical Review B **65** (2002) 052408

IWASA K., HANNAN A., KOHGI MA. BRADEN M., MIGNOT J.M., KITAWAZA H., SUZUKI T. - Crystal lattice modulation and phonon anomaly associated with strong p-f mixing effect of CeSb
Applied Physics A **74** (2002) S1179-S1181

KEIMER B., HE H., BOURGES P., SIDIS Y., ULRICH C., REGNAULT L.P., PAILHES S., BERZIGIAROVA N.S., KOLESNIKOV N.N. - Inelastic neutron scattering study of $Tl_2Ba_2Cu_{6+\delta}$
Journal of Physics and Chemistry of Solids **63** (2002) 2243-2246.

KOHGI M., IWASA K., MIGNOT J.M., FAK B., GEGENWART P., LANG M., OCHIAI A., OAKI H., SUZUKI T. - Staggered field effect on the one-dimensional S=1/2 antiferromagnet Yb_4As_3
Physical Review Letters **86** (2001) 2439-2442

KOHGI M., IWASA K., MIGNOT J.-M., FAK B., HIESS A., GEGENWART P., LANG M., OCHIAI A., AOKI H., SUZUKI T. - Spin excitations of the one-dimensional S=12 Heisenberg antiferromagnet Yb_4As_3 under magnetic field.
Physica B **312&313** (2002) 359-361.

KOHGI M., IWASA K., MIGNOT J.-M., GUKASOV A., FAK B., HIESS A., OCHIAI A., AOKI H.. - Neutron scattering studies of the one-dimensional quantum spin magnetism in Yb_4As_3
Applied Physics A **74** (2002) S871-S873

LAZUKOV V.N., NEFEODOVA E.V., SIKOLENKO V.V., STAUB U., ALEKSEEV P.A., BRADEN M., NEMKOVSKI K.S., PRADERVAND C., SADIKOV I.P., SODERHOLM L., TIDEN N.N. - Lattice anomalies in CeNi unstable valence compound
Applied Physics A **74** (2002) S559-S561

LE BRAS G., KONSTANTINOVIC Z., COLSON D., FORGET A., CARTON J.P., AYACHE C., JEAN F., COLLIN G., DUMONT Y. - Anomalous electronic susceptibility in $Bi_2Sr_2CuO_{6+\delta}$ and comparison with other overdoped cuprates
Physical Review B **66** (2002) 174517

LOEWENHAUPT M., WITTE U., KRAMP S., BRADEN M., SVOBODA P. - Unusual phonon siftening in the Kondo lattice $CeCu_2$
Physica B **312-313** (2002) 181-183

LOSHKAREVA N. N., ARBUZOVA T. I., SMOLYAK I. B., SOLIN N. I., NAUMOV S. V., SUKHORUKOV YU. P., MOSTOVSHCHIKOVA E. V., VIGLIN N. A., KOROLYOV A. V., BALBASHOV A. M., HENNION M., MOUSSA F., PAPAVASSILIOU G. - Charge segregation in manganites with electron doping
Journal Magnetism and Magnetic Materials **242-245** (2002) 704-706.

MACFARLANE W. A., BOBROFF J., MENDELS P., CYROT L., ALLOUL H., BLANCHARD N., COLLIN G., MARUCCO J.-F. - Planar 17O NMR study of $Pr_yY_{1-y}Ba_2Cu_3O_{6+x}$.
Physical Review B 66 (2002) 024508

MIGNOT J.-M., GONCHARENKO I.N., MATSUMURA T., SUZUKI T. - Stabilisation of type I-antiferromagnetism in TmTe at P=6 Gpa
Journal Magnetism and Magnetic Materials **226-230** (2001) 211-213

MIGNOT J.-M., GUKASOV A., YANG C.P., LINK P., MATSUMURA T., SUZUKI T. - Antiferroquadrupolar order in the magnetic semiconductor TmTe
Journal Physical Society of Japan **71** (2002) Sppl. 39

MIKKE K., JANKOWSKA-KISIELINSKA J., HENNION B. - The generalized susceptibility of FCC Mn(38%Ni) alloy
Applied Physics A **74** (2002) S616-S618

MIKKE K., JANKOWSKA-KISIELINSKA J., HENNION B., UDOVENKO V.A., MILCZAREK J.J. - Spin waves in the intermetallic compound Mn
Applied Physics A 74 (2002) S670-S672

MOUSSA F., REUTLER P., HENNION M., RODRIGUEZ-CARVAJAL J., WANG F., REVCOLEVSCHI A., BÜCHNER B. - Strong spin wave anomalies in $La_{1-x}Sr_xMnO_3$, x=0.125.
Applied Physics A **74** (2002) S1790-S1792

ONUFRIEVA F., PFEUTY P. - Spin dynamics of a two-dimensional metal in a superconducting state : application to the high T_c cuprates
Physical Review B **65** (2002) 054515

OTT F. - Réflectivité hors spéculaire et diffraction de surface
Journal de Physique IV (France) **11** (2001) Pr9- pp. 67-101

OTTLIK A., PINTSCHOVIUS L., MULLER H., LOHE D. - Stresses., residual stresses and distortions developing during brazing of cemented carbide and steel joints with cylindrical geometry
ECRS 6: Proceedings of the 6th European Conference on Residual Stresses - Materails Science Forum **404** (2002) 233-238

PAPOULAR R.J., COLLIN G., COLSON D., VIALLET V. - Direct Imaging of fractional oxygen O_d in Hg-based high-T_c superconductors
Bayesian Inference and Maximum Entropy Methods in Science and Engineering, 21th International Workshop, edited by R.L. Fry, pp. 204-226

PAPOULAR R.J. - Imaging of disordered protons and oxygen atoms in molecular compounds of pharmaceutical interest an high-T_c superconducting oxides from neutron and X-ray data
Proceedings SCI 2002" vol. XVII, edited by N. Callaos, Y. He, J.A. Perez-Peraza, pp. 313-320

PARASOTE V., KENTZINGER E., PIERRON-BOHNES V., CADEVILLE M. C., KERRACHE A., ZEMIRLI M., BOUZAR H., HENNION B. - Order and migration energies in a $CoPt_3$ single crystal. Experimental determination from neutron scattering and Monte-Carlo simulations.
Diffusion and Defect Data--Solid State Data, Pt. A: Defect and Diffusion Forum **194-199** (2001) 403-410

PETITGRAND D. IVANOV , A.S., MALEYEV S.V. - Spin dynamics and magnetic order near the field-induced quantum critical point in Pr_2CuO_4
Applied Physics A **74** (2002) S853-S855

PINTSCHOVIUS L., REICHARDT W., BRADEN M., DHALENNE G., REVCOLEVSCHI A. - Lattice dynamics of stoichiometric and nonstoichiometric $La_{1.85}Sr_{0.15}CuO_4$
Physical Review B **64** (2001) 094510

PINTSCHOVIUS L., REICHARDT W., KLASER M., WOLF T., VON LOHNEYSEN H. - Pronounced in-plane anisotropy of phonon anomalies in $YBa_2Cu_3O_{6.6}$
Physical Review Letters **89** (2002) 037001

PROKES K., GUKASOV A., JAVORSKY P., SECHOVSKY V., MIHALIK M. - Magnetic anisotropy in UniGa determined by polarized neutrons
Physica B **301** (2001) 255-260

PROKES K., JAVORSKY P., GUKASOV A., BRUCK E., SECHOVSKY V. - Field induced change of the antiferromagnetic structure of UniAl
Physica B **312-313** (2002) 872-874

ROTTER M., KRAMP S., LOEWENHAUPT M., GRATZ E., SCHMIDT W., PYKA N.M., HENNION B., v.d.KAMP R. - Magnetic excitations in the antiferromagnetic phase of NdCu$_2$.
Applied Physics A **74** (2002) S751-S753

RÜCKER U., KENTZINGER E., TOPERVERG B., OTT F., BRÜCKEL T. - Layer-by-layer magnetometry of polarizing supermirrors
Applied Physics A **74** (2002) S607-S609

SADOWSKI J., MATHIEU R., SVEDLINDH P., KARLSTEEN M., KANSKI J., FU Y., DOMAGALA J. T., SZUSZKIEWICZ W., HENNION B., MAUDE D. K., AIREY R., HILL G. - Ferromagnetic GaMnAs/GaAs superlattices-MBE growth and magnetic properties.
Thin Solid Films **412** (2002) 122-128.

SECHOVSKY V., PROKES K., SVOBODA P. SYSHCHENKO O., CHERNYAVSKI O., SATO H., FUJITA T., SUZUKI T., DOERR M., ROTTER M., LOEWENHAUPT M., GUKASOV A. - Magnetic field induced irreversibility in UniAl
Journal of Applied Physics **89** (2001) 7639-7641

SIDIS Y., BOURGES P., KEIMER B., REGNAULT L. P., BOSSY J., IVANOV A., HENNION B., GAUTIER-PICARD P., COLLIN G. - Magnetic resonance peak and nonmagnetic impurities.
NATO Science Series, II: Mathematics, Physics and Chemistry (2001), 15(Open Problems in Strongly Correlated Electron Systems), 59-68.

SIDIS Y., ULRICH C., BOURGES P., BERNHARD C., NIEDERMAYER C., REGNAULT L. P., ANDERSEN N. H., KEIMER B. - Antiferromagnetic Ordering in Superconducting YBa$_2$Cu$_3$O$_{6.5}$.
Physical Review Letters **86** (2001) 4100-4103.

SIMON Ch., MERCONE S., GUIBLIN N., MARTIN C., BRULET A., ANDRE G. - Microphase separation in Pr$_{0.67}$Ca$_{0.33}$MnO$_3$ by small angle neutron scattering
Physical Review Letters **89** (2002) 207202

STRIDE J., GILLON B., GOUKASSOV A., LARIOVA J., CLERAC R., KAHN O. - Determination of the nuclear structure and spin density distribution in the cyano-bridged molecular based magnet K$_2$Mn$_3$(H$_2$O)$_6$[Mo(CN)$_7$]$_2$·6H$_2$O
Comptes Rendus de l'Académie des Sciences - Paris Chimie **4** (2001) 105-112

SZUSZKIEWICZ W., DYNOWSKA E., HENNION B., OTT F., JOUANNE M., MORHANGE J. F., KARLSTEEN M., SADOWSKI J. - Interlayer exchange coupling in short period GaMnAs/GaAs superlattices.
Acta Physica Polonica, A **100** (2001) 335-341

TRANQUADA J.M., NAKAJIMA K., BRADEN M., PINTSCHOVIUS L., MCQUEENEY R.J. - Bond-Stretching-Phonon Anomalies in Stripe-Ordered La$_{1.69}$Sr$_{0.31}$NiO$_4$
Physical Review Letters **88** (2002) 075505

VIRET M.; BERGER S.; GABUREAC M.; OTT F.; OLLIGS D.; PETEJ I.; GREGG J. F.; FERMON C.; FRANCINET G.; LE GOFF G., Magnetoresistance through a single nickel atom.
Physical Review B: 66 (2002) 220401

WANG NL., TIMUSK T., FRANCK JP., SCHWEISS P., BRADEN M., ERB A. - Oxygen isotope effect in the ab-plane reflectance of underdoped YBa$_2$Cu$_3$O$_{7-\delta}$
Physical Review Letters **89** (2002) 087003

WITTE U., KRAMP S., BRADEN M., SVOBODA P., LOEWENHAUPT M. - Crystal field-phonon coupling in the Kondo lattice CeCu$_2$
Applied Physics A **74** (2002) S571-S573

3 - MATERIALS SCIENCE

ALBERTINI G., CERETTI M., CAGLIOTI G., FIORI F., MONZANI R., VIVIANI L. - Residual stresses in AA6082 shrink-fit systems : finite element calculations and neutron diffraction measurements
Journal of Neutron Research **9** (2001) 459-467

ANNIBALI G., BRUNO G., FIORI F., GIULIANI A., MANESCU A., MARCANTONI M., TURQUIER F. - Neutron-diffraction measurements for residual stress analysis in automotive steel gears
Applied Physics A **74** Part 2 (2002) S1698-S1700

ASSERIN O., BRAHAM C., MILLET P., LODINI A. - Synchrotron, neutron and classical X-ray measurement in an electron beam welded martensitic steel
Journal of Neutron Research **9** (2001) 351-356

BACZMANSKI A.; BRAHAM C.; LODINI A.- Intergranular stresses determined by diffraction and self-consistent model.
Materials Science Forum (2002), 404-407
(ECRS 6, Proceedings of the 6th European Conference on Residual Stresses, 2002), 729-73

BARRALLIER L., FABRE A., MASSE J.-E., CERETTI M.- Residual stress measurements using neutron diffraction in magnesium alloy laser welded joints.
Materials Science Forum **404-407** (2002) 399-404

BARUCHEL J, LODINI A., ROMANZETTI S., RUSTICHELLI F., SCRIVANI A. - Phase-contrast imaging of thin biomaterials
Biomaterials **22** (2001) 1515-1520

BATTAGLIN G.; MENELLE A.; MONTECCHI M.; NICHELATTI E.; POLATO P. - Neutron reflectometry for the investigation of multilayer coatings for building applications
Glass Technology **43** (2002) 203-208

BECHADE J.L., MATHON M.H., BRANGER V., REGLE H., ALAMO A. - Texture analysis of oxide dispersion strenghtened (ODS) Fe alloys by X-ray and Neutron diffraction
Journal de Physique IV **12** (2002) 155-163

BOUCHARD P. J.; FIORI F.; TREIMER W. - Characterisation of creep cavitation damage in a stainless steel pressure vessel using small angle neutron scattering
Applied Physics A **74** (2002) S1689-S1691

BRUNO G., GIRARDIN E., GIULIANI A., KOSZEGI L., LEVY-TUBIANA R., MANESCU A., RUSTICHELLI F. - Residual stress determination in several MMC samples submitted to different operating conditions
Journal of Neutron Research **9** (2001) 107-117

CALEYO F., BAUDIN T., MATHON M.H., PENELLE R. - Comparison of severalk methods for the reproduction of the orientation distribution function from pole figures in medium to strong textured materials
European Physical Journal A **15** (2001) 85-96

PUBLICATIONS

CARRADO A., SPRAUEL J.-M., BARRALLIER L., LODINI A. - Neutron and synchrotron evaluation of residual stresses in coatings
Journal of Neutron Research **9** (2001) 193-200

CARRADO A., FIORI F., GIRARDIN E., PIRLING T., POWELL P., RUSTICHELLI F. - Neutron diffraction measurements of residual stresses in metal matrix composite samples.
Radiation Physics and Chemistry **61** (2001) 575-577.

CARRADO A.; SPRAUEL J. M.; BARRALLIER L.; LODINI A. - Synchrotron evaluation of residual stress in palladium alloy substrate.
Materials Science Forum (2002), 404-407
(ECRS 6, Proceedings of the 6th European Conference on Residual Stresses, 2002) 335-340.

CERETTI M., HIRSCHI K., MARINI B., SPRAUEL J.M., LAURIAT J.P., ELKAIM E. - Residual stresses and hardening near crack tip regions of austenitic steel
Applied Physics A **74** (2002) S1722-S1724

COFINO B., BRAHAM C., MILLET P., LODINI A. - Use of synchrotron radiation in the analysis of strains near the interface between a plasma-sprayed hydroxyapatite coating and a Ti-6Al-4V substrate
Journal of Neutron Research **9** (2001) 243-247

COPPOLA R.,. LAPP A, MAGNANI M., VALLI M. - Non-destructive investigation of microporosity in marbles by means of small angle neutron scattering.
Construction and Building Materials, **16** (2002) 223-27

COPPOLA R., LAPP A, MAGNANI M., VALLI M. - Small angle neutron scattering investigation of microporosity in marbles
Applied Physics A **74** (2002) S1066-S1068

COPPOLA R., GLATTLI H., VALLI M**.** - Polarized SANS study of microstructural evolution in a martensitic steel for fusion reactors
Applied Physics A **74** Part 2 (2002) S1055-S1057

DILIGENT-BERVEILLER S., GAUTIER E., WEISBECKER P., MATHON M.H., IUNG T., REGLE H., ZIMMER P. - Influence of coiling temperature on recrystallization of Cu-bearing Ti-IF steels
Proceedings of the 21st Riso International Symposium on Materials Science : Recrystallization – Fundamental Aspects and Relations to Deformation Microstructure, Editors : N. Hansen, X. Huang, D. Juul Jensen, E.M. Lauridsen, T. Leffers W. Pantleon, T.J. Sabin, J.A. Wert
Journal de Physique IV : Proceedings (2001), 11(Pr4) 69-76.

DILIGENT-BERVEILLER S., AEBY-GAUTIER E., WEISBECKER P., MATHON MH., LUNG T., REGLE H., ZIMMER P. – Recrystallization kinetics and associated textures of Cu-bearing Ti-IF steels
Journal de Physique IV 11 (PR4) (2001) 69-76

ETTER A.L., MATHON M.H., BAUDIN T., BRANGER V., PENELLE R. - Influence of the cold rolled reduction on the stored energy and the recrystallization texture in a Fe-53%Ni alloy
Scripta Materialia **46** (2002) 311-317

ETTER A.L., MATHON M.H., BAUDIN T., PENELLE R - A method of determination of stored energy in a single and dual phase cold rolled materials
Materials Science Forum **408-410** (2002) 583-588

FIORI F.; MARCANTONI M. - Neutron-diffraction measurement of residual stresses in Al-Cu cold-cut welding. .
Applied Physics A: **74** (2002) S1695-S1697

FITZPATRICK M.E., WITHERS P.J., BACZMANSKI A., HUTCHINGS M.T., LEVY R., CERETTI M., LODINI A. - Changes in the misfit stresses in an Al/SiC$_p$ metal matrix composite under plastic strain
Acta Materialia **50** (2002) 1031-1040

GALDEANO S., CHAFFON L., MATHON M.H., VINCENT E., ANDRE G., de NOVION C.H. - Characterisation of the ball-milled Cu$_{80}$(Fe$_{0.3}$Co$_{0.7}$)$_{20}$ compound and effects of the milling conditions on its nanostructure.
Materials Science Forum **360-362** (2001) 367-372

GALDEANO S., MATHON M.H., CHAFFRON L., ANDRÉ G., VINCENT E., TRAVERSE A., DE NOVION C.H. - Study of the nanocrystalline ball milled Cu80 (Fe$_{0.3}$Co$_{0.7}$)$_{20}$ compound
Applied Physics A**75** (2002) 1-3

GALDEANO S., MATHON M.H., CHAFFON L., ANDRE G., VINCENT E., TRAVERSE A., DE NOVION C.H. - Study of the nanocrystalline ball-milled Cu$_{80}$(Fe$_{0.3}$Co$_{0.7}$)$_{20}$ compound
Applied Physics A**74** (2002) S1046-S1948

GIGOUT D., BACZMANSKI A., OHMS C., YOUTSOS A. G., LODINI A. - Residual stresses in austeno-ferritic steel neutron diffraction and modelling.
Journal of Neutron Research **9** (2001) 65-70.

GROSSE M., STUHR U., CERETTI M., KOSZEGI L. - Measurement of radial strain in the cross section of a railway wheel hoop
Journal of Neutron Research **9** (2001) 489-493

GROSSE M., CERETTI M., OTTLINGER P. - Distribution of radial strain in a disc-braked railway wheel measured by neutron diffraction
Applied Physics A **74** (2002) S1400-S1402

GUEZOU J.C., CERETTI M., BAUDIN T., MATHON M.H., PENELLE R. - Elastic strain study in quartzites using neutron diffraction
Journal of Neutron Research **9** (2001) 357-362

JURA J., BAUDIN T., MATHON M.H., SWIATNICKI W., PENELLE R. - Microstructure and texture analysis in a cold-rolled austenitic-ferritic steel with duplex structure
Materials Science Forum **408-410** (2002) 1359-1364

KUSNIERZ J., KURPWSKI M., MATHON M.H., BAUDIN T., JASIENSKI Z., PENELLE R. - Effect of deformation path on torsion texture and stored energy of copper rods
Materials Science Forum **408-410** (2002) 625-630

KUSNIERZ J., MATHON M.H., BAUDIN T., JASIENSKI Z., PENELLE R. - Neutron diffraction study of texture and stored energy in ECA pressed copper
Materials Science Forum **408-410** (2002) 703-708

LABBE E., POISSON N., PRIOUL C., LODINI A. - Residual stress evaluation in railway wheel/axle
Journal of Neutron Research**9** (2001) 393-397

LETOUZE N., BRENNER R., CASTELNAU O., BECHADE J.L., MATHON M.H. - Residual strain distribution in Zircaloy-4 measured by neutron diffraction and estimated by homogenization techniques
Scripta Materials **47** (2002) 595-599

LETOUZE N., BRENNER R., BECHADE J.L., CASTELNAU O., MATHON M.H, BACROIX B. - Analyse par diffraction des neutrons des déformations résiduelles dans une alliage de Zirconium après un chargement thermomécanique
Journal de Physique IV **12**, PR6 (2002) 125-136

LEVY-TUBIANA R., MOLLIEX L., LODINI A. - Evaluation by neutron diffraction method of the level of stressesin Ti/SiC bling
Journal of Neutron Research **9** (2001) 431-434

LI A., LODINI A. - Micro- and macrostresses in a cold-rolled Al-SiC composite
Journal of Composite Materials 36 (7): 873-884 2002

LODINI A. - The recent development of neutronic techniques for determination of residual stresses.
Radiation Physics and Chemistry **61** (2001) 227-233.

LUKAS P., SITTNER P., LUGOVOY D., NEOV D., CERETTI M. - In situ neutron diffraction studies of the R-phase transformation in the NiTi shape memory alloy
Applied Physics A **74** (2002) S1121-S1123

MATHON M.H., de CARLAN Y., GEOFFROY G., AVERTY X., de NOVION C.H., ALAMO A. - Microstructural evolution of reduced and activation and conventional martensitic steels after thermal ageing and neutron irradiation
" Effects of Radiation on Materials " 20th International symposium, ASTM STP, Williamsburg, USA, 5-8 juin 2000
In " Effects of Radiation Materials " (2001) pp.674-693

MENIG R., PINTSCHOVIUS L., SCHULZE V., VOHRINGER O. - Depth profiles of macro residual stresses in thin shot peened steel plates determined by X-ray and neutron diffraction
Scripta Materialia **45** (2001):977-983

METELEV S. V., PLESHANOV N. K., MENELLE A., PUSENKOV V. M., SCHEBETOV A. F., SOROKO Z. N., UL'YANOV V. A. - The study of oxidation of thin metal films by neutron reflectometry.
Physica B **297** (2001) 122-125.

MILLET P., GIRARDIN E., BRAHAM C., LODINI A. - Residual stress analysis in implant coating using X-ray and neutron diffraction techniques
Journal of Neutron Research **9** (2001) 443-448

MILLET P., GIRARDIN E., BRAHAM C., LODINI A. - Stress influence on interface in plasma-sprayed hydroxyapatite coatings on titanium alloy.
Journal of Biomedical Materials Research **60** (2002) 679-684.

N'GUY-MARECHAL K., MENELLE A., GERGAUD P. - NiC/Ti supermirrors and stress evolution under neutron irradiation
Journal of Neutron Research **9** (2001) 71-78
PENELLE R.; BAUDIN T.; ETTER A. L.; SOLAS D. - Formation and control of the cube texture in Fe-Ni alloys.
Materials Science Forum **408-412** (2002) 739-747

PETTINARI F., PREM M., KREXNER G., CARON P., COUJOU A., KIRCHNER H.O.K., CLEMENT N. – Local order in industrial and model γ phases of superalloys
Acta Materialia **49** (2001) 2549-2556

PINTSCHOVIUS L., KAMPFE A., EIGENMANN B., LOHE D. - Residual stress analysis in actively brazed joints of aluminium nitride and copper using neutron and X-ray diffraction
Zeitschrift fur Metalkunde **92** (2001) 275-280

PINTSCHOVIUS L., KAMPFE A., EIGENMANN B., WICK A. - Determination of steep stress gradients at surfaces of interfaces by means of neutron diffraction
Journal of Neutron Research **9** (2001) 181-185

PREM M.; KREXNER G.; PETTINARI-STURMEL F.; CLEMENT N. - Temperature dependence of ordering in the γ-phase of Ni-based superalloys.
Applied Physics A: **74** (2002) S1112-S1114

SITTNER P., LUKAS P., NOVAK V., NEOV D., CERETTI M. - In Situ neutron diffraction study of stresses generated by shape memory alloys
Journal of Neutron Research **9** (2001) 143-150

TAKZEI G. A., MIREBEAU I., GUN'KO L. P., SURZHENKO O. B., CHEREPOV S. V., TROSCHENKOV YU. N. - The onset of a long-range ferromagnetic order in an ensemble of small ferromagnetic particles.
Materials Science Forum **373-376** (2001) 145-148.

TAMISIER-KAROLAK S L, PAGLIARUSCO S, HERRENKNECHT C, BRETTREICH M, HIRSCH A, CEOLIN R, BENSASSON R V, SZWARC H, MOUSSA F. - Electrophoretic behavior of a highly water-soluble dendro[60]fullerene.
Electrophoresis **22** (2001) 4341-6.

TIAN B., PARIS O., PREM M., PINK E., FRATZL P**.** – Serrated flow and related microstructures in an Al-8.4 at.% Li alloy
Journal of Materials Science **37** (2002) 1355-1361

TOLEDANO P., KREXNER G., PREM M., WEBER HP., DMITRIEV VP. – Theory of the martensitic transformation in cobalt
Physical Review B **64** (2001) 144104

TURQUIER F., STANIC V., CERETTI M., FIFCH A., LODINI A., RUSTICHELLI F. - Experimental investigation of thermal fatigue-induced strain in a tool steel coated with plasma-prayed, stabilised zirconia
Journal of Neutron Research **9** (2001) 405-409

ULBRICHT A., BOEHMERT J., DEWHURST C., MATHON M.H. - Microstructural investigations on Russian reactor pressure vessel steels by small angle neutron scattering
Applied Physics A **74** (2002) S1128-S1130

4 - LIQUIDS AND DISORDERED SYSTEMS

ALMASY L., BANKI P., BELLISSENT-FUNEL M.-C., BOKOR M., CSER L., JANCSO G., TOMPA K., ZANOTTI J.-M. - QENS and NMR studies of aqueous solutions of 3-picoline
Applied Physics A **74** (2002) S516-S518

ALMASY L., CSER L., JANCSO G. - Kirkwood-Buff integrals in aqueous solutions of 3-methylpiridine
Journal of Molecular Liquids **101** ((2002) 89-98

ALMASY L., JANCSO G., CSER L. - Application of SANS to the determination of Kirkwood-Buff integrals in liquid mixtures
Applied Physics A **74** (2002) S1376-S1378

ALVAREZ M., LOMBA E., VERKERK P., VAN DER AART S.A., BIONDUCCI M., MIREBEAU I., VAN DER LUGH W. - Neutron diffraction investigation of liquid alkali-gallium alloys. Giant cluster formation ?
Zeitschrift fur Anorganische und Allgemeine Chemie **628** (2002) 553-558

BAYON G., WINKLER B., KAHLE A., HENNION B., BOUTROUILLE P - Application of dynamic neutron imaging in the earth sciences to determine viscosities and densities of silicate melts.
Nondestructive Testing and Evaluation **16** (2001) 287-296.

BELLISSENT-FUNEL M.-C. - Structure of supercritical water
Journal of Molecular Liquids **90** (2001) 313-322

BONETTI M., CALMETTES P., BERVILLIER C. - Small-angle neutron scattering from supercritical heavy water at off-critical densities.
Journal of Chemical Physics **115** (2001) 4660-4669.

BRANCA C.; FARAONE A.; GALLI G.; MAGAZU S.; MAISANO G.; MIGLIARDO F. Characterization of "strong-fragile" behaviour of glass-forming aqueous solutions by neutron scattering
Applied Physics A: **74** (2002) S448-S449.

BRANCA C.; MAGAZU S.; MAISANO G.; MIGLIARDO F.; ROMEO G. - Vibrational versus relaxational contribution for disaccharide-water glass formers: neutron scattering evidence
Philosophical Magazine B:**82** (2002) 347-355

BYCHKOV E., PRICE D.L., LAPP A. - Universal trend of the Haven Ratio in Glasses : origin and structural evidence from neutron diffraction and small angle neutron scattering
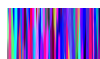Journal of Non Crystalline Solids **293-295** (2001) 211-219

CORMIER L., CALAS G., NEUVILLE DR., BELLISSENT R. - A high temperature neutron diffraction study of a titanosilicate glass
Journal of Non-Crystalline Solids **293** (2001) 510-516

COULET M.-V., CEOLIN R., BELLISSENT R., BERGMEN C, BEUNEU B., AMBROISE J.P., BICHARA C. - A new experimental method for studying phase separation through neutron diffraction : the case of As-rich liquid alloys in the As-S system
Journal of Non-Crystalline Solids **312-314** (2002) 404-408

FARAONE A., MAGAZA S., LECHNER R. E., LONGEVILLE S., MAISANO G., MAJOLINO D., MIGLIARDO P., WANDERLINGH U. - Quasielastic neutron scattering from trehalose aqueous solutions.
Journal of Chemical Physics **115** (2001) 3281-3286.

FRATINI E., CHEN S.H., BAGLIONI P., BELLISSENT-FUNEL M.C. - Age-dependent dynamics of water in hydrated cement paste
Physical Review E **64** (2001) 020201(R)

FRATINI E., CHEN S.H., BAGLIONI P., BELLISSENT-FUNEL M.C. - Quasi-elastic neutron scattering study of translational dynamics of hydration water in tricalcium silicate
Journal of Physical Chemistry B **106** (2002) 158-166

FRATINI E., FARAONE A., BAGLIONI P., BELLISSENT-FUNEL M.-C., CHEN S.-H. - Dynamic scaling of QENS spectra of glassy water in aging cement paste.
Physica A **304** (2002) 1-10.

GAMBI C.M.C., GIORDANO R., CHITTOFRATI A., PIERI R., BAGLIONI P., TEIXEIRA J. - SANS analysis of aqueous ionic perfluoropolyether micelles
Applied Physics A **74** (2002) S436-S438

GROSDIDIER B., BOS JL., GASSER JG., BELLISSENT R. - Chemical order of manganese-antimony liquid alloys obtained experimentally by the neutron "null matrix" method
Physics and Chemistry of Liquids **40** (2002) 553-580

HALM T., NZALI JN., HOYER W., MAY RP., BIONDUCCI A. - Short-range and medium-range order in molten Ga-Tl alloys
Journal of Non-Crystalline Solids **293** (2001) 182-186

HEDOUX A.,DORE J., GUINET Y., BELLISSENT-FUNEL M.-C., PREVOST D., DESCAMPS M., GRANDJEAN D. - Analysis of the local order in the glacial state of triphenyl phosphite by neutron diffraction
Physical Chemistry Chemical Physics **4** (2002) 5644-5648

JARDET K., MULLER C., BELLISSENT R., SATRE P., SEBAOUN A. - Temperature dependent X-ray and neutron diffraction study of the liquid-solid and solid-solid equilibria in the $Al_{29.2}Ga_{27}Zn_{43.8}$ ternary alloy
Journal of Alloys and Compounds **316** (2001) 179-188

MAGAZU S.; BRANCA C.; FARAONE A.; MIGLIARDO F.; MIGLIARDO P.; ROMEO G. - Comparison of disaccharide solutions across glass transition
Physica B: **301** (2001) 126-129.

PLANTEVIN O.; FAK B.; GLYDE H. R.; MULDERS N.; BOSSY J.; CODDENS G.; SCHOBER H. - Excitations of superfluid 4He in porous media: Aerogel and Vycor
Physical Review B **63** (2001) 224508

PLANTEVIN O.; GLYDE H.R.; FAK B.; BOSSY J.; ALBERGAMO F.; MULDERS N.; SCHOBER H - Excitations in liquid 4He in Geltech silica and localized Bose condensation
Physical Review B: **65** (2002) 224505

RATY JY., GODLEVSKY VV., GASPARD JP., BICHARA C., BIONDUCCI M., BELLISSENT R., CEOLIN R., CHELIKOWSKY JR., GHOSEZ P. - Distance correlations and dynamics of liquid GeSe: An ab initio molecular dynamics study
Physical Review B **64** (2001) 235209

RATY JY., GODLEVSKY VV., GASPARD JP., BICHARA C., BIONDUCCI M., BELLISSENT R., CEOLIN R., CHELIKOWSKY JR., GHOSEZ P**.** - Local structure of liquid GeTe via neutron scattering and ab initio simulations
Physical Review B **65** (2002) 115205

SIMONET V.; HIPPERT F.; AUDIER M.; BELLISSENT R. - Local order in liquids forming quasicrystals and approximant phases
Physical Review B **65** (2002) 024203

SWENSON J., BERGMAN R., BOWRON D. T., LONGEVILLE S. - Water structure and dynamics in a fully hydrated sodium vermiculite clay.
Philosophical Magazine B **82** (2002) 497-506.

TEIXEIRA J. - L'eau et les liaisons hydrogène
Encyclopaedia Universalis, La Science au présent 2001, 137-142

TEIXEIRA J. - L'étrange comportement de l'eau ultra-froide
Pour la Science 285 (2001) 84-91

5 - SOFT MATTER AND BIOMATERIALS

AKCASU AZ., JANNINK G., BENOIT H. - Application of the Sherman-Morisson formula to scattering problems by multi-component systems
European Physical Journal E **8** (2002) 315-319

ASCHI A., GHARBI A.H, BITRI L., CALMETTES P., DAOUD M., AGUIE-BEGHIN V., DOUILLARD R. - Structure and properties of adsorption layers of β-casein formed from guanidine hydrochloride rich solutions.
Langmuir **17** (2001) 1896-1904.

ASCHI A., GHARBI A.H, CALMETTES P., DAOUD M., AGUIE-BEGHIN V., DOUILLARD R. - Adsorption layers of β-casein at the air/water interface: Effect of guanidine hydrochloride.
Royal Society of Chemistry **276** (2002) 145-152.

BAUMERT J., ASMUSSEN B., GUTT C., KAHN R. - Pore-size dependence of the self-diffusion of hexane in silica gels
Journal of Chemical Physics **116** (2002) 10869-10876

BEAUDOIN E., LAPP A., HIORNS R.C., GRASSL B., FRANCOIS J. - Neutron scattering of hydrophobically modified poly(ethylene oxide) in aqueous solutions in the presence of latex particles
Polymer **43** (2002) 2677-2689

BAUDOUIN E., BORISOV O., LAPP A., BILLON L., HIORNS R.C., FRANÇOIS J. - Neutron Scattering Of Hydrophobically Modified Poly(ethylene oxide) in Aqueous Solutions.
Macromolecules **35** (2002) 7436 - 7447

BENOIT H., JANNINK G. - A few remarks on classic problems of scattering by polymer solutions and mixtures
Macromolecular Symposia **190** (2002) 43-54

BERRET J.-F., CRISTOBAL C., HERVE P., OBERDISSE J., GRILLO I. - Structure pf colloidal complexes obtained from neutral/polyelectrolyte copolymers and oppositely charged surfactants
European Physical Journal E **9** (2002) 301-311

BRAUN O., BOUE F., CANDAU F. - Microphase separation in weakly charged hydrophobic polyelectrolytes.
European Physical Journal E **7** (2002) 141-151.

BRUBACH J.B., MERMET A., FILABOZZI A., GERSCHEL A., LAIREZ D., KRAFFT M.P., ROY P. - Dependence of water dynamics upon confinement size
Journal of Physical Chemistry B **105** (2001) 430-435

BRULET A., FOURMAUX-DEMANGE V., COTTON J.P. - Temperature dependence of the conformation of a comb-like liquid crystalline polymer in a N_1 nematic phase
Macromolecules **34** (2001) 3077-3080

BRULET A., COTTON J.P. - Structure and dynamics of comb-like liquid crystalline polymers : studies as a function of the molecular weight
Recent Research Developments in Polymer Science **5** (2001) 93-138.

CARROT G., DIAMANTI S., MANUSZAK M., CHARLEUX B., VAIRON J.-P. - Atom transfer radical polimerization of n-butyl acrylate from silica nanoparticles
Journal of Polymer Science A **39** (2001) 4294-4301

CARROT G., RUTOT D., POTTIER A., DEGÉE P., HILBORN J., DUBOIS P. - Surface-initiated ring-opening polymerization: a versatile method for nanoparticle ordering
Macromolecules **35** (2001) 8400-8404

CASTELLETTO V., NOIREZ L. - Orientation of side chain liquid crystal polymers under shear constraint in the smectic phase
Molecular Crystal Liquid Crystal **362** (2001) 79-88

COUSIN F., DUBOIS E., CABUIL V., BOUE F., PERZYNSKI R. - Overview of the phase diagram of ionic magnetic colloidal dispersions
Brazilian Journal of Physics **31** (2001) 350-355

DUBOIS E., BOUE F. - Conformation of polystyrene sulfonate polyions in the presence of multivalent ions : small angle neutron scattering experiments
Macromolecules **34** (2001) 3684-3697

FADDA G.C., LAIREZ D., PELTA J. - Critical behavior of gelation probed by the dynamics of latex spheres
Physical Review E **63** (2001) 61405

FADDA G. C., LAIREZ D., PELTA J. - The sol-gel transition probed by the dynamics of latex particles studied by QELS.
Physica A **304** (2002) 103-110.

FAIVRE A., LEVELUT C., DURAND D., LONGEVILLE S., EHLERS G. - Influence of the microstructure of PPO-based glass-formers on their dynamics as investigated by neutron spin echo.
Journal of Non-Crystalline Solids **307-310** (2002) 712-718

GALANT, C., AMIEL, C., WINTGENS, V., SEBILLE, B., AUVRAY, L. - Ternary complexes with poly(β-cyclodextrin), cationic surfactant, and polyanion in dilute Aqueous solution: A viscometric and small-angle neutron scattering study
Langmuir **18** (2002) 9687-9695

GAZEAU F, DUBOIS E, BACRI J C, BOUE F, CEBERS A, PERZYNSKI R - Anisotropy of the structure factor of magnetic fluids under a field probed by small-angle neutron scattering.
Physical Review E **65** (2002) 031403

GILBERT E.P., AUVRAY L., LAL J. - Structure of charged polymer chains in confined geometry.
Materials Research Society Symposium Proceedings (2001) 651 (Dynamics in Small Confining Systems V) T1.3.1-T1.3.6.

GILBERT E.P., AUVRAY L., LAL J. - Structure of Polyelectrolyte Chains Confined in Nanoporous Glass.
Macromolecules **34** (2001) 4942-4948.

HELLWEG T., BRULET A.E, LAPP A., ROBERTSON D.LA, KOETZ J. - Temperature and polymer induced structural changes in SDS/decanol based multilamellar vesicles.
Physical Chemistry Chemical Physics **4** (2002) 2612-2616.

HERVE P., DESTARAC M., BERRET J.-F., LAL J., OBERDISSE J., GRILLO I. - Novel core-shell structure for colloids made of neutral/polyelectrolyte diblock copolymers and oppositely charged surfactants.
Europhysics Letters **58** (2002) 912-918.

JARROUX N., GUEGAN P., AUVRAY L., CHERADAME H. - High yield of polyrotaxanes by control of the blocking reaction kinetics.
American Chemical Society. (2001) 221st PMSE-585..

JEAN B., BOKIAS G., LEE L.T., ILLIOPOULOS I., CABANE B. - Microphase separation of cationic poly(N-isopropylacrylamide) copolymers in water : effect of the migration of charges
Colloid and Polymer Science **280** (2002) 908-914

JEAN B., LEE L.T. - Effects of sodium dodecyl sulfate poly(N-isopropylacrylamide) adsorption at the air-water interface above the lower critical solubility temperature
Colloid and Polymer Science **280** (2002) 689-694

JESTIN J., LEE LT., PRIVAT M., ZALCZER G. - Test of the universality of the critical adsorption profile by neutron reflection
European Physical Journal B **24** (2001) 541-547

KISELEV M.A., JANICH M., LESIEUR P., HOELL A., OBERDISSE J., PEPY G., KISSELEV A.M., GAPIENKO I.V., GUTBERLET T., AKSENOV V.L. - DMPC vesicles and mixed DMPC/C12E8 micelles orientation in strong magnetic fields
Applied Physics A **74** (2002) S1239-S1241

KISELEV M.A., JANICH M., LESIEUR P., HOELL A., OBERDISSE J., PEPY G., KISSELEV A.M., GAPIENKO I.V., GUTBERLET T., AKSENOV V.L. - DMPC multilamellar vesicles and mixed DMPC/$C_{12}E_8$ micelles orientation in strong magnetic fields.
FLNP 2001 annual report. JINR pub D-2002-80 (2002) 129-131.

KRATZ K., LAPP A., EIMER W., HELLWEG T. - Volume transition and structure of triethyleneglycol dimethacrylate, ethylenglykol dimethacrylate, and N,N'-methylene bis-acrylamide cross-linked poly(N-isopropyl acrylamide) microgels : a small angle neutron and dynamic light scattering study.
Colloids and Surfaces A **197** (2002) 55-67

LAL J., AUVRAY L - Interaction of polymer with discotic clay particles.
Molecular Crystals and Liquid Crystals Science and Technology, **356** (2001) 503-515.

LAL J., ABERNATHY D., AUVRAY L., DIAT O., GRUBEL G. - Dynamics and correlations in magnetic colloidal systems studied by X-ray photon correlation spectroscopy.
European Physical Journal E **4** (2001) 263-271.

LAL J., GILBERT E. P., AUVRAY L - Confinement of neutral and charged polymer chains in nanoporous glass.
Physica A **304** (2002) 244-248.

LASIC D.D., JOANNIC R., KELLER B.C., FREDERIK P.M., AUVRAY L. - Spontaneous vesiculation
Advanced Colloid Interface Science **89-90** (2001) 337-349

LECOMMANDOUX S., CHECOT F., BORSALI R., SCHAPPACHER M., DEFFIEUX A.,BRULET A., COTTON J.P. - Effect of dense grafting on the polystyrene brushes conformation : determination of the persistent length in solution
Macromolecules **35** 52002) 8878-8881

LEGRAND L., ROSENMAN I., BOUE F., ROBERT M.-C - Effect of the substitution of light by heavy water on lysozyme KCl and $NaNO_3$ solubility.
Journal of Crystal Growth **232** (2001) 244-249.

LEN A., HARMAT P. , PEPY G., ROSTA L. - SANS investigation of potassium morphology in bubble inclusions of sintered tungsten
Applied Physics A **74** (2002) S1418-S1420

MARZOLIN C., AUROY P., DERUELLE M., FOLKERS J.P., LEGER L., MENELLE A.- Neutron reflectometry study of the segment-density profiles in end-grafted and irreversibilly adsorbed layers of polymer in good solvents
Macromolecules **34** (2001) 8694-8700

PUBLICATIONS

MASCHKE U., GOGIBUS N., NOIREZ L., EWEN B., WAGNER T., BENMOUNA M. - Liquid crystal 8CB/deuterated polystyrene: investigations by small angle neutron scattering.
Molecular Crystals and Liquid Crystals Science and Technology, A **367** (2001) 259-266

NOIREZ L., UNGERANK M., STELZER F. - Dependence of the stereoregularity on the structure and the conformation of side-chain liquid crystalline polynorbornenes of various spacer lengths.
Macromolecules **34** (2001) 7885-7893

NOIREZ L. - The role of the smectic layer crossings in the rheology of side-chain liquid crystalline polymers.
Molecular Crystals and Liquid Crystals Science and Technology, A **364** (2001) 289-294.

OBERDISSE J., DEME B. - Structure of latex-silica nanocomposite films : a small-angle neutron scattering study
Macromolecules **35** (2002) 4397-4405

OBERDISSE J., IANNIRUBERTO G., GRECO F., MARRUCCI G. - Primitive-chain Brownian simulations of entangled rubbers.
Europhysics Letters **58** (2002) 530-536.

OBERDISSE J. - Structure and rheological properties of latex-silica nanocomposite films : stress-strain isotherms
Macromolecules **35** (2002) 9441-9450

PEPY G., KUKLIN A. - An orientation process to study nuclear membranes by small angle neutron diffraction
Nuclear Instruments and Methods in Physics Research B **185** (2001) 198-203

PEPY G., NOIREZ L., BARONI P. - Pressure induced mesophases in side-chain polymer liquid crystal revealed by neutron diffraction.
Molecular Crystals and Liquid Crystals Science and Technology A **365** (2001) 279-285.

PERREUR C., HABAS J.P., FRANCOIS J., PEYRELASSE J, LAPP A. - Rheological and small-angle neutron scattering studies of aqueous solutions of branched PEO-PPO-PEO copolymer
Physical Revew E **63** (2001) 31505/1-11

PERREUR C., J.P. HABAS, FRANCOIS J., PEYRELASSE J, LAPP A. - Determination of the rheological properties of aqueous solutions of branched PEO-PPO-PEO copolymers. Confrontation with small-angle neutron scattering studies
Macromolar Symposium **166** (2001) 127-137

PERREUR C., J.P. HABAS, FRANCOIS J., PEYRELASSE J, LAPP A. - Determination of the structure of the organized phase of PEO-PPO-PEO in aqueous solutions by small angle neutron scattering under flow.
Physical Review E **65** (2002) 041802

POPOVA A., GEOFFROY G., GARTNER E.M., LAPP A. - Calcium silicate hydrates studied by small-angle neutron scattering (SANS)
Journal of the American Ceramic Society **85** (2002) 1303-305

PUJOLLE-ROBIC C., NOIREZ L. - Observation of shear-induced nematic-isotropic transition in side-chain liquid crystal polymers
Nature **409** (2001) 167-171

PUJOLLE-ROBIC C., OLMSTED P.D., NOIREZ L. - Transient and stationary flow behaviour of side chain liquid crystalline polymers : evidence of a shear-induced isotropic to nematic phase transition
Europhysics Letters **59** (2002) 364-369

RATHGEBER S., MONKENBUSCH M., KREITSCHMANN M., URBAN V., BRULET A. - Dynamics of star-burst dendrimers in solution in relation to their structural properties.
Journal of Chemical Physics **117** (2002) 4047-4062.

RETSOS H., TERZIS A.F., ANASTASIADIS S.H., ANASTASSOPOULOS D.L., TOPRAKCIOGLU C., THEODOROU D.N., SMITH G.S., MENELLE A., GILL R.E., HADZIIOANNOU G., GALLOT Y. - Mushrooms and brushes in thin films of diblock copolymer/homopolymer mixtures
Macromolecules **35** (2002) 1116-1132

ROLLET AL., SIMONIN JP., TURQ P., GEBEL G., KAHN R., VANDAIS A., NOEL JP., MALVEAU C., CANET D. - Self-diffusion of ions at different time scales in a porous and charged medium: The nafion membrane
Journal of Physical Chemistry B **105** (2001) 4503-4509

RUSS T., BRENN R., ABEL F., BOUE F., GEOGHEGAN M. - Reptation and interdiffusion in polystyrene networks
European Physical Journal E **4** (2001) 419-433

SAITO S., HASHIMOTO T., MORFIN I., LINDNER P., BOUE F. - Structures in a semidilute polymer solution induced under steady shear flow as studied by small angle light and neutron scattering
Macromolecules **35** (2002) 445-459

SCAFFEI L., LANZI L., GAMBI C.M.C., GIORDANO R., BAGLIONI P., TEIXEIRA J. - Study by SANS of sodium dodecyl sulfate micelles with the macocyclic ligand [2.2.2.]-cryptand
Journal of Physical Chemistry B **106** (2002) 10771-10776

SCHALCHLI-PLASZCZYNSKI A., AUVRAY L. - Vesicle-to-micelle transition induced by grafted diblock copolymers.
European Physical Journal E **7** (2002) 339-344.

VIERTLER K., WEWERKA A., NOIREZ L., STELZER F. - Synthesis and characterization of SCLC-homopolymers and blockcopolymers.
NATO Science Series II: Mathematics, Physics and Chemistry **56** (2002) 143-155.

6 - LIFE SCIENCES

BELLISSENT-FUNEL M.-C. - Structure and relaxational dynamics of interfacial water
Studies in Surface Science and Catalysis (eds. Y. Iwasawa, N. Oyama and H. Kunieda) **132** (2001) 657-662

BELLISSENT-FUNEL M.-C. - Structure of confined water
Journal of Physics : Condensed Matter **13** (2001) 9165-9177

BELLISSENT-FUNEL M.-C. - Water near hydrophilic surface.
Journal of Molecular Liquids **96-97** (2002) 287-304.

CHEN S.H., LIAO C.Y., HUANG H.W., WEISS T.M., BELLISSENT-FUNEL M.C., SETTE F. - Collective dynamics in fully hydrated phospholipid bilayers studied by inelastic X-ray scattering
Physical Review Letters **86** (2001) 740-743

CHEN S.H., BELLISSENT-FUNEL M.-C., Editors - Special Section Containing Articles on Scattering Studies of Mesoscopic Scale Structure and Dynamics in Soft Matter. [In: J. Phys. Condens. Matter, 2001, **13**]. 428 pp. Publisher: (Institute of Physics Publishing, Bristol, UK)

DELLERUE S., PETRESCU A.-J., SMITH J.C., BELLISSENT-FUNEL M.-C. - Radially softening diffusive motions in a globular protein.
Biophysical Journal **81** (2001) 1666-1676.

FADDA G. C., LAIREZ D. - Evidence for a rigid structure in lysozyme fractal aggregates.
Physica A **304** (2002) 271-275.

GALL A., ROBERT B., COGDELL R. J., BELLISSENT-FUNEL M.-C., FRASER N. J. - Probing the binding sites of exchanged chlorophyll a in LH2 by Raman and site-selection fluorescence spectroscopies.
FEBS Letters **491** (2001) 143-147.

GALL A., DELLERUE S., LAPOUGE K., ROBERT B., BELLISSENT-FUNEL M.-C. - Small angle neutron scattering measurements on the membrane protein subunit B777 in a detergent microemulsion.
Biopolymers **58** (2001) 231-234.

GALL A., ELLERVEE A., BELLISSENT-FUNEL M.-C., ROBERT B., FREIBERG A. - Effect of high pressure on the photochemical reaction center from Rhodobacter sphaeroides R26.1.
Biophysical Journal **80** (2001) 1487-1497.

GALL A., SEGUIN J., ROBERT B., BELLISSENT-FUNEL M.C. - The first steps in monitoring the internal dynamics of bacterial photochemical reaction center
Journal of Physical Chemistry B **106** (2002) 6303-6309

GALL A., SEGUIN J., ROBERT B., BELLISSENT-FUNEL M.-C. - Membrane proteins in bulk solution can be used for quasi-elastic neutron scattering studies : the case for the photochemical reaction center
Journal of Physical Chemistry B **106** (2002) 6303-6309

HINSEN K., PETRESCU A.J., DELLERUE S., BELLISSENT-FUNEL M.-C., KNELLER G.R. - Liquid-like and solid-like motions in proteins.
Journal of Molecular Liquids **98-99** (2002) 381-398.

KOPER I., PETRY W., BELLISSENT-FUNEL M.-C. - Hindered protein dynamics in the presence of a cryoprotecting agent
Applied Physics A, **74** (2002) S1257-S1259

LOUPIAC C., BONETTI M., PIN S., CALMETTES P. - High-pressure effects on horse heart metmyoglobin studied by small-angle neutron scattering
European Journal of Biochemistry **269** (2002) 4731-4737.

MIDDENDORF HD., WANDERLINGH UN., HAYWARD RL., ALBERGAMO F. - Neutron Compton scattering from aligned collagen fibres
Physica A **304** (2002) 266-270

PAUTHE E., PELTA J., PATEL S., LAIREZ D., GOUBARD F. - Temperature induced beta-aggregation of fibronectin in aqueous solution
Biochimica et Biophysica Acta **1597** (2002) 12-21.

PEREZ J., VACHETTE P., RUSSO D., DESMADRIL M., DURAND D. - Heat-induced unfolding of neocarzinostatin., a small all-beta protein investigated by small-angle X-ray scattering
Journal of Molecular Biology **308** (2001) 721-743

RUSSO D., DURAND D., CALMETTES P., DESMADRIL M. - Characterization of the denatured states distribution of neocarzinostatin by small-angle neutron scattering and differential scanning calorimetry.
Biochemistry **40** (2001) 3958-3966.

RUSSO D., PEREZ J., ZANOTTI J.M., DESMADRIL M., DURAND D. - Dynamic transition associated with the thermal denaturation of a small beta protein
Biophysical Journal **82** (2002) 2792-2800

SWENSON J., BERGMAN R., LONGEVILLE S. - A neutron spin-echo study of confined water.
Journal of Chemical Physics **115** (2001) 11299-11305.

SWENSON J., BERGMAN R., LONGEVILLE S., HOWELLS W. S. - Dynamics of 2D-water as studied by quasi-elastic neutron scattering and neutron resonance spin-echo.
Physica B **301** (2001) 28-34

SWENSON J., BERGMAN R., LONGEVILLE S. - Experimental support for a dynamic transition of confined water.
Journal of Non-Crystalline Solids) **307-310** (2002) 573-578.

WANDERLINGH U.N., ALBERGAMO F., HAYWARD R.L., MIDDENDORF H.D. - Biophysical applications of neutron Compton scattering
Applied Physics A **74** (2002) S1283-S1286

ZANOTTI J.-M., PARELLO J., BELLISSENT-FUNEL M.-C. Influence of hydration and calcium binding on the parvalbumin protein dynamics
Applied Physics A **74** (2002) S1277-S1279

7 - MODELLING

AUBRY S., KOPIDAKIS G., MORGANTE A.M., TSIRONIS G.P. - Analytic conditions for tagered energy transfer between nonlinear oscillators or discrete breathers
Physica B **296** (2001) 222-236

AUBRY S., KOPIDAKIS G. - Aspects of discrete breathers and new directions
"Nonlinearity and Disorder : Theory and Applications " Editors : F. Abdullaev, O. Bang, M.P. Sorensen, NATO SCIENCE SERIES VOL. 45 P. 81-98 (2001)

AUBRY S., KOPIDAKIS G., KADELBURG V. - Variational proof for hard discrete breathers in some classes of hamiltonian dynamical systems
Discrete and Continuous Dynamical Systems – Series B **1** (2001) 271-298

CAVADINI N., STRÄSSLE TH., ALLENSPACH P., CANFIELD P.C., BOURGES P.H. - CEF nature of the magnetic excitations in ordered $HoNi_2B_2C$
European Physical Journal B **29** (2002) 377-384

JOHANSSON M. - Decay of discrete breathers through inelastic multiphonon scattering
Physical Review E **63** (2001) 37601

JOHANSSON M. - Growth and decay of weakly pertuirbated discrete breathers
"Nonlinearity and Disorder : Theory and Applications " Editors : F. Abdullaev, O. Bang, M.P. Sorensen, NATO Science Series Vol. 45 p197-203 (2001)

JOHANSSON M., MORGANTE A.M., AUBRY S., KOPIDAKIS G. - Standing wave instabilities, breathers formation and thermalization in Hamiltonian anharmonic lattices
European Physical Journal B **29** (2002) 279-283

KOPIDAKIS G., AUBRY S., TSIRONIS G.P. - Targeted energy transfer through discrete breathers in nonlinear systems
Physical Review Letters **87** (2001) 165501

KOPIDAKIS G., AUBRY S. - Discrete breathers in realistic models : hydrocarbon structures
Physica B **296** (2001) 237-250

MORGANTE A.M., JOHANSSON M., KOPIDAKIS G., AUBRY S.- Standing waves in 1D nonlinear lattices
"Nonlinearity and Disorder : Theory and Applications " Editors : F. Abdullaev, O. Bang, M.P. Sorensen
NATO Science Series Vol. 45 p. 205-211 (2001)

MORGANTE A.M., JOHANSSON M., KOPIDAKIS G., AUBRY S. - Standing wave instabilities in a chain of nonlinear coupled ascillators
Physica D **162** (2002) 53-94

MORGANTE A.M., JOHANSSON M.,AUBRY S., KOPIDAKIS G. - Breather-phonon resonances in finite-size lattices "phantom breathers
Journal of Physics. A. **35** (2002) 4999-5021

PAPOULAR R.J. - Automated estimations of asymmetric linewidth parameters for high-resolution X-ray & Neutron powder diffraction data
Materials Science Forum **378-381** (2001) 262-267

POGOSSIAN S. P., MENELLE A., YOUSSEF J. BEN, EL HARFAOUI M., LE GALL H. - Observation of polarization insensitive neutron waveguide modes in magnetic multilayered structures.
Journal of Physics D **34** (2001) 1872-1877.

PROVILLE L., AUBRY S. - Many polaron states in the Holstein-Hubberd model
Journal of Statistical Physics **106** (2002) 1185-1195

RODRIGUEZ-CARVAJAL J. - Recent developments of the program FullProf
CPD Newsletter **26** (2001) 12-19

RODRIGUEZ-CARVAJAL J. - Magnetic structure determination from powder diffraction symmetry analysis and simulated annealing.
Materials Science Forum **378-381** (2001) 268-273.

RODRIGUEZ-CARVAJAL J. - Magnetic structure determination from powder diffraction using the program FullProf.
Applied Crystallography **18** (2001) 30-36

ROISNEL T., RODRIGUEZ-CARVAJAL J. - WinPLOTR: A Windows tool for powder diffraction pattern analysis.
Materials Science Forum **378-381** (2001) 118-123.

8 - INSTRUMENTATION

BARONI P., PUJOLLE-ROBIC C., NOIREZ L. - An integrated neutron Couette system for non-equilibrium studies of polymers under flow
Review of Scientific Instruments **72** (2001) 2686-2690

BARONI P., PEPY G. - Connecting a sapphire window to a high pressure flange
Review of Scientific Instruments (Notes) **72** (2002) 480-481

DOAN T.D., OTT F., MENELLE A., HUMBERT P., FERMON C., PREJBEANU I.L., RÜCKER U. - New evanescent neutron wave diffractometer at LLB
Applied Physics A **74** (2002) S186-S188

OTT F., HUMBERT P., FERMON C., MENELLE A. - Dynamical calculation of neutron scattering on a magnetic grating at grazing incidence
Physica B **297** (2001) 189-193.

PLESHANOV N.K., BODNARCHUK V., GAEHLER R., KORNEEV D.A., MENELLE A., METELEV S.V., PUSENKOV V.M., SCHEBETOV A.F., UL'YANOV V.A. - The use of remanent supermirrors for polarized neutron reeflectometry with phase analysis
Physica B **297** (2001) 126-130

POGOSSIAN S. P., LE GALL H., BEN-YOUSSEF J., MENELLE A. - Coupling between neutron spin states in a proposed new spin directional coupler.
Journal Magnetism and Magnetic Materials **237** (2001) 302-308.

LLB Laboratoire Léon Brillouin

Intensity (a.u.) vs 2θ (Degrees)

Ambient pressure

2.9 GPa

$Tb(Mn,Al)_2 D_1$

5.9 GPa

8.3 GPa

G6.1 at LLB (Saclay,F)

CENTRE NATIONAL DE LA RECHERCHE SCIENTIFIQUE

cea